High performance flame retardant rigid polyurethane foam with high thermal insulation

Pablo Alberto Acuña Domínguez

Tesis depositada en cumplimiento parcial de los requisitos para el grado de Doctor en Ciencia e Ingeniería de Materiales

Universidad Carlos III de Madrid

Director(es):

De-Yi Wang

Tutor/a:

Olga Martín Cádiz

March 2021

DEDICATORIA

Dedico esta tesis doctoral a mi familia, a mi madre Rosa, mi padre Antonio, mi hermana Antía y a mis abuelos Edelmiro, Felisa e Isabel, los cual siempre me han apoyado a conseguir mis metas académicas. Gracias a ellos, he conseguido finalizar esta tesis y labrarme un futuro en el mundo investigador, científico y profesional.

También dedico esto tesis a la ciencia en general, sin la cual, el progreso como sociedad al margen de los dictámenes políticos, no sería posible.

AGRADECIMIENTOS

Firstly, I would like to acknowledge my supervisor, Dr. De-Yi Wang for the past five years. Thanks for your excellent support, patience, and words of encouragement to me as well as guidance on becoming a real scientist. Also, thanks to Dr. Ehsan Naderi Kalali for teaching me lots of expertise and guidance in my first PhD year as well as in the industrial projects involved. I have learned to work with industrial companies and to transform research and development into products to the market. Many thanks to Nerea Pérez, who have helped and supported me in both professional and personal life as well as being an excellent laboratory manager to our group. Also, thanks to important members of our group such as the Dr. Lu Zhang; who is an excellent researcher with great potential and a football fan, Jing Zhang; who is an important personal friend and honest person who can be whatever she wants in the future and Dr. Zhi Li; a nice person with a great academic future in China, all of them doing the PhD at the same time as me. Special thanks to Jimena de la Vega, who implanted very demanded improvements to our group, that helped all of us a lot in developing our daily work satisfactorily. Personal thanks to all my friends that I met in IMDEA such as Jaime Castro, Marcos Cejuela, Hugo Mora, Ángel Alvaredo, Cecilia Andradas, Miguel Valdés, Juan Carlos Fernández, Cemre Ozmenci, Laura Cabana, Verónica Fernández and my Galician mates Xaquín Rodiles and Alejandro Rodríguez. I was very lucky to work with them and share friendship during all my happy days in Madrid. Acknowledgement also goes to Dr. Vignesh Babu Heeralal, Dr. Yetang Pan, Dr. Guangzhong Yin and all my group members for the time I spent with them during my PhD days into our HPPN research group. Thanks to Dr. Juan Pedro Fernández, Dr. Vanesa Martínez, José Luis Jiménez, Marcos Angulo, Miguel de la Cruz and all the lab technicians for helping me to use the instruments in the laboratories. Acknowledgement goes to Rosa Mª Bazán, Mariana Huerta, Eduardo Troche, Miguel Ángel Rodiel, Vanessa Rodríguez and all the administration persons in 4th floor. Special thanks to Javier Llorca and Ignacio Romero, directors of the institute during my time in IMDEA. The support from my parents, grandparents, sister and all my family members were always the best encouragement to get and pursued my doctoral degree. This was an opportunity worth to cherish and a fully recommend to anyone interested in research and development and Science. Finally, thanks to all the good and bad experiences in the past five years that had enriched me both personal and professionally inside IMDEA materials institute.

Pablo Acuña, February 2021.

CONTENIDOS PUBLICADOS Y PRESENTADOS

- P. Acuña, M. Santiago-Calvo, F. Villafañe, M. A. Rodríguez-Perez, J. Rosas, and D. Y. Wang*, "Impact of expandable graphite on flame retardancy and mechanical properties of rigid polyurethane foam," *Polym. Compos.*, 2018.
    - Author: Pablo Acuña
    - Corresponding author: De-Yi Wang
    - URL: https://onlinelibrary.wiley.com/doi/pdf/10.1002/pc.25127
    - DOI: https://doi.org/10.1002/pc.25127
    - Partially included in **Chapter 4** with an explicit reference at the introduction section

- P. Acuña, Z. Li, M. Santiago-Calvo, F. Villafañe, M. Ángel Rodríguez-Perez, and D. Y. Wang*, "Influence of the characteristics of expandable graphite on the morphology, thermal properties, fire behaviour and compression performance of a rigid polyurethane foam," *Polymers (Basel).*, vol. 11, no. 1, 2019.
    - Author: Pablo Acuña
    - Corresponding author: De-Yi Wang
    - URL: https://www.mdpi.com/2073-4360/11/1/168
    - DOI: https://doi.org/10.3390/polym11010168
    - Totally included **Chapter 4** with an explicit reference at the introduction section

- P. Acuña, X. Lin, M. Santiago-Calvo, Z. Shao, N. Pérez, F. Villafañe, M. Ángel Rodríguez-Perez, D. Y. Wang*, "Synergistic effect of expandable graphite and phenylphosphonic-aniline salt on flame retardancy of rigid polyurethane foam", Polym. Degrad. Stab., Volume 179, September 2020, 109274.
    - Author: Pablo Acuña
    - Corresponding author: De-Yi Wang
    - URL: https://www.sciencedirect.com/science/article/pii/S0141391020302068?via%3Dihub
    - DOI: https://doi.org/10.1016/j.polymdegradstab.2020.109274
    - Totally included **Chapter 5** with an explicit reference at the introduction section

- P. Acuña, J. Zhang, G.-Z. Yin, X. Q. Liu, D. Y. Wang*, “Bio-based rigid polyurethane foam from castor oil with excellent flame retardancy and high insulation capacity via cooperation with carbon-based materials”, J. Mater. Sci., 2020
    - Author: Pablo Acuña
    - Corresponding author: De-Yi Wang
    - URL: https://link.springer.com/article/10.1007/s10853-020-05125-0
    - DOI: https://doi.org/10.1007/s10853-020-05125-0
    - Totally included in **Chapters 6** and **7** with an explicit reference at the introduction section

- P. Acuña, J. Zhang, G.-Z. Yin and D. Y. Wang*, “Highly flame-retardant bio-based rigid polyurethane foam using functional polyols derived from castor oil and modified graphene oxide”, (submittted)
    - Author: Pablo Acuña
    - Corresponding author: De-Yi Wang
    - *Waiting DOI and URL*
    - Totally included in **Chapter 7** and waiting for the publication.

OTROS MÉRITOS DE INVESTIGACIÓN

- N. Pérez, X. L. Qi, S. Nie, **P. Acuña**, M. J. Chen and D. Y. Wang*. "Flame Retardant Polypropylene Composites with Low Densities". Materials 2019, 12(1), 152;
    - DOI: https://doi.org/10.3390/ma12010152
    - Not included on this thesis

- S. de Juan, J. Zhang, **P. Acuña**, S. Nie, Z. Liu, W. Zhang, M. L. Puertas, A. Esteban-Cubillo, J. Santarén and D. Y. Wang*. "An efficient approach to improving fire retardancy and smoke suppression for intumescent flame-retardant polypropylene composites via incorporating organo-modified sepiolite". Fire and materials, 43, 8, 2019.
    - DOI: https://doi.org/10.1002/fam.2757
    - Not included on this thesis

Abstract

The fire hazard of polymeric materials causes fatal losses to people´s life, property and on top of that, commonly it derives to social problems due to these damages. The integral fire-hazard assessment was involved in thermal conductivity, ignition behavior, heat release, smoke production and toxic effluents. Polyurethane (PU), is one of the most used materials in our daily life´s, being integral part of freezers, cars, buildings, footwear, food packaging …etc. Indeed, PU is a very versatile material, being found on different applications, such as elastomers, adhesives, thermoplastics and on top of that, rigid (RPUF) and flexible (FPUF) foams. However, as most of the polymeric materials, it is very flammable with high risk of fire spreading. For that reason, fire/flame retardants (FRs) are commonly used as useful solutions to avoid the risk of a fire. In this PhD thesis, the thermal and fire behavior of different fire-retardant systems of RPUFs has been systematically investigated. The thermal conductivity has been of special importance particularly in terms of nanofillers-based polymers, as the commercial use of RPUFs is mainly as insulators. This thesis aimed also at the study of the mechanical properties of fire-retardant RPUF as it can be commonly used as mechanical reinforcement as well as the cellular structure, due to the direct influence in both thermal conductivity and mechanical performance. The nanostructures used as FR additives on this thesis include carbon-based materials such as expandable graphite (EG) and graphene oxide (GO) as well as novel synthesized phosphorous-nitrogen-based FRs (P-N FRs). Besides, the use of green natural resources to obtain RPUFs, partly suppressing the use of petroleum-based materials, has been encouraged on this thesis. The studies based on these solutions to obtain higher thermal and fire stability as well as good mechanical performance were explored separately with the FR mechanism investigation. In detail, the strategies based on novel concepts were adopted to obtain high flame retardancy (**Chapter 4**), synergistic effect to achieve higher compressive strength (**Chapter 5**) and the use of new natural resources combined with high thermal insulation (**Chapter 6**). Obtaining multifunctional properties into one sole system was demonstrated in **Chapter 7**.

1) In terms of flame retardancy, the use of EG as FR additive offered a feasible solution. The use of three different EGs (EG1, EG2 and EG3) with different particle size and rate of expansion was primarily investigated in a commercial foam. The big size of EG affects the structure of the foam by reducing its cell size, increasing the density and so, the thermal conductivity. The internal cellular structure of the PU gets dramatically affected by EG, thus the compressive performance of the foam was diminished due to slippage between the damaged

cellular structure and the EG. Above all, EG acted as an excellent additive FR which reduces the heat released (peak (PHRR) and total heat (THR)), total smoke production (TSP) and mass loss in a commercial RPUF (cone calorimeter test (CCT), 50 kW/m^2). The different particle size (EG1/EG2 and EG3) and rate of expansion (EG1 and EG2/EG3) were highlighted inside this research. It was discovered that to have an outstanding FR effect, it is necessary to use high particle size and high rate of expansion, with the aim of maximizing the performance of EG as FR. The particle size maximizes the blocking effect of EG and the rate of expansion favors lower smoke production; i.e. mass transfer. For this reason, PHRR, THR, TSP and mass loss were incredibly improved by EG with a high particle size and high rate of expansion (EG3). A loading up to 8 wt. % was enough to achieve V-0 rating in the vertical burning test (UL94). Indeed, PHRR was incredibly reduced up to a 51 %, THR was reduced up to a 47 %, TSP was reduced up to an impressive 82 % and mass loss were reduced by a 39 % less compared to the commercial reference PU. On the other hand, it was seen that the high particle size of EG3, affects negatively on the cellular structure, leading to a dramatic decrease of the compressive strength compared to the neat RPUF or a lower particle size EG-filled foam (EG1/EG2).

2) In terms of improved flame retardancy by a synergistic effect and higher compressive strength, solving the problem with EG, a system combining P-N FRs and EG was designed. It was reported in the literature that phosphorous species can impart good flame retardancy on RPUF by acting as synergistic agents for other FRs. Phenylphosphonic-aniline salt (FR1) was synthetized and used as a synergistic with EG at 8 wt. % loading into a commercial RPUF. A ratio of 12/1 (EG/FR1) was demonstrated to obtain the highest results with respect to flame retardancy and compressive strength. The optimal sample RPU3 increased the limited oxygen index (LOI) value from 19.2 % to 29.8 % and reached V-0 rating on the UL94 test. The PHRR was reduced up to 45 %, THR decreased to a 24 % and the TSP 58 %. It is highlighted that the optimal sample obtained better FR results than the sample with only EG at 8 wt. % loading, confirming a synergistic improved effect between FR1 and EG. A combined synergistic FR mechanism by the barrier effect of EG in condense phase and radical capture mechanism of FR1 in gas phase was proposed after a deep study. Finally, aiming to solve the commonly known low performance of EG-based RPUFs in the compression strength, it was discovered that the compressive strength of the new foams increased a 9 % compared with the reference commercial foam. There is a good interfacial adhesion between FR1 and PU matrix besides an increasing density of the foam provoked by the stiff phenyl groups in the FR1 structure and the proposed reaction of isocyanate (-NCO) groups at the PU end chains and FR1 to produce urea

groups. However, an increase in thermal conductivity was observed as the FR1 content increased. The thermogravimetric analysis (TGA) indeed indicated that EG and FR1 accelerated the degradation of the foam but increased the char residue.

3) In terms of thermal insulation and the use of natural resources to obtain a RPUF, A system based on a modification of castor oil; a natural oil with secondary hydroxyl (-OH) groups, and the use of novel nanomaterials, such as GO was proposed. First, castor oil was modified to increase the number of primary -OH groups, as they react faster with -NCO groups to produce a more crosslinked structure. Secondly, the double bonds of the remainder castor oil unsaturated fatty acid structure were used as an essential part and they were epoxidized. Finally, with the aim of getting a polyol with intrinsic flame retardancy, a commonly known phosphonic acid was used as modifier to be introduced into the epoxidized oil structure via ring opening reaction. With these modifications, a polyol with intrinsic flame retardancy, higher viscosity and increased OH number was synthetized (CPPA). This polyol was used as a substitute for the commercial polyol from the previous reference foam and produced a novel biobased FR RPUF (BIO2). This novel idea was able to reduce the thermal conductivity by a 14 % to only 33.8 mW/mK with respect to the commercial foam as well as maintained the density at levels closer to the ones used as the commercial insulators. Also, the LOI increased up to a 24 %. Following this incredible result, EG and GO were used as additives due to its previously studied flame retardancy and thermal insulation effect, respectively. BIO2/EG/GO; with 6 wt.% of additives, including 0.5 wt. % of GO, was able to obtain reduced thermal conductivity (34.2 mW/mK) as well as a V-0 rating in the UL94 test. The covalent bonds between GO and the PU matrix increased the crosslinking density of the foam and the gas barrier effect of GO; towards the lower cell size achieved, improved the insulation capacity of the foam. Moreover, the LOI was increased to 27.2 %. The reason behind is the combination of a condensed phase barrier insulation effect against heat and mass transfer from EG and GO towards an intumescent FR effect of CPPA. The use of EG as previously stated, reduced the compressive strength whereas on the other hand, GO was able to maintain the compressive strength closer to the initial value of BIO2.

4) In terms of the multifunctional properties, the combination of thermal insulation, flame retardancy and high compressive strength into one unique system was proposed and demonstrated. GO was modified by a novel and green method with a P-N FR (FP1) to achieve higher flame retardancy and higher compressive strength and it was used in comparison to BIO2/EG/GO. PGO; the modification of GO with FP1, as an additive was able to improve the

characteristics of GO by an incredible manner. The thermal insulation was maintained at similar levels with only a slight increase because of the density increment. The LOI was as a high as 27.6 % and reduced the individual average after-flame time to only 1.6 s in 5 samples for the UL94 test. Following this, BIO2/EG/PGO was able to decrease the PHRR and THR at low levels compared to BIO2. PHRR was decreased a 50 % and THR a 7 %, meaning an improved FR effect compared to BIO2 or GO. Unfortunately, the TSP increased due to an intense gas-phase FR effect of PGO and CPPA. Finally, the compressive performance was incredible improved to about a 25 % compared to BIO2. The chemical grafting of P-N FRs into GO surface, principally by the chemical bond of -NH- with epoxy groups, lead to more free -OH groups, which subsequently can be ready to form bonds with the -NCO groups at the end of the PU chains, thus increasing the crosslinking density and so, the compressive strength of PGO with respect to unmodified GO. After that, additional H-bonds between the urethane and urea linkages formed a strong covalent interface interaction, allowing effective load stress transfer from PU to PGO and dramatically increased the mechanical strength of the RPUF.

Resumen

El riesgo de incendio de los materiales poliméricos ocasiona pérdidas fatales en la vida de las personas, propiedades y además, comúnmente deriva en problemas sociales debido a estos daños. Para la evaluación integral del peligro de un incendio, están involucradas la conductividad térmica, comportamiento de ignición, liberación de calor y la producción de humo y efluentes tóxicos. El poliuretano (PU), es uno de los materiales más usados en nuestra vida diaria, siendo parte íntegra de materiales tales como congeladores, automóviles, edificios, calzado, envases de alimentación …etc. Además, es un material muy versátil, encontrándose en diferentes aplicaciones tales como elastómeros, adhesivos, termoplásticos y sobre todo, espuma rígida (RPUF) y flexible (FPUF). Sin embargo, como la mayoría de los materiales poliméricos, es un material inflamable con alto riesgo de extensión de la llama. Por esta razón, los retardantes de llama (FRs) son comúnmente usados como soluciones útiles para evitar el riesgo de incendio. En esta tesis doctoral, se ha investigado sistemáticamente el comportamiento térmico y a la llama de diferentes sistemas ignífugos de RPUF. La conductividad térmica ha sido de especial importancia, particularmente en términos de polímeros a base de nano-aditivos, ya que el uso comercial de RPUFs es principalmente como aislantes. La tesis se dirigió también al estudio de las propiedades mecánicas de RPUFs resistentes al fuego; ya que son comúnmente usadas como refuerzo estructural, así como al estudio de su estructura celular debido a la influencia directa de ésta en la conductividad térmica y rendimiento mecánico. Las nanoestructuras utilizadas como aditivos retardantes de llama en esta tesis incluyen materiales a base de carbono, tales como grafito expandible (EG) y óxido de grafeno (GO), así como nuevos retardantes de llama sintetizados en base a fósforo-nitrógeno (P-N FRs). Además, en esta tesis se ha fomentado el uso de recursos naturales para obtener RPUFs, suprimiendo parcialmente el uso de materiales derivados del petróleo. Los estudios basados en estas soluciones para obtener una mayor estabilidad térmica y al fuego, así como un buen rendimiento mecánico, se exploraron por separado con respecto a la investigación del mecanismo retardante de llama. En detalle, se adoptaron estrategias basadas en conceptos novedosos de alta retardancia de llama (**Capítulo 4**), efecto sinérgico para lograr mayor resistencia a la compresión (**Capítulo 5**) y el uso de nuevos recursos naturales combinados con alto aislamiento térmico (**Capítulo 6**). La obtención de propiedades multifuncionales en un único sistema fue demostrada en el **Capítulo 7**.

1) En términos de retardancia de llama, el uso de EG como aditivo retardante de llama ofreció una solución viable. El uso de tres EGs diferentes (EG1, EG2 y EG3) con diferente tamaño de partícula y tasa de expansión se investigó principalmente en una espuma comercial. El gran tamaño de partícula del EG afecta la estructura de la espuma reduciendo su tamaño de celda, aumentando la densidad y con ello, la conductividad térmica. La estructura celular interna del PU se ve dramáticamente afectada por el EG, por lo que el rendimiento a la compresión de la espuma se redujo debido al deslizamiento entre la estructura celular dañada y el EG. Principalmente, EG actuó como un aditivo retardante de llama excelente que reduce el calor liberado (pico (PHRR) y calor total (THR)), la producción de humo (TSP) y la pérdida de masa en una RPUF comercial (prueba de calorímetro de cono (CCT), 50 kW m^2). El diferente tamaño de partícula (EG1/EG2 y EG3) y la tasa de expansión (EG1 y EG2/EG3) fueron parámetros destacados dentro de esta investigación. Se descubrió que, para tener un efecto retardante de llama sobresaliente, es necesario utilizar un tamaño de partícula alto y una tasa de expansión alta, con el fin de maximizar el rendimiento de EG como FR. El tamaño de partícula maximiza el efecto de bloqueo de EG y la tasa de expansión favorece una menor producción de humo; es decir, transferencia de masa. Por esta razón, el PHRR, THR, la TSP y la pérdida de masa fueron increíblemente mejoradas por el EG con un alto tamaño de partícula y alta tasa de expansión (EG3). Una carga de hasta 8 % en peso fue suficiente para alcanzar la clasificación V-0 en la prueba de combustión vertical (UL94). De hecho, el PHRR se redujo hasta un 51 %, el THR se redujo hasta un 47 %, la TSP se redujo hasta un impresionante 82 % y la pérdida de masa se redujo increíblemente en un 39 % menos en comparación con la referencia comercial PU. Por otro lado, se vio que el alto tamaño de partícula de EG3 afecta negativamente a la estructura celular, lo que lleva a una disminución dramática de la resistencia a la compresión en comparación con la RPUF pura o una espuma con carga aditiva de EG de menor tamaño de partícula (EG1/EG2).

2) En términos de retardancia de llama mejorada a través de un efecto sinérgico y mayor resistencia a la compresión; resolviendo el problema previo con EG, se diseñó un sistema que combina un P-N FR y EG. Está reportado en la bibliografía que las especies de fósforo pueden impartir una buena resistencia a la llama en RPUF actuando como agentes sinérgicos para otros FRs. Una sal fenilfosfónico-anilina (FR1) se sintetizó y se usó como un aditivo sinérgico con EG a un 8 % en peso, al mismo porcentaje de carga que en una RPUF comercial como en el capítulo anterior. Se demostró que una relación de 12/1 (EG/FR1) obtiene los mejores resultados en términos de retardancia de llama y resistencia a la compresión. La muestra óptima

RPU3 aumentó el valor del índice de oxígeno limitante (LOI) del 19.2 % al 29.8 % y alcanzó la clasificación V-0 en la prueba de UL94. El PHRR se redujo hasta un 45 %, el THR disminuyó a un 24 % y la TSP a un 58 %. Se destaca que la muestra óptima obtuvo mejores resultados retardantes de llama que la muestra con solo EG a un 8 % en peso, lo que confirma un efecto mejorado sinérgico entre FR1 y EG. Después de un estudio profundo, se propuso un mecanismo retardante de llama sinérgico combinado por el efecto barrera de EG en fase de condensación y un mecanismo de captura de radicales por el FR1 en fase gaseosa. Finalmente, con el objetivo de solucionar el comúnmente conocido bajo rendimiento de los RPUFs basados en EG en la resistencia a la compresión, se descubrió que la resistencia a la compresión de las nuevas espumas aumentó un 9 % respecto a la referencia comercial. Existe una buena adhesión interfacial entre el FR1 y la matriz de PU, además de una densidad creciente de la espuma, provocada por los grupos fenilo rígidos en la estructura de FR1 y la reacción propuesta de isocianato (-NCO) al final de las cadenas de PU y FR1 para producir grupos urea. Sin embargo, se observó un aumento en la conductividad térmica a medida que aumentaba el contenido de FR1 aumentaba. El análisis termogravimétrico (TGA) indicó que EG y FR1 aceleraron conjuntamente la degradación de la espuma, pero aumentaron el residuo de carbón.

3) En términos de aislamiento térmico y uso de recursos naturales para obtener una RPUF, un sistema basado en una modificación del aceite de ricino; un aceite natural con grupos hidroxilo (-OH) secundarios, y se propuso el uso de nanomateriales novedosos, tales como el GO. Primero, se modificó el aceite de ricino para aumentar la cantidad de grupos -OH primarios, ya que reaccionan más rápido con los grupos -NCO para producir una estructura más reticulada. En segundo lugar, el doble enlace de la estructura ácido graso insaturado del aceite de ricino restante se utilizó como parte clave y se transformó en un anillo epoxi vía epoxidación. Finalmente, con el objetivo de obtener un poliol con resistencia al fuego intrínseca, se utilizó un ácido fosfónico comúnmente conocido como modificador para introducirlo en la estructura epoxidizada mediante la reacción de apertura del anillo. Con estas modificaciones, se sintetizó un poliol con retardo de llama intrínseco, mayor viscosidad y aumento de índice de hidroxilo (OH number) (CPPA). Este poliol se utilizó como sustituto del poliol comercial de la espuma de referencia anterior y produjo una nueva RPUF ignífuga de base biológica (BIO2). Esta idea novedosa logró reducir la conductividad térmica en un 14 % a solo 33.8 mW/mK con respecto a la espuma comercial, además de mantener la densidad en niveles más cercanos a los utilizados como aislantes comerciales. Además, el LOI aumentó hasta un 24.0 %. Tras este increíble resultado, EG y GO se utilizaron como aditivos debido a su efecto retardante de llama y

aislamiento térmico previamente estudiado, respectivamente. BIO2/EG/GO; con 6 % en peso de aditivos, incluyendo un 0.5 % en peso de GO, fue capaz de obtener una conductividad térmica reducida (34.2 mW/mK), así como una clasificación V-0 en la prueba UL94. Los enlaces covalentes entre la matriz de GO y PU aumentaron la densidad de reticulación de la espuma y el efecto de barrera frente a gases de GO, además de reducir el tamaño de las células de PU, mejoraron la capacidad de aislamiento de la espuma. Además, el LOI se incrementó hasta el 27.2 %. La razón detrás es la combinación de un efecto barrera de aislamiento en fase condensada contra la transferencia de calor y masa de EG y GO y un efecto FR intumescente del CPPA. El uso de EG, como se indicó anteriormente, redujo la resistencia a la compresión, mientras que GO pudo mantenerse más cerca de la resistencia a la compresión inicial de BIO2.

4) En términos de propiedades multifuncionales, la combinación de aislamiento térmico, retardancia de llama y alta resistencia a la compresión en un solo sistema, se obtuvo con una modificación de GO mediante un método nuevo y ecológico con un P-N FR (FP1) y se utilizó en comparación con BIO2/EG/GO. PGO; la modificación de GO con FP1, como aditivo fue capaz de mejorar las características de GO de una manera increíble. El aislamiento térmico se mantuvo en niveles similares con solo un ligero aumento de densidad. El LOI fue tan alto como 27.6 % y redujo el tiempo medio individual de combustión a solo 1.6 s en 5 muestras para la prueba de UL94. Después de esto, BIO2 EG/PGO pudo disminuir la PHRR y la THR a niveles bajos comparado con BIO2. El PHRR se redujo en un 50 % y el THR en un 7 % comparado con BIO2, lo que significa un efecto retardante de llama mejorado. Desafortunadamente, la TSP aumentó debido a un intenso efecto retardante de llama en fase gaseosa de PGO y CPPA. Finalmente, el rendimiento de compresión se mejoró increíblemente a aproximadamente un 25 % en comparación con BIO2. La inserción química de P-N FRs en la superficie GO, principalmente por el enlace químico de -NH- con grupos epoxi, conduce a más grupos -OH libres, que posteriormente pueden estar listos para formar enlaces con los grupos -NCO al final de las cadenas de PU, aumentando así la densidad de reticulación y de esta forma, la resistencia a la compresión de PGO con respecto a un GO sin modificar. Después de eso, enlaces de hidrógeno entre los enlaces uretano y urea formados forman una fuerte interacción covalente con la matriz polimérica, permitiendo una transferencia de tensión de carga efectiva de PU a PGO y aumentando dramáticamente la resistencia mecánica de la RPUF.

Preface

This thesis is submitted for the degree of Doctor of Philosophy in Materials Science and Engineering of the Carlos III University of Madrid (UC3M). The research described in this thesis was carried out at IMDEA Materials Institute (Madrid, Spain) during the period September 2016 to June 2019 under the supervision of Prof. Dr. De-Yi Wang, senior researcher at IMDEA Materials Institute. The results obtained during this thesis have been published in peer-reviewed international journals in Materials Science and chemistry, including *Polymer Composites, Polymers, Polymer Degradation and Stability, Journal of Materials Science* …etc. Indeed, some parts of this work have been well received at international conferences like the *2nd Asia-Oceania symposium for fire safety materials science and engineering*, October 2017 (Shenzhen, China) as well as COST Action programs. Moreover, the knowledge, experience and the scientific training received during this PhD, was of interest for the companies and helped me to start a professional career in the private industrial sector.

To the best of my knowledge, the work described in this dissertation is original, except where due reference has been made to the work of others or my own publications, and nothing is included which is the outcome of work done in collaboration, unless otherwise stated. No part of this dissertation, or any similar to it, has been, or is currently being, submitted for any degree or other qualification at any other university.

Pablo Alberto Acuña Domínguez

Madrid

February 2021

Contents

Abbreviations

(9,10-dihydro-9-oxaphosphaphenanthrene-10-oxide) (DOPO)
1,4-diazabicyclo [2.2.2] octane (DABCO)
4,4-diphenylmethane di-isocyanate (MDI)
Acetic acid (HAc)
Alkoxy (C-O-C)
Allylamine (AA)
Aluminium trihydroxide (ATH)
Ammonium polyphosphate (APP)
Carbon dioxide (CO_2)
Carbon monoxide (CO)
Carbon nanotubes (CNT)
Carbonyl (-C=O)
Coatings, adhesives, sealants, elastomers (CASE)
Cone calorimeter test (CCT)
Dibutyltin diacetate (DBTDA)
Dibutyltin dilaurate (DBTDL)
Diethanolamine (DEOA)
Diethylene glycol (DEG)
Diethylether (DEE)
Differential thermogravimetry (DTG)
Dimethyl methylphosphonate (DMMP)
Dimethylcyclohexylamine (DMCHA)
Dimethylethanolamine (DMEA)
European Chemicals agency (ECHA)
Expandable graphite (EG)
Fire retardant/flame retardant(s) (FR)
Flexible polyurethane foam(s) (FPUF)
Fourier transform infrared spectroscopy (FTIR)
Graphene nanosheets (GNSs)
Graphene oxide (GO)
Hard segments (HS)
Heat release rate (HRR)
Hydrochloric acid (HCl)
Hydrofluorocarbons (HFC´s)
Hydrogen cyanide (HCN)
Hydrogen halide (HX)
Hydrogen peroxide (H_2O_2)
Hydroxyl (-OH)
Intumescent flame retardant (s) (IFR)
Isocyanate (s) (-NCO)
Layered-double-hydroxides (LDH)
Limited oxygen index (LOI)
Magnesium hydroxide (MDH)
Mean cell size (Φ_{3D})
Melamine-DOPO (MADP/DOPO)
Methanol (MeOH)
Molecular weight (MW)
Multi-walled carbon nanotubes (MWNT)
Nitrogen (gas) (N_2)
Nitrogen-based flame retardant(s) (N-FR)
Nuclear magnetic resonance (NMR)
Open cell content % (OC %)
Oxygen (gas) (O_2)
Peak of heat released rate (PHRR)
Phenylphosphonic acid (PPA)
Phenylphosphonic dichloride (PPDCl)
Phenylphosphonic-aniline salt (FR1)
Phosphoric acid (H_3PO_4)
Phosphorous-based flame retardant(s) (P-FR)
Phosphorous-nitrogen flame retardant(s) (P-N FR)
Polyester (PEST)
Polyether (PE)
Polyisocyanurate foam(s) (PIR)
Polymeric MDI (PMDI/PAPI)
Polytetramethylene ether glycol (PTMEG)
Polyurethane(s) (PU)
Potassium permanganate ($KMnO_4$)
P-phenylenediamine (PPD)
p-Toluenesulfonyl Isocyanate (TSI)

Reduced graphene oxide (rGO)
Rigid polyurethane foam(s)(RPUF)
Scanning electron microscopy (SEM)
Sodium chloride (NaCl)
Sodium methoxide (NaOMe)
Soft segments (SS)
Sulfuric acid (H_2SO_4)
Temperature at 5 % weight loss (T_5 wt.%)
Temperature at maximum weight loss rate ($T_{max)}$
Tetramethyl silane (TMS)
Thermogravimetric analysis (TGA)
Thermogravimetric analysis coupled to Fourier transform infrared spectroscopy (TGA-FTIR)
Time to ignition (TTI)
Toluene di-isocyanate (TDI)
Total heat released (THR)
Total smoke production (TSP)
Triethylamine (TEA)
triethylamine hydrochloride (TEA-HCl
Triethylenediamine (TEDA)
Triphenylphosphine (TPhP)
Tris(2-chloro-1-methylethyl) phosphate (TCPP)
Vertical burning test (UL94)
Volatile organic compounds (VOCs)
X-ray photoelectron spectroscopy (XPS)

Schemes

Figures

Tables

CHAPTER 1

1. Introduction

"Nothing in life is to be feared, it is only to be understood. Now is the time to understand more, so that we may fear less"

-Marie Curie

1.1. Background: Flammability of rigid PU foams (RPUFs)

PU is a kind of organic material and-like many other organic materials such as cotton, paper, wood, wool, etc.-can ignite and burn if exposed to an enough heat source. The common raw material products of PU; di-isocyanates (di-NCOs) and polyols, are mostly derived from crude oil. Due to this chemical origin, PU is a very flammable product with a high risk of fire spreading and so, their applications are sometimes restricted. Furthermore, the most common application for RPUFs is related to insulation; mainly in refrigerators and structural materials, commonly allocated on industrial buildings and domestic houses. The proximity of RPUFs to heat sources, such as ovens, heaters, big chemical containers, or electrical plugs, increases exponentially the risk of fire accident and fire spreading.

The high flammability of RPUFs is mainly caused by their porous structure, which increases the surface contact area between the material and air, thus being easily exposed to flames [1], [2]. Indeed, during a fire burning scenario, some harmful gases can be released to the environment. Hydrogen cyanide (HCN), a harmful gas that can be generated from PU foams in residence fires, directly related to the amount of char formed and its nitrogen content [3]. This gas inhibits the respiration system during a fire and it is inherently poisonous [4]. In addition, carbon monoxide (CO) and carbon dioxide (CO_2) are commonly released to the environment during a fire accident. CO is colorless, odorless, and tasteless but highly toxic. It is generated in case of incomplete combustion of combustible materials. As it is commonly known, CO substitutes gaseous oxygen (O_2) from hemoglobin; as it is around 220 times more affine; to produce carboxyhemoglobin, which usurps the space in hemoglobin that normally carries O_2 into the blood [5], causing slowly what is called "sweet death". When the amount of CO in the

air reaches 1 %, the people will lose consciousness after several counts of inhalation. After 1–2 min, the people may die of poisoning. CO_2, although with slight toxicity, it will reduce the O_2 content of air in the fire, also giving people a threat to life. In a normal fire, when CO_2, concentration increases to 5 %, people will die of choking [6]. On the other hand, it is commonly known that CO_2 is one of the most important agents concerning the global warming. As a resume, neat RPUFs are very flammable materials, with a high risk of a fast fire propagation along with potential deaths due to the release of toxic HCN and CO along with other chemical materials, with proved implications on the global warming and the environment. Therefore, modification of PU foams with FRs is a key factor to obtain high fire resistance PU composites.

1.2. Motivation for the development of FR RPUF composites

The motivation of my study resides in the fact that there is an increasing necessity all around the world on a higher safety against fire accidents, along with the increasing number of fire accidents occurring recently in Spain. Due to the increasing use of plastic materials during all the XX and XXI centuries (commonly derived from crude oil and so, quite flammable) on food packaging, households, construction, automotive, supermarkets and others, the risk of a fire spreading accident is increasing continuously into our daily life.

Spain is one of the European countries with higher risk of fire accidents due to his warm weather, number of sun hours, the global climate warnings and the increasing risk of desertification that is suffering most of the Spanish territory. A map from the Spanish agriculture department regarding the desertification risk in Spain is shown in **Figure 1-1** [7]. Because of this phenomenon, the risk of accidents with relation to fire in Spain is huge and it is expected to be a key increasing problem in the following years.

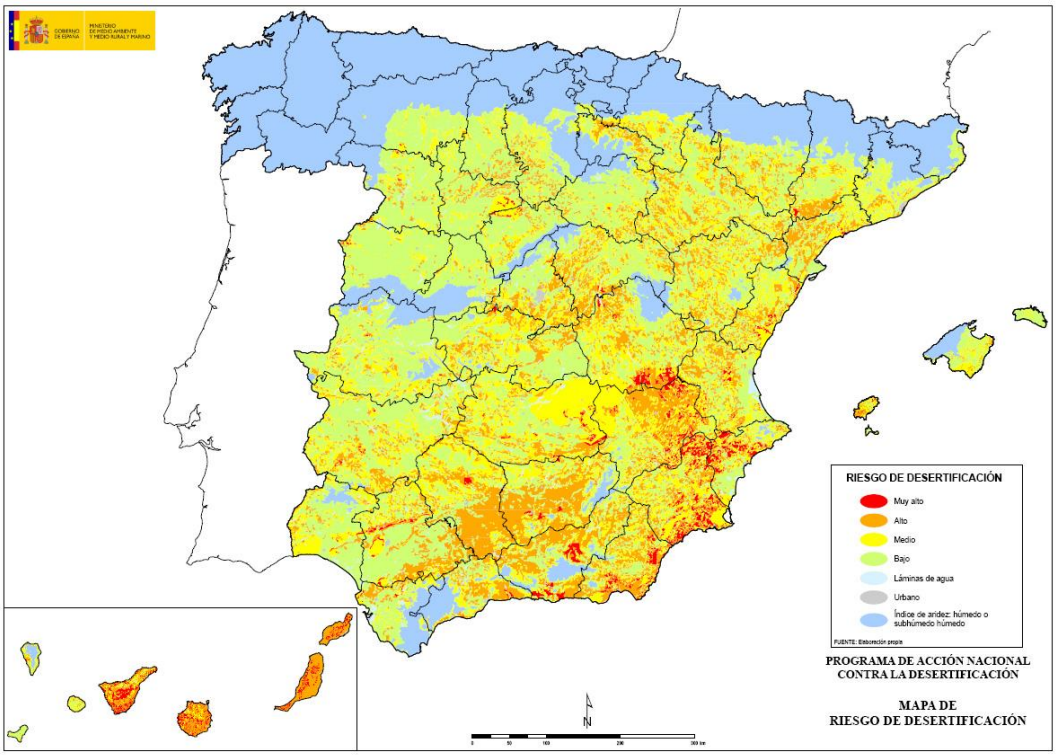

Figure 1-1. Map for the desertification risk in Spain. Programa de Acción Nacional contra la Desertificación (PAND) Ministerio de Medio Ambiente, Medio Rural y Marino. Madrid (2008) [7].

In accordance with this problematic, it can be noticed the multiple industrial accidents related with the fire that happened in Spain during the past years. For example, in 2015, *CEPSA*, devoted to petroleum-based materials, suffered its second fire accident in 2 years in Cerceda (A Coruña, Spain), and it was due to the PU residues in some containers [8]. In the year 2016, in Moaña (Pontevedra, Spain) one company (*Fandicosta*) was destroyed by a fire accident [9]. The accident produced environmental damage as well as economic problems to the company, which had to build a new ship to their products. According to the authorities, the reason behind this accident was the PU foam structure, which was located isolating the freezers of the company products such as fish, seafood, etc., ignited by an electrical problem and finally, damaging all the building. In 2018, *Frigoríficos de Vigo*, mainly dedicated to frozen seafood and so, equipped with big freezers with isolating PU, which was also damaged by a fire [10]. In 2019, the *Oceanogràfic de València*, a scientific museum, suffered a big fire accident due to the PU artificial decorative PU-based stone [11]. Lastly, in 2020, a company situated in Sant Cugat del Vallès (Barcelona, Spain) suffered a fire, intoxicating ten people due to the fire of

some pallets with PU foam [12]. Several examples of many companies on different industrial areas of Spain can led us to understand, the dimension of this problematic.

From this point of view, my motivation is heading to stop this kind of fire accidents, which are not only dangerous for people´s lives but also cause damage to companies and the economic activity of important places in Spain. Therefore, novel FR PU foam solutions needs to be developed to obtain novel high performance RPUF composites.

1.3. Objective of the study

Based on the discussion above, the main objective of this study is to improve the FR, thermal insulation, and mechanical properties of RPUFs. The most important and interesting research is to deeply investigate the mechanism behind the FR behavior, the mechanical properties performance (mainly compressive strength) and the cellular structure inside the PU foam. In order to reduce the flammability of RPUFs, suitable compounds should be carefully selected. The components of as-synthesized novel FRs on this study are inspired by the current literature and firstly designed by our group. The objectives of the study are divided into several points and concluded as:

1) To obtain good FR and low smoke production in a RPUF with non-halogenated FRs
2) To improve the mechanical compressive performance of a FR RPUF
3) To study the FR mechanisms of different RPUFs
4) To improve the thermal insulation properties of flame retardant RPUFs
5) To introduce biobased sources-based flame retardant RPUF

To endow RPUF with flame retardancy, good compressive strength and thermal insulation, different systems will be selected. Each system contributes with different benefits:

- Inorganic FRs such as expandable graphite (EG), impart excellent flame retardancy without toxicity.
- Phosphorous-based FRs (P-FRs) are a very good synergistic agent with carbon-based materials that improve flame retardancy and mechanical properties on RPUF.
- Reactive natural-based FR polyols substitute petroleum-based polyols and impart high flame retardancy towards good mechanical properties.
- Graphene oxide (GO) interacts with -NCO to impart higher flame retardancy and thermal insulation.

- Modification of GO with P-N FRs improve both flame retardancy and mechanical properties of the RPUF.

1.4. Outline of the thesis

The dissertation is divided into seven core chapters regarding the preparation, chemical characterization, cellular structure, FR, mechanical properties and the study of the mechanism of the FR performance for different RPUFs. **Chapter 2** explains the different PU technologies for foams and reviews the current progress of RPUF-based FR composites. The preparation, cellular characterization, flame retardancy and compressive performance of modified RPUFs with addition of EG as FR is discussed in **Chapter 4**. **Chapter 5** studies the synergistic effect on the flame retardancy and compressive performance between the previously selected EG and a new synthesized P-N FR salt (FR1). **Chapter 6** reveals the synthesis and characterization of a FR biobased polyol and the use of GO to achieve a high insulation biobased RPUF. Finally, **Chapter 7** represents the preparation methods and characterization techniques for the results of the RPUF composites by the use of a modified GO (PGO) to achieve a high insulation and outstanding mechanical properties biobased RPUF. Finally, the recommendation for the future work, list of publications and references explained in the thesis chapters.

CHAPTER 2

2. State of the art

"Extraordinary claims require extraordinary evidence"

-Carl Sagan

2.1. PU foam

PU was discovered by Dr. Otto Bayer back in 1937 inside the laboratories of the former German company I.G. Farbenindustrie (Leverkusen, Germany). Initially, it was intended to be a competitor of polyamide fibers (*Nylon*), discovered by DuPont (USA) but finally, it was patented on 13th of November of 1937 as a "*product obtained by the polyaddition of isocyanate and polyol*" DRP 728.981 imperial German patent (*Deutsche Reichspatent*). After that, as its failure for using it as fibers was confirmed, it led to a new material in a foam cellular structure shape, which found its own market after the II world war. In 1952, the flexible-type foam PU (FPUF) was made by the mixture of toluene di-isocyanate (TDI) and polyester (PEST) polyols [13]. Later, the use of 4,4-diphenylmethane di-isocyanate (MDI) and polytetramethylene ether glycol (PTMEG) (30/70) [14], lead to a fiber called *Spandex*, commonly known as *Lycra*, which was produced by Dupont and finally, extended the market of PU to fabrics. Then, in the 60`s, RPUF entered the market in the form of sandwich structure, protected by two metallic layers and focused mainly on the construction sector. The development of polyisocyanurate foams (PIR) by the use of poly-methylene diphenyl di-isocyanate (PMDI/PAPI), making foams with good thermal and flame resistance, upgraded even more the PU market for their use on freezers as an insulator, until the present day [15]. Over the years, their use was amplified to many new industrial sectors, such as automotive or aeronautics. In the 90's, their main improvement was the introduction of viscoelastic PU foams, widely used nowadays on our beds. In the XXI century, the direction of the research of PU is moving towards environmental-friendly and sustainable solutions due to the current concerns regarding climate warnings and depleting fossil-fuel resources.

A foam is a composite solid-gas material. The continuous phase is the PU polymer and the discontinuous phase is the gas phase [16]. The process to produce a PU foam starts with a reaction between a di-NCO and a diol or polyol and creates a urethane bond. Furthermore, the presence of a chain extender, catalyst, and/or other additives are commonly present along PU formulation and allows a product with high versatility. To obtain a PU foam, blowing agent (water or organic gases) and surfactants (commonly silicone derivatives) are mandatory additives.

Due to the recent environmental concerns, the use of the previously used chlorinated agents as blowing agents was changed towards alkanes, CO_2 or water among others. In the same line, to avoid the use of petroleum-based raw materials, the industry along with companies are developing PU foams with high biobased content. Following this, one of the most interesting topics nowadays, is the use of vegetable-oils as a replacement of traditionally used crude-oil based polyols. Unfortunately, most of the initial characteristics of the petroleum-based foam are deteriorated (mainly mechanical-related properties) and so, new ideas need to be applied on this material. The challenge is open to all the researchers.

2.1.1. *PU market*

Currently, PU is a widely used and leading-market polymer among the thermosetting plastic market. The industry may be segmented by product into foams (flexible and rigid), coatings, adhesives, sealants, elastomers (CASE) and other products. PU foams are the most important products among the PU market (**Figure 2-1 a**) [17]. Inherent properties of RPUFs and FPUFs such as structural stability, allow the production of thermally insulating products and cushioning materials. RPUFs are widely used for energy conservation in the construction and automotive field due to their excellent strength to weight ratio, thermal insulation performance and mechanical properties [18]. It can be observed that the construction field, furniture and electronics, have a PU market share higher than 70 % (**Figure 2-1 a**). However, this end-user applications have a very high risk of fire accident. Indeed, the PU market size was USD 54 billion in 2015 and is projected to grow at a 7 % rate from 2016 to 2025. The European PU market was valued at USD 16 billion in 2015. Besides, the revenues related to PU applications in Europe, are dominated by FPUF and RPUF (**Figure 2-1 b**) [19]. Due to these expectations of future growing demand and multiple uses along different industrial fields, the prospects about the use and research related to PU foams and its flammability, is expected to be highly encouraged.

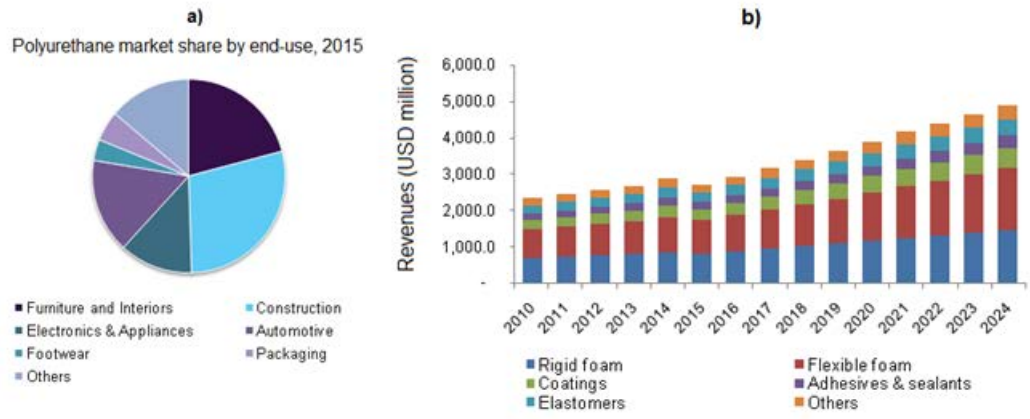

Figure 2-1. a) PU market share by end-use (2015) and b) Germany PU market revenue by product, 2010 – 2024 from *Grandviewresearch.com* [17], [19] .

2.1.2. *Isocyanates (-NCOs)*

Isocyanates (-NCOs) are an essential component for the PU production. They can be di- or polyfunctional -NCO which contains two or more -NCO groups per molecule. These can be aliphatic, cyclic or aromatic. The -NCO group dominates the reactivity of isocyanates. Due the continued double bond -N=C=O, the carbon atom is a very electrophilic atom with positive charge, thus being easily attacked by nucleophiles with negative charge like hydroxyl (-OH) groups from polyols. Among the most common -NCO to prepare PU foams, it can be highlighted aromatic -NCO such as MDI and TDI (**Figure 2-2**). Aromatic -NCOs are more reactive than aliphatic or cyclic -NCOs as the negative charge on the structure gets delocalized along the aromatic group, being a molecule with high resonance [20]. For that reason, to prepare a RPUF, -NCOs with high aromaticity, like MDI; mainly commercialized as 4,4´-isomer, are preferred. Indeed, TDI has a higher reactivity than MDI.

MDI is commercialized in various forms and functionalities, being the most important ones: pure MDI, "crude" MDI and polymeric MDI (PMDI). Pure 4,4´-MDI is used mainly in elastomers, whereas PMDI and the commonly known 'crude' MDI (mixture of 4,4´-isomer and isomers with higher molecular weight (MW) (PMDI)) are especially used in highly crosslinked PUs, such as RPUFs. On the other hand, TDI is commercialized using a mixture of the 2,4 and 2,6 isomers (TDI 80/20 having 80 % 2,4 TDI and 20 % 2,6 TDI and TDI 65/35 having 65 %

2,4 TDI and 35 % 2,6 TDI) or 2,4 TDI as pure isomer, commonly used for the preparation of FPUFs [15], [16].

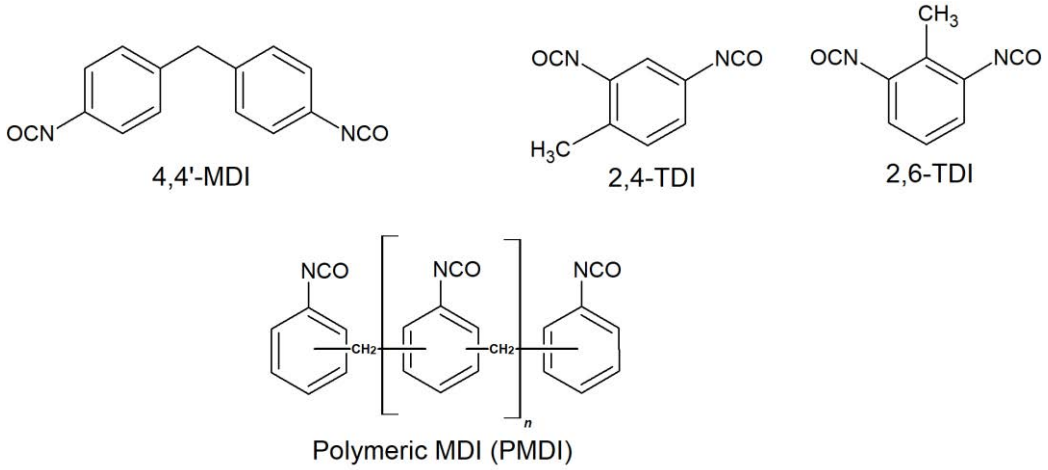

Figure 2-2. Illustration of MDI, TDI and PMDI aromatic isocyanate chemical structures.

2.1.3. *Polyols*

Polyols are a kind of chemical compound with multiple -OH groups inside its structure. They can be divided into polyester (PEST) and polyether (PE) polyols (**Figure 2-3**). PESTs have high abrasion resistance, and they hold up very well the thermal oxidation and/or mineral oils and greases attacks. However, they are susceptible to hydrolysis due to the presence of ester groups, and this also leads to the deterioration of their mechanical properties. On the other hand, PEs possess high hydrolysis and microorganism resistance as well as low temperature flexibility. Besides, they are weak to the UV light exposure.

The characteristics of a polyol, such as MW and hydroxyl number (OH number), determines the elasticity/rigidity of a PU as they influence the crosslinking degree of the polymer. Polyols represent the “soft domain” or “soft segment” (SS) of the polymer, whereas the urethane linkages (and urea linkages), because of the possibility of association by hydrogen bonds, generate the commonly known “hard domain” or “hard segments” (HS) of a PU [16]. The HS mainly consist of a rigid di-NCO and a chain extender moieties [21]. In the case of PU foams, rigid PEST structures (with highly branched structure) will result on a RPUF whereas a FPUF is obtained with less branched PEST. Also, on one hand, RPUFs are made from low MW polyols (a few hundred units; 300-1000 Da) with high functionality, whereas FPUFs are obtained from high MW polyols (from 2000 to 10,000 Da) with low functionality [16], [22], [23]. The high elasticity of FPUF is given by the high MW and mobility of the polyol segment

and the low crosslinking density due to the low functionality [16]. In addition, Polyols for RPUF use raw materials containing higher number of -OH groups [23].

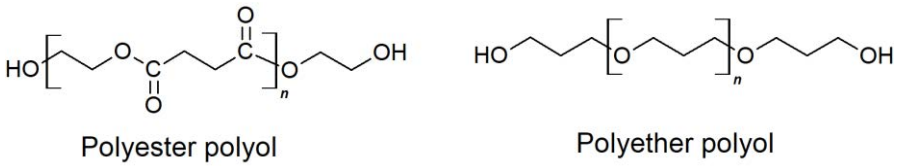

Figure 2-3. Illustration of the PEST and PE polyol chemical structures.

As it was previously described, vegetable oils can be used as polyols for the PU production. An excellent example of biobased PEST is Castor oil, with contains natural -OH groups inside its structure. Many other vegetable oils are available; like palm oil or linseed oil; which can also be transformed into a PEST polyol trough a chemical modification.

2.1.4. *Additives*

Along with a polyol and an -NCO, some additives may also be required during PU production, not only to control or modify the reaction conditions but also to finish or modify the final product. These additives include catalysts, chain extenders, crosslinkers, blowing agents and others.

a) *Catalysts*

Catalysts are added in the PU production to promote the reaction rate, lower temperatures and lowering curing temperatures and times. The reaction between -NCO groups and -OH groups is slow at room temperature. This slow speed is due to the phase incompatibility of the polar and less dense polyol phase and the relatively non-polar and denser -NCO phase. Therefore, a suitable surfactant and suitable catalysts are required to get a faster reaction rate between them [20]. Many chemical compounds can be used for this purpose, mainly including aliphatic and aromatic amines as well as organometallics [20]:

- Amine catalysts: Traditionally consist of tertiary amines, such as dimethylcyclohexylamine (DMCHA), dimethylethanolamine (DMEA), 1,4-diazabicyclo [2.2.2] octane (DABCO) and triethylenediamine (TEDA).

- Organometallic compounds: The most common are dibutyltin dilaurate (DBTDL), dibutyltin diacetate (DBTDA), but also alkali metal salts of carboxylic acids and phenols (calcium, magnesium, strontium, barium, salts of hexanoic, octanoic, naphthenic, linolenic acid) are widely used as catalysts.

b) *Chain extenders and crosslinkers*

Difunctional low MW diols (functionality = 2) (diethylene glycol (DEG), 1,4-butanediol, 1,6-hexanediol, cyclohexanedimethanol, diamines or hydroxylamines) are used as chain extenders in PU synthesis, while those with functionality ≥ 3 are used as crosslinkers.

As mentioned, PU consists of hard (HS) and soft segments (SS). HS belong to urethane links whereas the SS belong to the polyol linkages [24]. The domains of the HS urethane serve as cross-linkers for the domains of the segment amorphous PEST (or PE). This interface separation arises due to the incompatibility and immiscibility (while both phases are amorphous) of the segments (low melting and non-polar) with the HSs (high melting). Therefore, crystallization does not have any effect on phase separation. Generally, the HSs, which are produced from -NCO and chain extenders, are immobile and stiff, while on the other hand, the segments, which are produced from the polyols, can move freely and often appear in foil forms [20]. Proper selection of the chain extender could also influence the chemical resistance, heat and mechanical properties of the PU.

Since -NCO are too sensitive to moisture or water even in traces, the final mechanical properties of the RPUF are deteriorated if water is present at high amounts in the formulation. For that reason, moisture scavengers, which react more favorable with water than an -NCO, could be incorporated to cut off/eliminate the water influence during PU synthesis [15]. Examples of common moisture scavengers include oxazolidine derivatives or zeolite type molecular sieves.

c) *Blowing agents*

One of the most important additives for PU foam production are the blowing agents. Blowing agents are used to produce PU foams with cellular structures by a foaming process. PU foams are formed by either physical blowing agents or chemical blowing agents. Physical blowing agent such as cyclopentane, isobutane, CO_2 and hydrofluorocarbons (HFC´s) expand PU by vaporization, resulting in an endothermic reaction. On the contrary, chemical blowing agents

such as water, expand PU by CO_2 generated by the reaction between the blowing agent and -NCO; which "blows" the PU and produces heat, being this reaction exothermic [25] (**Figure 2-4**).

Traditionally, hydrocarbons were used as blowing agents due to its lower thermal conductivity as compared to water [25]. However, due to the environmental and the global warming concerns about HFC´s; they were phased out in 1996 in the developed countries [26]. Nowadays, the use of environmentally friendly blowing agents, such as water, is promoted. Besides, the increasing amount of water as blowing agent, helps to increase the kinetic rate formation of PU due to the heat formed.

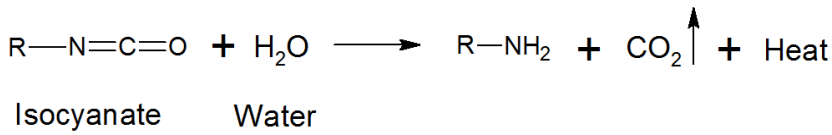

Figure 2-4. Illustration of the reaction between isocyanates (-NCO) and water (blowing reaction).

d) *Surfactants*

Surfactants are a kind a chemical compound which have a hydrophilic head and hydrophobic tail [27]. Due to this fact, surfactant molecules interpose themselves between water and water-insoluble substances, increasing the compatibility between different materials, such as catalyst, polyols or -NCO. Surfactants are commonly polysiloxane-polyoxyalkylene copolymers, silicone oils and some other organic compounds that perform several benefits to the foam structure, including: Increase of the compatibility of raw materials, decrease the surface tension, promotion of the nucleation of bubbles during mixing and the stabilization and regulation against collapse of the cell structure [20], [28].

In accordance with Lim et al. [29], in the absence of a surfactant, a foaming system will normally experience catastrophic coalescence and exhibit the event known as boiling. The loading of surfactant is of importance; small amount of surfactant, will form stable but imperfect foams whereas an increasing surfactant concentration, will impart to the foam system improved stability and cell-size control. At optimum concentrations, stable open-cell foams may be produced. If the loading is higher than the optimum, the cell-windows become over stabilized and the resulting foams are tighter with diminished physical properties. In accordance with the decreased surface tension, cell size diminished, and closed cell content increased, improving the cellular structure of the foam and its thermal conductivity gets decreased.

2.1.5. *The Chemistry of PU*

The Chemistry of PU foams is based on two different reactions (**Figure 2-5**). The first one is commonly known as "gelling reaction"; it involves the reaction of -NCO from isocyanates with -OH from polyols to form the urethane link and the second one, is the "blowing reaction"; involving the reaction of -NCO groups with water to produce CO_2 as gas. The different possible reactions of -NCO and other Hydrogen-active functional groups are showed in **Table 2-1** [16], [30].

-NCO reacts with -OH to form a urethane linkage (**Figure 2-5 a**). This reaction is an addition polymerization reaction of a di-NCO with compounds having a plurality of -OH groups (polyols). Primary -OH groups are around three times more reactive than secondary -OH groups and 200 times more reactive than tertiary -OH groups [16] (**Table 2-1**). The principal reaction leads to the formation of a crosslinked polymer (PU) since polyols with several -OH are used. The secondary reaction of a urethane group with an -NCO group to form an allophanate group is another possible way to further cross-link the polymer (**Figure 2-5 a.1**) [31]. However, this reaction needs a temperature greater than 110 ºC to occur and sometimes is preferable to avoid it if the viscosity increases too much.

The second reaction is the -NCO-water reaction, known as the "blowing reaction" (**Figure 2-5 b**), which forms the carbamic acid intermediate. Water is considered, in PU foam manufacture, as a chemical blowing agent, because the gas generation is a consequence of a chemical reaction [16]. Furthermore, carbamic acid; as an unstable compound, decomposes to give an amine and CO_2. Next, the formed amine group reacts with another -NCO group in the second step to give a disubstituted urea (**Figure 2-5 b.1**). It is important to mention that amines are much more reactive than the -OH compounds [16] as showed in **Table 2-1**. The third part of the blowing reaction contributes to chain extend the aromatic groups of the -NCO molecules to form linear HSs. This reaction involves the formation of biuret and allophanate linkages which could lead to the formation of covalent cross-linked structures (**Figure 2-5 b.2)**. In a similar way as the formation of allophanates, the temperature needed should be greater than 110 ºC. The correct balance between these reactions is required since it controls the foam stability and allows to achieve foams with tailored physical properties [32], [33].

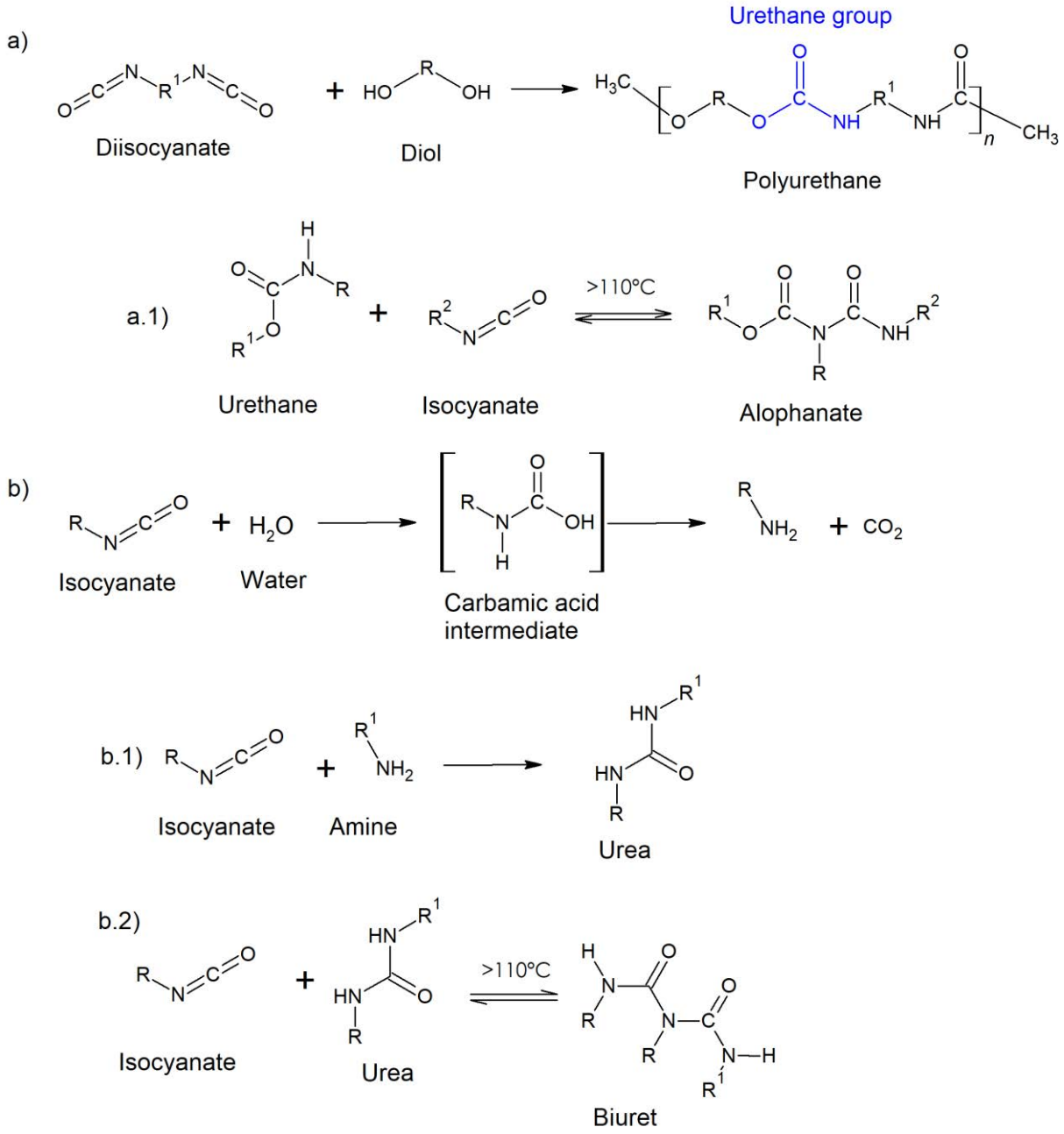

Figure 2-5. Illustration of a) Gelling reaction of a di-isocyanate with polyol to form PU and b) Blowing reaction of -NCO with water.

Table 2-1. Relative rate of reaction of H-active compounds with -NCO.

H-active functional group	Chemical structure	Relative reaction rate uncatalized at 25ºC	Type of linkage formed with -NCO
Primary aliphatic amine	R-NH_2	2500	Urea
Secondary aliphatic amine	R_2-NH	500-1250	Urea

Primary aromatic amine	Ar-NH_2	5-7.5	Urea
Primary -OH	R-CH_2-OH	2.5	Urethane
Water	H-O-H	2.5	Amine + CO_2
Secondary aromatic amine	Ar-NH-R	2.5	Urea
Carboxilic acid	R-COOH	1	Amide + CO_2
Secondary -OH	R_2-CH-OH	0.75	Urethane
Urea	R-NH-C=O-NH-R´	0.375	Biuret
Tertiary -OH	R_3-CH-OH	0.0125	Urethane
Phenolic -OH	Ar-OH	0.0025-0.00125	Urea
Urethane	R-NH-COOR´	0.0025	Allophanate

a) *Catalyst mechanism of PU formation: Amine and organometallic catalyzed reaction*

The catalyst addition allows the reaction to be performed at room temperature with very fast reaction rates. Commonly, tertiary amines and metal oxides are the most widely used catalyst for PU production (**Figure 2-6**) [34]. For RPUFs, the selection of the appropriate catalyst is of importance, as the increasing catalyst content decrease the cell size of the foam, having a big impact on the thermal conductivity [25].

In the **Figure 2-7 a)**, it can be observed the amine-catalyzed reaction of PU. The amine-catalyzed reaction can be explained by two possible mechanism: The first one is called "Baker´s mechanism" and the second one is denominated as "Farka´s mechanism" (**Figure 2-7 a.1)** and **Figure 2-7 a.2)** respectively) [32]. Tertiary amines are one of the best overall catalysts for PU production. They catalyze both NCO-OH and NCO-water reactions. Although they generally catalyze the NCO-water reaction better than the NCO-polyol reaction [32] . They also catalyze -NCO trimerization reactions (**Figure 2-8**), usually designated as polyisocyanurate reaction (PIR) and leading to a RPUF with better thermal stability and flame resistance [35]. Two main characteristics influence the effectivity of tertiary amines as catalysts; their structure as well as their basicity; catalytic activity increases with increased basicity and decreases with the steric hindrance on the nitrogen atom of amine. The ability to form hydrogen bonds and the spatial separation between active sites also affect their catalytic selectivity. Their catalytic action is performed by a complex formation between amine and -NCO, by donating the electrons on nitrogen atom of tertiary amine to the positively charged carbon atom of the -NCO. Despite their effectivity, one of the drawbacks of using tertiary amines is their offensive fish- like odor and high volatility. Increasing environmental concerns toward decreasing of emissions of

volatile organic compounds (VOCs) have contributed to the development of nonfugitive catalysts [32].

Organometallic catalysts on the other hand (**Figure 2-7 b)**) are widely used in PU applications due to their strong gelation activity. Their general feature is that they are much more effective in the NCO-OH reaction when aliphatic -NCOs are used than the tertiary amines, which are commonly used with aromatic -NCOs. In detail, metallic catalysts bear superiority over tertiary amines as they are comparatively less volatile and less toxic [15]. They form a complex with both -NCO and -OH groups. The positive metal center interacts with the electron rich "O" atom of both the -NCO and -OH groups forming an intermediate complex, thus resulting on a further rearrangement to from the urethane bond.

A right choice of catalyst for RPUF would be that both catalyst types are used. On this way, amine catalysts catalyze the -NCO-water reaction (blowing reaction) whereas organometallics work better as gelling catalysts [36], [37].

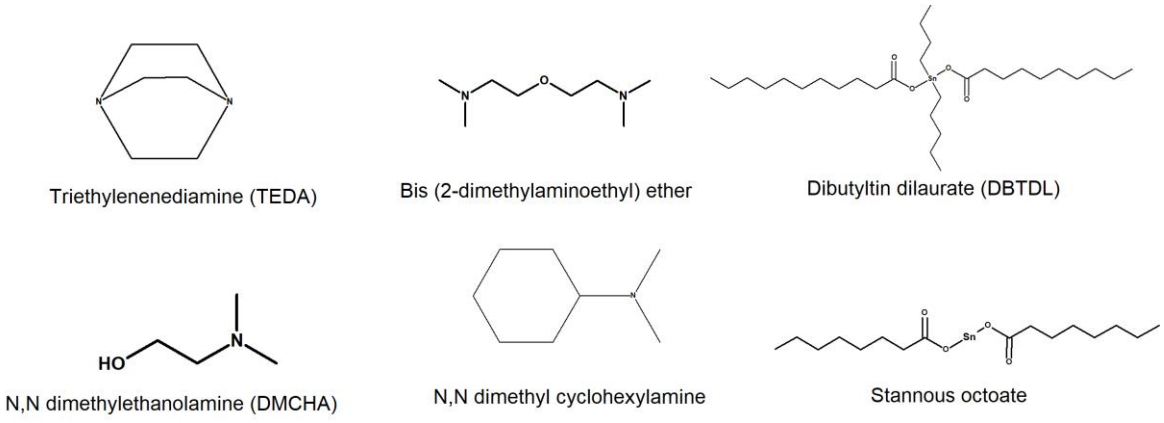

Figure 2-6. Typical catalyst for the reaction between -NCO and alcohols or water.

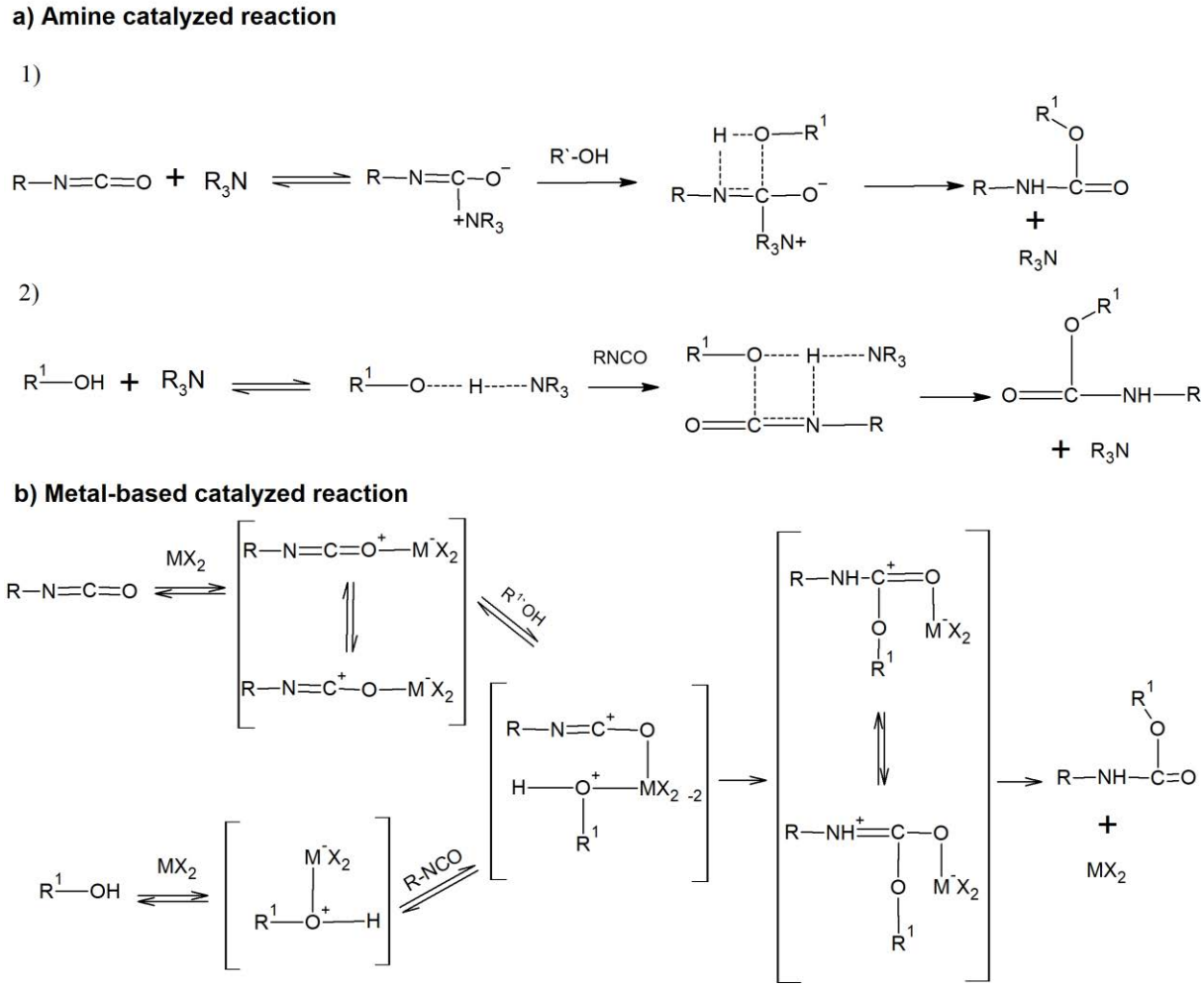

Figure 2-7. Illustration of the PU reaction catalyzed by a) tertiary amines and b) metal-based catalysts.

b) *Trimerization catalyst reaction:*

The trimerization reaction of -NCOs is a reaction which takes place in the presence of special catalysts with an excess of -NCO (NCO index = 200-600) [16]. The trimerization of -NCO is mainly present in the manufacture of RPUF and PIR, due to the higher thermal stability and improved flame retardance obtained, making them some of the most efficient thermal insulating products available. Highly crosslinked structures are formed **(Figure 2-8)**. Typical catalysts for PIR production are quaternary ammonium salts of tetraalkylmonoamine, some tertiary amines and alkali metal carboxylates [38]. Its effectivity was explained by the fact that oxyanionic bases are more nucleophilic and, consequently, more catalytically active than tertiary amines

with similar basicity. Alkali metal carboxylates salts such as potassium acetate and potassium 2-ethylhexanoate are commonly employed as trimerization catalysts [39], [40]. The industrial name of this catalyst are the brand DABCO-K brand from Air products [41].

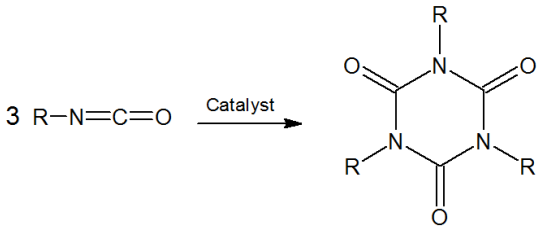

Figure 2-8. Illustration of the trimerization of PU catalyzed by a tertiary amine/ Tetraalkylammonium carboxylates to form an isocyanurate ring.

2.2. Combustion mechanism of polymers

Polymers are highly combustible due to their chemical structure, made up mainly of carbon and hydrogen. The polymer combustion reaction involves three main factors: one or more combustibles (reducing agents) a combustive (oxidizing agent, such as O_2 in the air), and a heat source which provides the activation energy (**Scheme 2-1**) [42].

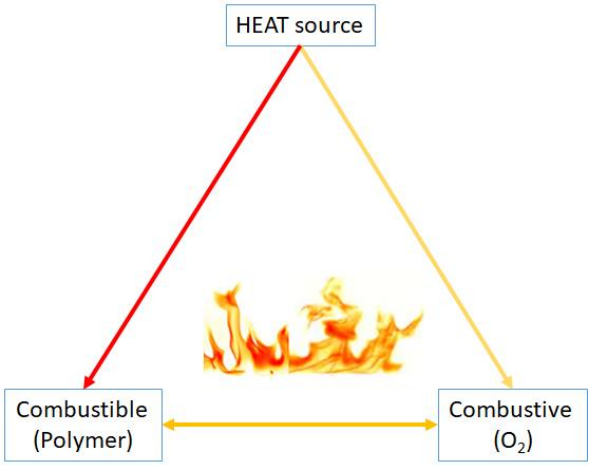

Scheme 2-1. Schematic illustration for the fire triangle combustion cycle.

In general, four major steps comprise polymer combustion process: Ignition, pyrolysis, combustion and feedback (**Scheme 2-2**) [43]. Indeed, the combustion mechanism involves two phases: Vapor (gas) and condensed phase. In the end of the process, radiant energy produced, goes back to condensed phase continuing the burning of the polymer until is totally degraded.

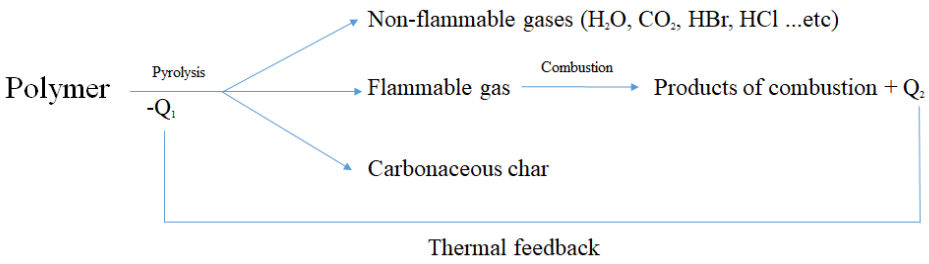

Scheme 2-2. Schematic illustration of the polymer combustion.

The process usually starts with an increase in the temperature of the material due to a heat source. Then, the solid polymer melts and decomposes to flammable gases through polymer bond scissions. The volatile gases of the resulting polymer fragments combine with the air and creates a combustible gaseous mixture called fuel, which propagates the fuel combustion by a branching reaction. This gaseous mixture ignites when the auto-ignition temperature (temperature at which the activation energy is achieved) is reached, liberating heat. Alternatively, the fuel can also ignite at a lower temperature (called the flash point) upon reaction with an external source of intense energy (such as a spark) [42]. Polymers, like other fuels, produce species upon pyrolysis capable of reaction with O_2 and produce the H_2-O_2 scheme which propagates the fuel combustion by the branching reaction (**Scheme 2-3**) [44]. The main exothermic reaction that provides most of the energy to maintain the flame is the (3) below [45]:

$$(1)\quad H\bullet + O_2 \rightarrow OH\bullet + O\bullet$$

$$(2)\quad O\bullet + H_2 \rightarrow OH\bullet + H\bullet$$

$$(3)\quad OH\bullet + CO \rightarrow CO_2 + H\bullet$$

Scheme 2-3. Schematic illustration of the polymer combustion mechanism.

The main action to stop the combustion process is performed by FR materials. In order to protect against fire, some actions can be taken: (a) reduce the heat evolved to below that required to sustain combustion; (b) modification of the pyrolysis process in order to reduce the amount of flammable volatiles emitted; (c) isolate the flame from O_2; or (d) reduce the heat flow back to the polymer to prevent further pyrolysis [45]. For this reason, to deal against the fire, the design of new FRs is a strong point. FRs can work by the addition of a FR to the polymer matrix or due to a chemical reaction with the polymer. The selection and use of a

designed FR for a particular polymer is a critical point in the FR field. Indeed, the study of the mechanism behind the FR process is one of the main points of the research activity.

2.3. Flame retardancy of PU foam

2.3.1. *Thermal degradation of PU by thermogravimetric analysis (TGA)*

The degradation of PU foams is fundamental to understand and to avoid the flammability problem associated with this polymer.

The thermal degradation of RPUF in nitrogen (N_2) and air showed a two-stage and three-stage process respectively. In a non-oxidizing N_2 atmosphere, commonly the first step occurs in the range 110-190 ºC and the second step begins around 220-250 ºC, finishing all the process about 600 ºC. The three-step process in air has its first step occurs in the range 110-190 ºC, its second starts at 210 and ends at about 400 ºC. Then, the final third step finishes being close to 670 ºC [46].

The TGA study here presented will be focused in N_2 atmosphere, which it will be the one used in our TGA analysis, as the degradation in air will be studied by the cone calorimeter test (CCT).

- **TGA under a non-oxidizing atmosphere (N_2):**

TGA is an excellent technique to analyze the degradation of polymeric materials. The analysis of the temperature pictures is commonly performed via differential thermogravimetry (DTG). In a non-oxidizing environment, the decomposition mechanism occurs via one of the three reactions or a combination of them presented below for the breaking of urethane bonds in the **Scheme 2-4** [46]:

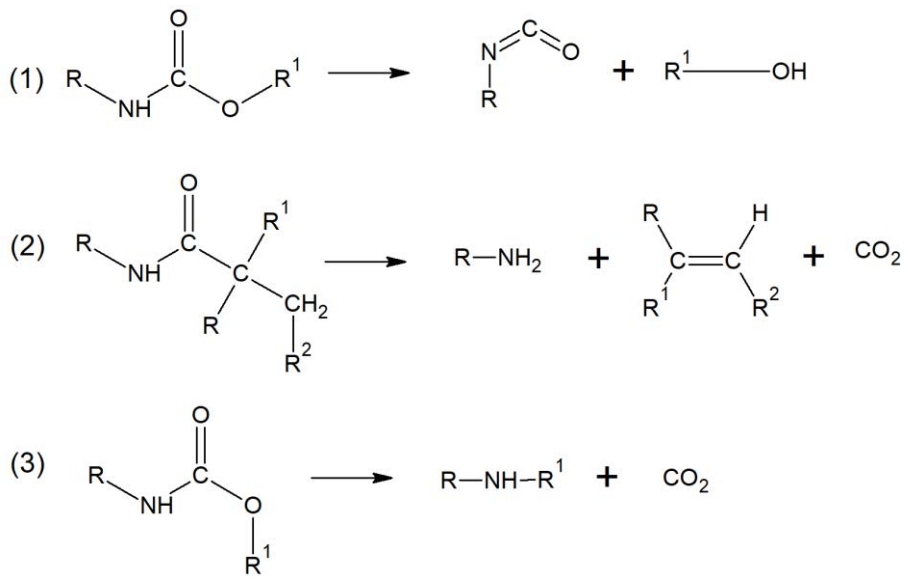

Scheme 2-4. Schematic illustration of the basic reactions for the thermal degradation of PUs.

A complete scheme showing a general PU decomposition process in a non-oxidizing environment was showed in **Scheme 2-5**, based on the reaction between -NCO and DEG and obtained from the work from L. Jiao et al. [46]. The **Step 1** of degradation for the neat RPUFs was between 100 and 200 ºC, associated to the evaporation of small molecules, such as the blowing agent, H_2O and CH_3OCH_3, along with unreacted -NCO monomers [46]. The **Step 2** of degradation occurred at higher temperatures than 200 ºC, and it is mainly due to the formation of the original PU components; -NCO and polyols; following reaction (1) in **Scheme 2-4**, due to the break of urethane bonds in HSs [46], [47]. Rupture of HSs takes place at a relatively low temperature and great amounts of -NCO are formed in the decomposition residues at the early stage. On the other hand, in the **Step 3**, the polyols segments start to decompose into some kinds of aliphatic ether alcohols olefins and CO_2 as temperature increases. Then, the products become more complex with temperature increasing, even epoxy compounds are formed as a result of interactions among evolved products. In the temperature range of 280-300 °C for N_2 and 320-350 °C for air, the -NCO monomers completely evaporate from PU in a narrow range of about 20-30 °C. From 260 °C in air and 320 °C in nitrogen, the degradation of polyols stats. At higher temperatures, reaction (2) and (3) from **Scheme 2-4** dominates the process. Compounds like nitrides, HCN and NO_2 are formed in the temperature range of 300-400 °C. At temperature above 500 °C (**Step 4**), the material residues continue to decompose into volatile products and other products derived from -NCO groups (such as primary and secondary amines or benzene alkyl) and then they decompose into volatile products like aliphatic alcohol with branched

chains, benzene alkyls and small molecule like CO_2 or NO_2, which are generated in the final stage of the degradation process around 600 ºC [46]. Finally, a complete thermal break-down of the chains yields a mixture of simple hydrocarbons, CO, CO_2, HCN, methanol (MeOH), acetonitrile, acrylonitrile, propionitrile, pyrrole, pyridine, aniline, benzonitrile, quinolone, phenyl-NCO and a complex char [48]. Compared to that in N_2, the degradation rate of PU materials during the process in air is accelerated significantly due to the presence of an oxidizing element like O_2. The initial reaction temperature of the whole reaction in N_2 is approximately 50 °C higher than that in air.

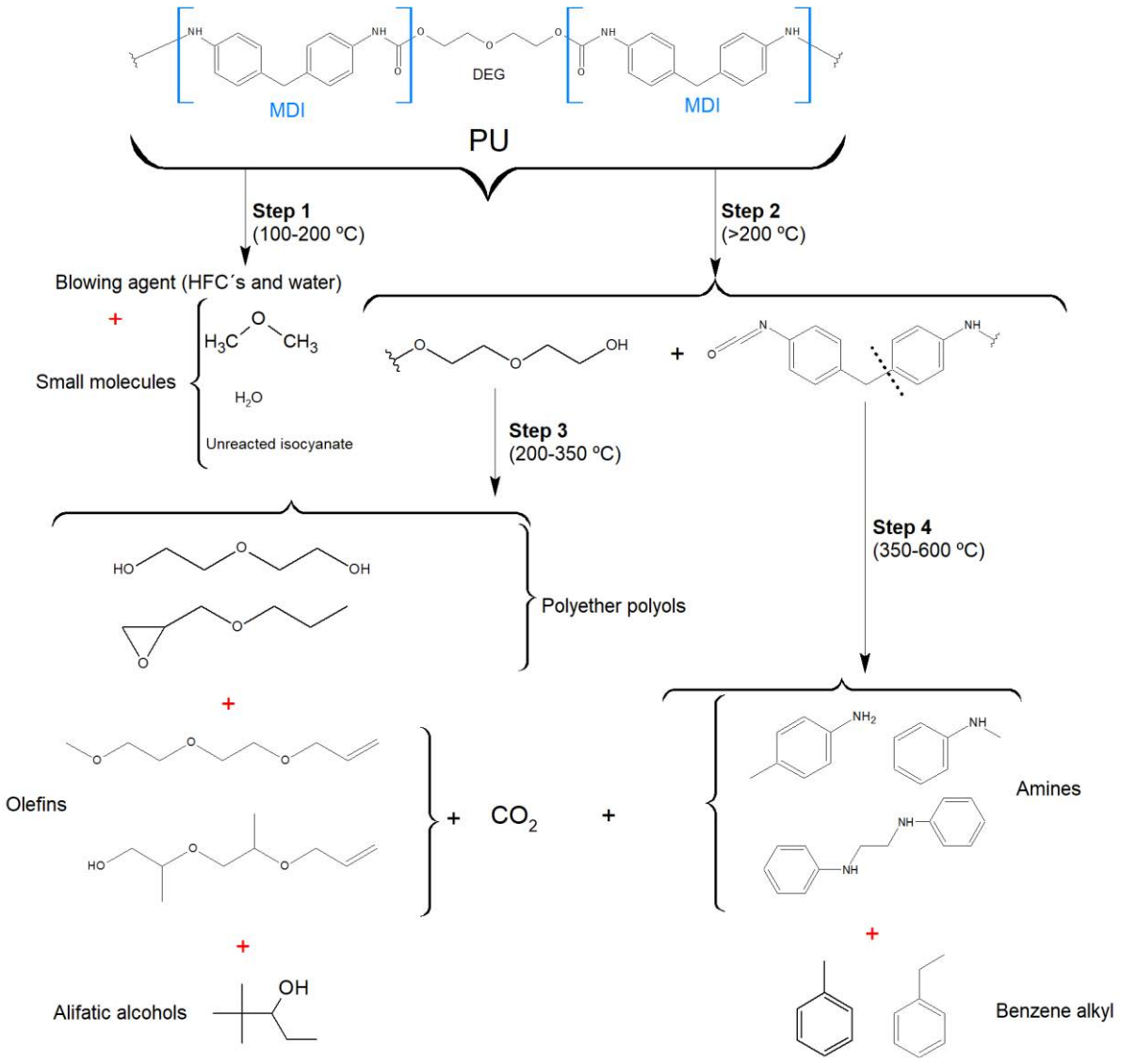

Scheme 2-5. Schematic illustration of the thermal degradation mechanism of PU under N_2 atmosphere [46].

As a resume, the mechanism of PU thermal degradation under non-oxidizing gaseous environment is resumed here: 1) Water as the blowing agent is released, 2) The urethane bond groups of PU break up into -NCO and polyols from about 200 °C, 3) Scission and depolymerization, resulting in weight loss and degradation of mechanical properties [48]; In the meantime, the polyols segments decompose to some kinds of aliphatic ether alcohols and the products become more complex by the interaction of the evolved products with each other, 4) In the range of 350-500 °C, primary and secondary amines, vinyl ethers and CO_2 become the dominant products of PU and 5) At temperature above 500 °C, the aliphatic alcohol with branched chains and benzene alkyls are generated [46].

2.3.2. *FRs for RPUF*

The FRs field could be classified into many different schemes; a) Mechanism by chemical or physical action, b) Interaction with the polymer matrix; additive or reactive and c) Chemical nature, which interfere with the combustion process at different stages inhibiting or even suppressing the combustion process. The amount of FRs suitable to achieve the desired level of fire safety can range from very low loading, in less than 1 wt. % for highly effective FRs (e.g., halogenated); up to more than 50 wt. % (for example in metal hydroxides). However, very big loadings of FRs could also affect the mechanical performance or the internal structure of the polymer, thus declining other typical polymeric properties.

a) *Mechanism classification:*

Flame retardancy in polymers can be firstly classified by its mechanism action; chemical or physical modification of the fire process, which can occur in either the gaseous or the condensed phase. Chemical action is usually more effective than physical action [49].

- **Chemical action:**

  - *Reaction in the gas phase:* The radical gas phase combustion process is interrupted by the FR, resulting in cooling of the system, reducing, and eventually suppressing the supply of flammable gases.

- *Reaction in the solid phase:* The FRs build up a char layer and shields the material against O_2 and the heat source. This char acts as a physical insulating layer between the gas phase and the condensed phase.

➢ **Physical action:**

- *Cooling:* Endothermic processes triggered by the chemical release of water, which colds the substrate to a temperature below that required for sustaining the combustion process. They could act in both gas and condensed phase.
- *Formation of a protective layer (coating):* The material is shielded with a solid or gaseous protective layer which protects him from heat and O_2 in the condensed phase.
- *Dilution:* Inert substances (fillers) and additives evolving non-combustible gases dilute the fuel in the solid and gaseous phases.

Action of the FRs can be summarized in the image below (**Scheme 2-6**) [50]:

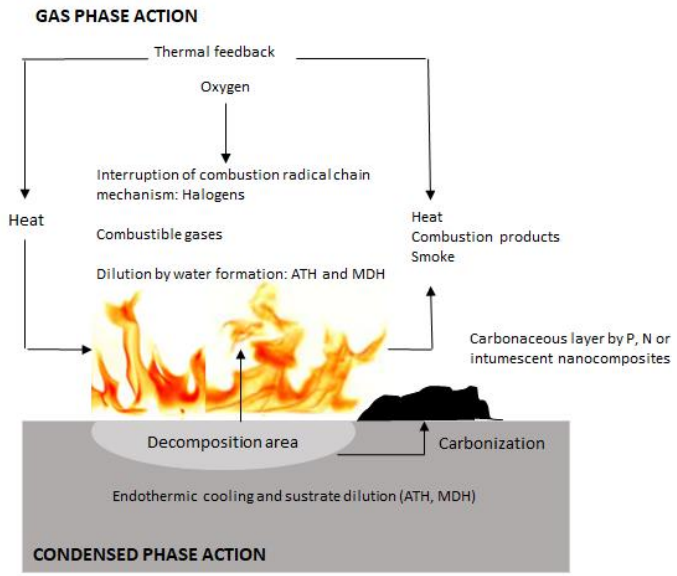

Scheme 2-6. Schematic illustration of the FRs action in gas and condensed phase.

b) *Chemical nature:*

Finally, depending on their chemical nature, they are divided between halogenated and non-halogenated FRs:

- **Halogenated FRs:**

Br, Cl-containing FRs were the most common FRs available in the market. Inside the halogenated FRs, brominated ones were the most popular because of their low amount necessary and good performance. However, some halogenated compounds have serious disadvantages, such as the evolution of harmful gases, corrosive smoke and pollution of environment [51]. For that reason, they are continually phased out because of environmental and health concerns. Currently, the research efforts have been carried out towards research in non-halogenated FR solutions.

Halogenated FRs are famous for their high FR efficiency, due to their action in the gas phase by inhibiting the exothermic oxidation reaction in the flame through radical scavenging, and thus decreasing the energy feedback to the polymer matrix. To slow down or stop the combustion, it is imperative to hinder the chain-branching reactions (1) and (2) from **Scheme 2-3** via radical scavenging. The inhibiting effects of halogen derivatives, usually chlorine and bromine, is considered to operate via the gas-phase mechanism [44] in **Scheme 2-7** . This effect in the first instance occurs either by releasing a halogen atom, if the FR molecule does not contain hydrogen, or by releasing a hydrogen halides (HX) (**Scheme 2-7 a**), being " M· " the residue of the FR molecule. Nonetheless, the halogen atom reacts with the fuel, producing hydrogen halide (**Scheme 2-7 b**). Finally, the hydrogen halide is believed to be the actual flame inhibitor by affecting the chain branching (**Scheme 2-7 c**):

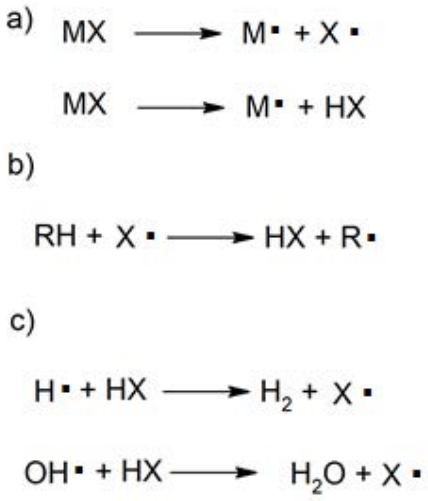

Scheme 2-7. Schematic illustration of the halogen FR mechanism.

However, despite their excellent FR efficiency, HX are considered toxic gases and particularly, corrosive gases (HCl, HBr …etc) which can affect respiratory systems and aquatic environment [52]. Following this idea, some polybrominated FRs were banned in EU to be used into electronic/electrical applications [53], [54]. Also most of the commonly used organophosphorous FRs containing halogens were evaluated by the European Chemicals agency (ECHA) and reported a risk from exposure in PU foams [55], [56] due to their potential toxicity and environmental problems arising from PU foam storage, transportation and also, combustion. However, environmental concerns related to the aforementioned emission of toxic gases from the combustion of halogenated FRs have led to the EU to require the development of new halogen-free FRs [57].

- **Non-halogenated FRs**

Non-halogenated FRs can be classified according to the list below:

- Inorganic FRs, such as metal hydroxides and expandable graphite (EG), etc.
- Phosphorous (P-FR) and Nitrogen-containing (N-FR) compounds (P-N FRs).
- Nanoscale FRs, such as, carbon nanotubes (CNT), graphene, clays, etc.

Both halogenated and non-halogenated FRs can be additive or reactive FRs, depending on their interaction and mixture with the polymer matrix [42]. These two methods have their advantages and drawbacks. Additive-type FRs; incorporated during the transformation process (i.e., By mixing), are simple technology with low cost but they have low compatibility and use to obtain poor mechanical performance. Additives commonly do not interact at this stage with the polymer and they are usually mineral fillers (inorganics), hybrids or organic compounds, which can also include macromolecules. On the other hand, reactive-type FRs, are highly compatible with the polymeric matrix and use to obtain good mechanical properties but unfortunately, they are usually expensive and complex [58]. Commonly, they are introduced into the polymer during synthesis or in a post-reaction process (e.g., via chemical grafting), being integrated in the polymer chains.

For the best of our concern, the most important non-halogenated FRs for RPUF are metal hydroxides, EG, phosphorous and nitrogen-containing compounds and new nano-scale FRS such as graphene derivatives.

- *Metal hydroxides*

Metal hydroxides are one of the most used halogen-free FRs for polymers. They are easy to obtain, very cheap and environmentally friendly. Among them, aluminum tri-hydroxide (ATH) and magnesium hydroxide (MDH) are the most common ones. Indeed, ATH is the most used FR in the world with around a 38 % market share [59]. The decomposition of the metal hydroxides upon a heat source, led to generation of metal oxides and water, following an endothermic reaction which absorbs energy from the ignition source (**Scheme 2-8)**. In detail, ATH starts to decompose at around 220 ºC whereas MDH can last until 330 ºC [60]. Besides the absorption of energy from the reaction, this mechanism also dilutes volatile polymer decomposition products by water vapors released. On top of that, the metal oxide formed, creates a protective insulating metal oxide layer under the polymer surface, protecting it from further decomposition. Their mechanism is a combination of gas phase and condensed phase FR effect and is responsible for reducing the heat release rate of the material and hence, reducing the amount of released toxic gases. However very big loadings of metal hydroxides ae commonly needed to achieve a good FR effect. As an example, the presence of about 40 wt. % of ATH into a RPUF, allowed to reach a 72.5 % in the LOI test [61]. Despite its good FR effect, high loadings of metal hydroxides usually accompany with side-effects, such as processing difficulties or deterioration in other properties, like mechanical properties in the final foam [62].

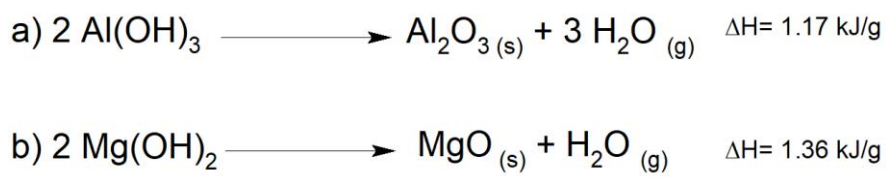

Scheme 2-8. Schematic illustration of the metal hydroxides FR mechanism.

- *Expandable graphite (EG)*

Expandable graphite (EG) is a non-halogenated additive inorganic-type FR, which is manufactured from flake graphite by treatment with strong acids like sulfuric (H_2SO_4) or nitric acid. These acids become crystalized and eventually intercalated into the graphite crystal structure (**Figure 2-9**) so as it expands or exfoliates when heated [63]. Commonly, EG expands

at around 180-200 ºC and these intercalation compounds decompose into gaseous products, what produces a higher inter-graphene layer pressure.

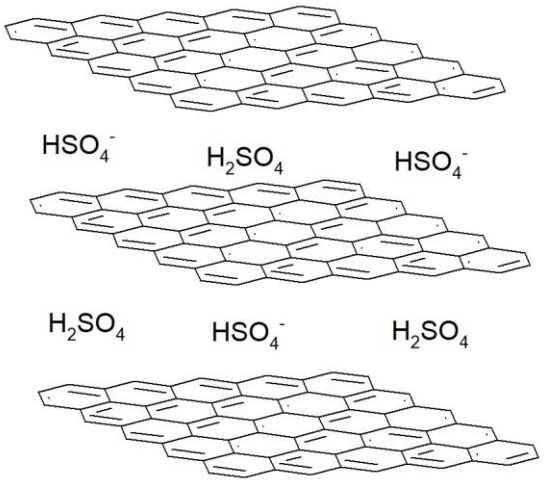

Figure 2-9. Illustration of the crystal structure of EG.

According to several authors [64], [65], the reaction of EG, is due to a redox process between high concentrated acids and the graphite that originates blowing gases and releases water (**Scheme 2-9**). Thus, the volume of the graphite may increase up to 300 times, lowering its density, and increasing the surface area. Once in the polymer during a burning process, EG forms a worm-like insulation carbonaceous protective layer in the condensed phase with the polymer, isolating the material from the heat and precluding mass transfer to the heat source [66]. The release of water and other volatiles also help to suffocate the flames [67].

$$C + 2H_2SO_4 \longrightarrow CO_2 + 2H_2O + 2SO_2$$

$$C + 4HNO_3 \longrightarrow CO_2 + 2H_2O + 4NO_2$$

Scheme 2-9. Schematic illustration of the FR mechanism reaction EG.

- *Phosphorous and Nitrogen-containing compounds*

  - Phosphorous-based FRs (P-FRs)

Phosphorous-containing FRs, particularly organophosphorus compounds, have taken a lot of attention as a good alternative to halogenated FRs, including cost-efficient, non-toxic gases released and lower loading than metal hydroxides are required to achieve good flame retardancy. One of the key points, is the different oxidation state of phosphorous [68], which open-up different organophosphorus compounds (**Figure 2-10**) and different FR efficiency.

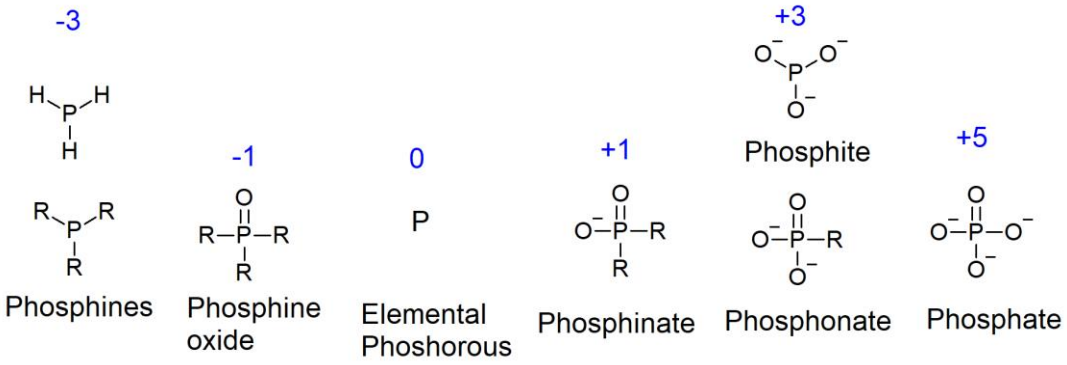

Figure 2-10. Illustration of the organophosphorus compounds depending on Phosphorous oxidation state (R=Alkyl).

P- FRs can act in the condensed phase or gas-phase. Their condensed phase mechanism is focused on the formation of a carbonaceous char layer which protects the polymer trough catalysis of the char formation [69], as well as the incorporation of as phosphorus-containing acids into the char, thus enriching the carbonaceous char by a charring process [70]. The charring effect is the strongest for phosphate, decreases with decreasing oxidation state and becomes of minor importance for phosphine oxide [71]. In their gas-phase action, they release radical fragments ($PO\cdot$ and $HPO_2\cdot$) which interact with the radicals from the combustion process ($H\cdot$ and $OH\cdot$ in **Scheme 2-3**), thus interrupting the normal combustion mechanism, in a similar way as halogenated FRs, and so, they improve the flame retardancy of the material (**Figure 2-11**) [72].

$$PO\bullet + H\bullet \rightarrow HPO$$
$$PO\bullet + OH\bullet \rightarrow HPO_2$$
$$HPO + H\bullet \rightarrow H_2 + PO\bullet$$
$$OH\bullet + H_2 + PO\bullet \rightarrow H_2O + HPO$$
$$HPO_2\bullet + H\bullet \rightarrow H_2O + PO$$
$$HPO_2\bullet + H\bullet \rightarrow H_2 + PO_2$$
$$HPO_2\bullet + OH\bullet \rightarrow H_2O + PO_2$$

Figure 2-11. Interactions between radicals from the flame and from P- FRs.

Many different P-FRs have been used in PU foams such as dimethyl methylphosphonate (DMMP) [73], [74], phosphates [75], phosphoramidates [76], red phosphorous [77], cyclophosphazenes [78], [79], but mostly 9,10-dihydro-9-oxaphosphaphenanthrene-10-oxide (DOPO) (**Figure 2-12**) and derivatives [80]–[82], including polyol modifications with DOPO [83]–[85].

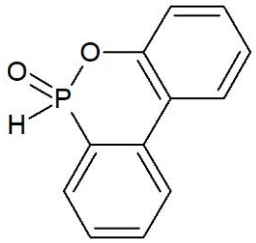

Figure 2-12. Illustration of the chemical structure of DOPO.

The use of P-based FRs has important implications in both flame retardancy and compressive performance of RPUF. Besides the reported increase in the flame retardancy, high loadings of P- FRs could lead to a cell collapse and so, decrease the compressive strength of the foam [86], [87]. On the other side, the compressive performance of PU with P- FRs had been also reported to increase [81], mostly when using specific conditions, such as low loadings of P-FRs [88], with presence of -OH groups to improve compatibility with PU matrix [89] and stiff phenyl groups on its chemical structure to impart rigidity to the structure [80], all of them had been reported as beneficial for the compression resistance of RPUF.

- Nitrogen-based FRs (N-FRs)

N-FRs have been also used to impart FR properties to RPUF. Commonly, the most important Nitrogen-based FR was Melamine (**Figure 2-13**). Melamine can generate melem and melam trough a de-ammoniation mechanism [90]. On one hand the ammonia gas released can dilute the fuel gases from the combustion process and so, inhibiting the flame. In the other hand, Nitrogen-rich compounds can play a similar role as phosphorous-based compounds by a charring effect. Several Nitrogen-rich compounds; such as melamine-derived compounds, have been studied on the literature like Urea formaldehyde and melam [91], melamine formaldehyde [92] melamine cyanurate and melamine polyphosphate [87], [93], [94], melamine-phosphinic salts [95], [96], melamine and cardanol polyol [97]. Furthermore, it is notable the synergistic effect between nitrogen-based compounds and phosphorous-based compounds [78], [79], [83], [98], [99], such as triazine and phosphates [100], melamine-DOPO polyol modifications (MADP/DOPO) [80] but mostly, ammonium polyphosphate (APP) [101]–[103].

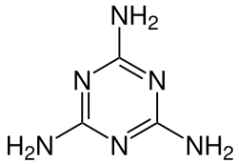

Figure 2-13. Illustration of the chemical structure of melamine.

P-FRs and N-FRs are a very good example of "intumescent" FRs (IFRs). A typical IFRs system is composed of three major components: an acid source, a carbon source and a blowing agent [104]. **Table 2-2** summarizes IFRs components. It can be observed that melamine compounds, PU and phosphate-amine compounds, are very common components of an IFR. APP is considered an excellent example. A proposed general mechanism to describe the development of the intumescent phenomenon is consisted on different steps (**Scheme 2-10**) [105]. The polymer softens, leading the FR exposed to the heat. Later, 1) the acid source decomposes and releases the inorganic acid; 2) the inorganic acid reacts with the carbon source via dehydration and carbonization starts; and finally, 3) released gases from the blowing agent and degradation products cause the carbonizing material to swell up; as the reaction nears completion, gelation and finally solidification occurs, the resulting solid is a multi-cellular foam. As the main mechanisms for IFRs are based on the formation of an intumescent char

barrier insulating the flammable volatiles, O_2 and heat, the difference in flame retardance of the above systems is greatly related to the char construction in the condensed phase [106].

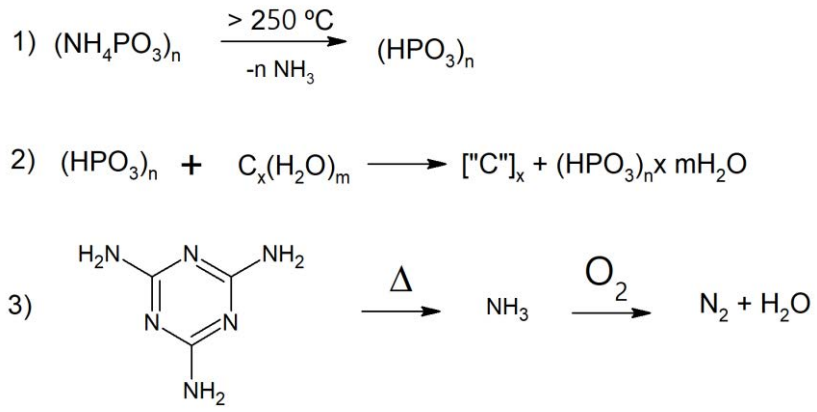

Scheme 2-10. Schematic illustration of the main steps of the IFRs mechanism.

Table 2-2. Summary of some typical components used in IFRs.

Acid source	Carbon source	Blowing agent
Phosphoric acid, phosphates and polyphosphates, H_2SO_4, sulfates, boric acid, borates and polyborates, ammonium salts, phosphates of amine or amide, melamine phosphate, alkyl phosphate, haloalhylphosphate	Starch, dextrin, sorbitol, mannitol, pentaerythritol, phenol-formaldehyde resin, char former polymers like PU or polycarbonate	Urea, Urea-formaldehyde resin, Melamine, Dicyandiamine

- *Nanoscale FRs:*

Nanoscale FRs are also a good solution that can improve the properties of a RPUF, mostly the thermal stability and compressive strength. The most important factor to take into account is the dispersion and compatibility of the nanomaterial into the polymer matrix [107]–[109] For instance, Hao-Kai Peng et al. [110] used 5 wt. % of Hydrotalcite to increase the compressive strength and the LOI up to 29 % in a RPUF. Moreover, Layered-double-hydroxides (LDH) were studied as excellent synergistic agents with other FRs, such as P-FRs [111], N-FRs [51] or EG [112]. Among others, mineral clays such as Montmorillonite, has been mostly used in RPUF as reinforcement to improve mechanical and thermal stability properties [113]–[116]. In

a similar way, sepiolite clay [117], [118] or metallic materials such as zirconium [119], could be used to impart functionality towards mechanical resistance to the PU foam. Indeed, nanomaterials from nature such as Cellulose, principally effects as synergistic agent regarding thermal stability, flame retardancy and compressive strength [120]–[123]. However, the most interesting nanomaterials come from the carbon family of materials [124], such as Fullerenes, Multi-walled CNTs (MWNT) and graphene derivatives [125], [126].

- Graphene derivatives

Graphene is a 2-dimensional (2D) sheet of sp^2 carbon atoms in a honeycomb structure [127]. Graphene and graphene-based materials such as graphene oxide (GO) [128] and reduced graphene oxide (rGO) [129]–[131] have drawn significant attention to the researchers all around the world in the past years, mostly due to their unique combination of properties, such as tensile strength [132], thermal conductivity [126] or electrical conductive properties [133]. To use it in RPUF, GO is preferred against rGO due its large number of oxygen-containing functional groups like -OH, alkoxy (C-O-C), carbonyl (-C=O), epoxy and others within the structure [134], which disrupt the conjugation of aromatic rings making it non-electrical conductive [135], hydrophilic [136], [137] and improving the thermal insulation capacity of the RPUFs [138], [139], due to GO contains more sp^3 but less sp^2 carbon atoms, with a low thermal conductivity (0.5-1 $Wm^{-1}k^{-1}$) [140]. On the other hand, rGO, which few less numbers of oxygen-containing groups from the elimination of these functionalities, is electrical conductive [137] and so, is more suitable for electrical applications [141]–[144]. It was reported that rGO can be used as FR at 2 wt. % along with IFRs (18 wt. %) to increase the LOI value up to 34 % with improved electrical properties [145].

GO has been mainly used to improve the tensile strength of PU, commonly, elastomers [146], [147]. Fortunately, many different research have recently been published using GO to impart flame retardancy into RPUF [148]. For example, Kim et al. [149] studied small amounts of GO and graphite (lower than 1 wt. % graphite and 0.1 wt. % GO, enhanced the microstructure, insulation capacity and mechanical strength compared with neat PUFs. Shi et al. used a GO-based coating to impart remarkable fire-resistance and smoke suppression to PU foams [150].. Also, in combination with cellulose [151], the thermal stability of the foam was improved. P-FRs have excellent synergistic FR effect with graphene, such as DOPO [99], [152]; melanin [150], with excellent gas-phase effect, phosphoramides [153] or IFRs [154]. Among them, the

work done by Cao et al. [155], used functionalized phosphorous-graphene as a filler to make a PU foam with high performances of good mechanical strength, low thermal conductivity (0.02975 W/(m·K)), fire resistance and low smoke release. These are just some examples about the future possibilities regarding graphene nanocomposites as FRs.

- *FR polyols:*

The raw materials of RPUF (polyols and -NCOs) are obtained from petroleum as feedstock. This dependency on petrochemical products is a challenge for the industry, as over the last years, depleting fossil reserves, fluctuation of petroleum prices, environmental concerns and the flammability of petroleum, have triggered growing interest in the development of bio-renewable feedstocks to substitute petrochemically derived counterparts in the production of many polymeric materials [156]. From many published literature, renewable sources can often substitute their petrochemical analogues.

In order to overcome this major drawbacks and the use of petroleum, one option is to replace the petroleum-based polyol by green sources, such us a modified natural-based polyols [157]. Several vegetable plants have seen used for this purpose, including rosin [82], [112], [114], rapeseed [158], [159], palm [116], [160]–[162], soybean [163]–[165] and mostly, Castor oil [111], [166]. However, these natural-based polyols suffer from the same problem as petroleum-based polyols, this is, lack of fire protection and the replacement of a petroleum-based polyol by a natural-based polyol, does not provide instantly high-flame retardancy efficiency. In addition, most of the natural-based oils does not contain any -OH groups; or non-primary OH-groups inside its structure, thus giving a RPUF with lower mechanical performance than its contra part from petroleum [167]–[169].

However, Castor oil is a natural-based oil which has secondary -OH groups along with double bonds inside its chemical structure [170], which can be easily modified by a chemical functionalization (**Figure 2-14**). Castor oil is highlighted because obtains the highest compressive strength and modulus due to a lower closed-cell content and thicker cell walls compared with other biobased polyols [171]. Nonetheless, primary -OH groups are preferred to obtain a RPUF with good structure stability, as they are more reactive than secondary ones, thus giving stability to the RPUF [172], [173]. Furthermore, the modification of the double bonds of castor oil can increase the reactivity of the polyol with -NCO, thus obtaining a RPUF with a good structure, high thermal stability, flame retardancy or better compressive strength. To increase the primary -OH groups content of castor oil, amidation with diethanolamine

(DEOA) is a common procedure [161], [174], [175] but also, transesterification with glycerol [166], [176], [177] or pentaerythritol [178], [179] are recommendable options. A combination of epoxy ring opening and transesterification of fatty acid triglycerides could lead to higher functionality, which would ensure high cross-link density of PU matrix that would convert to rigid PU foam with increased mechanical properties, good dimensional stability and high aging stability [180].

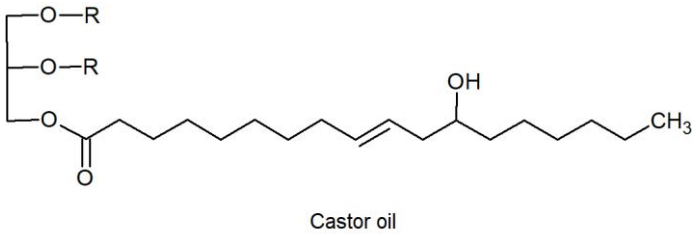

Castor oil

Figure 2-14. Illustration of the chemical structure of castor oil.

A well-known solution to overcome the flammability and structural problem of natural-based RPUF, is to introduce a reactive-FR-based polyol into the PU formula. Commonly, most of the reactive-FR polyols are phosphorus containing compounds [84], [111], [166], [181], as it is known to be a relationship between their efficiency and the phosphorus content [72]. Reactive polyols have indeed the advantage of having strong connections with the -NCO and avoid most of the incompatibility problems from additive FRs. In detail, organophosphorus compounds affects positively the char formation by the production of poly-(meta-phosphoric acid) [182]. Besides, this good compatibility influences positively on the mechanical properties; as bonds on the internal structure are stablished and insulation capacity of the foam can be increased [183], [184].

CHAPTER 3

3. Materials and experimental techniques

"Science knows no country, because knowledge belongs to humanity, and is the torch which illuminates the world"

-Louis Pasteur

3.1. Materials

RPUF with commercial formulation provided by Smooth-On (FormX Spain, Barcelona, Spain) was used in this study: FOAM-iT! ™ 5. The commercial PU raw materials were divided into two sides: A-side (referred to -NCO; NCO % = 30 %) and B-side (referred to polyol, also containing catalysts, surfactants and water as blowing agent). For the PU, the manufacturer provided the following data: Density: 80 Kg/m^3, viscosity: 300 cps, and mixing ratio: 100/87 (A:B) (1.15:1 weight ratio).

Three different types of EG: GHL PX 95 N, (Ash max. 5 %, moisture 1 %, volume expansion of 250 cm^3/g, starting temperature 180-220 ºC and 300 µm particle size, EG1), GHL PX 98 HE, (Ash max. 2 %, moisture 1 %, expansion volume of 350 cm^3/g, starting temperature 180-220 ºC and 300 µm particle size, EG2) and GHL PX 99 32 350, (Ash max. 1 %, moisture 1 %, expansion volume of 350 cm^3/g, starting temperature 150 ºC and 500 µm particle size, EG3), were kindly provided by Georg H. Luh, GmbH (Walluf, Germany).

For the FR1 synthesis in **Chapter 5***, P*-phenylenediamine (PPD, 98 %, Sigma-Aldrich), phenylphosphonic acid (PPA, >98 %, TCI Europe), MeOH (99.8 %, Merck) as a solvent. The products were used without any additional purification.

For the synthesis of CPPA in **Chapter 6**, castor oil, diethanolamine (DEOA, 98 %), sodium methoxide (NaOMe, 95 %), ethylacetate (99.5 %), Amberlite IR120 hydrogen form catalyst,

acetic acid (HAc, 99.8 %), hydrogen peroxide solution (H_2O_2, 30 % solution), toluene (99.8 %) and triphenylphosphine (TPhP, 99 %) were all purchased Sigma-Aldrich and used without further purification. Polycat 34, DABCO K-15 as catalyzer 1 and 2 respectively and DABCO DC193 as surfactant were kindly provided by Airproducts iberica (Bellaterra, Spain).

For GO synthesis in **Chapter 6**, potassium permanganate ($KMnO_4$, 98 %) was purchased from Alfa-Aesar whereas H_2SO_4 (95-97 %), phosphoric acid solution (H_3PO_4, 85 wt. %), hydrochloric acid (HCl, 37-38 %) and sodium chloride (NaCl) were purchased from Sigma-Aldrich and used as received.

For PGO synthesis in **Chapter 7**, phenylphosphonic dichloride (PPDCl, 90 %), allylamine (AA, 98 %), triethylamine (TEA, 99 %) and diethylether (DEE, 99.7 %) were purchased from Sigma-Aldrich and used as received.

3.2. Experimental techniques

3.2.1. *Characterization*

a) *Nuclear magnetic resonance (NMR)*

The chemical shifts of elements in the chemical structures of FR1, FP1, castor oil and its derivatives were studied via NMR spectroscopy. ^{1}H, ^{13}C and ^{31}P-NMR spectra were recorded on an NMR spectroscopy (Oxford AS400, UK) at room temperature using DMSO-d6 as a solvent. The chemical shifts are reported in parts per million (δ, ppm) relative to tetramethyl silane (TMS) as a reference for ^{1}H (400 Hz) and ^{13}C NMR (100 MHz). The ^{31}P NMR (162 MHz) spectra was referenced to 85 % H_3PO_4.

b) *Fourier transform infrared spectroscopy (FTIR)*

FTIR spectra for FR1, FP1, castor oil and its derivatives, GO, PGO and the foam samples were recorded on an FTIR Spectrometer (iS50, USA). The scanning range was from 4000 cm^{-1} to 500 cm^{-1} and the resolution was set as 4 cm^{-1}. Sample preparation was using the KBr pellets method.

c) *X-ray photoelectron spectroscopy (XPS)*

The XPS analysis for GO and PGO were carried out in a Thermo Scientific Multilab 2000 spectrometer (Thermo Scientific, Waltham, Massachusetts, USA) fitted dual-anode X-ray

source (Mg K alpha and Al K alpha with photon energies 1253.6 and 1486.7 eV respectively), and a 110 nm hemispherical sector analyzer. The core level spectra were fitted using Origin software package.

d) *Thermal gravimetric analysis (TGA)*

The thermal decomposition of the RPUFs was studied via TGA. The testing was performed on a thermogravimetric analyzer (Q50, USA) under N_2 gas. The sample gas purge flow rate was set as 90 mL/min. Samples weighing 7 ± 0.5 mg were tested over a temperature range from room temperature to 700 ºC with a heating rate of 10 ºC/ min.

e) *Scanning electron microscopy (SEM)*

The morphology of char residues after the cone calorimeter test was studied by SEM-EDS (EVO MA15, Germany). The samples were coated with a fine gold layer under 20 kV condition. In **Chapters 6** and **7**, The average cell size diameter (d) is measured from the total area of the SEM image and by counting the total number of cells including the half cells at the edges. Now dividing the total area by the number of cells gives the area of each cell as square with side, d. Then, the square root is taken to determine the average diameter of a cell in an image [185]. At least two images per sample were used to obtain the average cell size diameter and the standard deviation.

f) *Microstructure analysis*

For the microstructure analysis, several techniques were performed, and the main data obtained was divided into Open cell content % (OC %), and mean cell size (Φ_{3D}). The OC % was measured by using a gas pycnometer Accupyc II 1340 from Micromeritics, according to ASTM D6226-10. OC % was measured for three cylindrical samples of each material, after measuring their densities. Mean cell size (Φ_{3D}) was measured by SEM as showed earlier.

g) *Density*

Foam densities were measured as described by ASTM D1622/D1622M-14. Density was determined by dividing the weight of each sample by its corresponding volume in three different samples for each material.

h) *Viscosity*

Viscosity of the bio-polyols in **Chapter 6** was measured at 25 ºC with a Brookfield DV-E viscosimeter (Brookfield engineering, Massachusetts, US).

i) *Hydroxyl number (OH number)*

The OH number of the polyols in **Chapter 6** was measured according to ASTM E1899 [186]. Briefly, an appropriate amount of sample is weighted and dissolved in 10 g of a mixture of acetonitrile/toluene (70:30). Then, the same mass of p-Toluenesulfonyl Isocyanate (TSI) is added and reacted for a determined time. Then, 0.5-1 mL of distilled water was added to finish the reaction. Samples were then titrated with Tetrabutylammonium Hydroxide. The OH number of the bio-polyols were measured with a Titrando 904 automatic titrator (Metrohm AG, Herisau, Switzerland). All measures were run in duplicate.

j) *Acid value (AV)*

AV of the polyols in **Chapter 6** was measured by weighting the appropriate mass and dissolving it in Xylene/ethanol (75/25). The sample was titrated with a solution of KOH 0.1 N in MeOH. The AV of the bio-polyols were measured with a Titrando 904 automatic titrator (Metrohm AG, Herisau, Switzerland). All measures were run in duplicate.

k) *Isocyanate content (NCO %)*

NCO % of the part A of the commercial foam used on this thesis was measured with a Titrando 888 automatic titrator (Metrohm AG, Herisau, Switzerland) with HCl as titrant, Dibutylamine as reagent and methyl ethyl ketone as a solvent for the sample. All measures were run in duplicate.

l) *Thermal conductivity*

The thermal conductivity was determined at 20 ºC using a hot-disk transient plane source (TPS) thermal constant analyzer, according to ISO 22007-2:2008 method [187]. The measurements were performed using two cylindrical samples with a diameter of 30 mm and a height of 30 mm obtained from the same materials. A disk shaped TPS sensor with a diameter of 3.189 mm was used, after being located in contact with the xy plane (perpendicular to growth plane) of

the two samples for **Chapters 4** and **5**. In **Chapters 6** and **7**, the measurements were taken using two square samples cut from the same materials of 50 mm x 50 mm x 30 mm (length × width × thickness) with a sensor of diameter 9.9 mm.

3.2.2. *Fire behavior*

a) *Limited oxygen index (LOI)*

The LOI test was used to evaluate the minimum concentration of O_2 that supports the flaming combustion of a specimen in a flow-controlled mixture of O_2 and N_2. It is a technique for measuring the minimum oxygen concentration to support candle-like combustion of plastics over 3 min or until the testing sample is consumed for more than 5 cm from the top. Summarizing, the LOI test determines the amount of O_2 in the atmosphere necessary to start combustion and it reflects the flammability of the RPUFs. A higher LOI value indicates a greater efficiency for the FR. The oxygen index was described as follows. LOI values for flame-retarded RPUF samples were measured on an Oxygen Index Meter (Fire Testing Technology (FTT), UK) with a precision of ± 0.2 %, in accordance with ASTM D2863-97 [188]. The sheet dimensions of the samples were 130 mm × 10 mm × 10 mm (length × width × thickness). The typical LOI test equipment is illustrated in **Scheme 3-1** [189], which is taken from the standard mentioned above. Neat RPUF uses to show an LOI value of around 19.0 % [190].

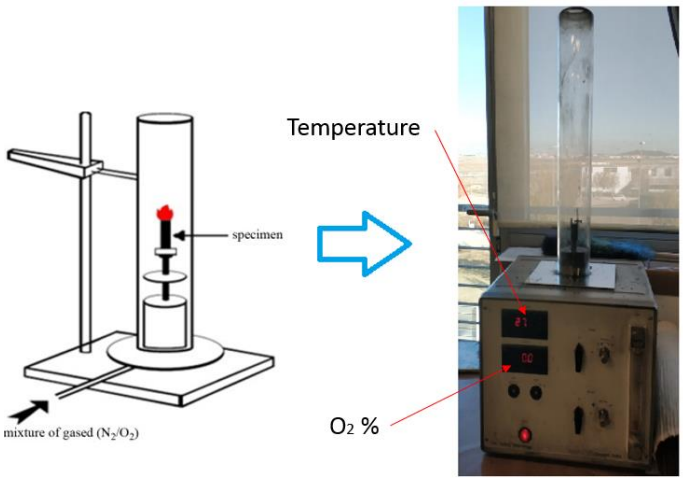

Scheme 3-1. Schematic illustration of the LOI test and tester.

b) *Vertical burning test (UL94)*

The vertical burning test (UL94) were developed by Underwriters Laboratories as combustion tests of polymeric materials for parts in devices and appliances. In terms of all the UL94 tests, vertical burning test is the most widely used measurement for examining the ignitability and flame spread of polymeric materials [124]. The UL94 test measures the ability of a sample to self-sustain ignition and propagation in an upward flame spread configuration. The UL94 test, is a measurement of the self-extinguish capacity of the sample sheet, based on the burning time after two continuous 10s ignitions. A piece of cotton (approximately 50 mm × 50 mm × 6 mm) was positioned 300 ± 10 mm below the end of the specimen in order to record whether any dripping induced ignition of the cotton. The Bunsen burner generates blue flame by consuming methane with a length of 20 mm and a power of 50 W. The vertical burning tests were carried in a UL94 Horizontal/Vertical Flame Chamber (FTT, UK) (**Figure 3-1**) in accordance with ASTM D3801 [191]. Five samples with sheet dimensions of 130 mm × 13 mm × 10 mm (length × width × thickness) were tested. **Scheme 3-2** illustrates a) the standard sample disposal and b) the criteria conditions of the UL94 test. The untreated neat RPUF cannot pass the UL94 rating because of its inherent flammability [190]. For a better understanding of the burning behavior, the average individual after-flame time for each sample studies were reported.

Figure 3-1. Picture of the vertical burning test (UL94) chamber.

a)

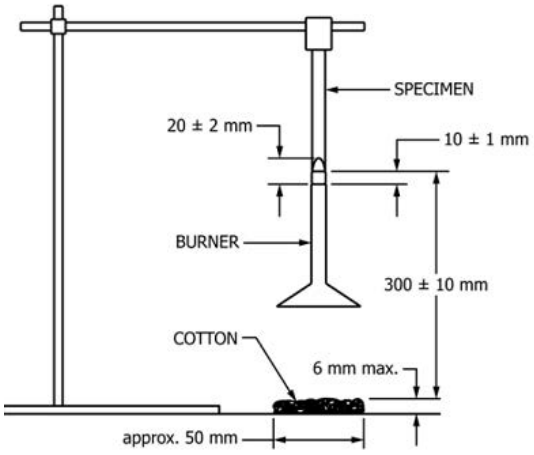

b)

Criteria Conditions	V-0	V-1	V-2
Afterflame time for each individual specimen, t_1 or t_2	≤10 s	≤30 s	≤30 s
Total afterflame time for any condition set (t_1 plus t_2 for the five specimens)	≤50 s	≤250 s	≤250 s
Afterflame plus afterglow time for each individual specimen after the second flame application (t_2 + t_3)	≤30 s	≤60 s	≤60 s
Afterflame or afterglow of any specimen up to the holding clamp	No	No	No
Cotton indicator ignited by flaming particles or drops	No	No	Yes

[A] If only one specimen from a set of five specimens does not comply with the requirements, another set of five specimens shall be tested. In the case of the total number of seconds of flaming, an additional set of five specimens shall be tested if the totals are in the range from 51 to 55 s for V-0 and from 251 to 255 s for V-1 and V-2. All specimens from this second set shall comply with the appropriate requirements in order for the material in that thickness to be classified V-0, V-1, or V-2.

Scheme 3-2. Schematic illustration of a) Vertical burning test (UL94) sample position and specimen size and b) UL94/vertical burning test classification criteria, in accordance with ASTM D3801.

c) *Cone calorimeter test (CCT)*

The Cone Calorimeter is a bench scale fire testing instrument and it provides a wealth of information on the combustion behavior of polymeric materials subjected to a heat flow and simulate a real fire scenario [192], [193]. The measuring principle of this test is that of O_2 consumption in the combustion gases of a specimen subjected to a defined heat flux [194]. It provides comprehensive insight into fire risk via parameters such as time to ignition (TTI), peak of heat release rate (PHRR), total heat released (THR), total smoke produced (TSP) and CO/CO_2 released into the smoke production and mass loss. The main parameter that determined during combustion in the cone calorimeter test is the PHRR, which is the basic parameter for fire modeling and evaluating fire behavior of materials. PHRR denotes the rate at which heat energy is released per unit area of the sample. It is recognized to be the most important parameter to quantify the size of fire and an effective FR system generally shows a lower PHRR value. A schematic view of the cone calorimeter is shown in **Scheme 3-3** [195]. CCTs were carried out using a cone calorimeter (FTT, UK) (**Scheme 3-3 b)**) and following the ISO 5660-1 standard [196]. Specimens with sheet dimensions of 100 mm × 100 mm × 30 mm (length × width × thickness) were irradiated at a heat flux of 50 kW/m^2. A specimen was placed under a cone shaped radiant heater under a metallic support enough to achieve 25 cm distance to the cone shuttles. The specimen was ignited once the pyrolysis products were ignited in the

atmosphere. The combustion products go through an instrument exhausted pipe and were filtered prior to detection by a gas analyzer.

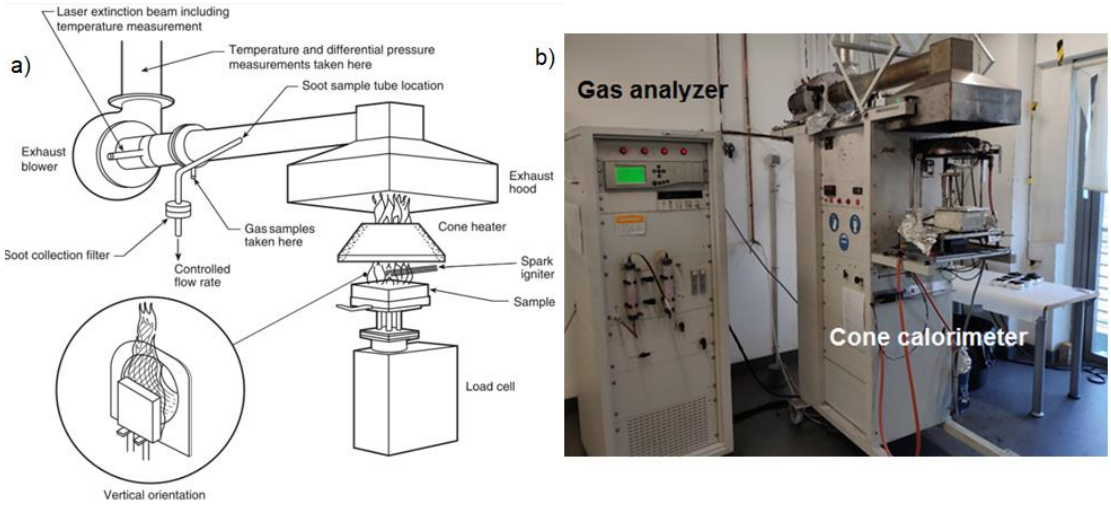

Scheme 3-3. Schematic illustration of a) View of the cone calorimeter and b) Dual cone calorimeter (FTT) equipment used for the CCT.

3.2.3. *Compression strength*

Compressive properties were tested with an INSTRON 5966 instrument (**Figure 3-2**) following ASTM D1621-00 standard [197]. Maximum of six specimens for each sample with size 50 mm × 50 mm × 30 mm (length × width × thickness) were tested. The compressive constant rate was 3 mm/min. The properties were measured in the direction of foam growth. The average compressive strength and average standard deviation are reported.

Figure 3-2. Picture of the dual column tabletop universal testing system (INSTRON 5966).

CHAPTER 4

4. Expandable graphite (EG): An efficient FR for RPUFs

"If I have a thousand ideas and only one turns out to be good, I am satisfied"

-Alfred Nobel

4.1. Introduction

RPUFs are widely used in some industries where the insulation and mechanical strength are highly necessary. In addition, they have an important use in the molding industry, being often present in costumes, due to his ability to be adapted to the mold before curing. However, polyol and -NCOs used to create RPUFs, come from petroleum, making the PU foam an easy flammable material. This of course, is an important drawback for some of their final applications. Therefore, FR additives are highly recommended to fulfil its practical demands [198]. Traditionally, halogenated FRs such as tris(2-chloro-1-methylethyl) phosphate (TCPP) [199], were widely use to achieve the FR requirements. However, the mentioned potential drawbacks of halogenated FRs [55] in **Chapter 2**, have increased the attention to discover new non-halogenated FRs. Considerable efforts have been made to improve the flame retardancy of RPUFs trough non-halogenated FRs. Thus, diverse inorganic fire-retardants have been already described, e.g., ATH [101], [102], achieving flame retardancy effect but with an extremely high loading that weakens the mechanical performance of the RPUF. In addition synergistic activity with other FRs such as EG, was reported to achieve an acceptable flame retardancy

effect [200]. EG is widely used as FR in RPUFs as well as in other polymers due to its low cost and effective condensed-phase FR mechanism [69], [201]. The behavior of RPUFs filled with EG as FR is known to be dependent on key parameters like density of the foam [202], [203], rate of expansion [204], [205] particle size [47], [206], [207], and distribution [1], [208]–[210] of EG. Unfortunately, the current literature did not study all the relevant properties together, thus leading to some contradictions and isolated conclusions.

In detail, the study of the different densities and compressive strength of the foams have importance influence in the FR performance, showing mainly that a higher density foam will have better FR properties [209] and compressive strength [203]. However, in order to achieve an acceptable FR performance, big loadings of EG (>15 wt. %) were commonly used, thus being one of the reasons for the dramatic decreasing on the mechanical properties, which is caused by affecting negatively the cellular structure and making the foaming process harder [73], [210]. Indeed, it has not been found a deep study regarding the effect of EG on the cellular structure and the reasons behind its mechanical performance results.

On the other hand, the effect of the particle size and the rate of expansion of the EG is maybe the critical point of this FR. Unfortunately, these parameters were only reported separately in the literature, with no clear conclusions about how these parameters affects in reality, the EG performance. The effect of particle size of EG on semi-rigid PU foams indicated that bigger particle sizes of EG gave better LOI, horizontal burning test and mechanical performance [210] and therefore, a significant improvement of the thermal stability [207]. The rate of expansion was studied by Lorenzetti [204], who concluded that the rate of expansion had no significant influence on the flame retardancy performance. On the contrary, Xiao-Liang Zhang et al. [205] indicated that the high efficiency of EG depends mainly on its expandability. Thus, based on the current literature, no conclusion may be drawn about which parameter is dominating the FR mechanism of EG to achieve a precise FR performance and to obtain acceptable mechanical properties. From our concern, the use of EG as an efficient non-halogenated FR needs a clear and deeper study and an optimization about its practical use. This information is a key point to investigate in detail the EG effectivity as FR.

The following chapter uses three different EGs (EG1; with 300 µm, and with 250 cm^3/g expansion rate, EG2; with 300 µm, and EG3; 500 µm, both with 350 cm^3/g expansion rate). The comparison between the three different EGs (EG1, EG2 and EG3) aims to stablish a quorum about the characteristics of the additive which are important to achieve good flame retardancy, good compressive strength and to give a clear conclusion which has not been

revealed in the current literature. The current chapter was based in two reported publication by our research group [211], [212].

4.2. Materials

4.2.1. *Materials*

RPUF commercial formulation provided by Smooth-On (FormX Spain, Barcelona, Spain) FOAM-iT! ™ 5 (PU). PU raw materials were divided into two sides: A-side (referred to -NCO) and B-side (referred to polyol, catalysts, surfactants and water as blowing agent). The weight mixing ratio between A and B was 100/87 (1.15). Three different types of EG were used: GHL PX 95 N, (Ash max. 5 %, moisture 1 %, volume expansion of 250 cm^3/g, starting temperature 180-220 ºC and 300 µm particle size, EG1), GHL PX 98 HE, (Ash max. 2 %, moisture 1%, expansion volume of 350 cm^3/g, starting temperature 180-220 ºC and 300 µm particle size, EG2) and GHL PX 99 32 350, (Ash max. 1 %, moisture 1%, expansion volume of 350 cm^3/g, starting temperature 150 ºC and 500 µm particle size, EG3), kindly provided by Georg H. Luh, GmbH (Germany).

4.2.2. *Foam preparation*

RPUFs with 0, 6, 8, and 10 wt. % EG were prepared using the one-shot and free-rising methods. The B-side parts of the RPUFs and EG were firstly mixed in a plastic beaker for 2 minutes with a mechanical stirrer at 1000 rpm until uniform dispersions were obtained. Then, the correct amount of -NCO (A-side) was added, and the mixture was stirred rapidly at 1200 rpm (for 30 s until the system became homogeneous) with a heidolph RZR-1 mechanical stirrer. The mixture was finally poured into a 250 mm × 250 mm × 60 mm open aluminum mold, where the RPUFs were raised in vertical direction at room temperature. After curing at room temperature for a minimum of 3 h, samples were cut according to the standards of the different test performed. RPUFs formulations are shown in **Table 4-1** below.

Table 4-1. The formulae of RPUF samples.

Sample	EG content (wt. %)
PU	0

EG1-6	6
EG2-6	6
EG3-6	6
EG1-8	8
EG2-8	8
EG3-8	8
EG1-10	10
EG2-10	10
EG3-10	10

4.3. Results and discussion

4.3.1. *Microstructure analysis and thermal conductivity*

a) *Cellular structure:*

The parameters studied were Open cell content % (OC %), mean cell size (Φ3D), density, and thermal conductivity. All these parameters are collected in **Table 4-2**.

Density is one of the most critical parameters of a RPUF, because it affects the distribution of the filler (EG) in the polymeric matrix, and so its impact on density determines its performance for many applications [112], [210] such as the strength, modulus, and energy absorption ability of the foam [48]. EG-filled RPUFs showed higher density than those of neat foam. This may be related to the increase of the polyol viscosity when EG was incorporated into the RPUF matrix, along with the very high density of EG particles cooperated to the RPUF matrix (for example, 2.2 g/cm^3 for EG1 versus *ac.* 0.1 g/cm^3 for neat PU foam). However, the three different particle sizes of EG impacted the RPUF´s density differently. As an example, an increase on average of 8.0 % was observed with the addition of EG1, of 4.8 % with EG2, and of 4.9 % with EG3. Considering the foams containing 10 wt. % EG, the density grew by 9.4 % for EG1 samples with respect to that of neat foam, by 6.9 % for EG2, and by 5.9 % for EG3. As a matter of fact, this phenomena was related to the impact of smaller EG particle size (EG1 and EG2 with 300 μm) on the neat foam, by decreasing the average cell size due to a nucleating effect during the foam formation, as reported by Luo et al. [207].

One decisive parameter in RPUFs is OC %, since closed cell structures are required for structural and thermal insulating applications. A slight increase in OC % compared to that of reference foam (6.9 %) was observed with the addition of EG particles. However, OC % was

similar for all different EG particles (between 9.1 % and 9.9 %), except for the foam containing EG3 at 6 wt. %, which was the highest (10.8 %), and for the foam containing EG1 at 8 wt. % (7.8 %), which had the lowest value for the EG-filled materials. This indicated that mostly, the greater the particle size of EG particles, the grater the OC % increases.

Cell size is a crucial factor influencing the properties of foams. The analysis of RPUF samples for SEM micrographs was shown in **Figure 4-1**. As previously described in other studies, EG particles have a nucleating effect during foam formation, decreasing the average cell size [47], [198]. In particular, the addition of EG1 promoted the highest cell size reduction (34 % for the sample with 6 wt. % content), whereas the average cell size reduction reached 30 % for EG1, 27 % for EG2, and 13 % for EG3. Therefore, the highest cell size reduction was obtained for EG particles with the lowest size (300 µm), due to the aggregation between particles [207]. Larger particle size of EG (EG3, 500 µm) enlarged the cell sizes, which was probably located mainly in the struts, that is, the intersection of several cells. On the other hand, the lower particle size EG (EG1 and EG2; 300 µm) were not located there due to the lower size compared with the neat foam (467 µm) [203]. The size of the EG particles used (300 or 500 µm) was in the same order as the mean cell size of foam, which might be the main reason behind EG particles being located between cell walls and struts [47] (**Figure 4-2**), thus modifying cellular structure.

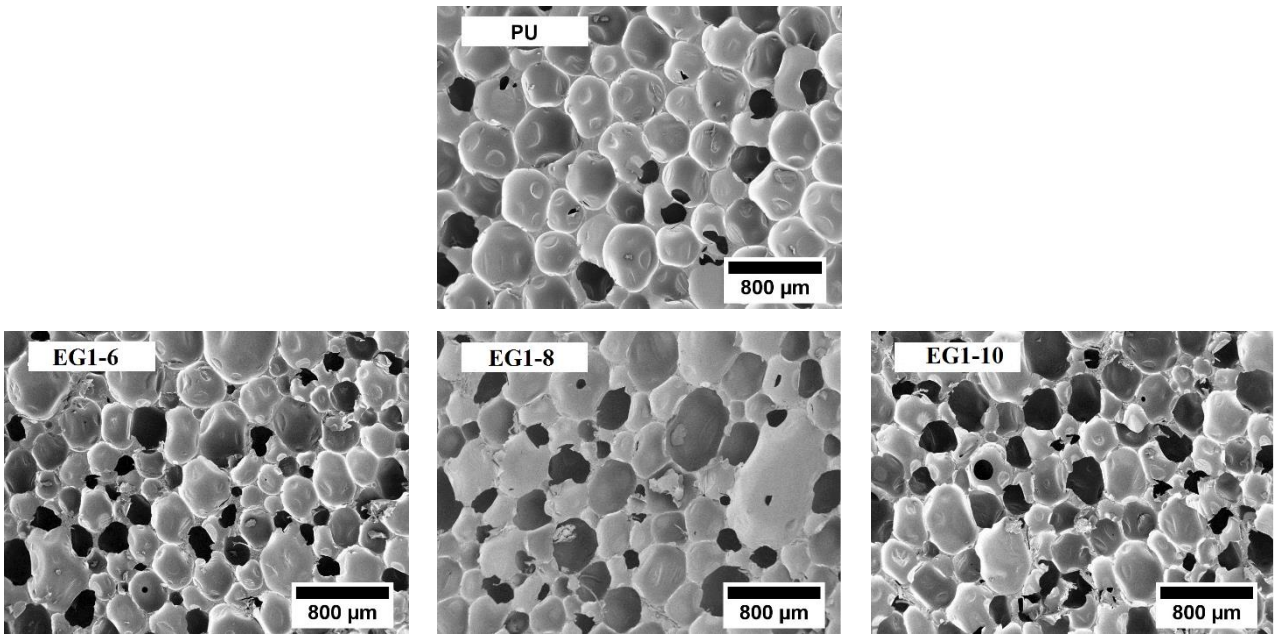

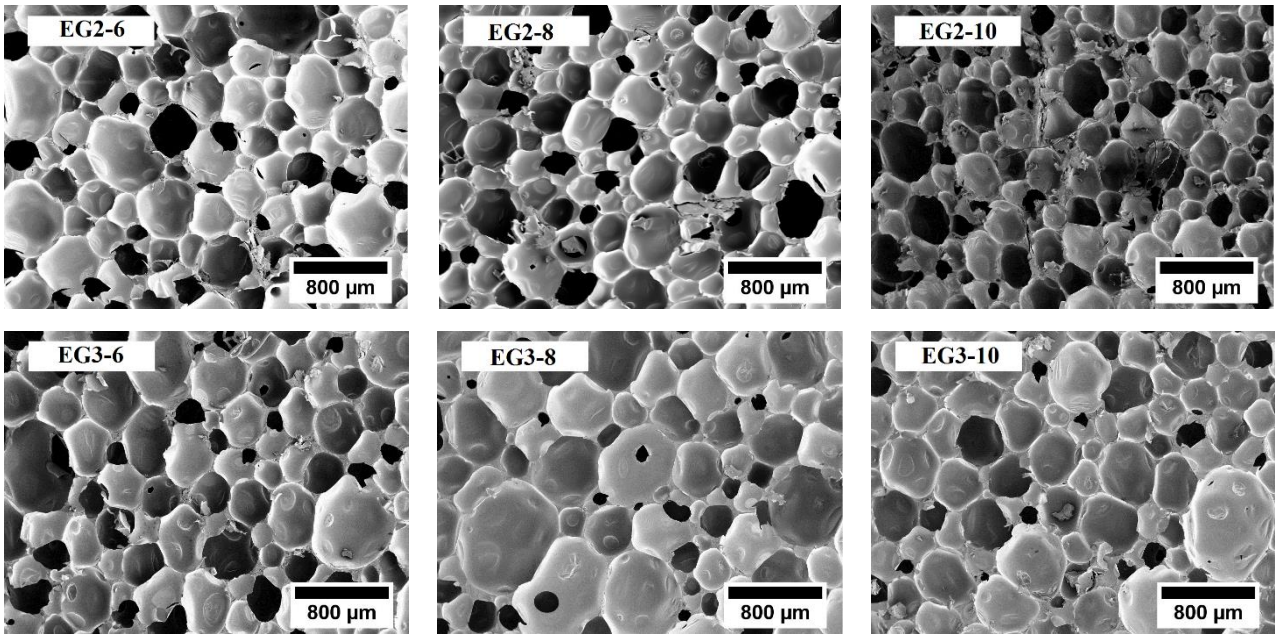

Figure 4-1. SEM micrographs of the growth plane of RPUF samples.

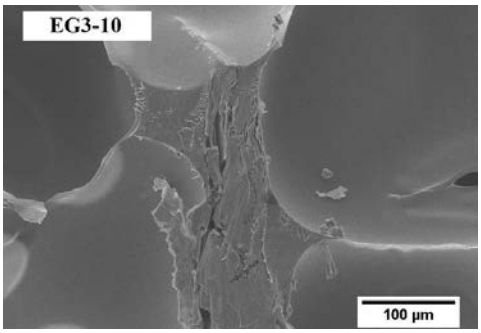

Figure 4-2. SEM micrograph of EG3-10 sample in the RPUF matrix.

b) *Thermal conductivity*

The thermal conductivity of RPUFs was measured to evaluate the effect of the different EGs as RPUFs are known to be one of the best insulating materials. They are highlighted by their low thermal conductivity, which is well represented as the sum of gas phase (λg), solid phase (λs), and radiative conductivity (λr) contribution [213]. According to Choi et al. [214], the conduction in the gas phase (λs) is the highest contributor with about 60 to 70 % of the total thermal conductivity. Besides, the introduction of fillers is commonly known to have a strong influence on the cell size and as consequence, on the thermal conductivity. On top of that, thermal conductivity generally decreases with decreasing cell size [215]. It is well known that particles in the RPUF formulation can act as nucleating agents, decreasing cell size and/or acting as infrared radiation blockers, which increases the extinction coefficient. Consequently,

this implied a decrease in radiation contribution (λr) to thermal conductivity. However, on this study, thermal conductivity increased with the addition of increasing amounts of EG particles, a phenomena which was reported in a related publication by our group [212]. Although the nucleation effect reduced the cell size of the foam; thus, reducing λr contribution, the increase of density increased the λs contribution. Besides, the intrinsic EG thermal conductivity weakens the thermal insulation efficiency of RPUF foams [216] adding a new conductive phase in the composite and increasing again the λs contribution to the thermal conductivity. Furthermore, the addition of EG particles slightly increased the OC % in the foams, which contributed to an increased thermal conductivity. These effects explained the higher thermal conductivity of EG-filled composites compared to neat RPUF.

Table 4-2. Main characteristics of the cellular structure of EG/PU foams, density, and thermal conductivity values.

Sample	Density (Kg/m^3)	OC (%)	Cell size (μm)	Thermal conductivity (mW/mK)
PU	95.9 ± 0.1	6.9 ± 0.2	467 ± 120	48.9 ± 0.1
EG1-6	100.9 ± 1.1	9.4 ± 0.4	310 ± 105	52.7 ± 0.2
EG1-8	104.7 ± 1.7	7.8 ± 0.6	339 ± 132	53.0 ± 0.2
EG1-10	104.9 ± 0.3	9.5 ± 0.1	339 ± 108	56.0 ± 0.1
EG2-6	96.5 ± 1.7	9.4 ± 1.5	329 ± 126	50.4 ± 0.1
EG2-8	99.6 ± 0.5	9.1 ± 0.1	349 ± 121	51.6 ± 0.2
EG2-10	102.8 ± 5	9.9 ± 0.2	340 ± 104	52.8 ± 0.2
EG3-6	97.5 ± 1.5	10.8 ± 0.7	423 ± 148	51.0 ± 0.3
EG3-8	102.7 ± 0.6	9.3 ± 1.2	383 ± 181	52.0 ± 0.2
EG3-10	101.6 ± 0.9	9.5 ± 0.6	408 ± 155	52.2 ± 0.4

4.3.2. *Thermal degradation*

TGA and differential thermogravimetry (DTG) analysis of neat RPUF (PU) and EG-filled RPUF samples on N_2 atmosphere are illustrated in **Figure 4-3** and the summarized data is collected in **Table 4-3**. The corresponding thermal parameters were the initial decomposition temperature ($T_{5\ wt.\ \%}$, namely the temperature at 5 % weight loss), the temperature at maximum weight loss rate (T_{max}, denoted as the peak value from the DTG curves), and the remaining

residue at the end of the test (wt. %). Both unfilled and EG-filled RPUFs showed a similar degradation curve for each sample. The degradation process of PU composites has been reported by many authors [48], [217]. Commonly is consisted of a two to three steps or even four step process, involving the degradation of the HS and SS of PU. The first step is due to degradation of the HS, which results in the formation of -NCO and alcohol, primary or secondary amine and olefin, and CO_2. The second step is the degradation of the SS by polyol de-polycondensation. The rate of the SS degradation depends on the SS structure and its three-dimensional arrangement. A detailed scheme was showed back in **Scheme 2-5**.

For the EG-filled foams, the degradation started earlier due to the intercalated acid inside the EG layers (**Figure 2-9**). The average of the first peak degradation temperature on the DTG curves for the EG1 samples (with lowest rate of expansion) was 194 °C. For EG2 and EG3 samples (both EGs with the same rate of expansion), they increased to 202 and to 201 °C, respectively. In other words, the higher rate of expansion, delayed the degradation starting point. For EG1, the average of the first step of degradation, without accounting into the loading, was in the range 121–223 °C, whereas it was 132–233 °C for EG2, and 136–228 °C for the particles with higher size EG3. The increasing range could be explained considering the higher rate of expansion combined with a bigger particle size of EG particles, which delayed the degradation path mechanism once the acid has been volatized. The average of the maximum degradation temperature (T_{max}) for EG1 was 310 °C, whereas it increased to 317 °C for EG2, and was slightly reduced to 315 °C for EG particles with higher size (EG3). Meanwhile, the residual char increased for all EG-filled RPUF with respect to neat PU. The residue wt. % increased along with the EG loading to reach a maximum of 22.6 wt. % for EG1. The char layer formed acted as a thermal barrier, protecting the foam from further decomposition and limiting the degradation of the PU matrix. Higher rate of expansion did not improve the char residue, neither did a higher particle size. A turning point regarding particle size and rate of expansion was found for EG1 samples, and they were the best according to the char residue wt. %. According to Y. Li. et al. [47], bigger particle size of EG did not influence the T_{max}, but in accordance with the high rate of expansion, more gases can be generated, resulting in less residual char for EG2 and EG3. Although the rate of expansion increased the degradation temperature, only minor influences were observed. Considering the effect of the different EGs in the foam, except for the residue wt. %, there were no important impacts on the PU degradation, as EG did not react with the PU matrix [218]. In addition, the characteristics of EG have low or negligible impact on the degradation on N_2 atmosphere.

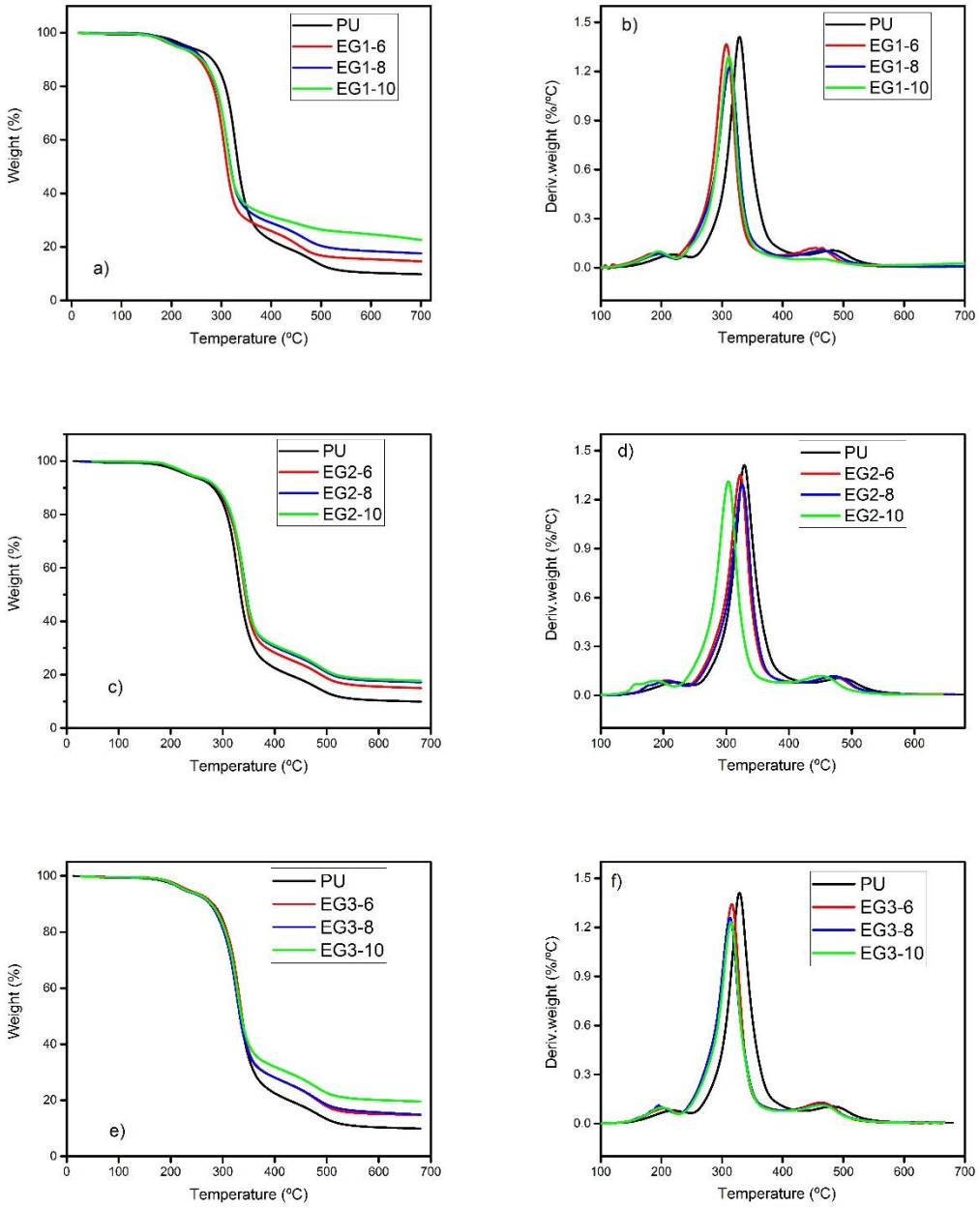

Figure 4-3. TGA and DTG curves for RPUF samples containing EG1 (a) and (b), EG2 (c) and (d), and EG3 (e) and (f).

Table 4-3. TGA data for EG/PU samples.

Sample	$T_{5\ wt.\%}$ (ºC)	T_{max} (ºC)	Residue (wt. %)
PU	231	329	9.8
EG1-6	231	307	14.6
EG1-8	238	313	17.6

EG1-10	228	311	22.6
EG2-6	236	322	15.0
EG2-8	237	325	17.2
EG2-10	238	303	17.7
EG3-6	234	316	14.8
EG3-8	226	313	14.9
EG3-10	229	315	19.6

4.3.3. *Fire behavior*

a) *LOI and UL94 tests:*

LOI and UL94 tests were performed, and the corresponding results are collected in **Table 4-4**. Indeed, to compare the RPUF specimens, the average burning time after twice ignition (t_1+ t_2) for each individual sample; the time in which the individual specimens from the UL94 tests were burning until the fire was total extinguished after the two consecutive ignitions—was herein recorded and presented as comparison. The LOI of neat RPUF (PU) was 19.2 %, indicating that it was a very flammable material under atmospheric conditions (*ca*. 21 % O_2). LOI values and UL94 rating increased along with the increasing amount of EG into the foam. V-0 rating in the vertical burning test was only achieved above 8 wt. % onwards on the EG1-RPUF sample, which provided a LOI value of 27.8 %. The sample containing 10 wt. % of EG1 increased by a 50 % the initial value of the PU to 29.8, whereas UL94 average burning time decreased (4.2 s) and maintained the V-0 rating. When EG1 was replaced by EG particles with a higher rate of expansion, such as EG2 (350 cm^3/g), the effects on the LOI values were positive. LOI increased from 27.8 to 30.0 % in EG2-8 and higher LOI values were achieved using 10 wt. % of EG2, showing a value of 31.8 %. UL94 rating of the EG2-8 and EG2-10 samples was indeed V-0. Despite the increasing burning time in the UL94 test, the performance of EG2 was almost like EG1 on the UL94 test. So, the rate of expansion of EG, had no big influence on the UL94 test, thus maintaining the same rating. Moreover, EG3, with higher particle size and same rate of expansion as EG2, obtained similar LOI performance. The LOI values were clearly improved with the increasing rate of expansion, which might be explained by the formation and densification of an isolation layer that became larger with increasing volume of the EG particles and formed a more intumescent char [210]. On the contrary, decrease in particle number

(caused by the higher particle size for the same loading) had no important effect on the formation of a compact isolation layer during the fire process, increasing slowly the LOI values as it was reported by other authors [204]. Interestingly, the UL94 values obtained by EG3-RPUFs were outstanding. In fact, a V-1 rating was achieved with a loading as low as 6 wt. % of EG3, whereas for 8 wt. % onwards, the UL94 rating was V-0 with an average t_1+t_2 time of only 2.9 s. An increasing amount of EG added into the foam should contribute to an increased barrier effect due to EG expansion, giving eventually a good fire performance [64], [66], [67], [219]. For this reason, EG3; the EG particles with higher size, should be able to create a more compact isolation layer, thus improving UL94 performance [207], [220]. In summary, the role of particle size and rate of expansion of EG, as intrinsic characteristics of the material, seemed to be crucial for the flame retardancy performance of EG-filled RPUFs. On one hand, the expansion rate was important for a variable O_2 % test as LOI, in which a higher concentration of O_2 could easily start a fire process. On the other hand, the particle size of EG3 was a key point on the UL94 test under ambient conditions in order to prevent fire spreading in a more efficient way [207].

Table 4-4. Limited oxygen index **(**LOI) and vertical burning (UL94) tests results of EG/PU samples.

Sample	EG loading (wt. %)	LOI (%)	UL94 Rating	Average time (t1+ t2) (s)
PU	0	19.2	NO RATING	>30
EG1-6	6	26.8	NO RATING	>30
EG2-6	6	28.0	NO RATING	>30
EG3-6	6	28.6	V-1	9.9 ± 5.3
EG1-8	8	27.8	V-0	7.4 ± 6-3
EG2-8	8	30.0	V-0	8.5 ± 4.2
EG3-8	8	29.2	V-0	5.6 ± 3.4
EG1-10	10	29.8	V-0	4.2 ± 3.3
EG2-10	10	31.8	V-0	5.8 ± 4-2
EG3-10	10	31.8	V-0	2.9 ± 2.0

b) *CCT test*

Cone calorimeter test (CCT) based on the O_2-combustion principle test was performed at a heat flux of 50 kW/m^2. The potential fire disaster can be assessed by the following parameters: PHRR (Peak Heat Release Rate), TSP (Total Smoke Production), THR (Total Heat Released), and mass loss rate (Mass %). All these data for the RPUFs are summarized in **Table 4-5**. Each RPUF loaded with different EG types was discussed individually.

The PHRR and TSP curves for the PU foams loaded with EG1 are shown in **Figure 4-4**, whereas their THR and mass loss curves are displayed in **Figure 4-5**. It is noteworthy that the samples rapidly raised their maximum peak value (PHRR) after ignition. The porosity of the foam structure facilitates a large surface contact area between the polymeric material and the air, currently being more exposed to the heat [2]. As showed in **Figure 4-4**, the samples showed two-peak curves for the PHRR. The first peak is assigned to the development of the intumescent protective char and the second peak is due to the gradual degradation of the protective layer as the sample is continuously exposed to heat [179]. For instance, neat RPUFs burned fiercely once ignited and exhibited a peak value of 220 kW/m². The maximum values of these second peaks decreased as the amount of EG increased, since pyrolysis at the bottom parts of the samples was then blocked by the EG expansion mechanism [204], [207]. The results of EG1 in a RPUF were already reported in a previous publication by our group and included on this chapter [212]. In detail, the addition of EG1 reduced PHRR values by 32, 39, and 49 % for the samples containing 6, 8, and 10 wt. % of EG, respectively, with the lowest peak for the EG1-10 samples being 111 kW/m². TSP is a critical parameter, since smoke is a dangerous agent on a fire scenario, and mainly due to the toxicity of CO. Hence, reducing the TSP evidenced a good FR effect. TSP of neat PU showed a value of 10.4 m², and the addition of EG continuously reduced the TSP reference value: they were reduced by 25, 63 and 81 % in the samples containing 6, 8 and 10 wt. % of EG respectively, with the lowest value for the EG1-10 sample being 2.0 m².

THR curves for RPUFs loaded with EG1 are shown in **Figure 4-5**. THR of the reference sample (PU) gave a value of 68.7 MJ/m². The introduction of EG continuously reduced this value by 18, 34, and 27 % for samples containing 6, 8, and 10 wt. %, respectively of EG1, with the lowest value for the EG1-8 sample being 45.3 MJ/m². The mass loss rate is another important parameter in order to evaluate the FR properties of a polymer. In our case, mass loss of the neat PU sample showed a value of 87 wt. %. In this way, most polymers were transformed into volatiles during the process. Significantly, the addition of EG reduced this reference value

by 17, 28, and 33 % for samples containing 6, 8, and 10 wt. % of EG, respectively, the lowest mass loss for the EG1-10 sample being 54 wt. %. For our EG-filled RPUFs, increasing quantities due to the EG expansion led to the formation of a carbon char when exposed to a heat source, thus improving the polymer flame retardancy. As concluded previously by other scientists, the intumescent char formed by the EG expansion contributed to the flame suppression and limited heat and mass transfers from the polymer to the heat source, thereby preventing further decomposition and limiting RPUFs' weight loss [18], [47], [179], [207].

PHRR and TSP curves for RPUFs loaded with EG2 are shown in **Figure 4-6**. THR and mass loss curves are plotted in **Figure 4-7.** As well as EG1 samples, EG2-filled RPUF samples reached their maximum peak very rapidly; less than 20 s. Thus, the time of EG2-10 increased by 5 s compared to that of EG1. Alike, the addition of EG reduced the PHRR value of neat PU continuously by a 25, 42, and 48 % in the samples containing 6, 8, and 10 wt. % of EG2, respectively, with the lowest peak for the sample with EG2-10 being 113 kW/m². In this way, the addition of EG2 reduced continuously the reference TSP values (PU) by a 52, 79, and 79 % in the samples containing 6, 8, and 10 wt. % of EG2, respectively. Then, 2.1 m² was shown as the lowest value for the sample with EG2-10.

THR and mass loss curves for RPUF containing EG2 are shown in **Figure 4-7**. The introduction of EG2 also reduced the THR value continuously by a 29, 43, and 40 % in the samples containing 6, 8, and 10 wt % of EG2, respectively, with the lowest result for the sample EG2-8 being 38.9 MJ/m². The addition of EG2 also reduced the reference value of mass loss up to a 34 % reduction on EG2-10. So far, 53 wt. % was the lowest amount of mass loss during the experiment for the sample EG2-10.

PHRR and TSP for the RPUFs loaded with EG3 are shown in **Figure 4-8**. THR and mass loss are displayed in **Figure 4-9.** As described above for previous samples, PU containing EG3 again reached their PHRR before 15 s, in the same range as other EGs. In this case, the addition of EG also reduced the reference PHRR value continuously by a 43, 51, and 54 % for the samples containing 6, 8, and 10 wt. % of EG3, respectively, with the lowest peak for the sample with EG3-10 being 101 kW/m². Thus, the addition of EG3 also continuously reduced the TSP reference value by a 67, 82, and 84 % for samples containing 6, 8, and 10 wt. % of EG respectively. In this case, an impressive 1.7 m² was the lowest value for the EG3-10 sample.

THR and mass loss curves for RPUFs containing EG3 are shown in **Figure 4-9**. Again, the introduction of EG3 reduced the reference value by 18, 47, and 47 % for the samples containing 6, 8, and 10 wt. % of EG3, respectively, with the lowest result for a sample with higher EG wt.

% as EG3-10 being 36.3 MJ/m². Therefore, the addition of EG3 also reduced the reference value of mass loss by 18, 39, and 37 % for the samples containing 6, 8, and 10 wt. % of EG3, respectively. The lowest amount of mass loss during the cone calorimeter test for the sample with 8 wt. % EG3 was 49 wt. %.

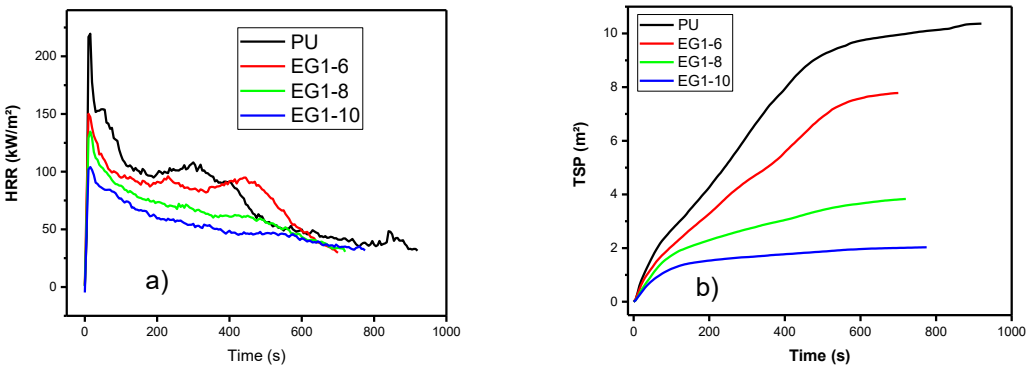

Figure 4-4. a) HRR and b) TSP curves of EG1/PU samples at 50 kW/m^2.

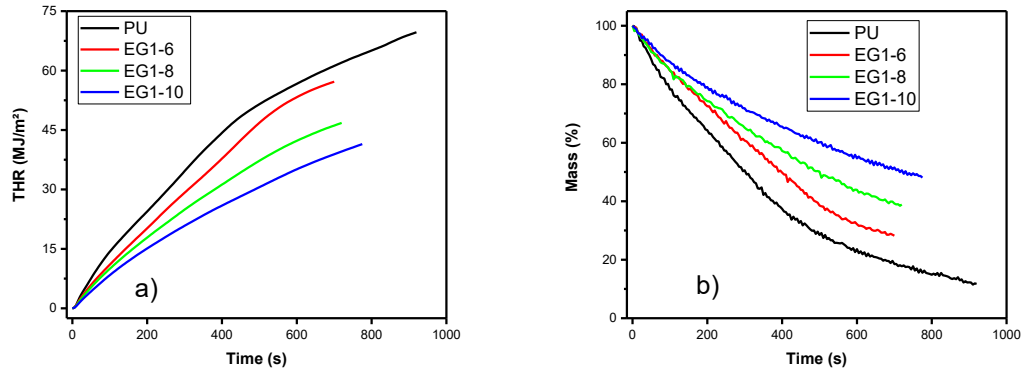

Figure 4-5. a) THR and b) mass loss curves of EG1/PU samples at 50 kW/m^2.

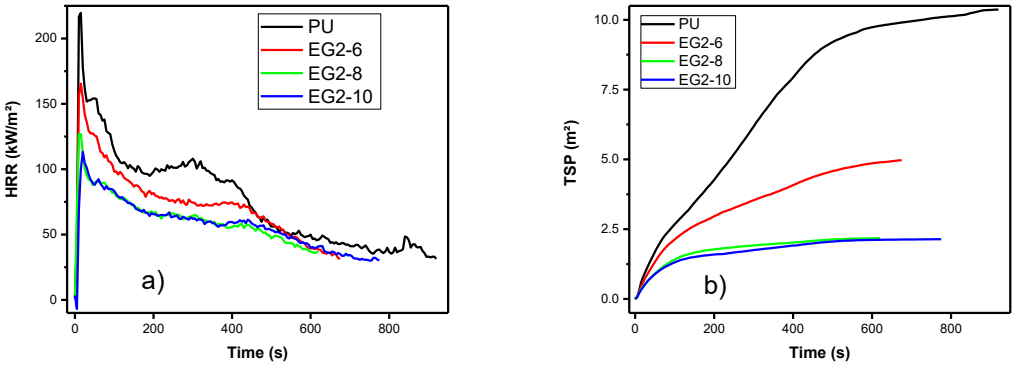

Figure 4-6. a) HRR and b) TSP curves of EG2/PU samples at 50 kW/m^2.

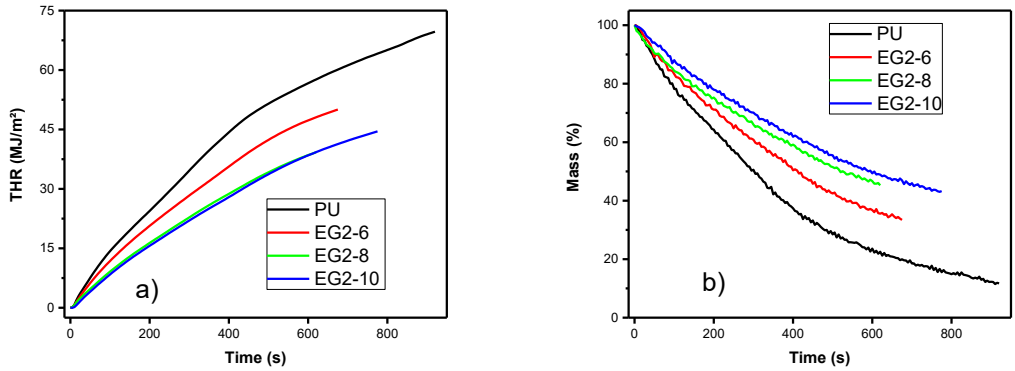

Figure 4-7. a) THR and b) mass loss curves of EG2/PU samples at 50 kW/m^2.

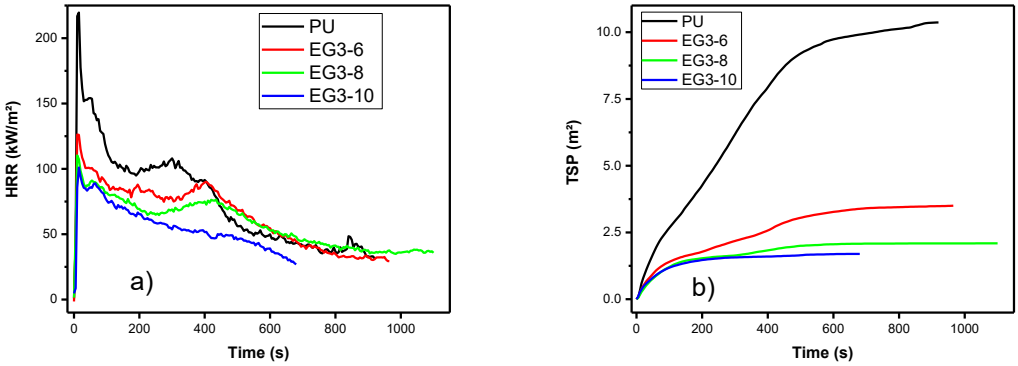

Figure 4-8. a) HRR and b) TSP curves of EG3/PU samples at 50 kW/m^2.

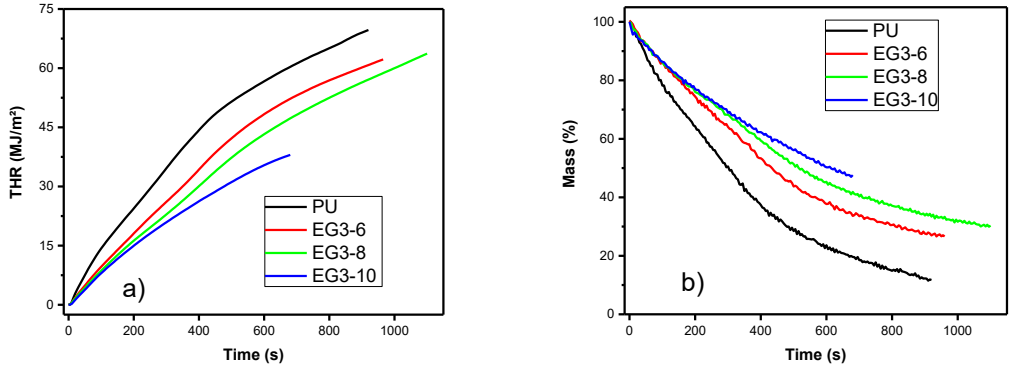

Figure 4-9. a) THR and b) mass loss curves of EG3/PU at 50 kW/m^2.

Table 4-5. Data of EG/RPUF composites at 50 kW/m^2 from CCT.

Sample	PHRR (kW/m²)	THR (MJ/m²)	TSP (m²)	Mass loss (wt. %)
PU	220 ± 39	68.7 ± 15.4	10.4 ± 0.4	87
EG1-6	150 ± 14	56.2 ± 4.4	7.8 ± 1.3	71
EG2-6	165 ± 4	48.8 ± 0.8	4.9 ± 0.6	66
EG3-6	126 ± 2	56.4 ± 3.4	3.4 ± 0.1	69
EG1-8	135 ± 8	45.3 ± 1.7	3.8 ± 0.2	59
EG2-8	127 ± 9	38.9 ± 3.5	2.2 ± 0.7	54
EG3-8	107 ± 2	36.7 ± 19.1	1.9 ± 0.2	49
EG1-10	111 ± 5	50.3 ± 7.6	2.0 ± 0.1	54
EG2-10	113 ± 7	41.3 ± 0.5	2.1 ± 0.4	53
EG3-10	101 ± 7	36.3 ± 0.8	1.7 ± 0.5	50

c) *FR and smoke suppression behavior*

In order to clarify which could be the intrinsic characteristics of EG that are decisive for its performance as FR, an analysis including the impact of the particle size and the rate of expansion on the FR performance was carried out here. Thus, the effect of the rate of expansion could be studied by comparing EG1 and EG2; bearing in mind that these two types of EG had the same particle size but different rates of expansion (250 and 350 cm^3/g, respectively). The PHRR at the maximum difference point was 6 % lower for EG2, which had a higher rate of expansion. Afterwards, THR of samples with a 10 wt. % of EG was 18 % lower for the foams with EG2, although it was a 15 % lower considering the average values. One possible explanation could be that the heat could not be transferred so smoothly through a higher volume material after the worm-like expansion of EG and gets dissipated easily. In this case, a higher amount of PU remained unaltered in the condensed phase, which was not available for pyrolysis, eventually reducing the THR [204]. On the other side, EG2 reduced the smoke production (TSP) at higher rates than EG1, with a maximum reduction of a 43 % lower than EG1 when an 8 wt. % EG2 was used. On average, the amount of smoke produced was a 24 % lower for EG2. Interestingly the above difference between EGs decreased with an increase in EG loading. Finally, the mass lost during the cone calorimeter test was slightly lower for EG2. All in all, these results support that EG2 was a better FR than EG1 and so, a higher expansion rate is beneficial for a better FR effect. The above mentioned higher performance could be

explained considering the fact that a higher expansion of EG promoted the development of a thicker worm structure, which can block more efficiently the heat and mass transfer during the pyrolysis, leading to lower values of PHRR, THR, and smoke production [47], [204]. It can be concluded that the higher rate of expansion of EG2, has a very positive effect regarding the THR but mostly the TSP, where the differences were highlighted at lower loadings of EG, with a higher effectivity at higher rates of EG expansion.

On the other hand, to study the effect of particle size on flame retardancy, the behavior of EG3 and EG2 was compared next, taking into consideration that particle size increased from 300 to 500 μm, whereas the rate of expansion remained unaltered (350 cm^3/g). Commonly, bigger particle sizes or bigger expansion rates lead to higher FR performance [221]–[224]. Consequently, the PHRR of EG3 samples was 24 %, 15 %, and 11 % lower than that of EG2 samples containing 6, 8, and 10 wt. % of EG3, respectively. In other words, particles with higher size were able to reduce more efficiently the PHRR. Considering the average values, the decrease of PHRR for EG2 was 17 % lower than that of EG3. Even so, when the amount of EG increased, this difference was continuously reduced. In a similar trend, EG3 also reduced the smoke production (TSP) at higher rates than EG2. In fact, a 30, 13, and 20 % reduction with respect to EG2 was obtained for samples containing 6, 8, and 10 wt. % of EG3 respectively. On average, EG3 reduced the TSP by a 21 %. This data indicated that particles of higher sizes formed a more stable char barrier, which blocked the smoke production, as described by others authors [47], [207], [210]. On the other hand, the THR of the sample with EG3 was higher for those samples containing 8 wt. % of EG or less. Even though particles of higher sizes favored char barrier formation, bigger cracks could occur at the surface, thus reducing the effect of heat blocking and increasing THR as consequence [207]. Moreover, the thermal conductivity increased with the average cell size; as reported on the morphology analysis above in **4.3.1.b)**; and with the breaking of the cell walls [210]. Finally, when comparing the mass loss rate of both samples, those containing EG3 reduced the mass loss rate compared to EG2-filled RPUFs. This was due to the increasing number of particles forming a char barrier, and thus forming a more compact isolation layer [207]. For this reason, the heat flux delivered to the pyrolysis front of the sample was also reduced [204]. On the contrary, at 6 wt. % of EG3, a higher amount of gases could be generated, as the small number of particles could not form a sufficient barrier to hinder heat penetration [207]. Therefore, the defects in structure also became larger, resulting in a less stable structure, and producing less amounts of residual char [207]. When the loading increased, the char became more compact and the initial PU structure remained almost

unaltered, reducing the mass loss rate along with the previously mentioned parameters. Therefore, the combination of higher particle sizes and higher rates of expansion had a beneficial effect on the formation of a compact residual char, which was the main characteristic of the mechanism of EG as FR [201]. In summary, the higher the particle size, the bigger impact on the results of the cone calorimeter test, such as PHRR and THR, but mostly TSP. At the same time, a higher rate of expansion was a necessary characteristic of this FR to obtain an outstanding performance.

4.3.4. *Compressive strength*

Compression tests are mandatory to completely characterize the foams due to its common use in the market as insulation material and reinforcement. Herein the compression tests were performed at a constant rate of 3 mm/min, the data obtained are shown in **Figure 4-10**, and collected in **Table 4-6**.

The compressive strength of the RPUF decreased slightly with the addition of any kind of EG. The average compressive strength of EG1 decreased by 6 % compared to neat foam, whereas EG2 and EG3 decreased by a 3 and 4 %, respectively. Also, it decreased on average from 1 to 9 % with the increasing loading of EG. A very interesting effect of EGs was found at lower loadings (6 wt. %), where a correlation was observed between the cell size and the compressive strength. Thus, the lowest cell size obtained (EG1-6), gave the lowest compressive strength result as opposed to that the highest cell size obtained (EG3-6), gave the highest compressive strength result. This effect was associated to the dispersion of EG into RPUF at lower loadings, where the effect of particle size was more important on the cell size and compressive strength due the homogeneity of cell size distribution, thus highlighting the differences. However, higher loadings of EG were associated with an increase in cell diameter, significant cell rupture, collapse, and brittleness, since EG particles can go through the cells damaging their structure [176], [207], thus reducing the crosslinking density of the polymer matrix [225].

In summary, the mechanical performance worsened, even though density increased due to the addition of EG particles. All these results were in accordance with the previous findings of Thirumal et al. [203], [210] and Modesti et al. [226]. Specifically, the compression performance of the RPUF loaded with EG3-10 decreased by a dramatic 15 % compared to the neat foam. The EG3 particles formed aggregates due to poor dispersion and decreased the compression performance at higher rates [198], [210]. Besides, the increase in EG size particles caused larger

defects in the PU structure, as a result of a poor interfacial adhesion between EG and the PU matrix. For that reason, slippage among these two components took place, resulting in a bigger decrease in the compressive performance, which was in accordance with previous reports by Yi Li et al. [207]. Therefore, the EG-RPUF structure became inhomogeneous, and consequently the compression performance was slightly worse than that of neat RPUF [198], [204], [227].

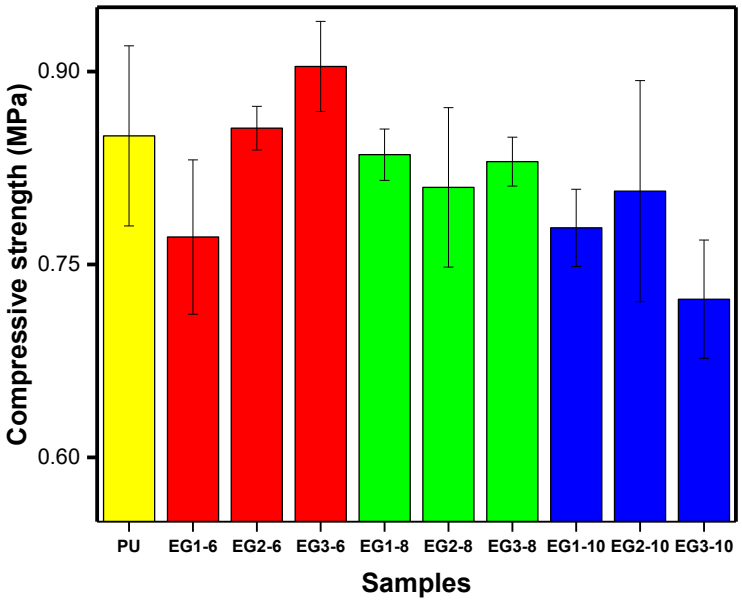

Figure 4-10. Compressive strength of EG/PU samples at 3 mm/min constant rate.

Table 4-6. Mechanical data of EG/RPUF samples.

Sample	Compressive strength (MPa)	Density (Kg/m^3)
PU	0.85 ± 0.07	95.9 ± 0.1
EG1-6	0.77 ± 0.06	100.9 ± 0.3
EG2-6	0.86 ± 0.02	97.2 ± 1.7
EG3-6	0.90 ± 0.04	97.5 ± 1.5
EG1-8	0.84 ± 0.02	104.7 ± 1.7
EG2-8	0.81 ± 0.06	101.7 ± 2.6
EG3-8	0.83 ± 0.02	102.7 ± 0.6
EG1-10	0.78 ± 0.03	104.9 ± 0.3
EG2-10	0.81 ± 0.09	102.5 ± 3.1
EG3-10	0.72 ± 0.05	101.6 ± 0.9

4.4. Conclusions

In the **Chapter 4**, the effect of EG as a non-halogenated additive for a commercial RPUF was completely studied. The impact of EG in a commercial RPUF, regarding cellular structure, thermal conductivity, flame retardancy and compressive strength was explained in detail. Three different EGs (EG1, EG2 and EG3) were compared in the same RPUF. Commonly, the big particle size of EG reduced the cell size of the foam whereas increased the density and thermal conductivity. The internal cellular structure of the PU gets dramatically affected by EG. Above all, EG acted as an excellent additive FR which reduces the HRR, THR, TSP and mass loss on a commercial RPUF. However, the compression strength of the resultant RPUF was worse than the neat PU foam. The compressive performance of the foam was diminished due to slippage between the cellular structure and so, decreases the compressive strength.

The fire performance of EG was studied based on two important characteristics of the material that seems to dominate its good FR effect: Particle size and the rate of expansion. Following this, three different EGs based on different particle size (EG1/EG2 and EG3) and rate of expansion (EG1 and EG2/EG3) were herein studied and compared. As is lighted up on this research, to have an optimal FR effect, it is necessary to have high particle size and high rate of expansion, in order to maximize the performance of EG. The particle size maximizes the blocking effect of EG and the rate of expansion favors lower smoke production; i.e. mass transfer. For this reason, PHRR, THR, TSP and mass loss were incredibly improved by EG with a high particle size and high rate of expansion (EG3). Just 8 wt. % was enough loading to achieve V-0 rating in the UL94 test. On the other hand, the high particle size of EG3, affects negatively on the cellular structure, leading to an even lower compressive strength compared to the neat RPUF or a lower particle size EG-filled foam (EG1/EG2). Indeed, the thermal conductivity was independent about these mentioned characteristics but was very dependent on the EG loading and density of the foam.

CHAPTER 5

5. Synergistic effect of EG and a P-N FR salt on the flame retardancy of a RPUF

"A country without research is a country without development"

-Margarita Salas Falgueras

5.1. Introduction

The problematic about the flammability of RPUFs can be solved through many different paths. As showed in **Chapter 4**, the addition of an inorganic FR with a strong condensed phase effect like EG, can impart high flame resistance to a RPUF. Another of the possible ways is to combine different FRs with different action mechanisms to achieve a synergistic effect, which obtains higher results than the sole sum of the individual FR additives. Considering the excellent performance of EG as unique additive, the compressive strength of the foam was deteriorated due to the poor compatibility between EG and RPUF matrix as reported in the previous chapter, which limits the application of EG into these foams. Besides EG, another kind of important FRs are P-FRs. Several kinds of P-FRs were used in the literature as halogen-free FRs. Among them, IFRs and P-FRs such as APP [101], DMMP [73], cyclophosphazenes [78] or DOPO [80], were studied in both flame retardancy and compressive performance of modified RPUFs. The compressive strength is of great importance for the development of RPUF, used

mainly as an insulator or reinforcement. Most of FRs prepared from organic phosphorous acid or oganophosphinic acid, work in condensed phase [69], [70] by forming polyphosphoric acid, which accelerates the dehydration of polymer matrix and the formation of carbon layers. Moreover, some phosphorus-containing FRs can release large amount of molecular fragments radical such as P· and PO·, which act as radical scavengers in gas phase to achieve outstanding FR results [72]. In addition, based on their good compatibility with the RPUF matrix [89] [80] and high efficiency [88], it is possible to achieve better FR performance and higher compressive strength. Therefore, the development of RPUF with both high-performance flame retardancy and good mechanical properties is valuable for the industry.

The main objective of the work showed in this chapter is to develop an efficient synergistic P-N FR agent in combination with EG as FR additives in a RPUF to improve both FR and mechanical properties. To carry out this idea, bis(4-aminoanilinium) phenylphosphonate (FR1); a phenylphosphonic aniline salt, was synthesized under specific conditions and added into PU matrix along with EG at varied ratios to prepare a new FR composite foam. In this work, a commercial RPUF formulation was flame retarded by adding 8 wt. % EG and FR1. Different ratios (8:1 and 12:1) of EG to FR1 were designed. The effect of these different additives on the cellular structure, thermal properties, flame retardancy and compression strength of a commercial RPUF were discussed. The synergistic effect of EG and FR1 with respect to the FR mechanism was discussed. The current chapter was based in a recently reported publication by our group [228].

5.2. Materials

5.2.1. *Materials*

PU commercial foam (FOAM-iT! ™ 5, RPU) provided by Smooth-On (Form X Spain, Barcelona, Spain). Expandable graphite (EG, *EG3* from **Chapter 4**), GHL PX 99 32 350, kindly provided by Georg H. Luh GmbH (Germany). P-phenylenediamine (PPD, 98 %, Sigma-Aldrich), phenylphosphonic acid (PPA, >98%, TCI Europe) a**s** reactants and MeOH (99.8%, Merck) as a solvent. The products were used without any additional purification.

5.2.2. *Synthesis of 4 N, N'-bis(4-aminophenyl)-P-phenylphosphonic diamide (FR1)*

The route to synthesize FR1 is presented on **Figure 5-1**. First, PPD (28.2 g, 0.26 mol) was dissolved on 200 mL of MeOH in a 1000 mL round flask under magnetic stirring around 30 min until a red transparent solution was obtained. Secondly, in a separate glass, a solution of PPA (20.6 g, 0.13 mol) on 200 mL of MeOH was prepared and passed to a dropping flask. Afterwards, the solution of PPA was added slowly dropwise over the PPD solution at room temperature around 20 min. Finally, the reaction was stirred during 16 h at room temperature. In the early beginning of the reaction, the solution became very thick and viscous by a white precipitant and after 16 h, a turbid violet liquid solution was obtained. Thereafter, the precipitant was vacuum-assisted filtrated and washed with MeOH for several times until a transparent washing MeOH and a clear white slurry were observed. The white slurry was dried over vacuum at 70 ºC during 3 h. Thus, FR1 was obtained as a white solid with a 55.2% yield.

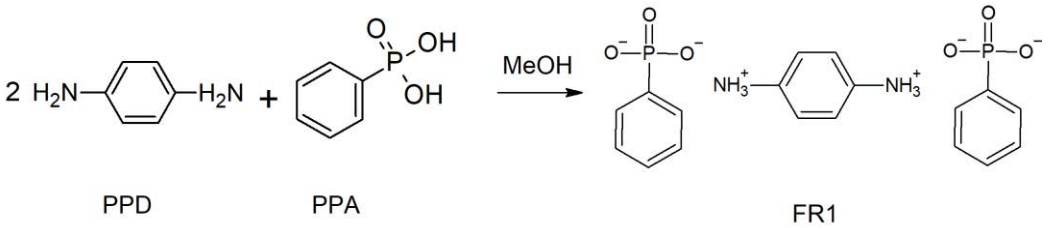

Figure 5-1. Proposed reaction of PPD and PPA to form FR1.

5.3. Results and discussion

5.3.1. *Characterization of FR1*

a) *FTIR*

The FTIR spectra of FR1 is shown in **Figure 5-2**. The peaks can be related to: 1518 cm^{-1} (C=C (Ph)) [229], 3051 cm^{-1} (C-H (Ph)) [230], 1220 cm^{-1}(P=O), 1050 and 819 cm^{-1} (P-O) [98], [231], 982 cm^{-1} (P-OH from a salt) [88], 1488 and 1591 cm^{-1} (P-Ph) [232], 3471 and 3384 cm^{-1} (primary-amines, $-NH_2$), 1631 cm^{-1} (N-H bending) and 775 cm^{-1} (N-H wag). Moreover, it can be assessed at 3135 cm^{-1} the vibration of the $-NH_3^+$ group [95], [96] and the phosphonic acid structure by the peaks at 2361 [95], [155] and 2590 cm^{-1}, which reflects the P-OH vibrations, always present in the FTIR spectra of phosphonates containing hydrogen phosphonate groups [88].

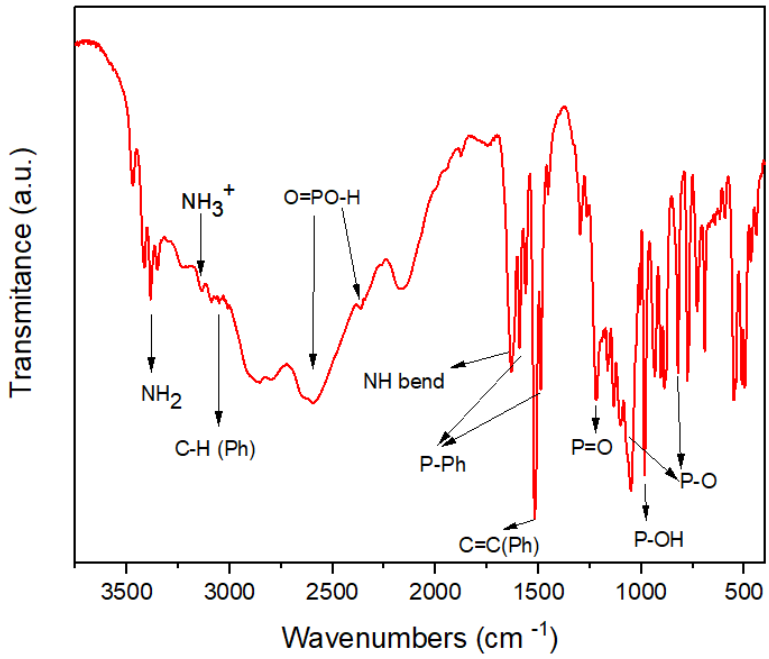

Figure 5-2. FTIR spectra of FR1 compound.

b) *NMR*

The structure was also evaluated by NMR. First, in the ^{31}P spectra (**Figure 5-3**) only one sharp peak located at 12.2 ppm, indicating a pure phenyl phosphonic-aniline salt with phosphonate-based skeleton phosphorous structure was obtained ($O=P(R)(OR)_2$. Secondly, the ^{1}H NMR spectra of the synthetized FR1 is presented in **Figure 5-4**. The assignment of each peak was marked. The integral area of peaks located at 7.6 ppm, 7.4 ppm and 6.6 ppm are 2.14, 3.087 and 2.21 respectively. Because of there is no peak of $-NH_2$ group appeared at range 3-4 ppm, it suggests that all the PPD reacted with PPA to form ammonium salt. Finally, on the ^{13}C NMR spectra (**Figure 5-5**), signal **1** was found at 131.1 ppm whereas **2** and **3** appeared at 118 ppm. Indeed, the signal of 128.5 was attributed to signal **4**. These are the carbons related to the PPD structure. The carbons related to the PPA structure (**5** to **8**), were found at 128.4 (**7**), 130.8 (**6**), 130.9 (**5**), and 131.0 (**8**). The analysis suggests a repeating unit based on the structure reported.

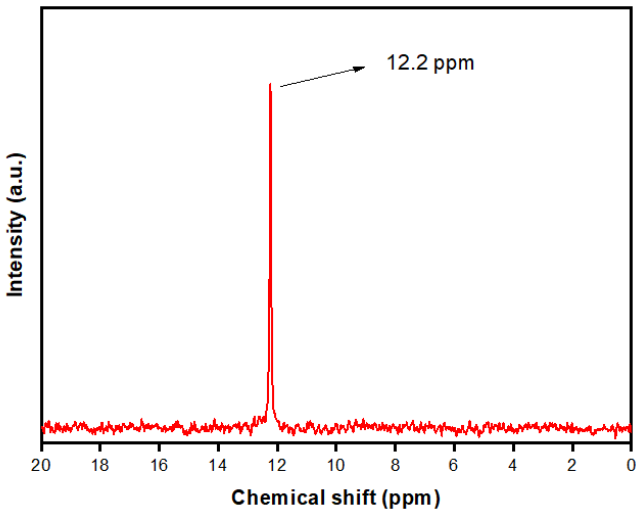

Figure 5-3. ^{31}P NMR spectra of FR1 compound.

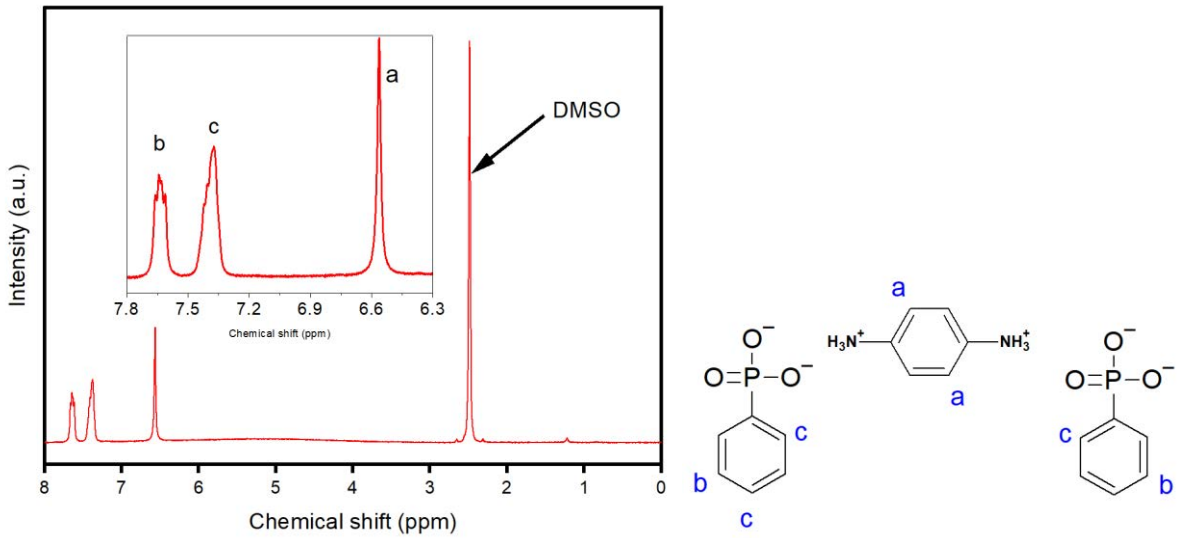

Figure 5-4. ^{1}H NMR spectra of FR1 compound.

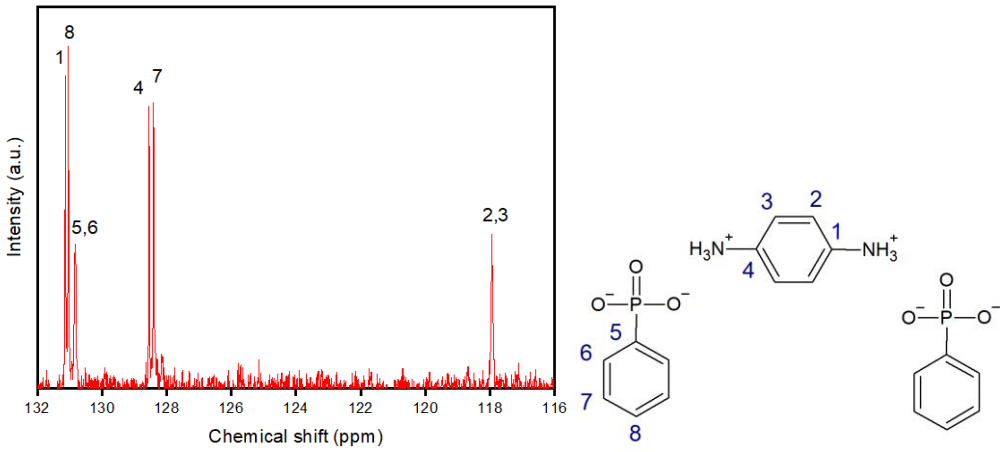

Figure 5-5. ^{13}C NMR spectra of FR1 compound.

5.3.2. *Foam preparation*

Neat PU foam (RPU) and FR RPUFs with 8 wt. % FRs were prepared by one-shot and free-rising method. The constant total amount of 8 wt. % FRs was chosen as reference ratio according to **Chapter 4** and the related publication [211]. Depending on the different ratios of EG and FR1 (100:0, 8:1 and 12:1), the samples were defined as RPU1, RPU2 and RPU3. Firstly, the B-side of the PU containing polyol, EG and FR1 were mixed by one-shot technique on a plastic beaker for 2 min with the help of a mechanical stirrer at 1000 rpm to prepare a uniform dispersion. Then, the correct amount of -NCO (A-side) was added and the mixture was stirred fast at 1200 rpm for 30 s until the system became homogeneous. The mixture was finally poured into a 250 mm × 250 mm × 60 mm open Aluminum mold, where the RPUFs raised in the vertical direction. After curing at room temperature for a minimum of 3 h, samples were cut according to the standards for the different test performed. The reference samples (PU and RPU1) were prepared following the same procedure without or with EG respectively. Formulations are plotted on the **Table 5-1** below**.**

Table 5-1. Formulae of EGFR1/RPUF composites.

Sample	PU resin (wt. %)	EG (wt. %)	FR1 (wt. %)	Ratio EG/FR1
RPU	100	0	0	-
RPU1	92	8	0	100/0

RPU2	92	7.1	0.9	8
RPU3	92	7.4	0.6	12

5.3.3. *Study of the cellular structure and thermal conductivity*

a) *Cellular structure and properties of final foams*

The effects of EG and EG-FR1 on the RPU samples on density, OC %, cellular morphology and thermal conductivity of RPUFs under study are evaluated and the corresponding results are listed in **Table 5-2**. SEM micrographs and the correlation between thermal conductivity and density for each sample are shown in **Figure 5-6** and **Figure 5-7** respectively.

The density is an important parameter, which determines the performance and final applications of PU foams. When EG or EG-FR1 was incorporated in RPUF, the foam density was increased in all the samples (**Table 5-2**). The density increased remarkably when FR1 was introduced in the RPU2 and RPU3. The reason is that FR1 is a reactive FR which can stablish bonds with the -NCO groups generating urea groups. As a consequence, the FR1 increased the degree of crosslinking in the foam structure. It was reported by Bhoyate et al. that the increasing phosphorous content in the foams would increase the density [233]. The density of the RPU2 sample with the highest FR1 content (0.9 wt. %) was the highest, followed by RPU3.

Regarding the OC %, all the foams had a closed cell structure since OC % has been always lower than 10 % (**Table 5-2**). Moreover, there was a slight decrease in OC % when FR1 was added. OC % decreased from 9.3 % for RPU1 to 6.5 % for the foam with higher content of FR1 (0.9 wt. %) RPU2. This decrease in OC % could be related to the generation of a more cross-linked solid phase with the incorporation of FR1.

Figure 5-6 shows the effect of EG and FR1 on the cellular structure of RPUF. It is clearly observed that the addition of 8 wt. % of EG (with 500 µm size) produced a significant decrease in cell size and also a more heterogeneous cellular structure compared with the neat PU. However, the presence of FR1 in the RPUF increased the cell size. The cell structure is still uniform after introducing of FR1 and showed from the analysis of SEM images (**Table 5-2**). The cell size decreased from 467 for neat PU sample to 383 µm for RPU1 sample due to the nucleation effect of the EG. In the case of foams with EG and FR1, the cell size increased when

the FR1 content was increased, showing a lineal correlation between the cell size and the FR1 content. It was reported by several authors that the phosphorous content in the foam, would lead to an increase of the cell size [182] [181]. Indeed, the presence of the P-N FRs increased the cell size during foaming because after their addition, the nucleation efficiency improved, which in turn increased the number of bubbles [234], thus augmenting the size of the cells.

Since the thermal properties are vital for RPUF applications, the thermal conductivity of the foams under study was measured and the values are collected in **Table 5-2** and thermal conductivity versus density for the RPU foams was shown in **Figure 5-7**. As explained in the previous **Chapter 4**, the thermal conductivity of RPUFs is well represented by the addition of three heat conduction mechanisms: conduction through the solid phase (λs), conduction through the gas phase (λg) and thermal radiation (λr) [213]. Despite the fact that EG addition could reduce the λr contribution to the thermal conductivity decreasing cell size as in the case of RPU1 and/or acting as infrared radiation absorbent [235] as in the case of samples with EG-FR1, the thermal conductivity increased in all the samples with FRs of this study. RPU1 increased the thermal conductivity due to the intrinsic thermal conductivity of graphite; especially for higher EG contents (above 6 wt. %) [225] and the increase on the density. For RPU2 and RPU3, the thermal conductivity increased with the introduction of FR1 as compared to RPU1. This could be explained considering the increase in the λs due to the following reasons: the increased density with the FR1 incorporation and the formation of a network of interconnected conductive EG particles throughout the insulating PU matrix, which together increased the thermal conductivity. It is shown in **Figure 5-7** a clear linear correlation between the thermal conductivity and the density, indicating that density is one of the main reasons justifying the increased thermal conductivity of the foams.

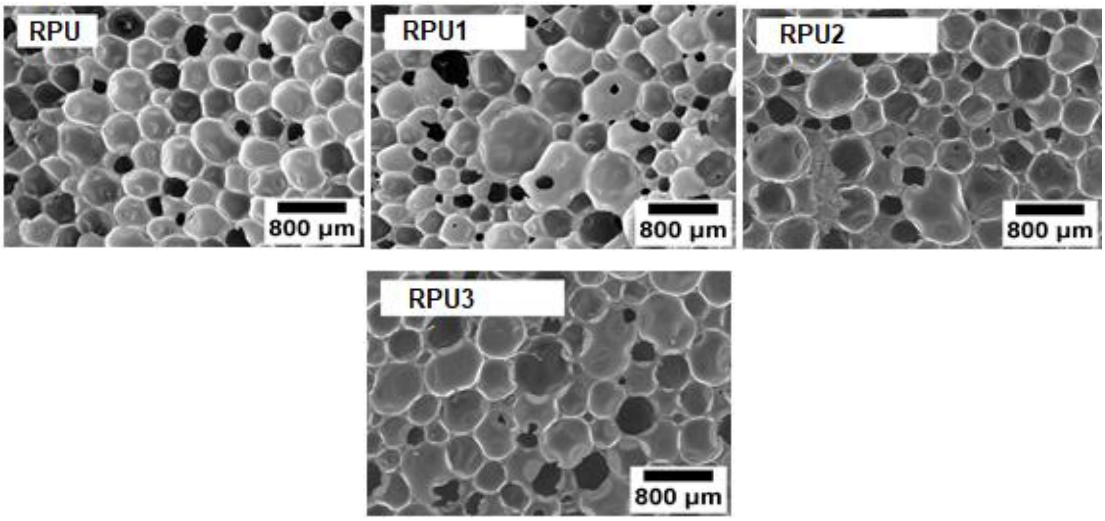

Figure 5-6. SEM micrographs of the EG/FR1-RPUFs under study.

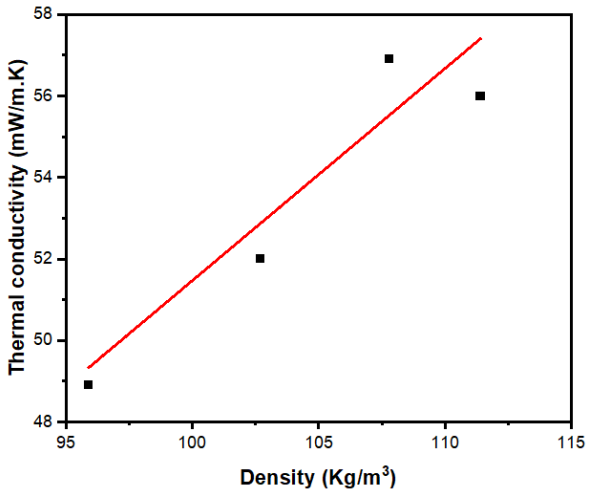

Figure 5-7. Thermal conductivity versus density for the foams under study.

Table 5-2. Density, OC %, mean cell size and thermal conductivity for each foam under study.

Sample	Density (Kg/m^3)	OC (%)	Mean cell size (µm)	Thermal conductivity (mW/mK)
RPU	95.9 ± 0.1	6.9 ± 0.2	467 ± 120	48.9 ± 0.1
RPU1	102.7 ± 0.6	9.3 ± 1.2	383 ± 181	52.0 ± 0.2

RPU2	111.4 ± 3.0	6.5 ± 1.9	495 ± 151	56.0 ± 0.3
RPU3	107.8 ± 4.1	8.5 ± 1.1	487 ± 160	56.9 ± 0.3

5.3.4. *Thermal degradation*

TGA is one of the most relevant analysis to evaluate the thermal properties of the RPUFs. TGA and DTG analysis of the studied samples under N_2 atmosphere are illustrated in **Figure 5-8** and **Figure 5-9**, whereas the parameters obtained were collected in **Table 5-3**. The corresponding thermal parameters were: $T_{5\ wt.\ \%}$, T_{max} and the remaining residue at the end of the test (wt. %).

All the studied samples showed a similar degradation curve. The degradative process consisted of a 2-steps process [48], [211]. The first step of degradation for RPU was between 150 and 250 ºC with *ca*. 7% weight loss. $T_{5\ wt.\ \%}$ for this sample was indeed 231.1 ºC. This step may be associated to the evaporation of small molecules and unreacted -NCO monomers [46]. The second step of degradation occurred between 250 ºC and 620 ºC, and it is mainly due to the formation of the original PU components (-NCO and polyols) by the break of urethane bonds in the HS [47]. First, polyol structures in the SS start to decompose and then, as the -NCO formed remains, products with more complexity are formed. Finally, these compounds decompose into volatile products like CO_2, HCN or NO_2, which are generated in the final stage of the degradation process [217].

When RPU1 and EG-FR1 series of samples were analyzed, the degradation of the material started earlier than neat PU. For RPU and RPU1, the $T_{5\ wt.\ \%}$ on the DTG curves for the RPU were 231.1 and 226.0 ºC respectively. There is not a big difference between them, as EG slightly reacts with PU [218]. However, the earlier degradation temperature of the EG-filled RPUF was attributed mainly to the oxidation and degradation of the polymer matrix promoted by the residual acid inside the layers of EG [64], [207] and its higher thermal conductivity. For the EGFR1 samples, the $T_{5\ wt.\ \%}$ was lower than RPU1. Meanwhile, the T_{max} for the RPU was 328.7 ºC, whereas it decreased smoothly to 327.4 ºC for RPU1, and is further reduced for the EGFR1samples series, meaning that FR1, accelerated the degradation mechanism of PU by a catalytic effect of the derived phosphate compounds [2], [48], [69]. It could be explained by the

release of phosphorous-based compounds from FR1 degradative mechanism, which catalyzes the decomposition of the RPUF matrix to its initial components (-NCO and polyols) and so, increasing the degradation rate of the RPUF [69], [76] (**Scheme 5-1**). Also, the increasing thermal conductivity of RPU2 and RPU3 (**Table 5-2**) contributed to conduct the heat faster trough the PU structure.

On the other hand, the residual char increased for all samples containing FR1 with respect to RPU and RPU1. The residue amount increased up to a maximum of 17.2 wt. % for RPU3 while RPU1, showed only 14.9 wt. %. Bearing in mind the "worm" barrier effect of EG, with increases the char residue in the foam [69], FR1 catalyzed the degradation of PU but increased dramatically the char residue remaining at the end of the process [48], [231]. Thus, supported that a reinforced char layer was formed which acted as a thermal barrier, protecting the foam from further decomposition and limiting the degradation of the PU matrix in the latter stages of the degradation process. The explanation behind this phenomena was mainly due to the charring effect from the FR1 phosphorous FR decomposition, similar to commonly known phosphorous-based FRs [2], [80], [106]. Phosphate released compounds from FR1 could decompose to form poly(phosphoric acid), which catalyzes char formation to a more stable species, such as urea or isocyanurate as reported by Velencoso et al. [236]. Therefore, EG and FR1 combined together as additives, promoted the formation of additional char residues synergistically.

Table 5-3. TGA data for EGFR1 samples.

Sample	$T_{5\ wt.\ \%}$ (ºC)	T_{max} (ºC)	Wt. % Residue
RPU	231.1	328.7	9.8
RPU1	226.0	327.4	14.9
RPU2	224.2	323.6	16.7
RPU3	222.9	323.3	17.2

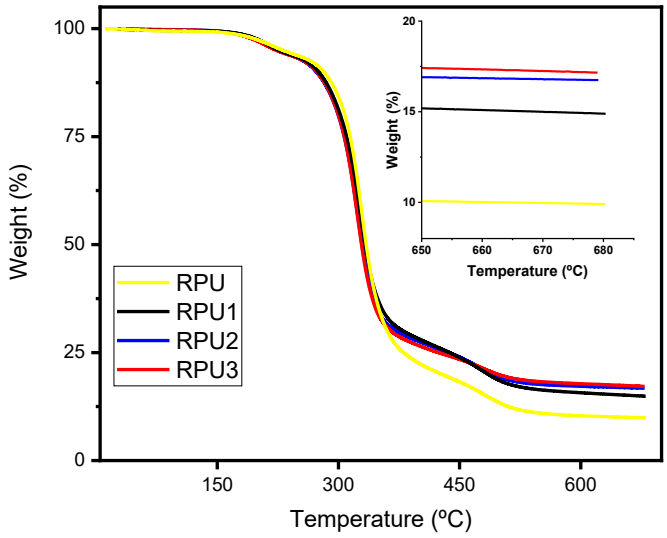

Figure 5-8. TGA curves of EGFR1 samples.

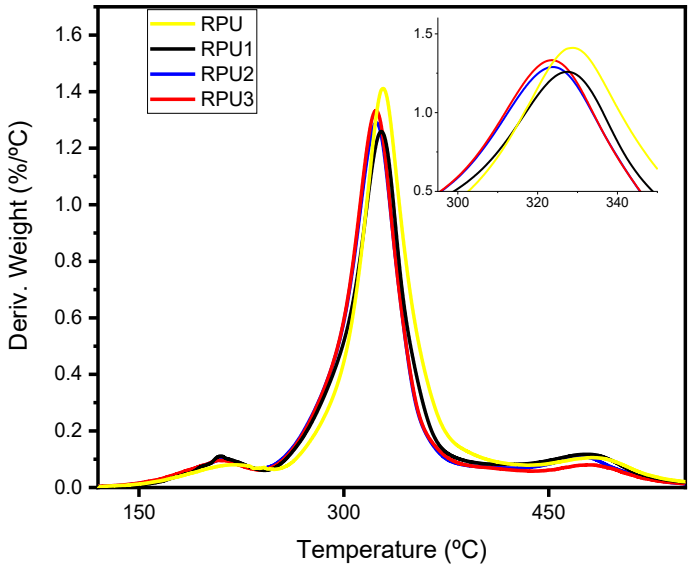

Figure 5-9. DTG curves of EGFR1 samples.

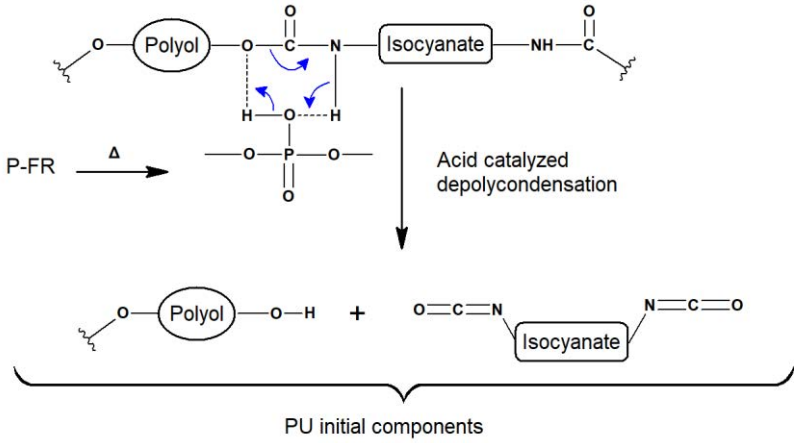

Scheme 5-1. Schematic illustration of the catalytic action for the de-polycondensation reaction of PU by released phosphoric acid during the degradation of P-FRs [76].

5.3.5. *Fire behavior*

a) *LOI and UL94 tests*

LOI and UL94 tests of all the RPUF specimens have been performed, and the data were collected in **Table 5-4** and **Figure 5-10 d)**. As showed in the previous chapter, the LOI values of the reference RPU foam is just 19.2 % and the value of RPU1 increased to 29.2 %. EG inhibited the flame spread as a good isolating material into RPUFs. To further improve the fire performance of RPU1, a phosphorous-containing FR1 was mixed with EG to prepare RPU2 and RPU3 foams. The LOI value of RPU3 increased to 29.8 % with 0.6 % FR1 addition, showing a potential synergistic effect between EG and FR1 as additive FRs. However, the LOI value of RPU2 was turn lower than RPU1. It means that higher FR1 content will accelerate the fire spreading through the sample and the FR performance would be decreased.

Under the UL94 test, RPU, as a neat and flammable PU sample, was not classified under UL94 test standards. The reference RPU1 foam containing 8 wt. % EG achieved V-0 rating according to the standards of the UL-94 test. It can be observed that with addition of FR1, RPU2 and RPU3 can maintain V-0 rating as well. Furthermore, with the aim of investigating on the detailed performance under the UL94 test, the average after flame time ($t_1 + t_2$) for each individual sample was reported. It can be observed that the burning rate was clearly diminished when using a ratio of EG to FR1 of 12:1 (RPU3). But for the RPU2 specimen, the flame keeps longer since more FR1 was added, which is in accordance with the results of LOI test.

Therefore, the additive combination of these two FRs obtained the highest standards among LOI and UL94 tests at 8 wt. % loading when the ratio of EG and FR1 was 12:1.

Table 5-4. LOI and UL94 tests results for the EGFR1 samples.

Sample	LOI (%)	UL94 rating	Average time (t_1+ t_2) (s)
RPU	19.2	NO RATING	>30
RPU1	29.2	V-0	5.6 ± 3.4
RPU2	28.4	V-0	6.1 ± 5.4
RPU3	29.8	V-0	5.1 ± 1.2

b) *CCT test*

CCT was performed at a heat flux of 50 kW/m^2. The parameters evaluated were: PHRR, TSP and THR. The curves for the samples regarding PHRR and TSP and THR are shown in **Figure 5-10 a-c)** respectively. The CCT data are summarized in **Table 5-5**. An analysis of the smoke behavior was included in **Figure 5-11** and **Table 5-6.** The samples were evaluated based on these parameters.

First, the HRR curves for the RPUF samples were analyzed (**Figure 5-10 a)**). The PHRR was rapidly raised after the ignition (less than 3s). The low thermal inertia of insulating foams and the porous structure of RPUFs increased the contact area between the matrix and oxygen [1], thus igniting the samples fast. PHRR was 181 kW/m² for the commercial reference RPU without any FR additive. For the RPU1 reference sample, PHRR value decreased to 130 kW/m², which is nearly 28 % reduction with respect to RPU. For the FR1-containing samples, the PHRR values of RPU2 and RPU3 were reduced 35 % and 45 % with respect to RPU respectively. The results of RPU3 disclosed a synergistic effect between EG and FR1 at 12:1 ratio, which means that the two additive FRs could work together to inhibit the combustion intensity and reduced the spreading speed of the flame. However, with the slight increase of FR1 in RPU2, the PHRR value is higher than RPU3, meaning that an increasing loading of FR1 could not be beneficial as compared with EG, which is in accordance with the fire performance in the UL94 and LOI tests.

THR (**Figure 5-10 c**) is a measurement of the heat released by combustion during a given time. The reference sample PU showed a THR value of 51 MJ/m². The introduction of EG

reduced this value by 32 % for the RPU1 sample. On the contrary, the introduction of FR1 in RPU2 and RPU3, slightly increased the THR values with respect to RPU1. This result suggests that the fragments released by FR1 during combustion were further burned, increasing the THR of EGFR1 samples in comparison with RPU1 [237].

Because of the danger of smoke in a fire hazard is the biggest threat to people's lives, reducing the smoke production (TSP) (**Figure 5-10 b**) was also a signal of a good FR effect. The TSP value of RPU was 6.5 m², while the addition of 8 wt. % EG reduced the reference TSP value to 2.3 m², meaning a dramatic 65 % reduction with respect to the neat foam. The EG addition reduced the smoke production due to the formation of a char barrier, which blocks the mass transfer and most of the PU materials remained in char residue. However, with the addition of FR1, the smoke production is slightly increased in both RPU2 and RPU3 compared to RPU1. It can be related to the fire reaction was interrupted by radical capture mechanism in gas phase, which was proved in some published work [4]. Several authors [2], [18] proposed a mechanism explanation for this phenomena in which the phosphorous FRs, promoted charring on the condensed phase and releasing larger molecular fragments and non-combustible gases on the gas phase, leading to a stronger smoke [237]. Moreover, this gas-phase mechanism can be used to explain the increase of the CO yield, and reduction of the complete combustion products (CO_2) as reported in **Figure 5-11** [69].

Table 5-5. Data of EGFR1 composites at 50 kW/ m^2 from CCT.

Sample	PHRR (kW/m²)	THR (MJ/m²)	TSP (m²)
RPU	181 ± 10	51 ± 6	6.5 ± 0.6
RPU1	130 ± 17	35 ± 3	2.3 ± 0.5
RPU2	118 ± 2	47 ± 1	3.3 ± 0.2
RPU3	100 ± 4	39 ± 1	2.7 ± 0.4

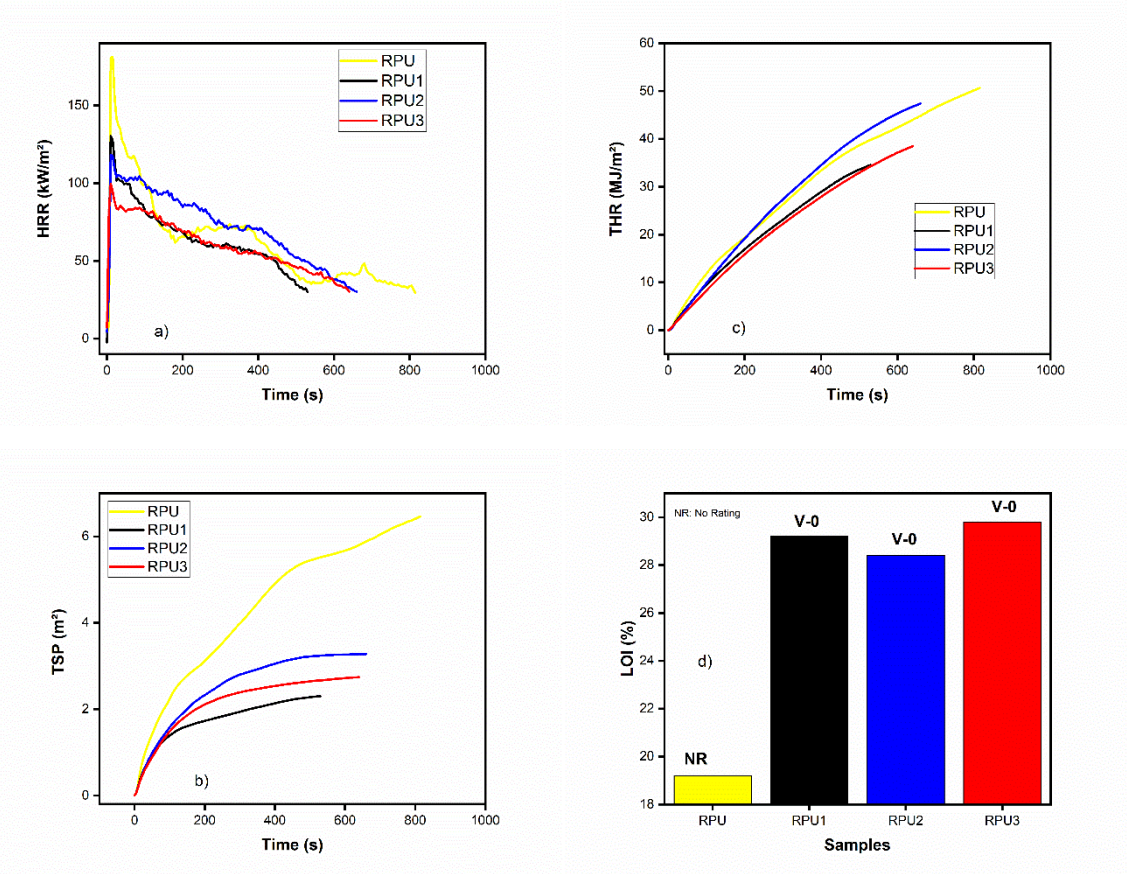

Figure 5-10. a) HRR, b) TSP and c) THR curves of EGFR1 samples at 50 kW/m^2 and d) LOI and UL94 test.

➢ Smoking behavior analysis

The smoking behavior of the analyzed samples was performed through the analysis of the COP and CO_2P (CO and CO_2 production respectively). The curves for Av-COP, Av-CO_2P (average COP and CO_2P respectively) and the average COP/CO_2P ratio were presented in **Figure 5-11** and the data was showed in **Table 5-6.**

The CO production curves were showed in **Figure 5-11 a)**. The production of CO was diminished when adding EG as FR in comparison with the neat PU foam. The average COP production for RPU was 1.42 mg/s whereas this value, was decreased an impressive 37 % in the RPU1 sample. Moreover, the addition of FR1 contributes differently to the COP. Compared to RPU1, the curves of RPU2 showed higher CO production, mostly before 250 s. On the other hand, RPU3, showed reduced CO production over the time, delaying in a very effective way

the CO released. Attending to the average values of the CO production (Av-COP) on **Table 5-6** and **Figure 5-11 a)**, RPU2 and RPU3 showed reduced CO production with respect to RPU. Interestingly, RPU3 obtained the lowest Av-COP value with only 0.74 mg/s, which it was a 17 % lower than RPU1 and an impressive 48 % reduction with respect to the original PU neat foam (RPU). Thus, a loading of around 0.6 wt. % of FR1 was beneficial for the CO reduction.

The production of CO_2 was showed on **Figure 5-11 b)**, and **Table 5-6**. **Figure 5-11 b)**, showed that the production of CO_2 was increased when adding EG as a FR in comparison with the neat PU foam. The average CO_2 production (Av-CO_2P) for the neat PU foam was 42.6 mg/s whereas this value, was increased a 9 % in the RPU1 sample. A possible explanation for this phenomena resides in the fact that EG releases CO_2 when expanding, in accordance to Camino et al. [64], thus increasing the CO_2 production. Moreover, the addition of FR1 contributes again differently to the CO_2P. By comparison with the neat PU sample, all the samples with FR1 as an additive, increased the CO_2P. This effect was reported by Modesti et al. [226], explaining that the decrease in flame temperature due to the endothermic reaction of a phosphorous-based FR, lead to a higher production of CO_2 instead of CO, in accordance to the **equation 1** below:.

$$CO_2 + C \rightleftharpoons 2\,CO \qquad \Delta H = +172\ kJ/mol \quad (1)$$

Attending to the average values of the CO_2P (Av-CO_2P) on **Table 5-6** and **Figure 5-11 b)**, RPU3 showed reduced CO_2 production with respect to the reference RPU1. In detail, the reduction was about a 5 % with respect to RPU1. On the other hand, RPU2 increased the CO_2P up to a 13 %. The average CO/CO_2 ratio was plotted on **Figure 5-11 c)** and the data was shown in **Table 5-6**. As previously described by Modesti et al. [201], the greater this ratio, the lower the combustion completeness, and therefore the greater the toxicity of the smokes developed and consequently the more dangerous the material. The highest COP/CO_2P ratio was obtained by RPU, due to the lack of FR effectivity. Thus, the combustion of PU foam is a harmful process of a very dangerous material with high CO production from the flammability point of view. As far as EG entered the system, the CO/CO_2 ratio was decreased up to a 42 %. The addition of FR1 in RPU2, boosted the ratio up to a maximum of a 12 % higher than RPU1. From that point, the increasing EG to FR1 ratio diminished the CO/CO_2 until a minimum of a 50 % reduction with respect to RPU for the RPU3 sample, which obtained the lowest CO/CO_2 ratio. Owing to this fact, the combustion phenomena for the samples with FR1 as a FR, is more effective, due

to the higher CO_2 production but lower CO release [69]. For this reason, a synergistic effect, with lower CO production, was confirmed for the RPU3 sample based on the presented data. The CO production was dramatically reduced, improving the safety of the material and the average CO/CO_2 ratio was indeed improved.

Table 5-6. Average data of COP and CO_2P of the EGFR1 composites at 50 kW/ m^2 from CCT.

Samples	Av-COP (mg/s)	Av-CO2P (mg/s)	Av-COP/Av-CO2P (mg/mg)
RPU	1.42	42.6	0.0334
RPU1	0.89	46.5	0.0192
RPU2	1.13	52.5	0.0215
RPU3	0.74	44.3	0.0168

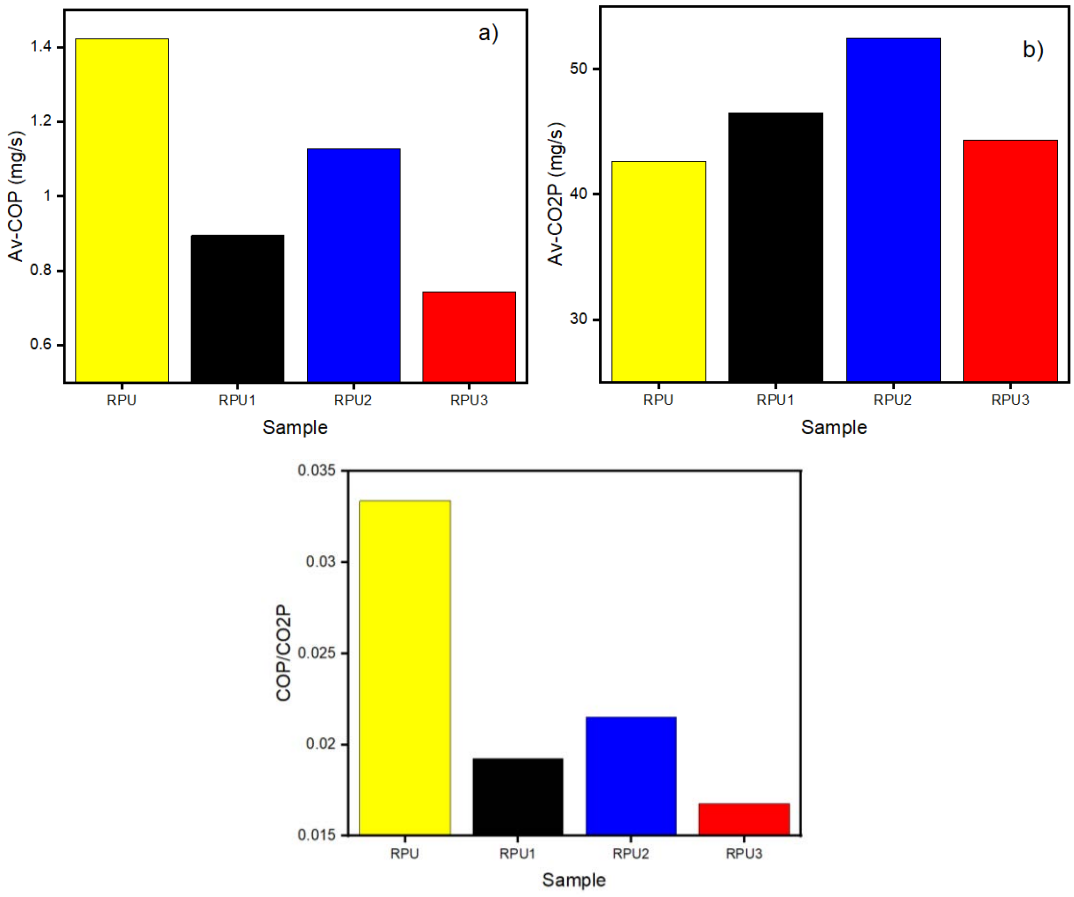

Figure 5-11. a) Av-COP and b) Av-CO_2P and c) COP/CO_2P ratio of EGFR1 samples at 50 kW/m^2 after CCT.

- **SEM char analysis**

The chars were indeed analyzed by SEM after the CCT (**Figure 5-12**). In the RPU1 char, it can be observed the "worm-like" particles created by EG expansion. However, the char showed many cracks and holes were heat could penetrate, thus showing the damage on the structure by EG (**Figure 5-12 a, b**). Then, RPU3 char was analyzed. It can also be clearly seen the worm structure produced by EG expansion upon heat covering all the char structure. Indeed, round FR1 particles can be observed completing and reinforcing the char formed (**Figure 5-12 c and d)**. Thus, confirm the synergistic char structure between both FRs.

Moreover, and EDX analysis of the chars were performed to analyze the elements present on the char structure (**Figure 5-13**). The analysis of RPU1 (**Figure 5-13 a**), revealed the only presence of C and O. On the other hand, RPU3 (**Figure 5-13 b**) showed an increase on the intensity of O and the presence of P, probably due to the formation of poly-phosphoric acid (by the poly-condensation reaction of phosphoric acid when the temperature is increasing) and enriches the char carbonaceous layer produced by EG [70], [106], [152], [238].

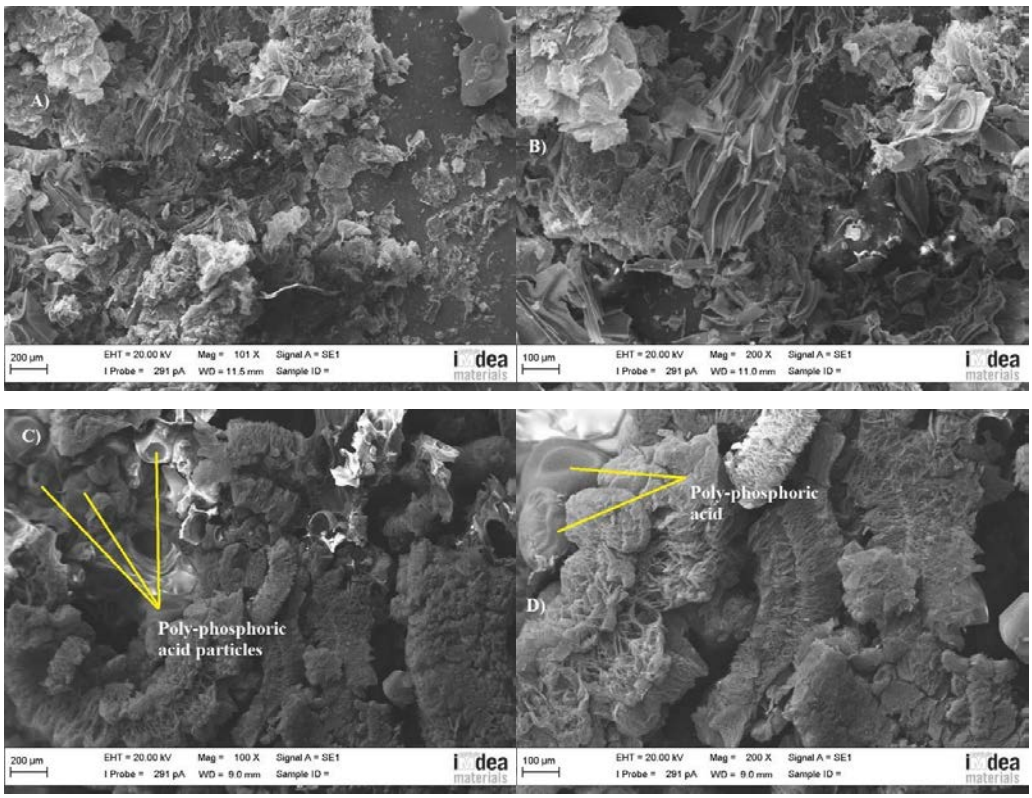

Figure 5-12. SEM chars observed by SEM of a), b) RPU1 and c), d) RPU3.

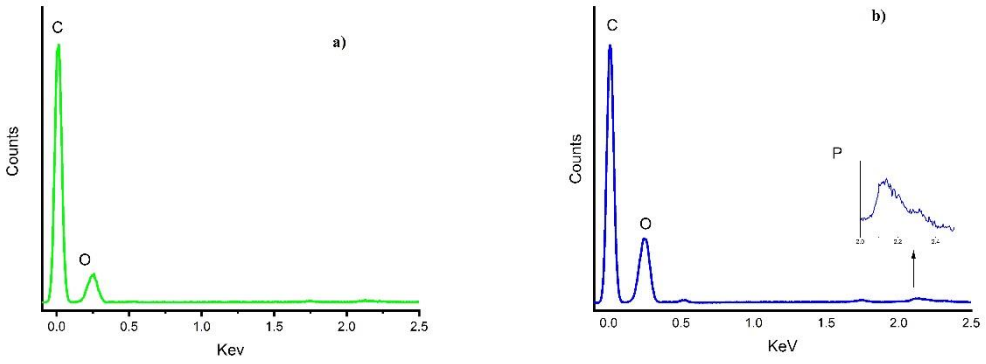

Figure 5-13. EDX elemental analysis of a) RPU1 and b) RPU3.

c) *FR proposed mechanism*

The FR mechanism of synergistic effect of EG/FR1 compounds in RPU3 was proposed in **Figure 5-14**. Firstly, EG expands and produces some gases during combustion [64], which blows the graphite structure to form some worm-like char protective layer (**Figure 5-14 a)** [64], [210]. The shaggy char barrier was able to block the fire and heat spread [69]. For the FR1 FR, two-action mechanism was proposed [1], [73], [231]. On one hand, the decomposition of FR1 evolves radical P-based scavengers such as phenyl-PO· and PO·, which can capture the free radicals (**Figure 5-14 b)** and interrupt the combustion process along with the release of gaseous NH_3, diluting the combustible gases [95], [239], [240]. On the other hand, a char forming with a reinforcing effect by FR1 in combination with that of EG, which enhanced the FR action as suggested by Wang X. et al. [18] and showed in **Figure 5-14 c)**. In general, the proposed mechanism based on a gas phase action of FR1 and the condensed phase action of FR1 and EG, could enhance the FR performance of a RPUF [2], [82], [106], [204].

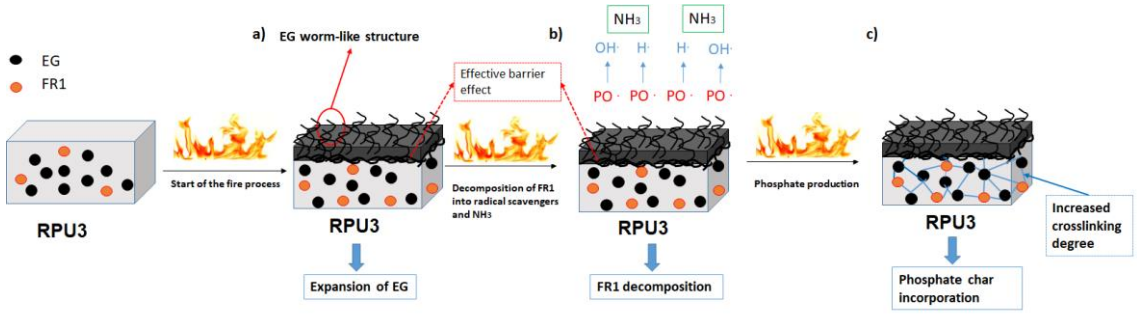

Figure 5-14. Proposed FR mechanism of RPU3.

5.3.6. *Compressive strength*

Compression tests were performed at a constant rate of 3 mm/min, and the data obtained for the compressive strength are shown in **Table 5-7**. The compressive strength of the samples decreased slightly with the addition of EG, in accordance with previous results [210], [211], [226]. The poor interfacial adhesion between EG and the PU matrix and the large particle size of EG, leads to slippage among these two components and damages the cell walls, affecting to the integrity of the foam. This effect lead to an inhomogeneous structure and resulted in a decrease of the compressive strength performance [47]. Nevertheless, the compression strength of both RPU2 and RPU3 increased with the addition of FR1. In RPU2, the compression strength was 0.89 MPa, higher than the reference RPU value by a 5 %. When the ratio of EG/FR1 was 12:1, the compression strength raised up to a maximum of 0.92 MPa, a 9 % higher than RPU. It suggests that FR1 can be a potential synergistic agent to solve the negative effects of EG in the foam structure, mainly by increasing the density of RPUFs. Despite that other P-FRs such as DMMP, have a plasticizer effect that increases the cell size and reduces the compressive strength of the foam [241], [242], it was reported by several authors that the introduction of a P-FR on a PU matrix improved the compressive strength of the RPUF [18], [80]–[82], [181], [243], [244]. Several factors could explain these phenomena and its influence on the density. Mostly, the stiff phenyl groups on the FR1 chemical structure, imparted rigidity to the structure due to the lower chain mobility. Owing to the presence of an H-active specie, such as FR1, it could also react with -NCO [80] and produce urea groups (**Figure 2-5 b.1**) as N-H compounds are much more reactive than the -OH compounds [16]. This effect provided a reinforcing effect to the RPUF and improved the mechanical properties as the HS of PU was enhanced [245]. However, this conclusion needs further evidence in future studies.

Table 5-7. Mechanical properties of EGFR1 samples.

Sample	Compressive strength (MPa)	Standard deviation (%)
PU	0.85 ± 0.06	7.4
RPU1	0.83 ± 0.02	2.3
RPU2	0.89 ± 0.02	2.5
RPU3	0.92 ± 0.03	3.7

5.4. Conclusions

In this work, the influences of EG and FR1 compounds on the properties of RPUF matrix were studied by comparing the cellular structure, thermal, fire and mechanical properties. FR1 was prepared successfully, and its chemical structure as a phenylphophonic aniline salt was confirmed by FTIR, ^{1}H, ^{31}P and ^{13}C NMR spectroscopy. The foam density increased with the inclusion of EG and FR1 in the PU matrix, since the amine groups of FR1 could react with the PU components. Regarding the thermal properties, FR1 increased the thermal conductivity mostly due to the previously mentioned increase of density. The degradation of PU was accelerated due to the release of H_3PO_4, which catalyzed PU de-polycondensation, and the char residue increased as well due to the production of poly-phosphoric acid and more thermally stable PU-derived species. The performance of the FR-RPUFs in the LOI and UL94 tests was improved. The LOI of RPU3; increased to 29.8 % and the UL94 obtained V-0 rating. In the CCT, the parameters PHRR, THR and TSP were improved with respect to those of the neat foam. However, as the loading of FR1 continues to increase to 0.9 wt. % (RPU2), the fire performances of RPU2 become worse. A synergistic FR mode that combinates that of a barrier against the fire by the EG expansion and a condensed phase charring effect towards a gas-phase quenching effect by the addition of FR1 was proposed to explain these results. Finally, the compression performance showed that EG-FR1 filled RPUFs had better compressive strength than those of RPU and RPU1. The reason was mainly due to the stiff phenyl groups of FR1 and covalent bonds formed between FR1 and -NCO which increased the density. Therefore, in accordance with the results presented, a synergistic effect between EG and FR1 in the RPUF matrix was herein demonstrated.

CHAPTER 6

6. The effective use of GO into a novel partly biobased synthetized RPUF

"The present is theirs; the future, for which I really worked, is mine"

-Nikola Tesla

6.1. Introduction

Traditionally, the raw materials of RPUFs (polyols and -NCO) are obtained from petroleum as feedstock. However, over the last years, the ecological, political and economic problems related to petroleum along with the flammability of the petroleum derivatives, made it grow interest in the development of alternative bio-renewable feedstocks for the chemical industry [246]. Polyols can be obtained from green vegetable sources to replace the common petroleum-based ones [157]. One of the best natural raw material for a bio-polyol synthesis is castor oil. Castor-oil is a natural oil with a fatty acid structure containing double bonds from ricinoleic acid and secondary -OH groups into his chemical structure [170]. Nonetheless, primary -OH groups are preferred for a polyol as they are around three times more reactive than secondary ones, thus giving stability to the RPUF [173]. To increase the primary -OH group content of castor oil, transamidation with DEOA is a widely reported procedure [175]. Apart from that, it has been reported by Wang et al. [247] that the use of castor oil as polyol in a high percentage (60 wt.

%) could improve the compression performance of a PU foam. However, to impart flame retardancy, deeper changes are still necessary. The double bonds of castor oil can be modified by several process. In order to obtain a FR polyol, first an epoxidation followed by ring-opening reaction with the desired FR modifier is the procedure suggested by several authors [166], [248]. Commonly, most of the reactive-FR polyols are phosphorus containing compounds, as it is known to be a relationship between their FR efficiency and the phosphorus content [249]. Also, their good interactions with -NCO influences positively on density [166], insulation [183], compressive strength [80], [181], and char formation [182].

On the other hand, carbon derivatives; like EG, has proved to obtain good FR results in the previous chapters of this thesis. However, the decreasing compressive performance obtained is still a problem for insulating RPUF materials and the industry. In the recent years, another derived-carbon materials such as graphene derivatives, have increased growing attention to all researchers [124]. Commonly, graphene-based materials such as GO and rGO have gain importance thanks to their unique combination of properties, such as mechanical strength and thermal stability [250] or electrical properties [251]. To use it in RPUF, GO is preferred instead of rGO due to its large number of oxygen-containing functional groups, showing hydrophilic in nature [134] as well as disrupt the conjugation of aromatic rings, thus improving the electrical insulation capacity [126], [252] and the thermal insulation properties of the RPUF [138]. These oxygen functionalities on the GO surface provide interesting benefits for PU nanocomposites in relation to the thermal conductivity and mechanical performance. They can act as scattering points for the phonons transmission [253] and decrease the thermal conductivity as well as increase the interfacial adhesion with the PU matrix and improve the mechanical properties [127], [146]. Indeed, the compression properties of graphene derivatives in PU foams have been studied by several authors, including Liu et al. [254], who used 3 wt. % of graphene to improve the compressive performance of TPU foam for about a 185 % or Pokharel et al. [147], improving the mechanical properties of PU nanocomposites by the enhancement of HS and SS of PU structure with 4 wt. % of GO loading. Yan et al. [215] reported that graphene nanosheets (GNSs) could enhance the compression and thermal stability of RPUFs even more than CNTs at very low loading of GNSs (0.3 wt. %). Moreover, the combination of carbon materials is highly desirable to impart different characteristics. For example, Kim et al. [149] used GO and graphite, to enhance the microstructure and mechanical strength of PU foams or Jiang et al. [255], who used GO/carbon fiber combination to improve the tensile strength of PU elastomers.

However, not very much research has been done to improve both the flame retardancy and compressive strength of natural-based PU products by using different carbon derivatives.

Herein we describe the synthesis of a new-efficient biobased FR polyol obtained from a modified-vegetable oil functionalized with phosphorous FR and the addition of EG combined with small amount of GO as FRs. The as-created RPUF was studied and its influence on the thermal, FR and mechanical properties will be discussed. The present chapter was based in a recent publication from our research group [256].

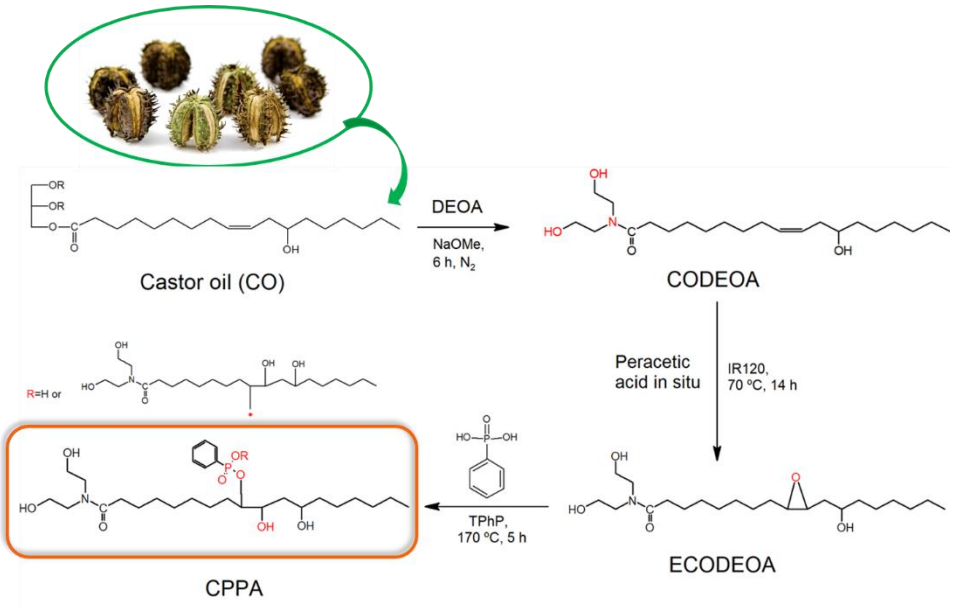

Scheme 6-1. Schematic representation for the synthesis of the FR polyol.

6.2. Materials

6.2.1. *Materials*

PU raw materials are provided by Smooth-On (FormX Spain, Spain) FOAM-IT! ™ 5. This foam was used as commercial reference and their -NCO (Part A, NCO % = 30 %) and weight mixing ratio (1.15:1 between both A and B components) were the selected ones to compare and obtain a density close to the commercial insulation foams. Castor oil, DEOA (98 %), NaOMe (95 %), ethyl acetate (99.5 %), Amberlite IR120 hydrogen form catalyst, HAc (99.8 %), H_2O_2 (30 % solution), toluene (99.8 %) and TPhP (99 %) were all purchased Sigma-Aldrich and used without further purification. Polycat 34 and DABCO K-15 as catalyser 1 and 2 respectively and DABCO DC193 as surfactant were kindly provided by Airproducts iberica (Bellaterra, Spain).

PPA (98 %) was purchased from TCI Europe. EG, GHL PX 98 HE (300 µm particle size) for GO synthesis and GHL PX 99 32 350 (expansion volume of 350 cm^3/g, 500 µm particle size) as additive FR, were kindly provided by Georg H. Luh, GmbH (Walluf, Germany). $KMnO_4$ (98 %) was purchased from Alfa-Aesar whereas H_2SO_4 (95-97 %), H_3PO_4 solution (H_3PO_4, 85 wt. %), HCl (37-38 %) and NaCl were all purchased from Sigma-Aldrich and used without further purification.

6.2.2. *Synthesis of the biobased polyol (CPPA):*

a) *Synthesis of castor-oil diethanolamine (CODEOA)*

The procedure used was based on the literature [16]. In detail, 250 g (0.27 mol) of Castor oil and 0.5 g of NaOMe were introduced in a 500 mL three-necked round-bottom glass flask. Then, 52 mL (0.54 mol) of DEOA (mol ratio Castor oil/DEOA 1:2) were added dropwise to the flask. The transamidization of castor oil was performed at 110-120 ºC for 6 h under N_2 atmosphere. After that, the product was dissolved on ethyl acetate and cleaned with 15 wt. % NaCl solution until pH around 7 was achieved. Finally, the product was dried over Na_2SO_4 saturated solution and the solvent was evaporated in a rotatory evaporator. (294.35 g, 95.8 % yield). The resulting reaction is shown **Scheme 6-1**. ^{1}H NMR (DMSO-d_6, ppm): For Castor oil, δ 0.77 (-CH_3), 1.10–1.27 (-CH_2- of the long fatty acid chain), 1.33 and 2.08 (-C**H**$_2$–CH-(OH)), 1.93 (-CH_2-C=C), 1.49 (-C**H**$_2$-CH_2-COOR), 2.20 (-CH_2-C**H**$_2$-COOR), 4.0-4.18 (-C**H**$_2$-O-C=O), 5.15 (-CH_2-**CH**-CH_2-), 5.22–5.42 (-C**H**=C**H**-), 3.48 (-C**H**-OH); ^{13}C NMR (DMSO-d_6, ppm): 172.7, 130.9, 127.3, 70.7, 69.3, 62.4; FTIR (cm^{-1}, KBr window): C=O (1745 cm^{-1}), -OH stretching (3363 cm^{-1}), C=C stretching (3009 cm^{-1}) [248], -CH_2- bending (1457 cm^{-1}) [257], [258] and C–OH stretching (1159 cm^{-1}) [166]. For CODEOA, ^{1}H NMR (DMSO-d_6, ppm): 3.32 and 3.50 (N-(C**H**$_2$)$_2$-OH); ^{13}C NMR (DMSO-d_6, ppm): 59.0, 50.5 [248] ; FTIR (cm^{-1}, KBr window): N-H stretching (3405) and bending (1628) [258], C-N stretching (1057) [248]. The FTIR of Castor oil and CODEOA is shown in **Figure 6-1 a)** and the NMR spectra is shown in **Figure 6-2 a-b)** and **Figure 6-3 a-b).**

b) *Synthesis of epoxidized castor oil (ECODEOA)*

Epoxidation of CODEOA follows a commonly known procedure on the literature [248], [259]. In detail, in a three-necked round-bottom glass flask, CODEOA (150 g) was dissolved in

toluene (200 ml) at room temperature. Then, HAc (11.1 ml) and Amberlite IR120 (4.75 g) as resin catalyst were added following a literature procedure [260]. After 30 minutes stirring, H_2O_2 (60 mL) was added dropwise, and the reaction was heated at 70 ºC for 14 h. The reaction was first filtered to remove the catalyst. Then, organic-inorganic mixture was separated with a glass decanter funnel. Finally, the organic phase was cleaned with NaCl 15 wt. % solution until pH=7, dried over Na_2SO_4 saturated solution and the solvent was evaporated by vacuum distillation in a rotatory evaporator. (145.35 g, 93.0 % yield). ^{1}H NMR (DMSO-d_6, ppm): 2.98 (C**H**-O-C**H**) while is still present an amount of the double bond from unreacted CODEOA due to the not completion of the epoxidation reaction [259] and 2.3 (C-O-C-C**H$_2$**-C=C-) [166]. ^{13}C NMR (DMSO-d_6, ppm): 56.1 and 54.2 (C-O-C) along with a peak at 48.9 ppm in accordance to Ding et al [248]. Unreacted CODEOA is present. FTIR (cm^{-1}, KBr window): C-O-C (epoxy, 856) [166], although some unreacted monoglyceride polyol with C=C is still present at 3009 cm^{-1} in accordance to similar studies [166], [248]. The FTIR spectra of ECODEOA are shown in **Figure 6-1 a)**, whereas the NMR is shown in **Figure 6-2 c)** and **Figure 6-3 c).**

c) *Synthesis of castor oil functionalized PPA (CPPA)*

ECODEOA (100 g) was introduced in a two-necked round-bottom glass flask with stirring. The procedure was inspired by those similar in the literature [166], [248], [259]. TPhP (0.5 g) was added as ring opener catalyst. Then, PPA (39.4 g) was introduced trough a plastic funnel and the temperature was raised to 170 ºC. The reaction was performed during 3 h until a homogeneous mixture was obtained. Finally, the reaction was cooled down to room temperature and the product was collected as a viscous red liquid. (134.15 g, 96.3% yield). The procedure was summarized in **Scheme 6-1**. ^{1}H NMR (DMSO-d_6, ppm): 7.15-7.66 (-Ph, benzene ring) [248], 3.66 (C–O**H**) [166], [259] and 3.00 (**H**C-O-P). ^{13}C NMR (DMSO-d_6, ppm): 120-140 (-Ph, benzene ring). ^{31}P NMR (H_3PO_4, ppm): 13.1. FTIR (cm^{-1}, KBr window): -OH groups vibrations (3200-3400), C-H of Ph-H from PPA (3055) [183]. A detailed image was presented to show the peaks between 750-1800 cm^{-1} (**Figure 6-1 b)**): N-H stretching of amide group (1627) [175], the phenyl skeleton (1437) [183]; P-Ph bond (1463 and 1595 cm^{-1}) [85]; P=O (1137) [261]; P–O–C (1068) [153] and 750 (P-C) [183], confirming the reaction between PPA and epoxy group. The FTIR spectra of CPPA is shown in **Figure 6-1 a-b)**, whereas the NMR is shown in **Figure 6-2 d)**, **Figure 6-3 d)** and **Figure 6-4**. A proposal for the oligomeric structure is shown in **Figure 6-5**.

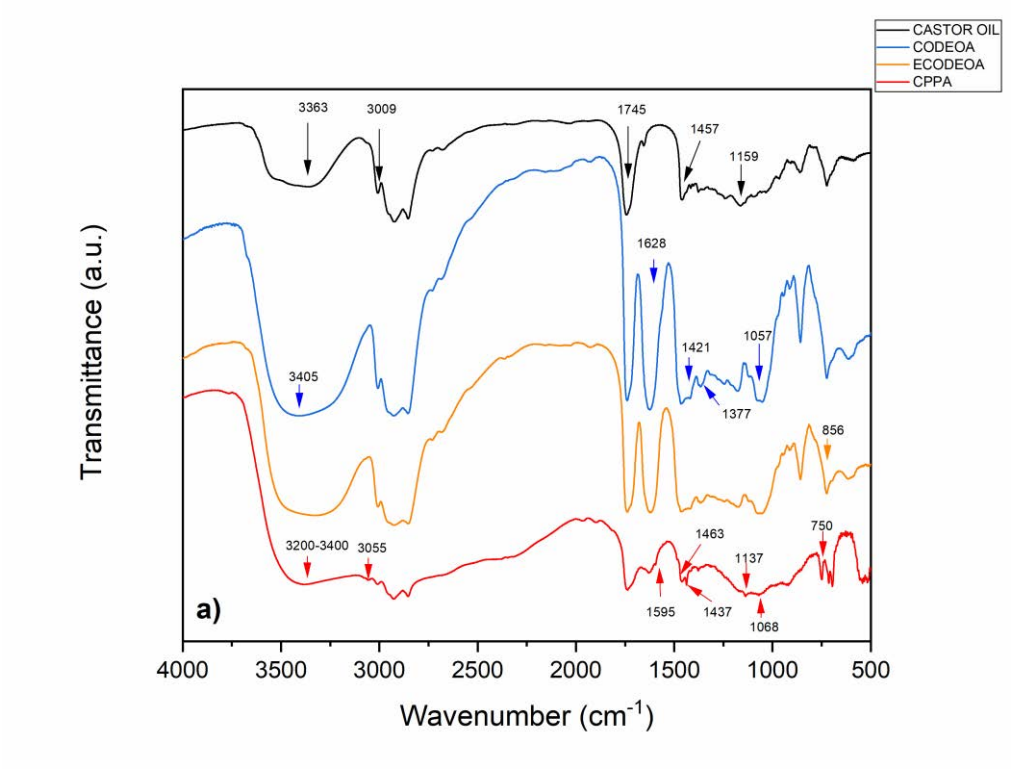
CASTOR OIL
CODEOA
ECODEOA
CPPA
3363
3009
1745
1457
1159
1628
1421
1057
3405
1377
856
3200-3400
3055
1463
750
1137
1595
1437
1068
a)
Transmittance (a.u.)
4000
3500
3000
2500
2000
1500
1000
500
Wavenumber (cm-1)

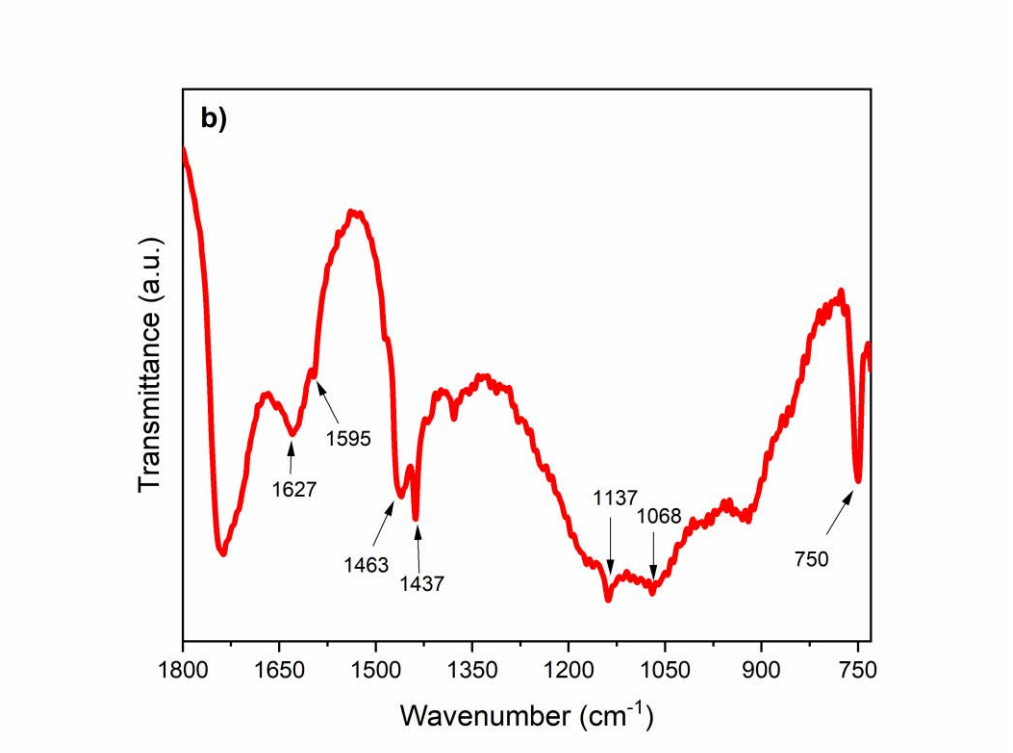
b)
Transmittance (a.u.)
1595
1627
1137
1068
1463
1437
750
1800
1650
1500
1350
1200
1050
900
750
Wavenumber (cm-1)

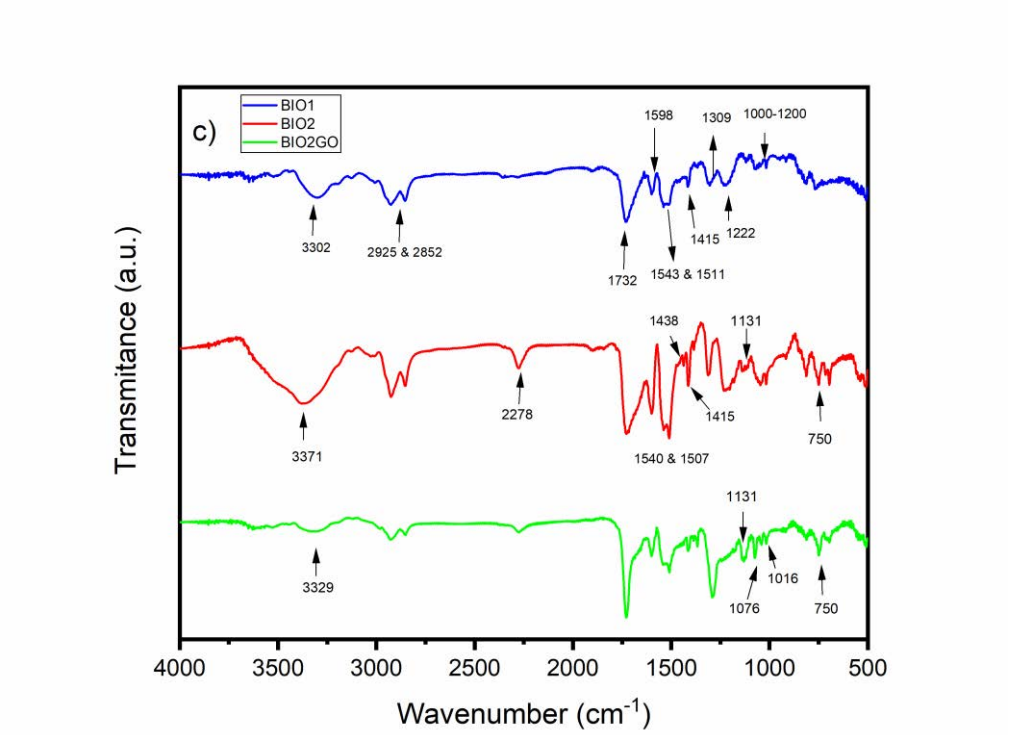

Figure 6-1. FTIR spectra of a) Castor oil polyol derivatives, b) detailed CPPA FTIR spectra (700-1800 cm^{-1}) and c) FTIR analysis of foam samples.

6.2.3. *Synthesis of Graphene oxide (GO)*

Graphene oxide (GO) was prepared following a modified improved Hummer´s method [252], [262]. In detail, 2 g of graphite (EG) were introduced in a 600 mL glass flask with a magnetic stirrer. Then, a mixture of (9:1 (v/v)) H_2SO_4 and H_3PO_4 (266 mL) was added and stirred for 10 min. After that, the oxidation process starts by adding $KMnO_4$ (12 g) and stirred the mixture by another 10 min. The flask was then placed into an ultrasonic bath equipped with a mechanical stirrer. The combination of mechanical stirring and ultrasonic treatment last for 3 h. During that process, the solution turns to a pale gray-green slurry and was transferred to a 1000 mL glass flask. 400 mL of ice are added slowly and the solution releases heat. After that, 6 mL of hydrogen peroxide was added slowly and the solution gives rise to enormous yellow bubbles. At the same time, the solution changed from gray green to gray-purple and finally a yellow bright color appeared on the solution. In order to wash the material, the solution was centrifuged to the removal of SO_4, K and Mn ions with 400 mL of HCl 10 % vol, 400 mL of NaCl 15 wt. % and distilled water until the pH of the supernatant reaches 6-7. Finally, the GO water

dispersion was placed in a petri glass and dried at 80 ºC for 15 h in an oven to obtain a solid GO.

6.3. Results and discussion

6.3.1. *Synthesis of modifiers CPPA and GO*

a) *Synthesis of CPPA*

First, CO was transformed into CODEOA by transamidization process. According to the literature, the product obtained is a mixture of two polyols [16], where two molecules of the diethanolamide polyol and one mole of the monoglyceride are obtained. The two absorptions bands in the FTIR spectra (**Figure 6-1)** connected to C-N bond (1377 cm^{-1} and 1421 cm^{-1}) and a band at 1741, related to some amount of DEOA-ester as a by-product of the reaction, revealed this fact as it was reported by Yakushin et al. [257]. CODEOA was used as reference polyol for comparison (BIO1). Then, CODEOA was epoxidized to form ECODEOA. This procedure is performed to transform the double bonds of CODEOA into epoxy rings, easy modified afterwards. Although, some double bonds from CODEOA are still present (**Figure 6-1 a)**). Finally, the epoxy ring of ECODEOA was opened by TPhP and PPA at 170 ºC to introduce the phosphorous-phenyl structure into the polyol, which was checked by FTIR (1068 cm^{-1} (P–O–C) [153] and 750 cm^{-1} (P-C) [183]) and NMR in **Figure 6-2 d), Figure 6-3 d)** and **Figure 6-4** (7-8 ppm, 120-140 ppm and 13.1 ppm in ^{1}H, ^{13}C NMR and ^{31}P-NMR respectively). Peaks around 3.00 and 3.66 ppm in the ^{1}H-NMR are the characteristic peaks of hydrogen generated from epoxy ring opening [230]. CPPA was used as a biobased FR polyol for BIO2 and the additive-filled samples. As reported here, CPPA could be consider a mixture of different related polyols (Several R variables in **Scheme 6-1**). As reported below in **Figure 6-5**, CPPA could be consider an oligomer mixture of different related polyols, with Rx and Ry as the basic structure and Rz as the hydrolyzed product. However, a certain number of impurities does not hinder the positive function of CPPA for the modification. It means it is not necessary to purify the product, which simplifies the process and further facilitates the practical application of the method. The characteristics of the synthetized polyols are plotted in **Table 6-1**.

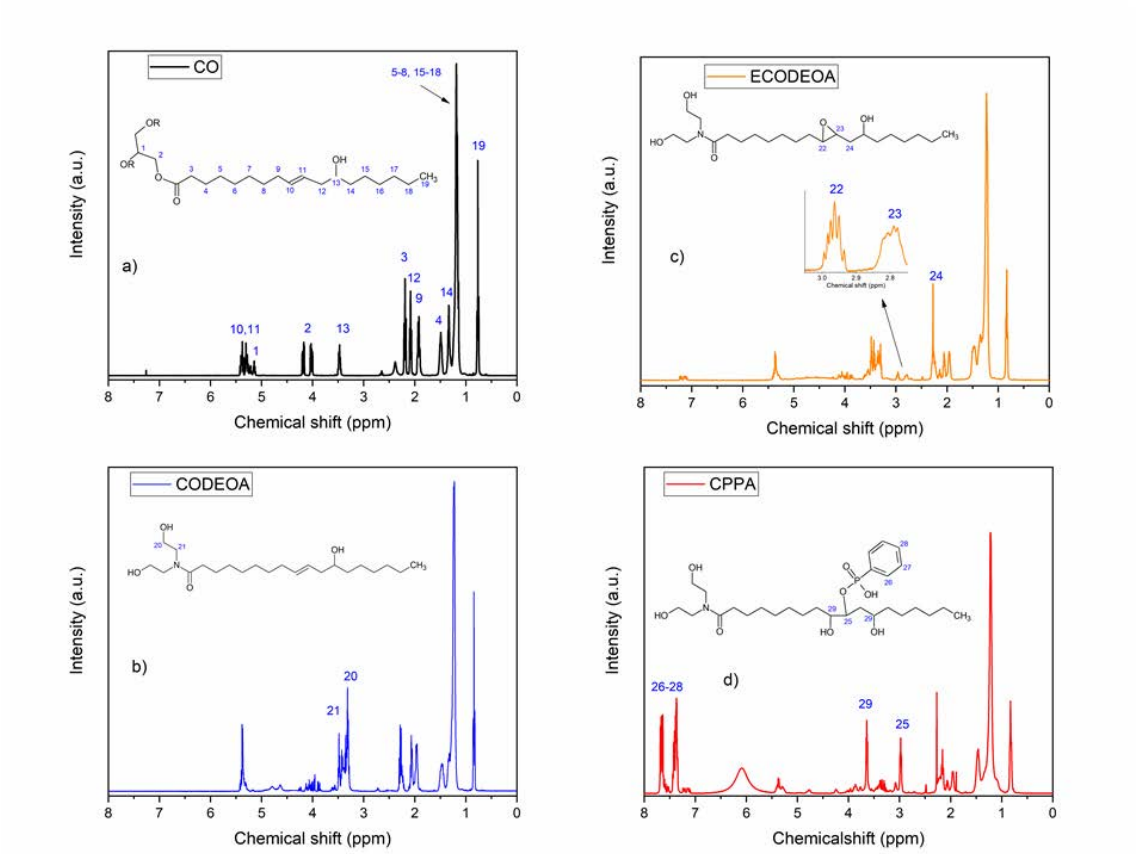

Figure 6-2. ^{1}H NMR spectra of castor oil derivatives.

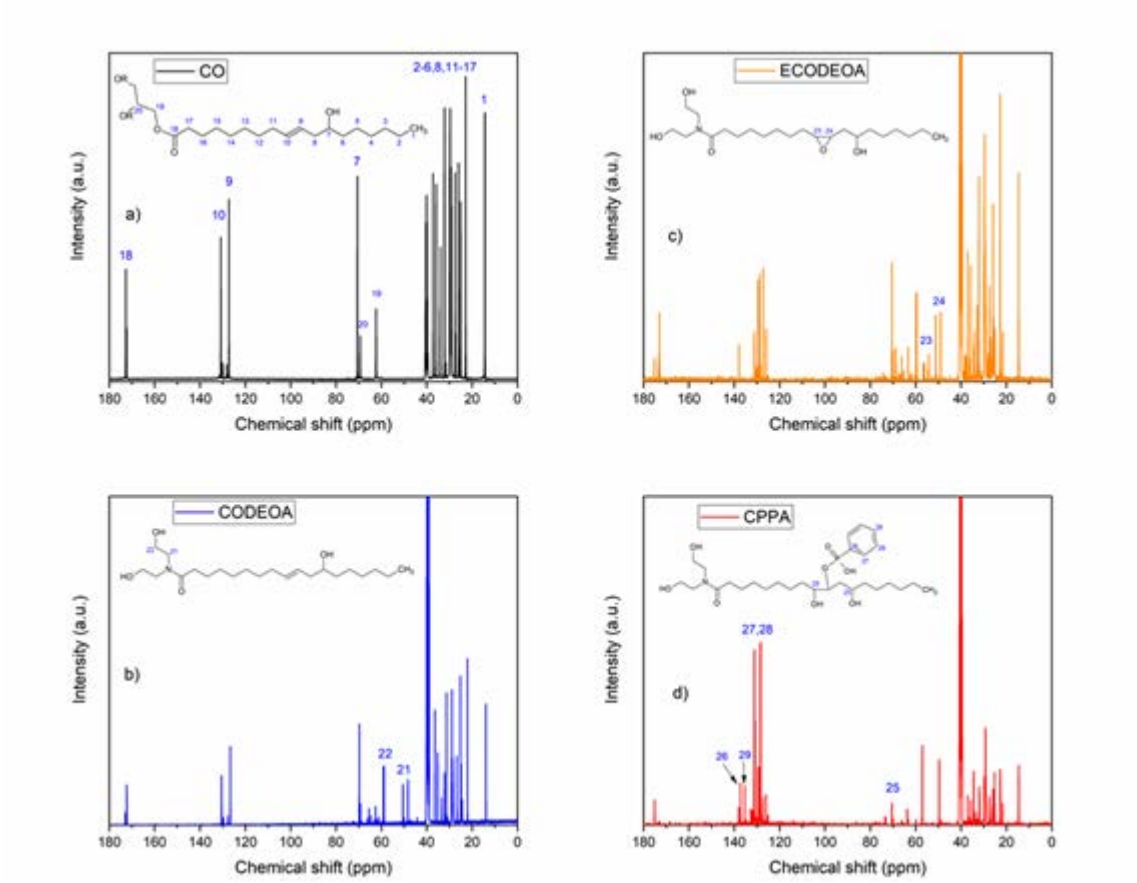

Figure 6-3. ^{13}C NMR spectra of castor oil derivatives.

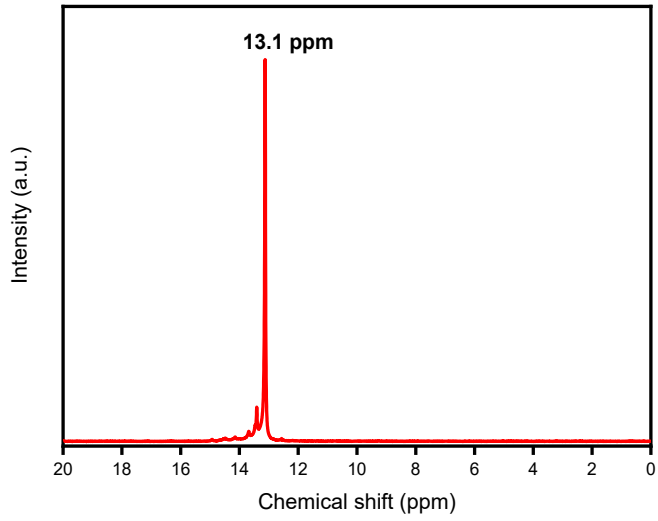

Figure 6-4. ^{31}P NMR spectra of CPPA.

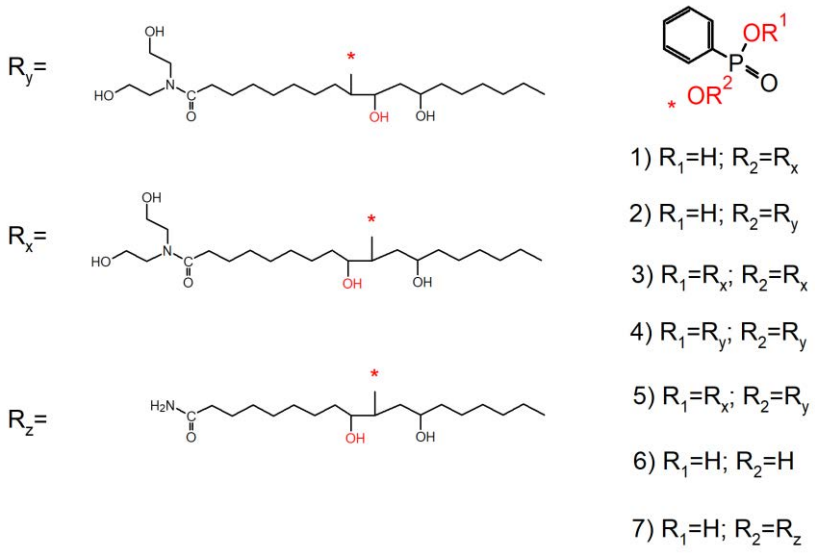

Figure 6-5. Illustration of the different chemical structures of oligomeric CPPA.

Table 6-1.Characteristics of the polyols used for the foam samples.

Biobased polyol	Measured OH number (mg/KOH/g)	Acid value (mg/KOH/g)	Corrected OH number (mg/KOH/g)	Viscosity at 25 ºC (mPas)
Castor oil	172	1	173	762
CODEOA	328	2	330	1704
CPPA	324	259	583	20850

b) *Synthesis of the modifier (GO)*

GO was synthesized and used as modifier for the biobased FR foam (BIO2). EG of GO were successfully analyzed by Raman spectroscopy (**Figure 6-6)** below. The spectra of EG displays a very intense G band at 1582 cm^{-1}, which corresponds to first-order scattering of the E_{2g} vibration mode and a 2D band at 2720 cm^{-1} due to the second-order two-phonon mode [263]. It was also present a small D band at 1350 cm^{-1}, which indicates the presence of defects due to the strong acid intercalation into the graphite layers for the preparation of EG [264]. For GO, the Raman spectra shows two main peaks related to the D and G bands. The D band becomes prominent, increasing the D/G ratio for GO with respect to EG. This increasing indicates an alteration in the graphite structure by the extensive oxidation and the presence of Oxygen groups [263], [265]. Also, the intensity of the 2D peak near 2710-2720 cm^{-1} decreased with the

increasing in oxidation degree, although the 2D-band was reported to be most likely suppressed by the "Pauli blocking" effect [252], [262]. The D/G intensity integrate area ratio are listed in **Table 6-2** and reflected the significant structural changes occurring during the chemical processing from pristine EG to GO. I_D/I_G for GO was 1.17, whereas it was only 0.29 for EG. The increase reflects more defects formed with the incorporation of oxygen-functional groups on the surface of GO [261] and confirming the successful preparation of GO.

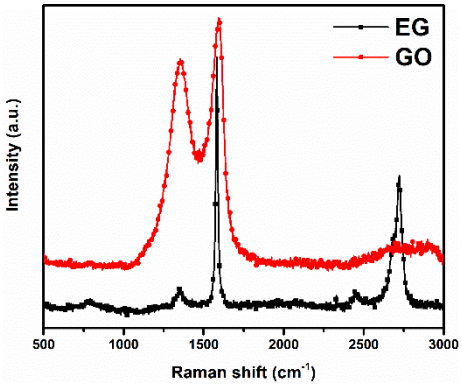

Figure 6-6. Raman spectra of EG and GO.

Table 6-2. Raman Peak Positions and D/G Intensity Ratio of EG and GO samples.

Sample	Peak of band D (cm^{-1})	Peak of band G (cm^{-1})	I_D/I_G integrate area ratio
EG	1356	1582	0.29
GO	1353	1593	1.17

c) *Foam preparation*

RPUFs were prepared mixing each component separately. First, biobased polyol (CODEOA or CPPA), catalyzer 1 and 2 were added along with the surfactant and water as blowing agent. The polyol mixture was stirred 1 min with a heidolph RZR-1 mechanical stirrer until a uniform, red-colored mixture was obtained. Finally, -NCO (Part A from the commercial RPUF) was added at an appropriate amount and the PU mixture was stirred at a high strength for a short time. BIO1 and BIO2 followed this procedure. The samples with the addition of EG and GO followed the same procedure but adding the additives in the polyol mixture (with CPPA) prior to the mixing with -NCO. In detail, GO was added to the polyol mixture and stirred for 1 min. Afterwards, EG was added and stirred again for 1 min to ensure full dispersion of the materials.

Finally, -NCO was added slowly, and the mixture was stirred for around 20 s until the materials begins to heat. The overall formulas are plotted in **Table 6-3**. The mixture was finally poured into a 250 mm × 250 mm × 60 mm open Aluminum mold, where the RPUFs raised freely in vertical direction. After curing at room temperature for a minimum of 24 h, samples were cut according to the standards for the different test performed. The formulations of the samples are plotted on **Table 6-4** below.

Table 6-3. Overall formulae of RPUF materials.

Component	BIO1	BIO2	BIO2/EG	BIO2/EG/GO
CODEOA	92.5	-	-	-
CPPA	-	92.5	92.5	92.5
Catalyzer 1	1.5	1.5	1.5	1.5
Catalyzer 2	0.5	0.5	0.5	0.5
Surfactant	4	4	4	4
Blowing agent	1.5	1.5	1.5	1.5
Total B*	100	100	100	100
Isocyanate (A)	115	115	115	115
Weight Ratio A/B	1.15	1.15	1.15	1.15
EG	-	-	13.7	12.6
GO	-	-	-	1.1

*B components (polyol, catalyzers, surfactant and blowing agent) are based on 100 g of material. The rest of the components are related to 100 g of B.

Table 6-4. Formulae of RPUF composites.

Sample	wt. % EG	wt. % GO
BIO1	-	-
BIO2	-	-
BIO2/EG	6	-
BIO2/EG/GO	5.5	0.5

6.3.2. *Foams sample FTIR analysis*

The foam samples were prepared according to section **6.3.1.c)** and a FTIR analysis was performed and showed in **Figure 6-1 c)**. BIO1 and BIO2 showed the typical peaks related to PU [247]. It can be observed an excess of -NCO by the -NCO group band at 2278 cm^{-1}. This -NCO excess and the use of water as blowing agent, favors the production of allophanate and thus, increased the intensity of the bands related to N-H (3371 cm^{-1}) and amide II (1540 and 1507 cm^{-1}), C-N stretching (1415 cm^{-1}) with respect to BIO1. The introduction of PPA in CPPA polyol was showed by the bands at 1438 (phenyl skeleton), 1131 (P=O), and 750 cm^{-1} (P-C) respectively. Moreover, the introduction of GO (BIO2/EG/GO) reduced the intensity of the unreacted -NCO associated peak in BIO2 and introduced two peaks at 1076 and 1016 cm^{-1}, attributed to the in-plane vibration of -OCO-NH- urethane group [266]. It also disappeared the bands around 3500 cm^{-1} related to free -OH and N-H, suggesting that the N-H groups are hydrogen bonded with GO as reported by Pokharel et al. [146]. Moreover, it increased the intensity of the urethane -C=O band (1728 cm^{-1}). This suggest a reaction between the -OH groups on surface of the GO and -NCO groups on the ends of PU chains to form urethane bonds [266] as well as hydrogen bonding between N-H from PU and GO [146].

6.3.3. *Cellular structure analysis and thermal conductivity of RPUF samples*

a) *Cellular structure analysis of RPUF samples*

The introduction and influence of graphitic particles into BIO2 cell structure can be observed in **Figure 6-7** and **Figure 6-8.** The different physical foam structures are showed in **Figure 6-9**. The average cell size diameter is showed in **Table 6-5**. It can be seen in **Figure 6-7 A)** and **Figure 6-9** a very big porous and non-homogenous structure of BIO1. The cell size of BIO1 was 812 µm, being clearly seen by the human eye. Due to presence of DEOA in CODEOA, the reaction between -NCO and polyols occurs at enhanced rates, producing higher amount of CO_2; which consequently "blows" the foam and produces a more porous structure with bigger cell size. **Figure 6-7 B)** shows a more regular shape cellular structure from BIO2 and the cell size was reduced a 72 % to 226 µm. The increasing viscosity of CPPA due to the presence of PPA in the structure (**Table 6-4**), has an effect in restraining the cell expansion during the foam formation and consequently, the cell size is reduced [165].

In **Figure 6-7 C)**, the introduction of very big particles of EG (500 µm); which are located inside the cell walls [267] (**Figure 6-8 B)**, produced many defects in the structure and rupture of the cells by a nucleation effect of the particles during the foam formation producing agglomerates, which consequently opened and increased the cell size of the foam [176] up to 692 µm and a 206 % with respect to BIO2. The damage in the cellular structure was attributed to the weak adhesion between the graphite flakes and the foam matrix [47]. However, it can be observed in **Figure 6-7 D)** and **Figure 6-8 C)** that the smaller particles of GO are better distributed than EG alone and produced a more homogeneous cellular structure. The good dispersion of GO can be attributed to the interactions between the oxygen groups on the GO surface and the PU matrix [266]. At the same time, GO acted as a dispersing agent, facilitating the dispersion of EG in PU and a strong interaction with the polymer matrix as reported by Pokharel et al. [128]. Therefore, the introduction of GO facilitates a smoother and more homogenous foam structure than EG alone and decreasing the cell size up to a 63 % with respect to BIO2/EG and 254 µm, which is beneficial for the thermal insulation as discussed above. However, by comparison with BIO2, the loading of about 0.5 wt. % was not beneficial for the cell size reduction probably due to an increase in the viscosity; assumed to be provoked by the strong interaction between the GO and the polyol via hydrogen bonding [146], that could lead to some agglomerates [138].

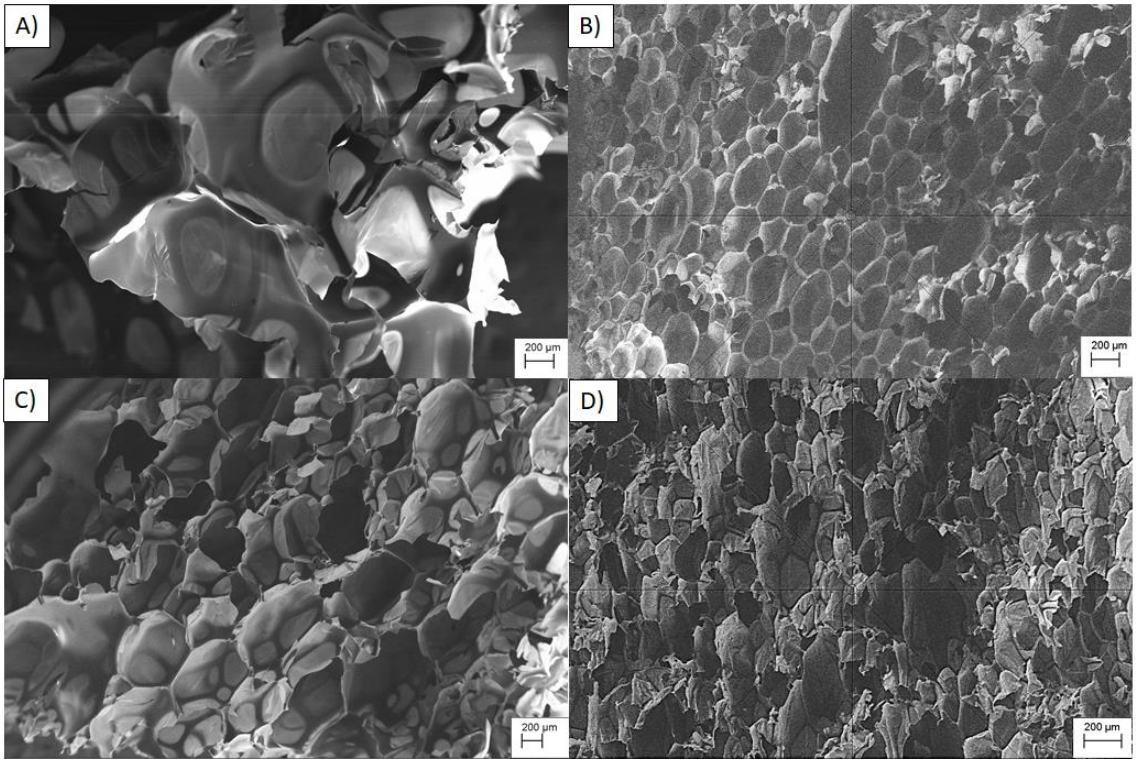

Figure 6-7. SEM micrographs of A) BIO1, B) BIO2, C) BIO2/EG and D) BIO2/EG/GO, foam samples showing their cell size.

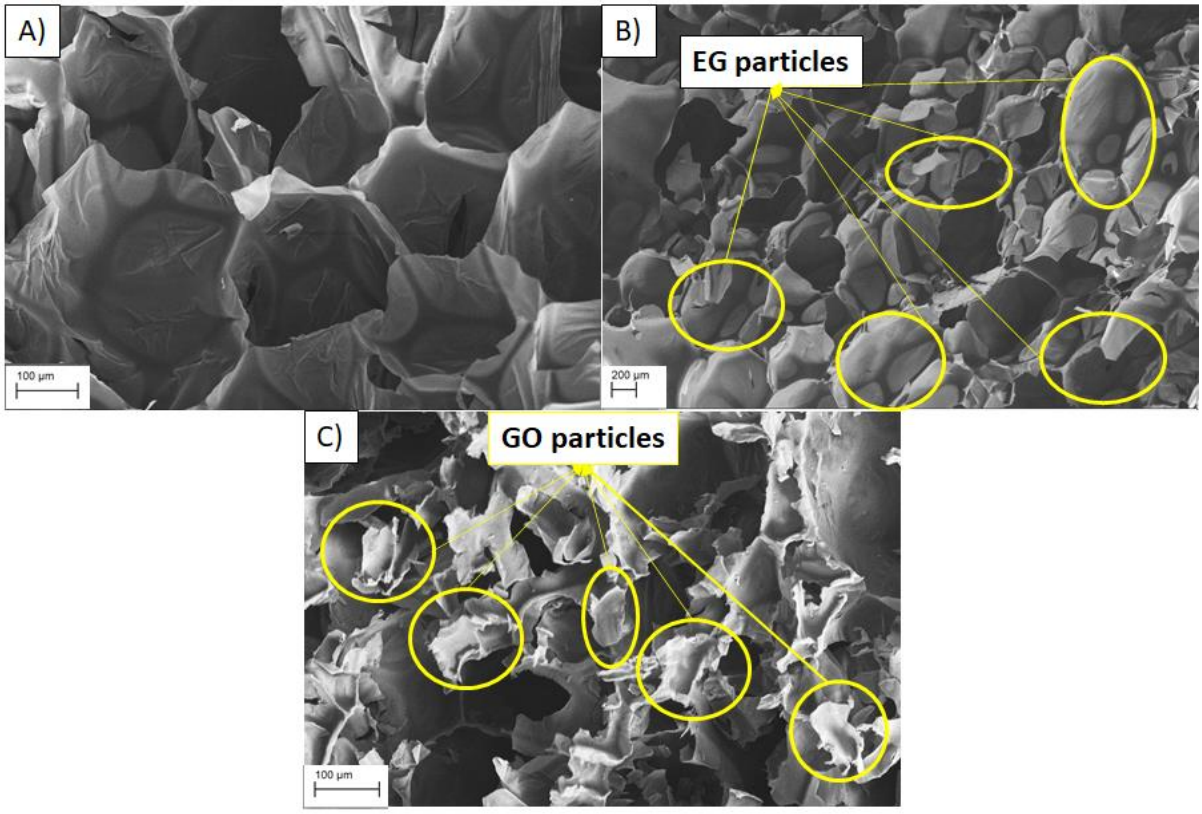

Figure 6-8. SEM micrographs of A)) BIO2, B) BIO2/EG and C) BIO2/EG/GO foam samples showing the FR additives distribution.

b) *Thermal conductivity of RPUF samples*

The thermal conductivity of biobased foam samples was herein measured to evaluate the effect of carbon materials, such as EG or GO on its cellular structure and showed in **Table 6-5**.

In our previous chapter, the commercial PU obtained a thermal conductivity of 48.9 mW/mK (**Table 4-2**). The same sample was measured here as described in the **Chapter 3** (materials section) and obtained a thermal conductivity of 39.4 mW/mK. The substitution of the commercial polyol by CODEOA, showed that BIO1 increased the value until 49.6 mW/mK. This value is similar to those obtained by Castor oil-based RPUF by previous authors [167]; as more open and ruptured cell were present in the foam network (**Figure 6-7 A)** and **Figure 6-9**); probably due to a more CO_2 production when reacting with -NCO, which blows the structure with the same mass and increases the cell size, leading to higher air convection that is not able to disperse the heat properly and so, increasing the thermal conductivity trough the cellular structure [156]. However, this led to a low-density foam (**Table 6-5**) which can still be

considered an insulating material similar to the commercial ones with density of 30.9 Kg/m^3. On the contrary, by using CPPA in BIO2, it reduced the thermal conductivity until an impressive 33.8 mW/Mk, a dramatic 32 % reduction with respect to BIO1 and a 14 % less than the commercial reference. Moreover, the use of CPPA instead of CODEOA as polyol, increased the density and decreased the cell size, as the viscosity of the polyol was higher and so, the polymer-forming reaction rate decreased, leading to a weak three-dimensional PU network [268]. The weaker cell walls were not strong enough to trap the CO_2 generated by the blowing reaction and CO_2 was emitted to the atmosphere. For that reason, BIO2 expanded less leading to a lower air convection and decreased the thermal conductivity [156].

On the other hand, the introduction of additives had a different impact. EG increased the density of the foam a 3 % in comparison with BIO2. The thermal conductivity increased with the addition of EG particles up to a 13 %, which could be explained considering the increase in conduction through the solid phase (λs), mostly due to the intrinsic high thermal conductivity of EG and density, which would weaken the thermal insulation efficiency of RPUF foams [216]. Also, as the addition of EG particles slightly increased the cell size in the foams, the segments of the polymer chains may gain mobility at lower temperatures [269], which contributed to increase the thermal conductivity. A similar behavior was found on previous works on our group regarding EG and RPUF [211], [212].

Finally, the substitution of 0.5 wt. % of EG by GO (BIO2/EG/GO), led to a decrease of the thermal conductivity around a 10 % compared to BIO2/EG. This fact confirmed the previously mentioned insulation effect of GO into foams. First of all, GO decreases the density of the foam up to a 8 % with respect to BIO2/EG. This effect was explained by the high hydrophilicity of GO and the water particles intercalated inside the GO structure [270], which can act as small blowing agents and producing CO_2, finally increasing the volume of the material and decreasing the density. GO also avoids the increase and/or the disruption of the cellular structure by the use of EG only [138], thus decreasing the λs. Due to the good interfacial adhesion of GO with the PU matrix, it facilitates the dispersion of EG, thus minimizing the EG cell damage. Consequently, the cell size decreased compared to BIO2/EG and it was closer to the values of BIO2. It has been also reported that GO enhances the gas barrier performance of PU [271], creating a commonly known "tortuous path" delaying at some extent, the diffusion of the gases [144]. It can be observed in **Figure 6-8 C)** the presence of some GO layers in the cell windows;

these layers can be helpful in decreasing blowing agent permeability through the cell windows [138] and so the λg.

Based on this, GO acts as radiation infrared blocker, decreasing the cell size and increasing the extinction coefficient of the cell walls [138], thus reducing the radiation contribution (λr) to the thermal conductivity [148]. At the same time, the better dispersion of EG due to the oxygen groups in the surface of GO and the interaction with the PU matrix, minimize the increase of λs and the damage to the cell structure from EG. Finally, GO, due to its gas barrier properties, will also reduce the gas conduction of the foam (λg), decreasing the heat transferred by this way. These three combined effects consequently reduce the thermal conductivity of the RPUF and confirmed the previously mentioned insulation effect of GO into RPUFs. There is a good agreement between the cell size and the thermal conductivity of the foams. where the lowest cell size, obtains the lowest thermal conductivity; thus, influencing in a lower gas conduction and so, obtaining lower thermal conductivity.

Table 6-5. Average cell size, thermal conductivity and density data results for the RPUF samples.

Sample	Average cell size diameter (μm)	Thermal conductivity (mW/mK)	Density (Kg/m^3)
Commercial PU	467 ± 120	39.4 ± 0.5	95.9
BIO1	812	49.6 ± 0.3	30.9
BIO2	226 ± 3	33.8 ± 0.3	31.8
BIO2/EG	692 ± 31	38.2 ± 0.6	32.9
BIO2/EG/GO	254 ± 6	34.2 ± 0.3	30.4

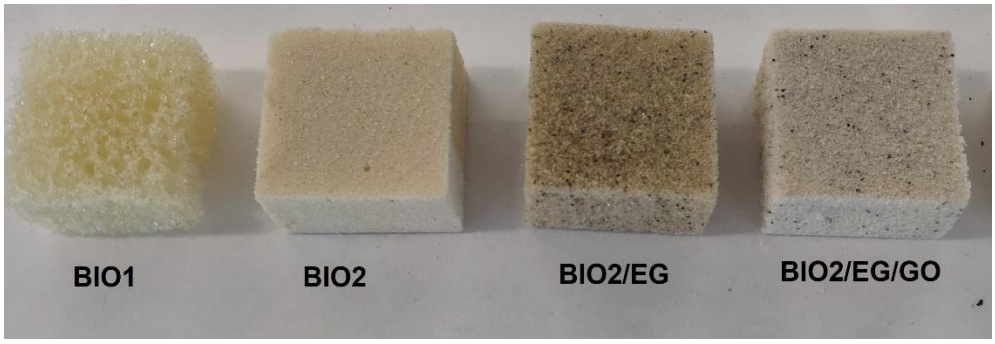

Figure 6-9. The different studied biobased-RPUF samples showing their different physical structure.

6.3.4. *Fire-retardant properties of RPUF samples*

a) *LOI and UL94 tests*

LOI and UL94 tests have been performed, and the data obtained are collected in **Table 6-6**. The average after-flame time (t_1+ t_2) was reported as comparison. The LOI values of the RPUF specimens with 6 wt. % of additives and without additives were measured. The reference foams (BIO1, BIO2 and BIO2/EG) showed a LOI value of 19.6 vol %, 24.0 vol % and 27.6 vol % respectively. This means that BIO1 was an inherently flammable material with lower LOI than the ambient O_2 value, probably due to the huge porous structure belonged to a low compatibility between CODEOA and -NCO. On the other hand, BIO2 and BIO2/EG are fireproof materials at ambient conditions. BIO2/EG increased the LOI value a 15 % compared with BIO2, meaning that the addition of EG dramatically increased the fire resistance. Subsequently, the samples containing EG along with GO (BIO2/EG/GO**)**, showed a stable LOI value around 27.2 vol%. The barrier condensed phase effect of EG is more effective than GO since GO does not "expand" as much as EG during the combustion process. This effect was probably due to a higher intercalated acid content of EG than GO; as GO was cleaned until pH=7, resulting in a higher expansion of EG than GO. Indeed, due to the conditions of the LOI test and the high oxygen concentration, EG will have better performance as FR as it could expand and block the fire feeding from the upper part of the specimen to the bottom.

The UL94 of BIO1 and BIO2, as a neat PU samples, showed that they were easy flammable materials and so, they were not classified under UL94 test standards. After that, the use of 6 wt.% of EG lead to an increase of the UL94 rating to V-2, due to dripping flaming particles

during the test which ignited the cotton. The cracks in the surface by EG addition; by a low compatibility with PU matrix [210], favored the entrance of heat through the internal porous structure of the foam and scattered the fire easily. On the other hand, the use of 0.5 wt. % of GO increased the rating to V-0. It has been reported that GO could have a synergistic barrier effect against oxygen penetration into the polymer matrix which can possibly stop the spreading of the fire [272]. The average after-flame time of each sample was only 3.6 s, the lowest among all the specimens tested. The different foam structure of BIO2/EG and BIO2/EG/GO (**Figure 6-9**), showed that the foam with EG has a more porous structure due to the incompatibility of EG and the PU matrix, whereas the foam with partly substituted GO, has a smoother structure. Also, it was observed a more homogenous structure and a better dispersion of EG and GO (**Figure 6-7**). This structural difference stops the propagation of the fire and the increase of temperature during the combustion process, thus having BIO2/EG/GO better UL94 test result than BIO2/EG. Indeed, the difference resides in the drops flaming particles; due to this porous structure, the flame "melts" the polymeric structure of BIO2/EG easily, whereas the smoothly structure of BIO2/EG/GO; due to the chemical connection between GO and the PU matrix that does not exist in the case of EG, favored a more integrated structure without dripping flame particles. For that reason, GO obtained a better UL94 rating than EG as additive for a RPUF.

As a comparison, similar density PU foams with another kind of nanomaterial like clays, obtained lower LOI and UL94 tests results with higher FR wt. % addition than the ones showed in the present manuscript [245], [273], [274]. Therefore, the combination of EG and GO as FRs obtained excellent fire resistance results at only 6 wt.% loading.

Table 6-6. LOI and UL94 tests results for the RPUF samples.

Sample	LOI (vol%)	UL94 rating	Average time (t1+ t2) (s)	Ignition of the Cotton
Commercial PU	19.2	NR	>30	Yes
BIO1	19.6	NR	>30	Yes
BIO2	24.0	NR	>30	Yes
BIO2/EG	27.6	V-2	5.3 ± 3.4	Yes
BIO2/EG/GO	27.2	V-0	3.6 ± 3.4	No

NR: No rating in UL-94 test

b) *CCT test*

CCT was performed at a heat flux of 50 kW/m^2. The fire behavior can be assessed by PHRR, THR and TSP. The samples were evaluated based on these parameters. The curves for the samples regarding these parameters are shown in **Figure 6-10,** the char residues are showed in **Figure 6-11,** the char SEM analysis in **Figure 6-12** and all the data are summarized in **Table 6-7**.

First, the HRR curves for the RPUF samples were analyzed in **Figure 6-10 a**). The PHRR was rapidly raised after the ignition (less than 3s) due to the intrinsic porosity of PU foams [2]. The flameout data for the filled-nanocomposites are all longer than that of neat RPUFs (BIO1 and BIO2), which is also a proof of the flame retardancy of the EG and GO-filled RPUF samples. The curves showed two different peaks; the first peak is attributed to the development of an intumescent efficient protective char layer; typically composed of three major components: an acid source, a carbon source and a blowing agent [104], whereas for the second peak, thermal feedback may also contribute when the pyrolysis front approaches the insulated back surface of the sample [204]. PHRR was 390 kW/m² for the reference BIO1 without any FR. BIO1 showed a huge difference between first and second peak as no intumescent char was formed (**Figure 6-11 A) and B)**). For that reason, the thermal feedback degraded even more the cellular structure in the second peak. On the other hand, BIO2 decreased the PHRR to 330 kW/m² with a slight 15 % decrease. BIO2 showed smaller second peak as this reduction was promoted by the intumescent char layer formed (**Figure 6-11 D**). The intumescent char was probably formed by the PU as carbon source, phosphinic acid as acid source and urea as blowing agent [275], since poly-NCO tend to form carbodiimide and urea when decompose [266]. Owing to the increase in phosphorous content of BIO2 compared to BIO1, an increased amount of phosphinic acid after decomposition of the foams was released and creates a phosphorous-rich protective char layer over the surface of the foam which reduces HRR and oxygen penetration [166]. When EG was introduced as additive, the curve displayed two smaller peaks and BIO2/EG obtained 168 kW/m² as PHRR. The reduction of the PHRR were a dramatic 57 % and 49 % with respect to BIO1 and BIO2 respectively. Although the aforementioned intumescent char was slightly restricted by the worm-like expansive structure created when EG was subjected to a heat source [64], the char formed was of higher quality (**Figure 6-11 F**). Interestingly, the second peak was slightly reduced as the pyrolysis at the bottom parts of the sample was blocked [204]. When 0.5 wt. % was depicted from EG

(BIO2/EG/GO), the PHRR increased a little to 178 kW/m². Although this increase is considered negligible, GO alone was not able to produce a continuous carbonaceous char layer compared to EG. Indeed, the second peak of GO-containing samples was increased. Therefore, EG is a slightly better FR than GO. It was reported that for nanocomposites, they can perform different in the flammability tests (LOI/UL94) than in the specific scenario tests (CCT) [276], due to influence of oxygen in the thermal conductivity on the gas phase and the viscosity of the polymer.

THR (**Figure 6-10 b**) is a measurement of the heat released by combustion during a given time. The reference sample BIO1 showed a THR value of 22.9 MJ/m². When it was functionalized with PPA (BIO2), the value decreases up to 18.3 MJ/m². The decrease was an impressive 20.1 %. The introduction of EG (BIO2/EG) reduced the reference value continuously by a 21.7 %. This is explained the EG thermally expanded and absorbed heat from the system in an endothermic way at 150-200 ºC, forming a worm-like protective layer on the foam surface [64]. After all, the use of GO, reduced the THR value until 17.3 MJ/m², a 5.6 % decrease compared to BIO2 and a 24.6 % with respect to BIO1. Several authors suggested that a good dispersion of GO could decrease the THR due to covalent bonds between PU matrix and oxygen-functionalized groups on the GO surface, which improve the network structure and enhanced the thermal stability of PU [266].

Bearing in mind the danger of smoke for people´s lives; including poisonous smoke and dust during a fire scenario, reduce the smoke production (TSP) (**Figure 6-10 c**) is also a signal of a good FR effect. TSP of BIO1 was 7.1 m². Then, BIO2 decreased the value up to a 27 % to 5.2 m². The previously mentioned formed intumescent char was probably the cause. The addition of EG also reduced the reference value to 5.2 m². Therefore, the worm-like structure forms a compact char layer which dilutes the oxygen concentration near the flame, blocks and limits the heat and the mass transfer from the polymer to the heat source, narrowing down further decomposition of the material while the smoke production was reduced [64], [210]. However, with the addition of GO (BIO2/EG/GO), TSP increased. The main reason is probably that depleting 0.5 wt. % of EG was not substituted efficiently by the same amount of GO to form an enough char barrier against the mass transfer compared to BIO2/EG. Also, the presence of reactive oxygen-functionalization on the GO surface; easily breakable by an external irradiation [277], increase the CO and CO_2 production along with steam, by the pyrolysis of these oxygen groups [253]. Thus the condensed phase FR effect was stronger against heat and mass transfer

for EG than GO and the addition of GO cannot effectively decrease the volatilization of flammable gases [152]. All in all, the differences between EG and GO could be considered negligible. Besides, the CCT results obtained for BIO2/EG/GO were a 19 %, 75 % and 42 % better than the commercial reference in **Chapter 4** (**Table 4-5**) with respect to PHRR, THR and TSP respectively.

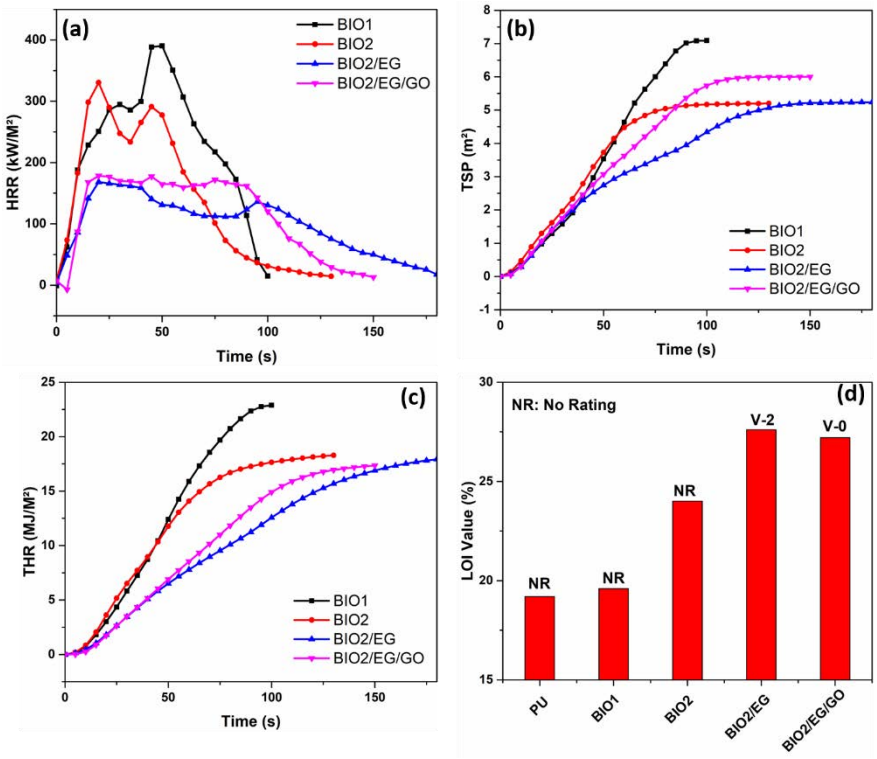

Figure 6-10. a) HRR, b) THR and c) TSP curves of RPUF samples at 50 kW/m^2.

Table 6-7. Data of biobased composites at 50 kW/m^2 from CCT.

Sample	PHRR (kW/m²)	THR (MJ/m²)	TSP (m²)
BIO1	390 ± 14	22.9 ± 0.1	7.1 ± 0.1
BIO2	330 ± 19	18.3 ± 1.9	5.2 ± 0.3
BIO2/EG	168 ± 10	17.9 ± 2.2	5.2 ± 0.3
BIO2/EG/GO	178 ± 9	17.3 ± 3.9	6.0 ± 0.1

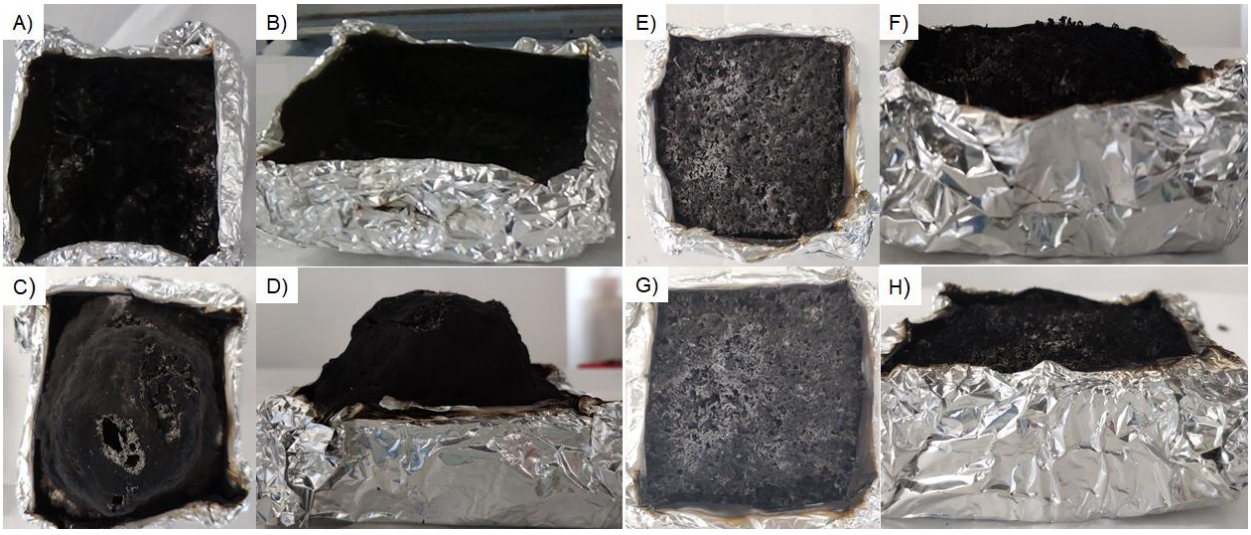

Figure 6-11. Char images of A, B) BIO1, C, D) BIO2, E, F) BIO2/EG, and G, H) BIO2/EG/GO after CCT.

- **Smoke behavior analysis**

A smoke production study based on the average CO and CO_2 production (Av-COP and Av-CO_2P) was performed and their ratio as CO % was showed **Table 6-8**. It can be observed that BIO1 produced the highest amount of CO and CO_2 during the combustion process. In BIO2, it obtained almost the same CO but decreased the CO_2 production up to a 38 %, which is indicative of an incomplete combustion and more gas-phase FR effect with an increased CO/CO2 ratio to 4.3 % [183]. The introduction of EG lead to a more important decrease of the CO and CO_2 production, reducing up to a 28 % and 55 % respectively with respect to BIO1 and 28 % and 27 % respectively compared to BIO2. However, the ratio COP/CO_2P increased again to 4.3 %. Finally, the substitution of 0.5 wt. % EG by GO lead to an increase of CO and CO_2 of about 21 and 9 % respectively compared to BIO2/EG. The pyrolysis of the oxygen-containing groups of GO, releasing CO, CO_2 and steam [253], may be the responsible for this increase. However, the production of CO and CO_2 is still reduced a 12 and 20 % respectively in comparison with BIO2. At the same time, the ratio COP/CO_2P increased to 4.7 %.

Table 6-8. Data of the CO and CO_2 production (mg/s) at 50 kW/m^2 from CCT.

Sample	Av-COP (mg/s)	Av-CO_2P (mg/s)	Ratio COP/CO_2P (%)

BIO1	3.73 ± 0.24	137.9 ± 4.4	2.70
BIO2	3.70 ± 0.17	85.7 ± 4.8	4.30
BIO2/EG	2.68 ± 0.16	62.6 ± 1.1	4.30
BIO2/EG/GO	3.24 ± 0.83	68.4 ± 12.4	4.70

- **SEM char analysis**

The chars were indeed analyzed by SEM after the CCT (**Figure 6-12**). Firstly, BIO2 inner and outer char were observed (**Figure 6-12 A) and B)**). The intumescent char was produced with a homogeneous structure but relatively weak and fragile. The inner char showed many cracks and holes where heat could penetrate, thus showing a bad quality char. Then, BIO2/EG chars (**Figure 6-12 C) and D))** were analyzed. It can be clearly seen the "worm-like" structure produced by EG expansion upon heat covering all the char structure. After that BIO2/EG/GO (**Figure 6-12 E) and F))** showed a similar char structure, however, small, layered insertions from GO could be observed. Indeed, layered GO can be observed attached to EG worm structures and producing a more compact char, confirming the synergistic char structure between both FRs

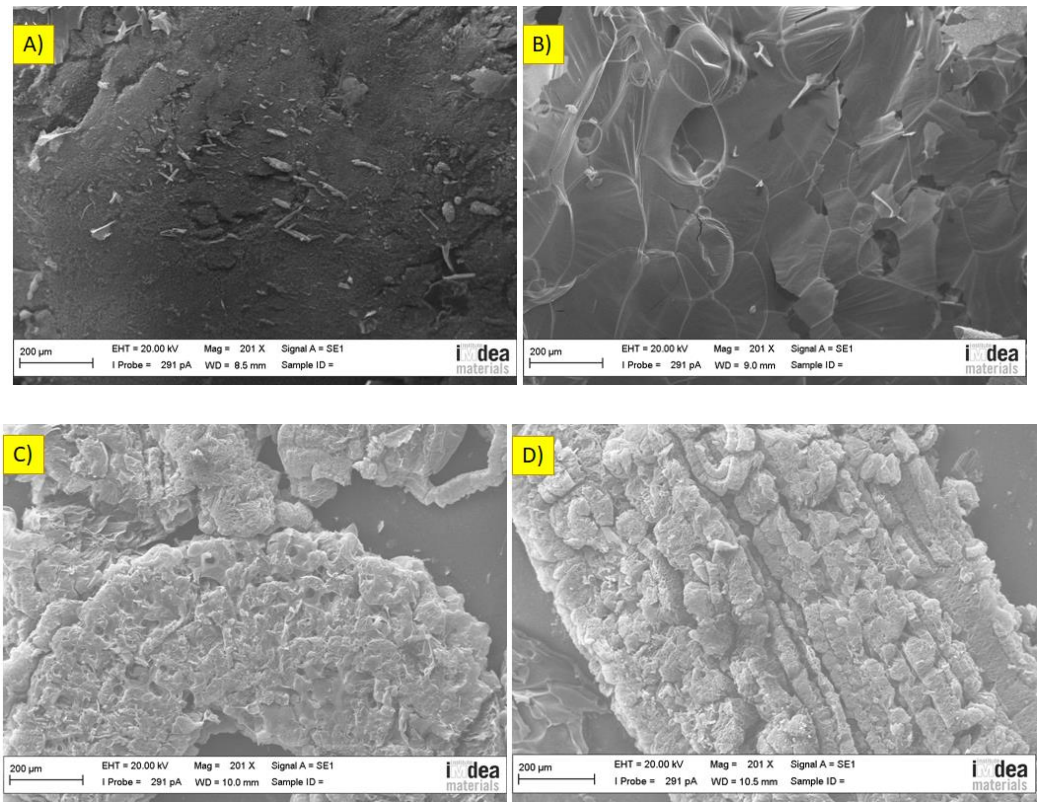

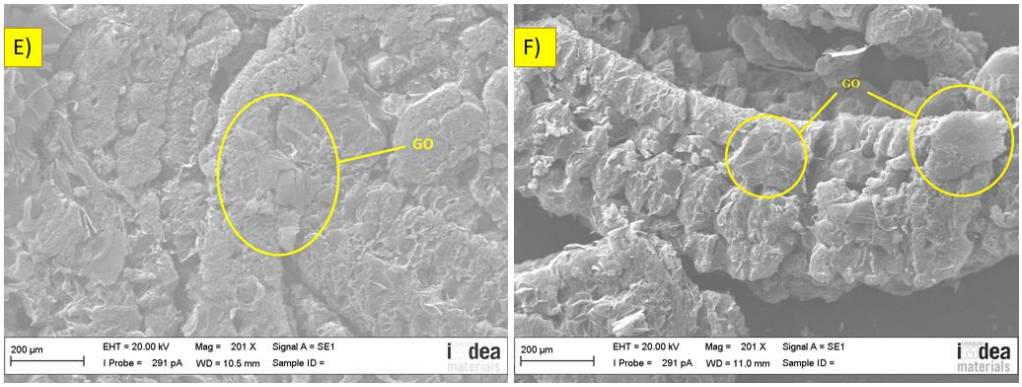

Figure 6-12. Char images of A,B) BIO2, C,D) BIO2/EG, E,F) BIO2/EG/GO analyzed by SEM.

c) *Proposed FR mechanism*

The mechanism proposed on this manuscript, is based on the synergistic combination of EG and GO, together with the FR polyol (CPPA). Following this, a condensed-phase FR action was proposed. Firstly, EG acts on the condensed phase by producing a dense char on the surface of PU, which limits the heat and mass transfer to the polymer and blocks the oxygen penetration. A similar behavior is also produced by GO (**Figure 6-13 b**). At the same time, the presence of phosphorous compounds (CPPA as liquid FR) and their thermal decomposition produced the release of phosphate and phosphinic species (H_3PO_3 and H_3PO_4) which acts in the gas-phase and permits the creation of an intumescent char [166] (**Figure 6-13 c**); these phosphorous species acted as an acid source, the PU matrix acted as char former and the rest of the gaseous products acted as blower (urea mainly), leading to an intumescent, foam-like char residue which finally acts like a barrier against the heat penetration (as showed in **Figure 6-11 D** and **Figure 6-12 A)** and **B)**). From 180 ºC, P-O-C bonds are thermally degraded and formed phosphoric acid [236]. Then, polyphosphoric acid was obtained by the polycondensation reaction of phosphoric acid when the temperature is increasing as showed in **Scheme 5-1**, catalyzing the formation of carbon layers [70] and enriches the char carbonaceous layer produced by EG and GO [106], acting as physical barrier, slowing down the heat and mass products transference between the matrix and the ambient. To sum up, a condensed phase mechanism by a charring behavior which leads intumescent and the barrier effect of EG and GO previously described, enhanced the FR action. This proposed mechanism is in accordance

to other authors about EG and phosphorous-based FR synergistic effect studies [2], [106]. The resume of the proposed mechanism is shown in **Figure 6-13.**

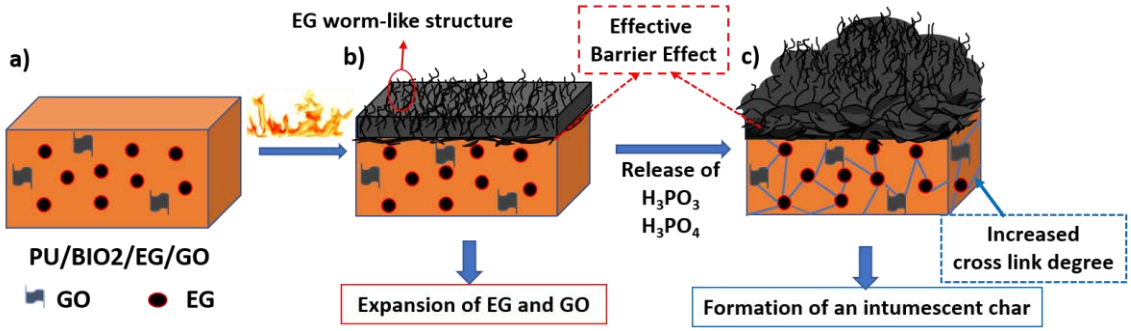

Figure 6-13. Proposed FR mechanism for the synergistic action between EG, GO and CPPA.

6.3.5. *Mechanical properties*

The introduction of additives in a polymeric matrix has commonly important effects on the compression properties. Also, density is related to a more compact cellular structures and influences positively on the compression strength. The data obtained for the compressive strength are shown in **Figure 6-15** and in **Table 6-9**. The compressive strength of BIO1 foam showed a value about 0.071 MPa. The huge porous structure and big cell size favored the propagation of micro-cracks and the fragility of the cell walls (**Figure 6-8**), thus debilitating the compression resistance of the foam. When using CPPA as polyol in BIO2, the compressive strength increased up to a 106 % compared to BIO1. The reason behind this improvement is that the viscosity was increased by the interaction of the higher quantity of -OH groups from the biobased polyol (CPPA) with -NCO groups, thus improving the interlayer network structure and increased the crosslinking density as it was reported before [166], [248]. When EG was introduced, the compressive strength of the samples decreased slightly up to a 25 %. As reported in previous chapters, the slippage between the components and the big size of EG, damages the cell walls and the integrity of the foam, leading to an inhomogeneous structure, increasing the average cell size of the foam with broken walls and resulting in a decrease of the compressive performance [210], [212]. In addition, the commercial reference of **Chapter 4** obtained higher compressive strength in a previous study probably due to the higher density and the absence of interfering additives in the cell structure [211] (**Table 4-6**). Therefore, the

compression performance of the biobased foam (BIO2) containing EG additives is slightly worse than that of the BIO2.

Nonetheless, based upon the results, the depleting of 0.5 wt. % of EG to GO, increased slightly the compression strength compared to EG, which is in accordance with the literature [149]. Besides, the dispersion of EG was enhanced and the average cell size was increased, being closer to the one of BIO2 (**Table 6-5**). The improvement in the properties upon the addition of GO may be attributable to the oxygen-functionalization of GO, improving the dispersion of GO and EG in the matrix and the strong interfacial interaction between the oxygen groups and the PU matrix. This good dispersion can be observed in **Figure 6-7** and **Figure 6-8**. -NCO groups at the ends of PU chains, could react with the -OH groups on the GO surface to form covalent bonds (**Figure 6-14**), thus increasing the crosslinking degree of PU [266]. On this way, a strong covalent interface interaction between the nanofiller (GO) and the HS of the PU polymeric matrix was formed, allowing effective load stress transfer from PU to GO and increased the mechanical strength [146]. However, three main aspects have been reported to consider: The intrinsic properties of the GO nanolayers, dispersion state of GO in the matrix and its interfacial interactions. Concluding that at higher loadings of GO, the interface diminishes and the mechanical performance become worse due to high agglomeration of GO and an effective reduction of the aspect ratio, that decreases the adhesion strength with the PU matrix [272].

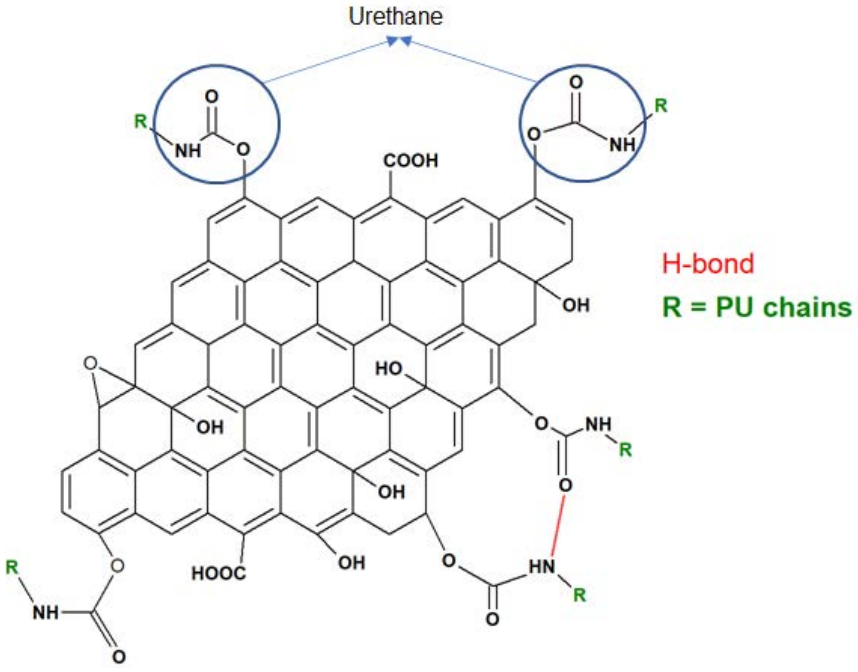

Figure 6-14. Interfacial interaction of GO with PU matrix.

Table 6-9. Compressive strength data of bio based RPUF samples.

Sample	Compressive strength (MPa)	Standard deviation (%)
BIO1	0.071 ± 0.004	5.7
BIO2	0.146 ± 0.013	8.6
BIO2/EG	0.109 ± 0.008	7.2
BIO2/EG/GO	0.112 ± 0.003	2.8

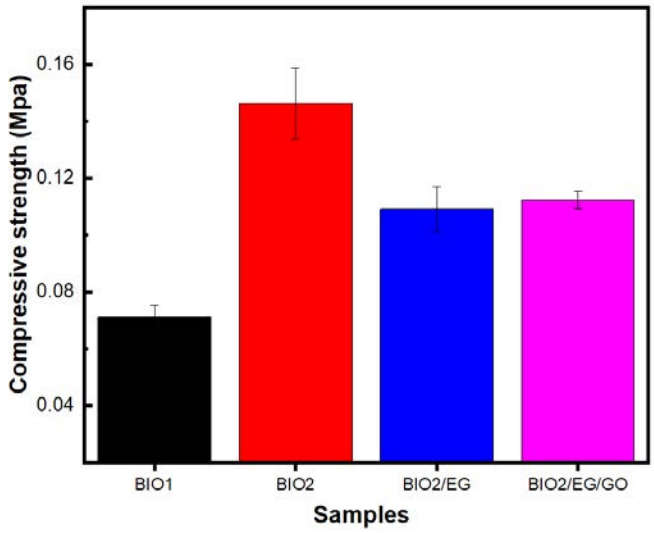

Figure 6-15. Compressive strength of RPUF samples at 3 mm/min constant rate.

6.4. Conclusions

The introduction of derived-carbon materials such as EG and GO into a biobased RPUF matrix was studied by the cellular structure, their thermal behavior, FR and compressive performance. The cellular structure showed that BIO2 decreased the cell size a 72 % compared to BIO1, whereas the introduction of EG increased the cell size a 206 % compared to BIO2 and GO reduced the cell size by a 63 % compared to BIO2/EG. The thermal conductivity of BIO2/EG/GO was decreased up to a 13 % compared to a similar commercial RPUF and a 10 % compared to BIO2/EG. The covalent bonds between GO and PU matrix increased the crosslinking density of the foam and the gas barrier effect of GO, towards the lower cell size, improved the insulation capacity of the foam. The fire properties showed a big improvement;

BIO2/EG/GO obtained a LOI of 27.2 % along with a V-0 rating in the vertical burning test, compared to 24.0 % and no rating obtained by BIO2 foam. Indeed, BIO2/EG obtained only V-2 rating in the vertical burning test. Moreover, CCT showed that BIO2/EG/GO improved the PHRR, THR and TSP a 54 %, 25 % and 15 % respectively with respect to BIO1. Also, PHRR and THR were improved a 46 % and 6 % with respect to BIO2 foam. The reason behind is the combination of a condensed phase barrier insulation effect against heat and mass transfer from EG and GO towards an intumescent effect of CPPA. Furthermore, the compressive strength showed an important improvement of a 58 % compared to BIO1. The good interfacial adhesion of GO structure and the PU matrix increase the crosslinking density and allows an effective load stress transfer from PU to GO which increased the mechanical strength of the foam compared to the addition of EG. This study provided a new strategy to develop high performance FR PU foam as fire safety thermal insulation material.

CHAPTER 7

7. Multifunctional biobased RPUF by using a modified GO

"I have not failed. I've just found 10,000 ways that won't work"

- Thomas A. Edison

7.1. Introduction

Graphene oxide (GO) is a carbon-based nanomaterial which contains large number of oxygen-based functional groups, such as epoxy, -OH and few others. Unlike graphene, the functional groups of GO disrupt the conjugation of aromatic rings and improve the insulation capacity of PU nanocomposites [126], [252]. This ability fits perfectly with the expected insulation capacity of RPUFs. In addition, GO improves the mechanical strength of the material by a good interaction with the PU matrix, principally -NCO with the oxygen-functionalities under the GO surface [147]. However, GO itself does not provide high FR efficiency to a RPUF, which is a very flammable material due to its porous structure as we have checked in the previous chapters. Many researchers supported the idea of a chemical functionalization of carbon nanomaterials as an effective way to improve their dispersion and to insure the development of strong interfacial interactions between the carbon nanomaterials and polymer matrixes at a molecular level [278]. It has been reported that the thermal conductivity of GO could decrease with the increasing oxidation an with the presence of doping defects [279]. In addition, GO is hydrophilic in nature, being easily dispersed in water. The presence of both aromatic (sp2) and aliphatic (sp3) domains increases the possible interactions on its surface [280]. The addition of some phosphorous compounds have been reported to obtain a more homogenous dispersion of carbon nanomaterials [244]. In detail, the grafting of phosphorus and/or nitrogen-containing

compounds onto the surface of GO, improve both the dispersion and FR capacity of the nanocomposites [154]. For example, DOPO grafted on GO, helped to disperse it in the polymer matrix and enhanced the formation of residue chars as reported by Sun et al. [261]. The presence of stiff phenyl groups on the chemical structure of the FR, beneficiates the compressive strength of RPUFs [80] as it was proved in **Chapter 5**. Finally, the good compatibility of P-N FRs with the PU matrix, endows RPUFs with increasing thermal insulation and mechanical properties [100].

Nowadays, several articles were published dealing with the properties of graphene derivatives in PU foams. For example, Zhou et al. [281], used functionalized graphene to duplicate the compressive performance of PU sponges. Furthermore, with the aim to increase other properties, Santiago-Calvo et al. [33] used graphene derivatives to reduce the thermal conductivity by a 25 % cell size reduction towards increasing the Young´s modulus of RPUFs. Recently, the functionalization of GO with phosphoric acid, dodecylbenzenesulfonic acid (DBSA), and polyaniline (PANI), provided anti-corrosion performance and better dispersion into waterborne PU coatings, mainly due to strong hydrogen bonds between the components [282]. Moreover, Chen et al. [190], functionalized GO to impart high thermal stability and flame retardancy to RPUFs at only 0.25 phr. However, not very much research has been done to improve several properties at once, such as the thermal resistance, flame retardancy and compressive strength of a biobased RPUF by using graphene derivatives.

Herein we describe the addition of EG combined with modified GO (PGO) into a bio-based FR RPUF (BIO2) from the previous chapter. The as-created RPUF was studied by the influence of PGO on the cellular structure, thermal, FR and mechanical properties. Indeed, the combination of natural-based polymeric products with improved thermal insulation, high flame retardancy and outstanding mechanical properties by using graphene-derivatives is a tremendous and exciting challenge. The current chapter is based on a submitted publication as pointed out in "*contenidos publicados y presentados*" section.

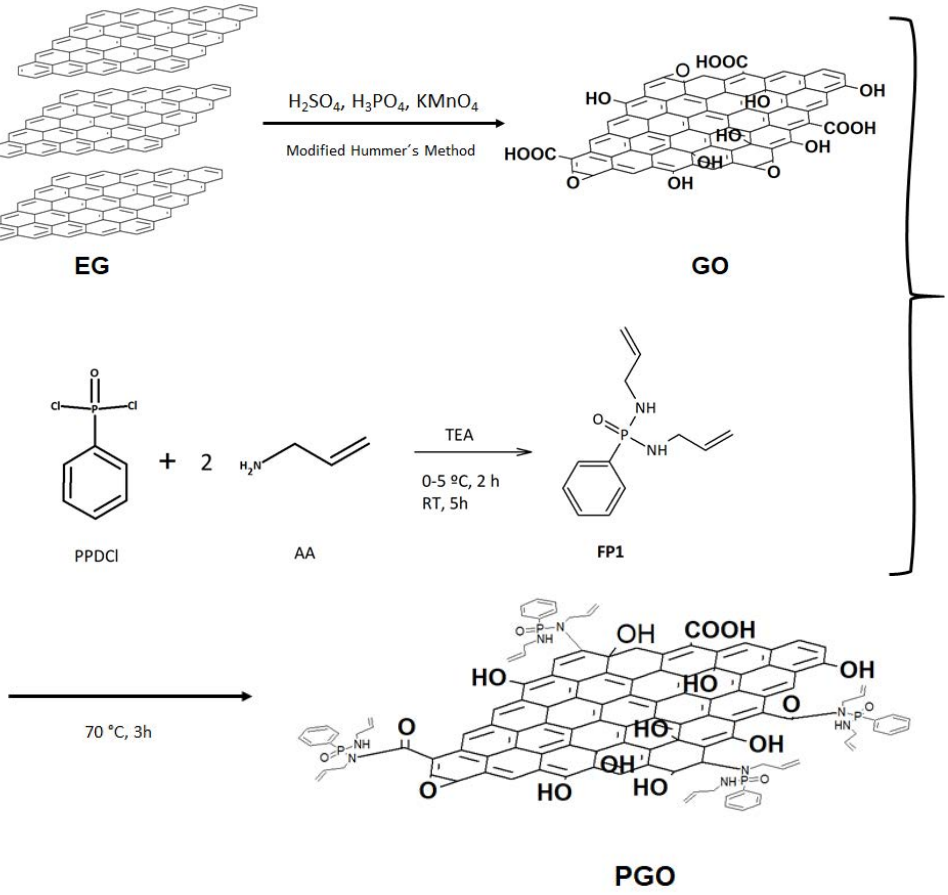

Scheme 7-1. Schematic illustration for the synthesis process of PGO.

7.2. Materials

7.2.1. *Materials*

Commercial RPUF reference as well as the Isocyanate for the biobased RPUFs was obtained from FOAM-IT! ™ 5 (Smooth-On, FormX Spain, Spain). CPPA from **Chapter 6**, Polycat 34 and DABCO K-15 as catalyst 1 and 2 respectively and DABCO DC193 as surfactant were kindly provided by Airproducts iberica (Bellaterra, Spain) and used to prepare the bio-based reference foam (BIO2). GO for the preparation of PGO was reported in section **6.3.1.b)** of the previous chapter. PPDCl (90 %), AA (98 %), TEA (99 %) and DEE (99.7 %) were purchased from Sigma-Aldrich and used as received.

7.2.2. *Preparation of PGO*

a) *Synthesis of FP1*

The preparation of N, N'-Diallyl-P-phenylphosphonicdiamide (FP1) was done according to a previous publication [283]. In detail, PPDCl (0.2 mol in 200 mL DEE) was added dropwise to a solution of AA (0.4 mol) and TEA (0.4 mol) in 200 mL DEE into a flask at 0-5 ºC and stirred during around 2 hours. Then, the stirring was continued at room temperature (RT) during 5 h. A white precipitant appeared, corresponding to triethylamine hydrochloride (TEA-HCl, 50.95 g, 92.5 % yield). The solid-liquid mixture was vacuum-assisted filtrated to eliminate TEA-HCl, and the rest of the solution was re-dissolved in acetone. The solution was vacuum-assisted evaporated to obtain FP1 (orange solid, 42.0 g, 89 % yield). ^{1}H NMR (DMSO-d6, ppm) (**Figure 7-1 a)**): 7.7-7.4 (Ar-H, 5H, **d-f**); 5.8(=CH, 2H, **b**); 5.2-5.0 (=CH_2, 4H, **a**); 4.6 (NH, 2H, **g**); 3.4 (-CH_2-, 4H, **c**). ^{13}C NMR (DMSO-d6, ppm) (**Figure 7-1 b)**): 138.5 (**a**), 132.2 (**g**), 132.0 (**f**), 131.4 (**e**), 128.6 (**d**), 115.0 (**a**), 43.1 (**c**). ^{31}P NMR (H_3PO_4, ppm) (**Figure 7-1 c)**): 20.8, confirming a phosphonate-based skeleton phosphorous structure (O=P(R)$(OR)_2$. NMR spectra of FP1 are shown in **Figure 7-1 a-c)**. FTIR (cm^{-1}, KBr window): -NH- stretching (3178), stretching of C-H of Ar and CH_2=CH (3010-3080), C-H of –CH_2- (2896, 2654), C=C of double bond and Ar (1643, 1592), P-Ar bond (1438), P=O (1180); P-N (1120) [99], C-N (1078) [284], C-H bending from vinyl group (996 and 915). FTIR spectra of FP1 was shown in **Figure 7-2**.

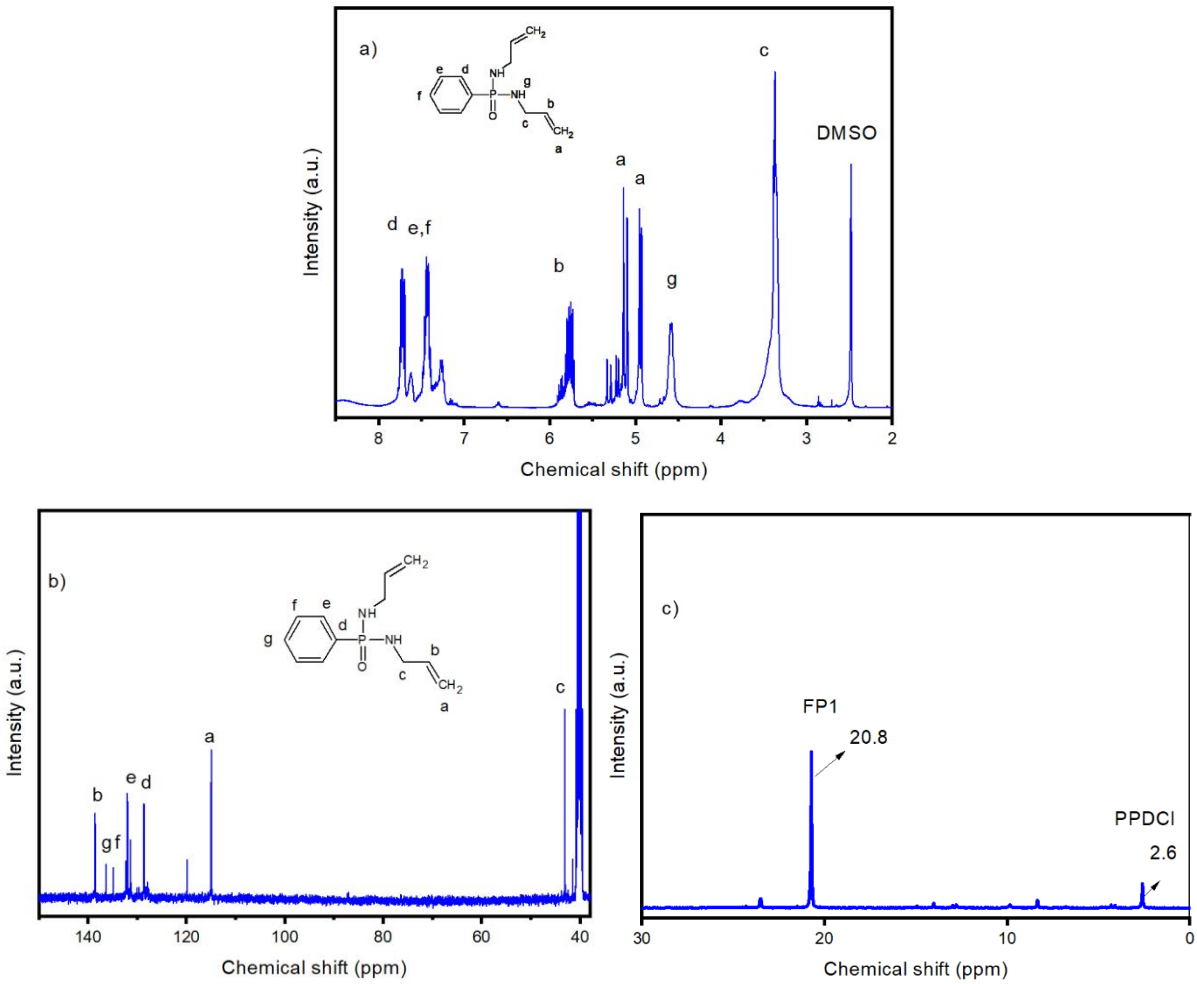

Figure 7-1. a) ^{1}H NMR spectra, b) ^{13}C NMR spectra and c) ^{31}P NMR spectra of FP1.

b) *Preparation of Phosphorous-functionalized Graphene Oxide (PGO)*

Graphene oxide (GO) was prepared following the procedure reported in **Chapter 6, section 6.3.1.b)** [256]. FTIR (cm^{-1}, KBr method): -OH (3460), C=O (1734), C=C (1631), C-OH (1380) and C-O-C (1107). The broad band assigned to -OH groups can also contain -COOH groups and intercalated water due to the hydrophilicity of GO [285]. The FTIR of GO (**Figure 7-2**) was in accordance with those from literature [286]. The proposed reaction to modify GO to obtain PGO is shown in **Scheme 7-1**. Dry and pulverized GO (1.5 g) was placed in a glass beaker under a hot plate calefactory plate equipped with a thermometer and magnetic stirrer. Inside the beaker, 300 mL of distilled water were added and stirred at 70 ºC during 1 h to disperse GO as it is hydrophilic and easily dispersed in water [280]. Then FP1 in a 1:1 mass relation to GO was added and the solution was continued stirred at 70 ºC during 3 h. After that, the mixture was vacuum filtrated and dried overnight at 80 ºC to obtain solid PGO. The FTIR

spectra for PGO is shown in **Figure 7-2**. FTIR (cm^{-1}, KBr window): 3693 (free -OH), 3612 (H-bonded -OH), 3411 (-NH- stretching) [287], 3000-3200 (C-H, Aryl and CH_2=CH) [99], 1620 (-NH- bending) [154], and 1385 (C-N stretching) [288], 1263 (P=O) [263], 1089 (P-N) [238], 1021 (C-N from FP1) and 805 (N-H wag). Taking into account this results, FP1 was successfully grafted onto GO surface by an amide/ester connections between oxygen groups from GO and NH bonds, as reported by several authors [137], [154], [238], [289], [290].

7.3. Results and discussion

7.3.1. *Characterization of modifiers and sample preparation*

a) *Characterization of PGO*

- **FTIR spectra of PGO:**

The FTIR spectra of GO, FP1 and PGO is shown in **Figure 7-2**. In GO, the oxygen-functionalized groups under its surface were reported. In PGO, after the modification with FP1, the previously assigned -OH stretching and the C-OH band for GO decreased significantly, in a similar way as reported from literature [152]. On the other hand, it could be distinguished, the principal modes of -OH groups, the smaller broad signal typical from free and isolated -OH groups at 3693 cm^{-1} and the H-bonded -OH groups at 3612 cm^{-1}. The other stretching modes of -OH groups from intermolecular bonding (intercalated H_2O and -COH within GO), are located in the broad band range between 3200-3600 cm^{-1} [154]. The presence of isolated -OH groups suggest the possibility a ring opening reaction between the N-H from the amine of PGO and the epoxy moiety of GO [287], [291]. In addition, the intermolecular bonded -OH peak is so broad that suggest interactions between O-H and -N-H groups [292]. Then, aromatic C-H groups, from GO and FP1, showed between 3000-3200 cm^{-1} and aliphatic from GO structure at 2800-2970 cm^{-1}. On this way, the FP1 functionalized structure on GO was showed by C=O from amides (1727 $cm^{-1)}$, N-H stretching (3406 cm^{-1}), bending (1620 cm^{-1}) from the epoxy ring opening [154], [289], [290] and C-N stretching (1385 cm^{-1}) [288]. Then, P=O (1263 cm^{-1}) [263], P-N (1089 cm^{-1}) [238] showed the phosphorous containing parts of FP1. Importantly, the N-H out of plane bend for primary and secondary amines, called “N-H wag” [293], [294] was found at 805 cm^{-1}. Taking into account these results, FP1 was successfully grafted onto GO surface by an amide/ester connections between oxygen groups from GO (-OH from -COOH and epoxy) and N-H bonds [137].

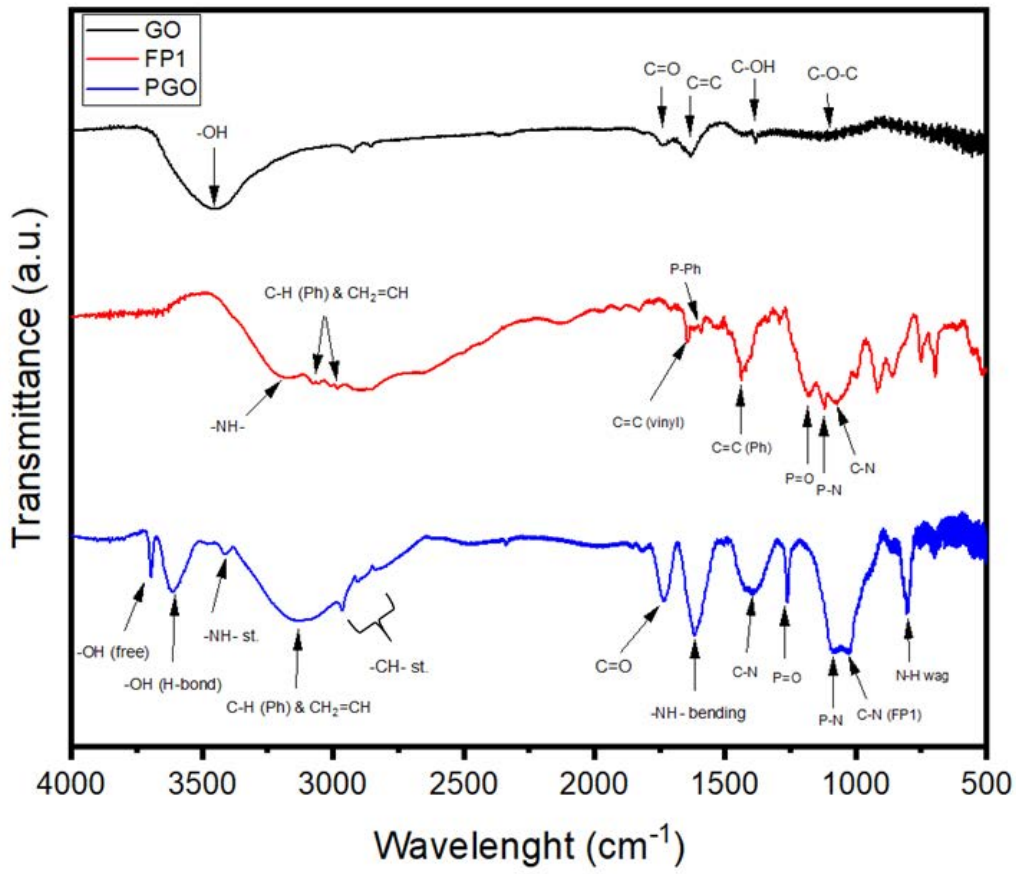

Figure 7-2. FTIR spectra of GO, FP1 and PGO.

- **Raman spectroscopy results of GO and PGO:**

The Raman spectra of EG, GO and PGO are shown in **Figure 7-3**. As reported previously in **Chapter 6**, the spectra of EG displayed a very intense G band at 1582 cm^{-1}, a 2D band at 2720 cm^{-1} and a smaller D band at 1350 cm^{-1}, which indicates the presence of inherent defects due to the strong acid intercalation into the layers for the preparation of EG [263]. For GO and PGO, the Raman spectra showed two main peaks related to a D and G band. The D band becomes more intense, thus increasing the D/G ratio for both GO and PGO with respect to EG due to the intense oxidation treatment and the presence of oxygen-groups [263] [265]. The G band is broadened and shifts to 1593 and 1590 cm^{-1} for GO and PGO respectively whereas the D band shifts downward to 1353 and 1354 cm^{-1} for GO and PGO respectively. This results are consistent with the work by Guo et al. [263]. The D/G intensity ratio are listed in **Table 7-1** and reflected the significant structural changes occurring during the chemical processing from pristine EG to GO and PGO. Due to the increase on the D band intensity, the D/G ratio for both

GO and PGO was enhanced with respect to EG. In this way, the increase in the I_D/I_G ratio, indicates changes on the EG and GO structure. I_D/I_G for GO was 1.17, whereas it increased to 1.49 in PGO. The increase reflects more defects formed with the incorporation of functional groups from FP1 by a chemical grafting on the surface of GO [152].

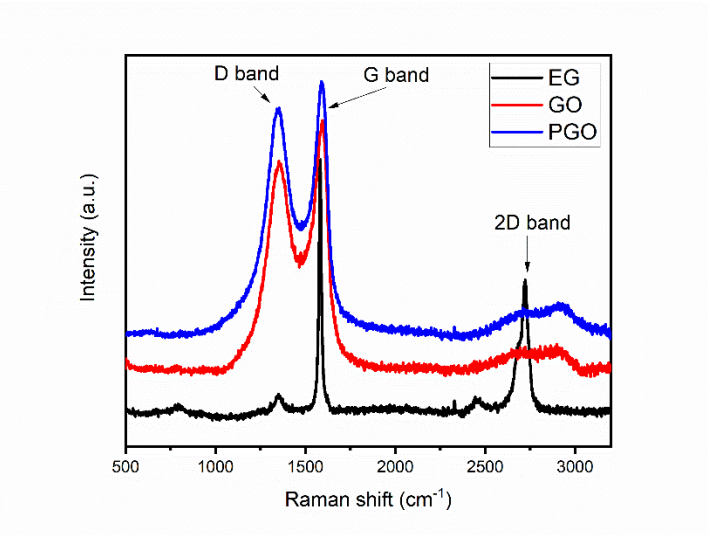

Figure 7-3. Raman spectra of EG, GO and PGO.

Table 7-1. Raman Peak Positions and D/G Intensity Ratio of EG, GO, and PGO samples.

Sample	Peak of band D (cm^{-1})	Peak of band G (cm^{-1})	I_D/I_G integrate area ratio
EG	1356	1582	0.29
GO	1353	1593	1.17
PGO	1354	1590	1.49

- **XPS spectroscopy results of GO and PGO:**

Figure 7-4 shows the XPS spectra of GO, PGO and their complete XPS scan. The C1s spectra of GO and PGO are showed in **Figure 7-4 a)** and **b)** respectively. The spectra of GO, only shows the presence of carbon and oxygen; the peak at 286.6 eV is attributed to sp2 carbon of graphite (C-C bond), and the peaks at 288.7 eV, 290.1 eV and 291.6 eV are typically attributed to oxygen containing groups such as -OH, epoxide, and carboxyl [295]. The corresponding C 1s spectra of PGO (**Figure 7-4 b)**), showed that the peaks attributed before to oxygen functionalities in the surface of GO, got their intensity decreased, indicating that most of the

oxygen functional groups have been successfully removed [296] . After the modification with FP1, an additional peak related to C-N (287.4 eV) appears [153] whereas the rest of oxygen-containing peaks like C-O (288.1 eV) and C=O (288.9 eV) and the carbonic peaks such as C-C (285.9 eV) are showed [290].

The full scan spectra of GO and PGO are depicted in **Figure 7-4 c)**. It can be observed also new peaks related to phosphorous (P2s and P2p), revealing the presence of FP1 into the GO surface [261], [296]. As a result of the grafting of FP1 into the GO surface, the individual components of a given XPS band arising from different environments shift to different extents confirming the reaction between those components according to Huang et al. [154]

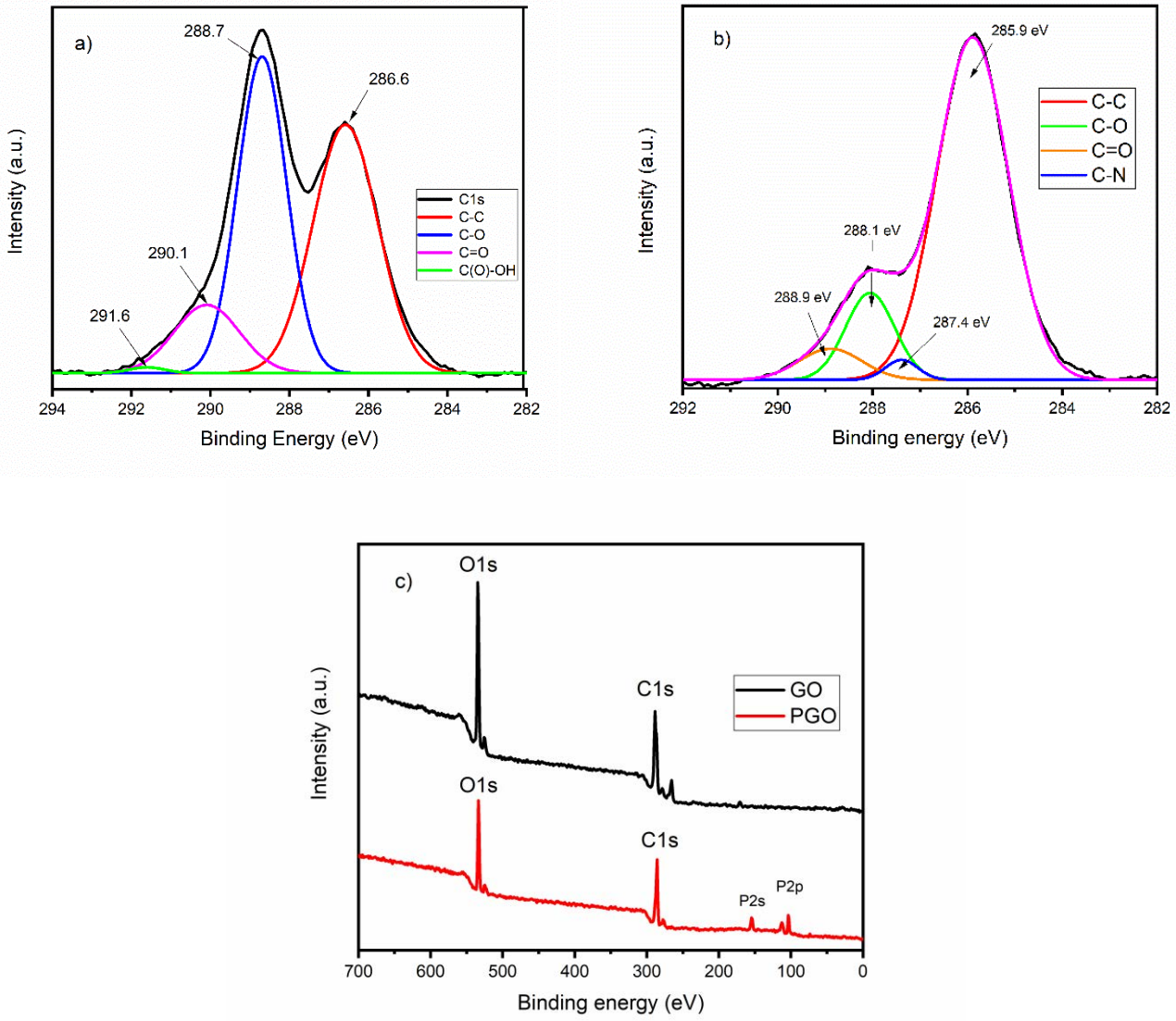

Figure 7-4. XPS spectra of a) GO, b) PGO and c) XPS full scan spectra comparison.

7.3.2. *Foam preparation and characterization*

RPUFs samples were prepared by mixing each component separately. A scheme showing the process is shown in **Scheme 7-2**. Firstly, bio-based polyol (CPPA), catalyzer 1 and 2 were added along with the surfactant and water as blowing agent. The polyol mixture was stirred 1 min with Heidolph RZR-1 mechanical stirrer until a uniform, red mixture was obtained. Then, isocyanate was added at an appropriate amount and then, the as-created PU mixture was stirred at a high strength until the beaker starts heating. The samples with the addition of EG, GO or PGO followed the same procedure but adding the additives in the polyol mixture prior to the mixing with isocyanate. The overall formulas are plotted in **Table 7-2**. The mixture was poured into a 250 mm × 250 mm × 60 mm open Aluminum mold, where the RPUFs raised freely in vertical direction. After curing at room temperature for a minimum of 24 h, samples were cut according to the standards for the different test performed. The foams were designed to obtain density close to the ones used for thermal insulation in buildings, which normally ranges between 20 kg/m³ and 50 kg/m³ [16], [233], [297].

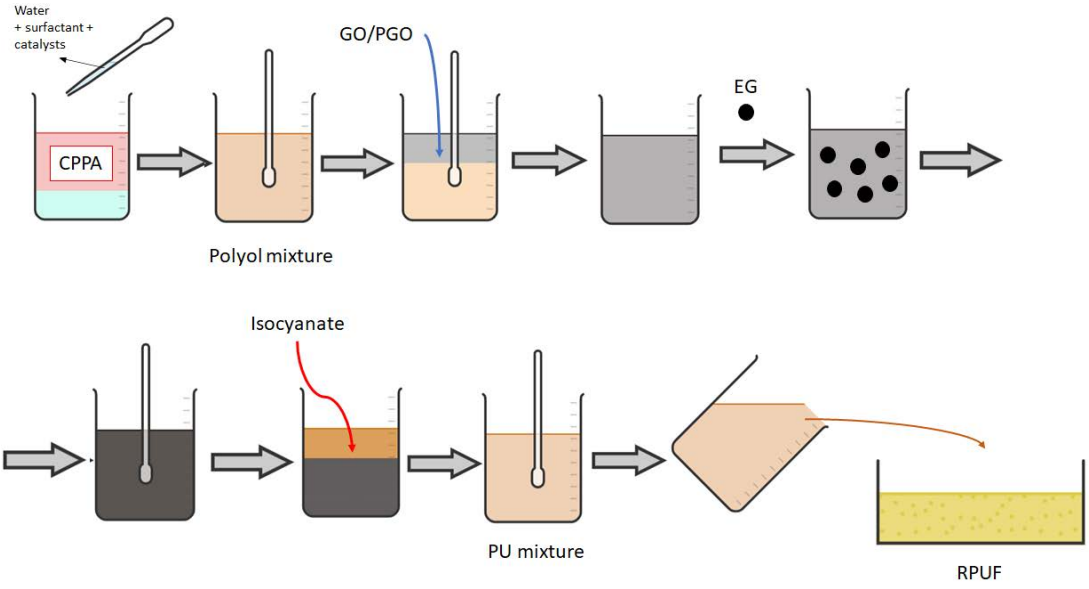

Scheme 7-2. Schematic representation of the manufacturing process of the RPUF samples.

Table 7-2. Formulae of RPUF materials.

Component	BIO2	BIO2/EG	BIO2/EG/GO	BIO2/EG/PGO
CPPA	92.5	92.5	92.5	92.5
Catalyzer 1	1.5	1.5	1.5	1.5
Catalyzer 2	0.5	0.5	0.5	0.5
Surfactant	4	4	4	4

Blowing agent	1.5	1.5	1.5	1.5
Total B*	100	100	100	100
Isocyanate (A)	115	115	115	115
EG	-	13.7	12.6	12.6
GO	-	-	1.1	-
PGO	-	-	-	1.1
Wt. % EG	0	6	5.5	5.5
Wt. % GO	0	0	0.5	0
Wt. % PGO	0	0	0	0.5

*B components (polyol, catalyzers, surfactant and blowing agent) are based on 100 g of material. The rest of the components are related to 100 g of B.

a) *Characterization of foam samples*

- **FTIR spectra of foam samples:**

The FTIR of the samples tested on this chapter is showed in **Figure 7-5**. First, it can still be observed the -NCO band form the excess used. The broad band between 3200-3700 was assigned to N-H stretching vibration [91], [294] and the -C=O peaks of urethane were found below 1710 cm^{-1}, which is an indicative of a huge H-bonded structure, which can include carbamate esters and amides [146], [288], [294], [298]. Besides, the -C=O band associated with urea formed bonds from the reaction of -NCO with amines from PGO was assigned between 1630 and 1680 cm^{-1} and included free and H-bonded urea [91], [245], [299]. Last, the C-N and N-H associated band of urea and urethane bands were found at 1537 and 1544 respectively [245], [294]. These spectra confirmed the successful introduction of PGO with the PU matrix and the reaction of -NCO from the excess of the PU end-chains with the amines present in the PGO structure. In addition, it can be observed enhanced H-bonds interactions due to the presence of -OH and N-H groups from PGO and the HS (including urea and urethane) of the RPUF.

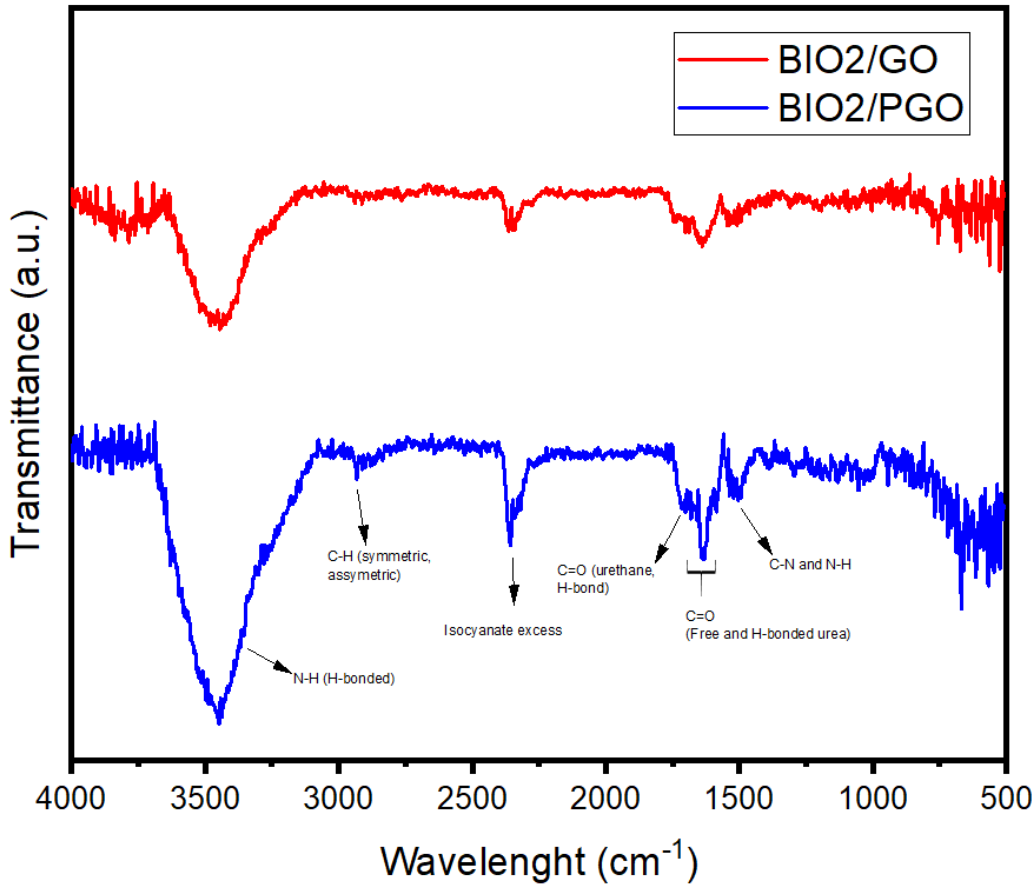

Figure 7-5. FTIR spectra of foam samples.

7.3.3. *Cellular structure analysis and thermal conductivity of RPUF samples*

a) *Cellular structure analysis*

The influence of the introduction of graphite-based particles into the BIO2 cell structure can be observed in **Figure 7-6.** The different physical foam structures are showed in **Figure 7-7.** The average cell size diameter is showed in **Table 7-3**. As showed in **Chapter 6,** BIO2 cell size was 226 µm (**Figure 7-6 A)**) and EG increased the cell size to 692 µm (**Figure 7-6 B)**). The weak adhesion between EG and the PU matrix [47] and the agglomerates formed by the bad dispersion with consequently nucleation of the EG particles during the foam formation, opened and increased the cell size of the BIO2/EG [176]. Due to the EG size (500 µm), the particles are located inside the cell walls [267]. The introduction of GO decreased the cell size up to 254 µm (**Figure 7-6 C)**). The dispersion of GO is better than EG and produced a more homogeneous cellular structure, attributed to the interactions between the oxygen groups on the GO surface and the PU matrix [266]. The dispersibility properties of GO, enhances the dispersion of EG and facilitated a strong interaction with the PU matrix [127], [128]. However, compared to

BIO2, GO was not beneficial for the cell size reduction due to a possible increase in the viscosity; mostly caused by an intense hydrogen bonding [146], which would lead to some agglomerates [138]. BIO2/EG/PGO showed interesting results in terms of cell size reduction, which will have impressive implications into the thermal resistance and mechanical performance. As it can be observed in **Figure 7-6 D))**, the cell size is remarkably reduced to 196 µm, meaning a 14 % reduction with respect to BIO2, a 72 % reduction with respect to the sample with only EG and a 23 % reduction with respect to BIO2/EG/GO. As stated in **Figure 7-13**, the interaction between the chemically attached FP1 of PGO and the -NCO from the PU matrix, would lead to an increasing viscosity and a lower foaming pressure [77], which consequently on one hand, reduces the cell size and on the other hand increased the density (**Table 7-3**). Besides, the amine functionalization of PGO would help to an improved dispersion of the fillers [238], [287], thus potentially diminishing the cell size increase effect which occurred by the EG addition.

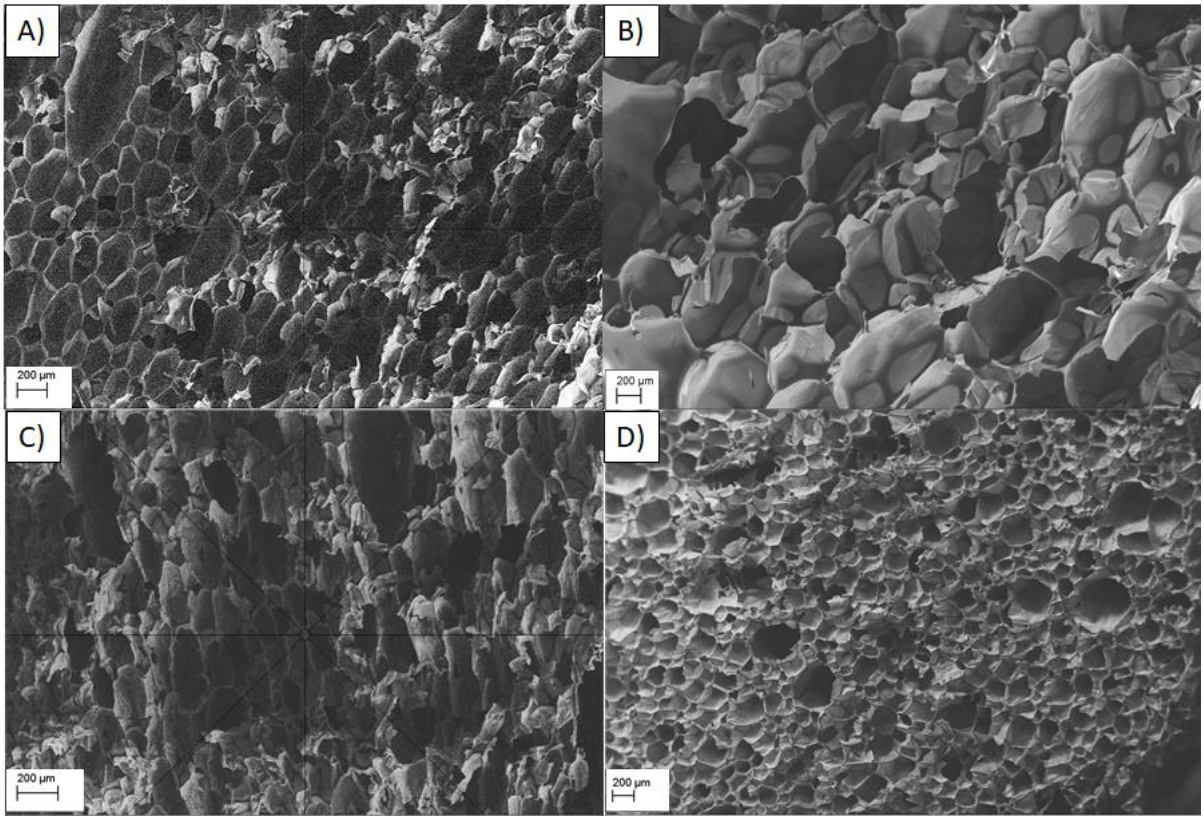

Figure 7-6. SEM micrographs of A) BIO2, B) BIO2/EG, C) BIO2/EG/GO and D) BIO2/EG/PGO foam samples.

b) *Thermal conductivity*

Due to the use of RPUFs as insulating materials, a low thermal conductivity is one of the most important parameters needed. Thermal conductivity generally decreases with decreasing cell size [215]. For that reason, to evaluate the effect of graphene-based materials, such as PGO in the cellular structure of the foams, the thermal conductivity was measured. The different foam structures are showed in **Figure 7-7**.

As showed in **Chapter 6**, the bio-based reference foam (BIO2) obtained a low thermal conductivity of 33.8 mW/Mk. The introduction of EG, increased the thermal conductivity up to 38.2 mW/Mk, increasing it up to an 13 % compared to that of BIO2 (**Table 7-3**). It was increased the conduction through the solid phase (λs) due to the intrinsic high thermal conductivity of EG and the slightly increase of the density and the cell size of the foams, that weakens the thermal insulation efficiency of RPUF foams [216].

The substitution of 0.5 wt. % of EG by GO (BIO2/EG/GO) and PGO (BIO2/EG/PGO), led to a decrease of the thermal conductivity around 10 % and 8 % respectively compared to BIO2/EG. Besides, PGO still reduced the thermal conductivity compared to a commercial PU by an 11 % (**Table 6-5**). As reported by Zhang et al. [300], GO sheets exhibit much lower thermal conductivity compared to that of pristine graphene due to the prevalence of oxygenic functional groups (e.g., epoxide, -OH, and carboxyl), high porosity and defect-induced scattering of phonons. Indeed, Santiago-Calvo et al. [33] showed that GO strongly reduces the cell size and consequently, the thermal conductivity is decreased. Three combined effects explain the previously mentioned improvement. First, due to the good interaction of GO and PGO with the PU matrix, the dispersion of EG was improved [128], as the presence of EG disrupts the cellular structure leading to a coarser cell structure [138]. In the case of PGO, amide and amine functionalities have been reported to achieve a more uniform distribution due to stronger interaction with the polymeric matrix [287], [292], [301]. This effect results in a reduction of the λs contribution. Secondly, graphene derivatives enhance the gas barrier performance of PU [271]. It was reported by Nguyen et al. [292] that functionalized GO creates a “tortuous path” for O_2 permeability, which delays at some extent, the diffusion of the gases through the PU cellular structure and giving O_2 barrier properties. The gas barrier capacity of GO and PGO, influences in a lower contribution of λg, thus decreasing the highest contributor of the thermal conductivity. Finally, GO and PGO act as radiation infrared blocker, decreasing the cell size and increasing the extinction coefficient of the cell walls [138], thus reducing the λr contribution to the thermal conductivity [148]. Although the smaller cell size of

BIO2/EG/PGO with respect to BIO2/EG/GO would represent a lower contribution of the λr to the thermal conductivity, the small difference between GO and PGO-filled RPUF; in terms of thermal conductivity, are negligible and ascribed to the increased density of BIO2/EG/PGO (**Table 7-3**). This density increase suggests an increasing λs besides the λr decrease due to a lower cell size, leading to an overall slightly higher thermal conductivity. The increase of density by the addition of PGO was mainly attributed to an increase of the polyol viscosity; due to the presence of stiff phenyl groups from FP1 [80], and the covalent interaction between PGO and the PU matrix. Furthermore, the proposed amide/ester bonds between oxygen-containing groups of GO and -NH from FP1 (**Scheme 7-1**), could increase the amount of free -OH groups on the surface of GO and being easy bonded to -NCO groups (**Figure 7-13**), thus finally increasing the crosslinking density of the composite.

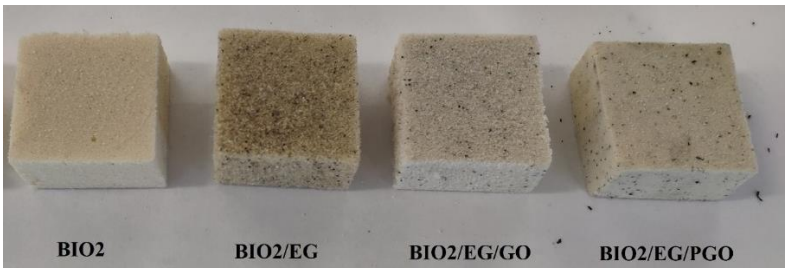

Figure 7-7. Physical structure of the different foam samples studied.

Table 7-3. Average cell size, thermal conductivity and density data results for the RPUF samples.

Sample	Average cell size diameter (μm)	Thermal conductivity (mW/mK)	Density (Kg/m^3)
BIO2	226 ± 3	33.8 ± 0.3	31.8
BIO2/EG	692 ± 31	38.2 ± 0.6	32.9
BIO2/EG/GO	254 ± 6	34.2 ± 0.3	30.4
BIO2/EG/PGO	196 ± 12	35.0 ± 0.2	34.6

7.3.4. *FR properties of RPUF samples*

a) *LOI and UL94 tests*

The data obtained from the LOI and UL94 tests are collected in **Table 7-4** and a draft is showed in **Figure 7-8 d)**. The average after flame time (t1+ t2) for each individual sample was included. As reported in **Chapter 6**, The LOI values of the reference foams (BIO2 and BIO2/EG) were

24.0 % and 27.6 % respectively. This means that the use of EG as FR obtained a LOI 15 % higher than BIO2. BIO2/EG/GO obtained a LOI value of 27.2 %. The barrier condensed phase effect of GO is less effective than EG since GO does not "expand" as much as EG as a result of the lower acid content between the layers due cleaning process to obtain GO. On the other hand, PGO increased the LOI value with respect to GO to 27.6 %. The higher density of BIO2/PGO (**Table 7-4**) and the presence of phosphorous containing species due to FP1, explained the better fire resistance with respect to the use of GO.

The UL94 of BIO2, as a neat PU sample, was not classified under the standard, being an easy flammable material. The use of 6 wt. % of EG increased the UL94 rating to V-2, because of small dripping flaming particles during the test which consequently ignited the cotton. The cracks on the surface of PU, favored the entrance of heat through the internal porous structure of the foam, increased the internal temperature and consequently melted the polymer, producing some dripping during the test. Besides, the after-flame time was 5.3 s. The use of 0.5 wt. % of GO increased the rating to V-0, with an after-flame time of only 3.6 s. The barrier effect against O_2 penetration into the polymer matrix for a well-dispersed graphene sheets was possibly the explanation as reported by Bian et al. [272]. In addition, PGO at 0.5 wt. % not only maintained the V-0 rating but the burning rate on BIO2/EG/PGO was clearly diminished compared to BIO2/EG/GO. The total burning time was reduced to only an impressive 1.6 s, being the lowest among all the specimens tested. Due to the addition of PGO, a continuous graphene network could be formed, increasing the viscosity and suppressing the melt-flow and dripping of the PU during combustion [72], [302], thus avoiding the dripping flame particles and obtaining a V-0 rating. Therefore, the combination of GO and FP1 (PGO) obtained good FR results among LOI and UL94 tests at only 0.5 wt. % loading of PGO into a RPUF.

Table 7-4. LOI and UL94 tests results for the RPUF samples.

Sample	LOI (%)	UL94 rating	Average time (t_1+ t_2) (s)	Dripping flame particles
BIO2	24.0	NR	>30	Yes
BIO2/EG	27.6	V-2	5.3 ± 3.4	Yes
BIO2/EG/GO	27.2	V-0	3.6 ± 3.4	No
BIO2/EG/PGO	27.6	V-0	1.6 ± 1.4	No

NR: No rating in UL-94 test

b) *CCT test*

Cone calorimeter test was performed at a heat flux of 50 kW/m^2. The typical CCT evaluated parameters were: PHRR, THR and TSP and their curves are shown in **Figure 7-8** with all the data are summarized in **Table 7-5**.

First, the HRR curves for the RPUF samples were analyzed in **Figure 7-8 a**). The PHRR was rapidly raised after the ignition (less than 3s) due to the porous structure of RPUFs. On the other hand, the flameout time for the additive filled RPUFs was longer than that of neat RPUF (BIO2). As in the previous chapters, the curves regarding the PHRR, showed two peaks. The first one is attributed to the development of an intumescent char-type layer [104], whereas for the second one, is caused by the degradation from continuous heat exposure during the test [179], [303] and thermal feedback [204]. BIO2 obtained a PHRR of 330 kW/m² with the production of an intumescent char layer (**Figure 7-9 B**). EG as an additive (BIO2/EG), obtained 168 kW/m² as PHRR and a reduction of the PHRR of a dramatic 49 % with respect to BIO2. However, the intumescent char previously formed by BIO2, was slightly restricted by the worm-like expansive and rigid structure created by EG [64] (**Figure 7-9 D**). When 0.5 wt. % was depicted from EG (BIO2/EG/GO), the PHRR increased a little to 178 kW/m². Although this increase is considered negligible, GO showed lower effectiveness in the formation of a carbonaceous char layer compared to EG. On the other hand, when PGO was used, some improvements were found: BIO2/EG/PGO decreased the PHRR to an impressive 165 kW/m², meaning a 50 % reduction with respect to BIO2. Although GO alone was not a good char former, the use of FP1 grafted on GO, added a synergistic effect by a gas-phase (composed by PO· radicals) [283] and a condensed charring effect by the incorporation of poly-phosphoric acid and phosphates into the char [152]. Thus, favoring a better char quality with higher intumescent effect (**Figure 7-9 H**) and reducing the PHRR.

THR (**Figure 7-8 b**) is a measurement of the heat released by combustion during a given time. The reference sample BIO2, obtained a THR of 18.3 MJ/m². The introduction of EG (BIO2/EG) reduced the reference value continuously by a 2.0 %, explained by heat absorption of the endothermic EG expansion [176]. The use of GO, reduced the THR value until 17.3 MJ/m², meaning a 5.6 % reduction with respect to BIO2. The good dispersion of GO into the matrix decrease the THR due to covalent bonds between PU matrix and oxygen-functionalized groups on the GO surface which reduces the thermal diffusion across the PU matrix and improves the thermal stability [266], [304]. Furthermore, the use of PGO get even more narrowed down the THR until a 6.6 % in comparison to BIO2. The reason behind is due to the

enhanced grafting of the PU chains onto the surface of graphene by the highly functionalized PGO, delayed the production of volatile degradation products and O_2 permeation due to the formation of a tortuous path [305] together with more char residue; by the carbonization effect of FP1, produced to isolate the heat release by a barrier effect previously mentioned [238]. The synergistic effect may be attributed to the decomposition of FP1 to yield phosphinic acid with strong dehydration effect during heating, along with the promotion of a cohesive and compact char layer during combustion, which together with EG forms a compact carbonaceous layer with stabilized structure [176].

Smoke is the most dangerous agent in a fire scenario. For this reason, the measurement of the TSP is a key part of the FR study (**Figure 7-8 c**). TSP of BIO2 was 5.2 m². The addition of EG did not improved the TSP value. Therefore, the interference of the worm-like structure of EG with the intumescent structure formed by BIO2 (**Figure 7-9 A-B**), reduced the effectivity of the protective char activity against the smoke production. However, with the addition of GO (BIO2/EG/GO), TSP increased due to the possible breaking of reactive oxygen-functionalization on the GO surface by the external heat flux irradiation [277], which may increase the CO and CO_2 production. Thus the condensed phase FR effect was stronger against heat and mass transfer for EG than GO and the addition of unmodified GO cannot effectively decrease the volatilization of flammable gases [152]. Finally, the use of modified GO (PGO) led to a decrease in the smoke production compared to unmodified GO. This can be explained by many reasons. First of all, the modification of GO led to less free-oxygen groups on the GO surface, thus avoiding the release of big quantities of CO and CO_2. Secondly, a gas phase effect by the presence of FP1 generates radical low MW phosphorous species (such as PO·) [283], which can hinder the radical combustion reaction by capturing the OH· and H· radicals in the combustion zone [82], leaving C-O species in the condensed phase to form a more efficient char layer produced by high carbonization [306]. Thirdly, the char layer formed blocks the mass heat and mass transfer, thus decreasing the amount of volatile gases and decreasing the TSP [152]. As a resume, the modified FR additive (PGO) has a slightly better gas inhibition effect on PU matrix than unmodified GO.

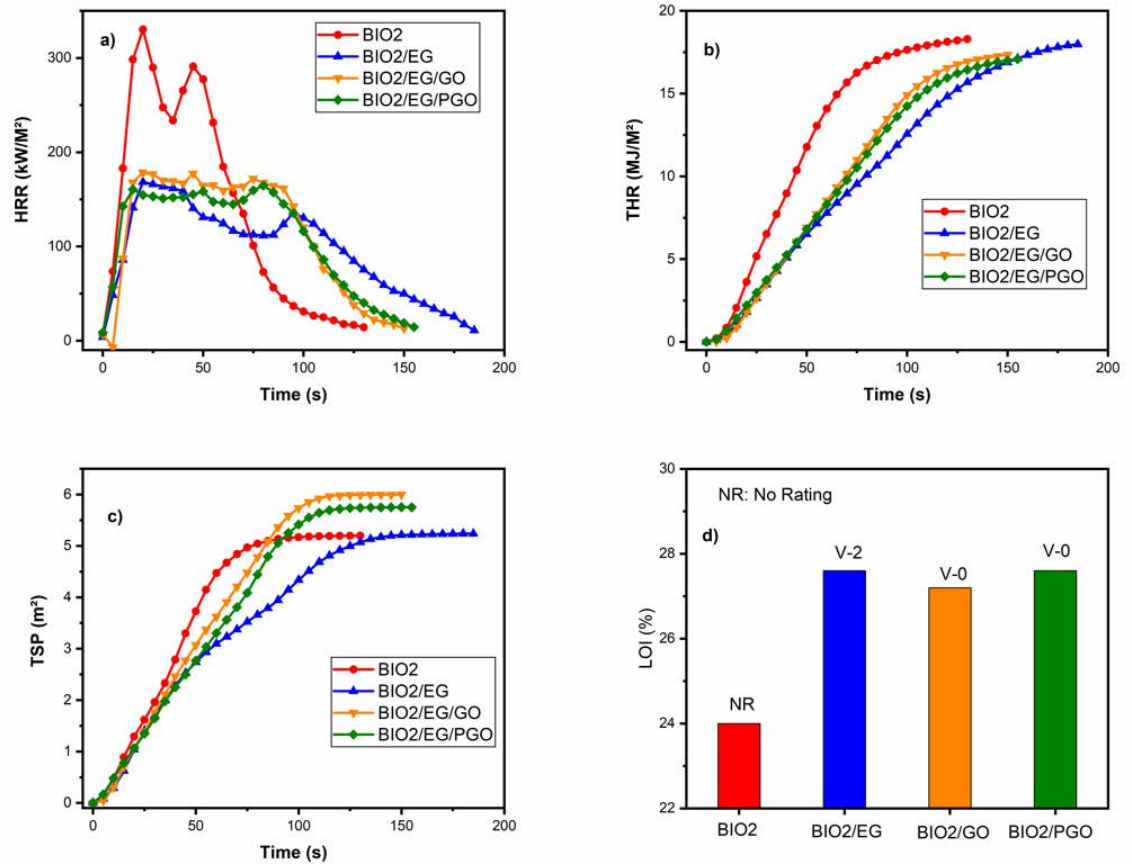

Figure 7-8. a) HRR and b) THR, c) TSP curves at 50 kW/m^2 and d) LOI and UL94 results for RPUF samples.

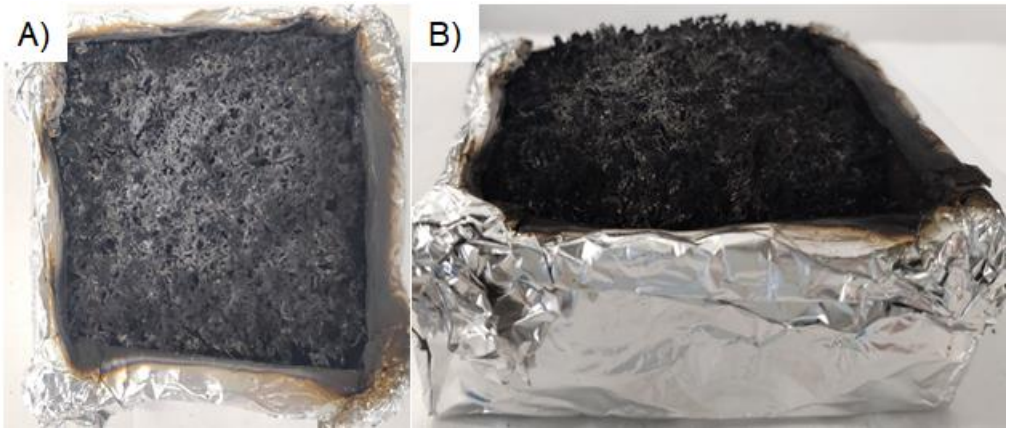

Figure 7-9. Char images of A, B) BIO2/EG/PGO after CCT.

Table 7-5. Data of CPPA/EG/GO composites at 50 kW/ m^2 from CCT.

Sample	PHRR (kW/m²)	THR (MJ/m²)	TSP (m²)
BIO2	330 ± 19	18.3 ± 1.9	5.2 ± 0.3

BIO2/EG	168 ± 10	17.9 ± 2.2	5.2 ± 0.3
BIO2/EG/GO	178 ± 9	17.3 ± 3.9	6.0 ± 0.1
BIO2/EG/PGO	165 ± 1	17.1 ± 3.9	5.8 ± 0.3

- **Smoke behavior analysis**

The smoke analysis based on the average CO and CO_2 production (Av-COP and Av-CO_2P) was performed for BIO2/EG/PGO and their ratio as CO % was showed **Table 7-6**. As showed in **Chapter 6**, EG decreased the CO and CO_2 production compared to BIO2 whereas GO increased it in comparison to EG due to the pyrolysis of the oxygen functionalities under the GO surface. However, the smoke gases production was still lower than BIO2. The introduction of PGO, decreased the COP and CO_2P a 14 % and 6 % respectively in comparison to GO. However, the results were still around a 3-4 % higher than EG. Interestingly, the ratio COP/CO_2P was also lower than GO.

Table 7-6. Data of the CO and CO_2 production (mg/s) at 50 kW/m^2 from CCT.

Sample	Av-COP (mg/s)	Av-CO_2P (mg/s)	Ratio COP/CO_2P (%)
BIO2	3.70 ± 0.17	85.7 ± 4.8	4.30
BIO2/EG	2.68 ± 0.16	62.6 ± 1.1	4.30
BIO2/EG/GO	3.24 ± 0.83	68.4 ± 12.4	4.70
BIO2/EG/PGO	2.80 ± 0.83	64.5 ± 8.9	4.34

- **SEM char analysis**

The chars of BIO2/EG/PGO were indeed analyzed by SEM after the CCT (**Figure 7-10**). It can be clearly seen the typical worm structure created by the EG expansion exposed to a heat source filling all the char structure. However, small and layered insertions from PGO could be observed (**Figure 7-10 A)**). PGO residues can be observed attached to EG worm structures and producing a high compact and robust char (**Figure 7-10 B)**), confirming the synergistic char structure between both FRs.

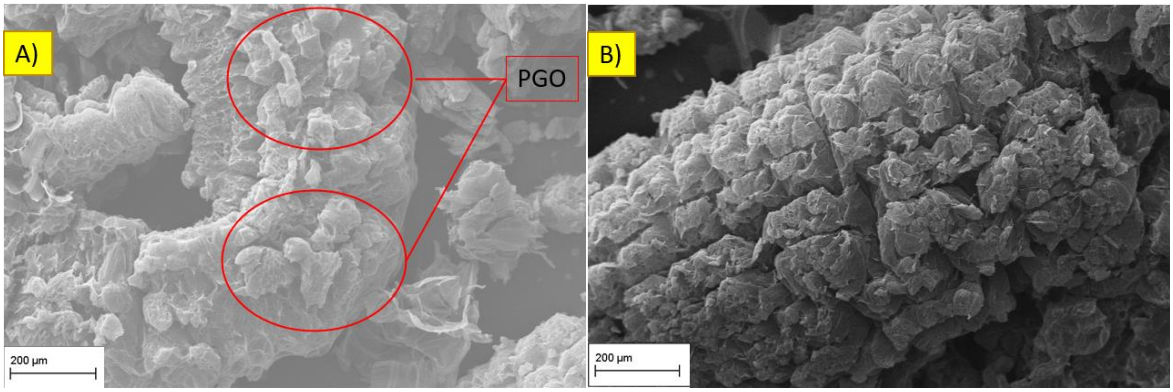

Figure 7-10. SEM Char images of A, B) BIO2/EG/PGO after CCT.

The results disclosed a synergistic effect between GO and FP1 the grafted on the surface, which means that the functionalization inhibited the combustion intensity efficiently and reduced the spreading speed of the flame at an equivalent unmodified GO loading, thus improving the fire performance of a biobased RPUF. However, both GO and PGO had higher TSP than EG. On one hand, GO produces a lower quality char barrier and the radical scavenger effect of PGO increases the production of CO by an incomplete and inefficient combustion [176] compared to EG alone. Indeed, it was reported that the presence of phosphorous species could lead to the release of larger and non-combustible fragments on the gas phase, thus leading to a ticker smoke [2].

c) *Proposed FR mechanism*

The mechanism proposed on this manuscript, is based on the synergistic combination of EG and PGO. The mechanism is shown in **Figure 7-11**. Following this, a two-phase action FR mechanism was proposed, similar to those form literature [231]. Firstly, EG acts on the condensed phase by producing a dense char on the surface of PU, which limits the heat and mass transfer to the polymer and blocks the O_2 penetration. A similar behavior is also produced by GO. At the same time, FP1 acts on the gas phase by releasing radical phosphorous species (like PO·) which captures the OH· and H· radicals in the combustion zone. At the same time, the presence of many phosphorous-containing compounds (like CPPA and FP1) and their thermal decomposition produced the release of phosphate and phosphinic species (H_3PO_3 and H_3PO_4) which permits the creation of an intumescent char [283]; these phosphorous species acted as an acid source, the PU matrix acted as char former and the rest of the gaseous products acted as blower (urea mainly), leading to an intumescent, foam-like char residue. Indeed, this phosphorous species catalyzes the formation of carbon layers (by the polycondensation reaction

of phosphoric acid when the temperature is increasing to create polyphosphoric acid) [152] and enriches the char carbonaceous layer produced by EG and GO [238]. This enriched char can act as physical barrier, slowing down the heat and mass products transference between the matrix and the ambient. In addition, non-combustible volatile products from the decomposition of CPPA and FP1 (NH_3, CO_2, water, NO_2, P_2O_5) could be released, diluting the combustible gases, mostly, the O_2 concentration [239]. Finally, the high density and thermally stable crosslinked thin film of oxides of phosphorus and nitrogen results in a phosphorus-nitrogen synergistic effect and yields an intumescent. To sum up, on one hand, a gas phase effect by FP1 and CPPA (mainly due to radical quenching mechanism to inhibit the combustion) and a condensed phase effect by charring and the barrier effect of EG and GO previously described, enhanced the FR action. This proposed mechanism is in accordance to other authors about EG and phosphorous-based FR synergistic effect studies [2], [82], [204].

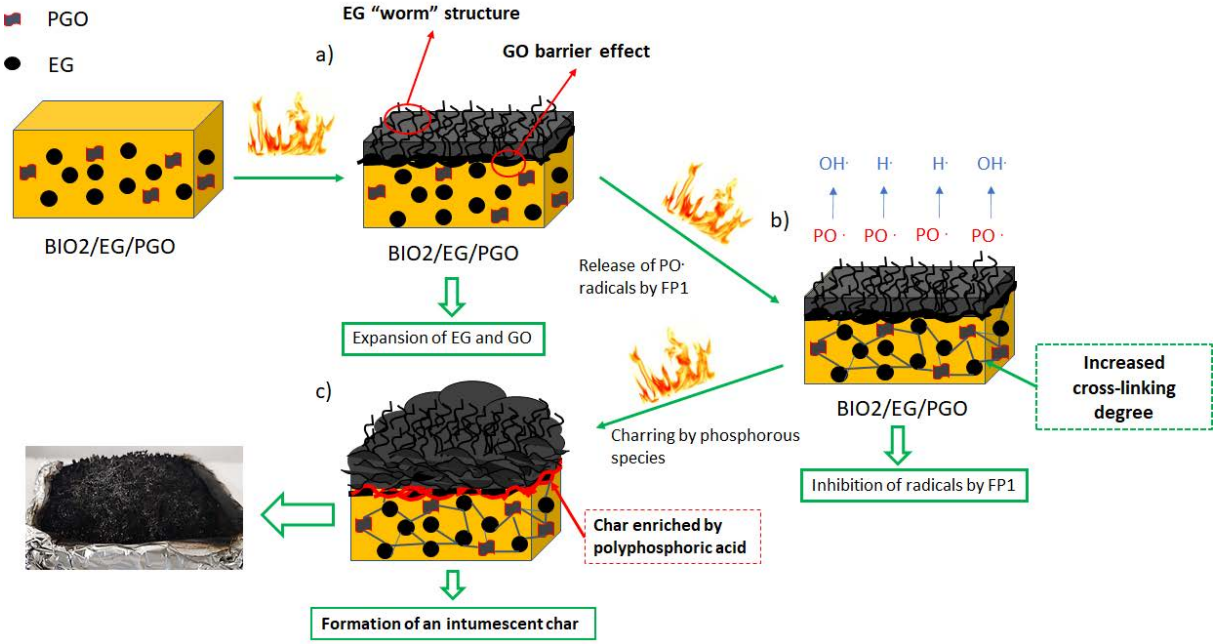

Figure 7-11. Proposed FR mechanism for the synergistic action between EG, and PGO.

7.3.5. *Mechanical properties*

Compressive strength tests were performed at a constant rate of 3 mm/min, and the data for compressive strength are shown in **Figure 7-12** and **Table 7-7**. The compressive strength of BIO2 foam showed a value about 0.146 MPa. When EG was introduced, the compressive strength of the samples decreased slightly up to a 25 % to 0.109 MPa due to slippage among EG and the PU matrix, leading to an inhomogeneous structure with increasing porosity [307]. Besides, the decreasing density, bigger cell size and broken walls (**Figure 7-6**) resulted in the

reduction of the compressive performance [210], [211]. The depleting of 0.5 wt. % of EG by GO, increased a little the compression strength, mostly attributable to the hydrophilic surface of GO [149], improving the dispersion of GO and EG in the matrix, and the strong interfacial interaction between the -NCO groups in the ends of PU chains and the oxygen groups (-OH among others) on the GO surface to form covalent bonds [266] (**Figure 7-13 a)**), thus increasing the crosslinking degree of the sample and improved slightly the compressive strength [266], [304]. However, with the functionalization in PGO, additional strength was imparted. When PGO was used, the compressive strength dramatically increased to 0.183 MPa, which means an increase of a 25 % with respect to BIO2 and a 63 % compared to BIO2/EG/GO. Several reasons explain this improvement. First, the chemical grafting of FP1 into GO surface, principally by the chemical bond of -NH- with epoxy/carboxylic acid groups lead to more free -OH groups, which subsequently can be ready to form covalent bonds with the -NCO from the PU end chains [256], [266]. This interaction led to a lower CO_2 produced from the "blowing reaction" and so, the foaming pressure is reduced decreasing the cell size and increasing the density. Then, it has been widely reported that PU can form hydrogen bonds with amine compounds [272], [308] that would strengthen the structure. Following this trend, the excess of isocyanate could react with the secondary amines of FP1; as secondary amines are more reactive than -OH groups (**Table 2-1**), producing urea linkages (which are stronger and more stable than urethane [298]). This interaction can led to an increasing crosslinking degree and branching structure that conducts increasing HS domains which impart additional strength to the PU structure [16], [309]. A similar result was reported by Bera et al. [298], who reported that besides urea linkages, amine-functionalized-GO can form additional bidentate H-bonding interactions with the PU chains, making the structure stiffer whereas the interactions between the urethane linkage of PU grafted GO and the HS of the adjacent PU chain, imparts only mono-dentate H-bonding, as showed back on **Figure 6-14**. Although this assumption needs further experimental evidence. Finally, the presence of stiff phenyl groups on the FP1 chemical structure, could help to increase the compressive performance [80]. These effects resulted in an increased compressive strength of PGO with respect to unmodified GO (**Figure 7-13**). According to Z.-J. Cao et al. [155], the chemical combination of functionalized GO, resulted in more regular cells, thicker cell walls, which may be responsible for the compressive strength improvement. The strong covalent interface interaction, allows effective load stress transfer from PU to PGO and slightly increased the mechanical strength compared to the EG-filled foam

[215]. This increased compressive strength can potentially reduce the thickness of RPUF to achieve an optimal thermal insulation effect [149].

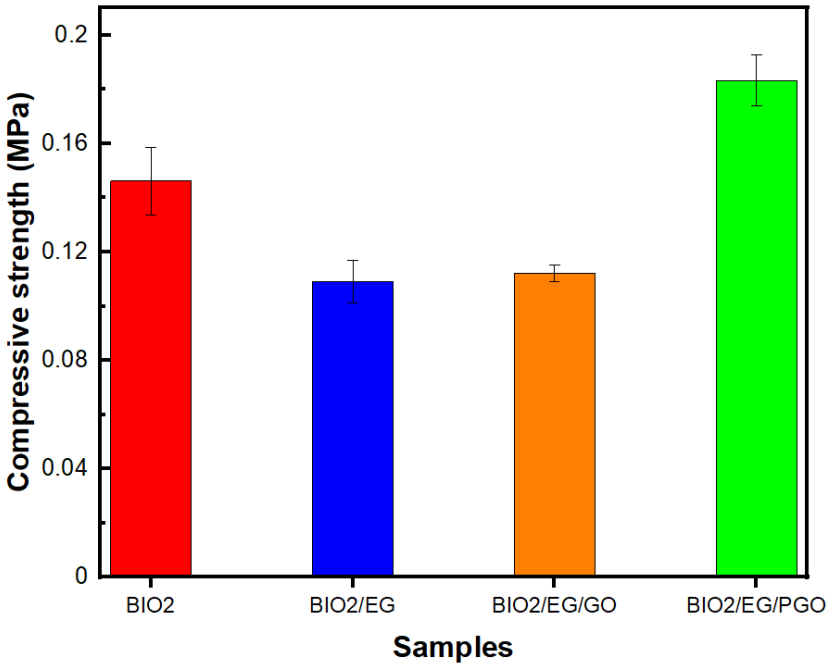

Figure 7-12. Compressive strength of RPUF samples at 3 mm/min constant rate.

Table 7-7. Compressive strength data of RPUF samples.

Sample	Compressive strength (MPa)	Standard deviation (%)
BIO2	0.146 ± 0.013	8.6
BIO2/EG	0.109 ± 0.008	7.2
BIO2/EG/GO	0.112 ± 0.003	2.8
BIO2/EG/PGO	0.183 ± 0.009	5.1

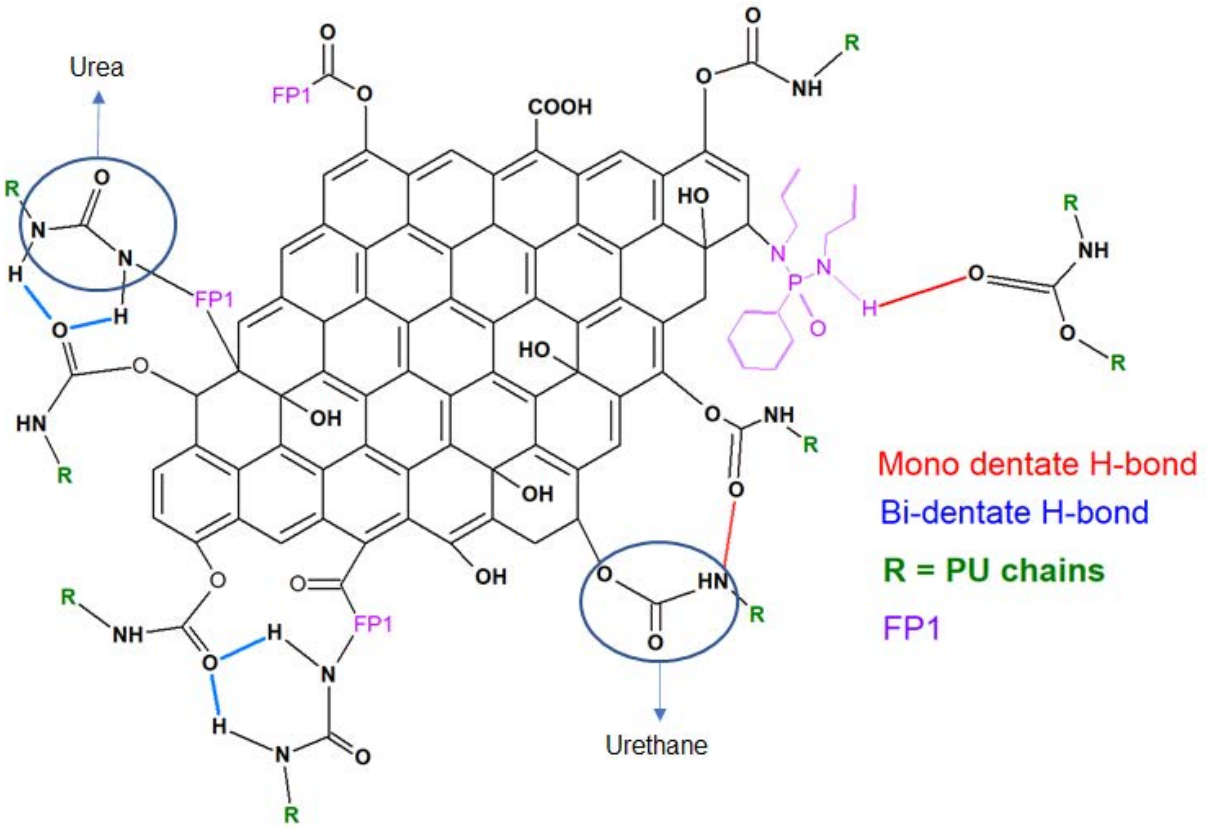

Figure 7-13. Illustration of the interfacial interaction of the interfacial interaction PGO and the PU matrix via hydrogen bonds, urethane and urea linkages.

7.4. Conclusions

Functionalized graphene oxide (PGO) as an additive FR into a bio-based a rigid PU foam matrix was studied by their cellular structure, thermal behavior, flame retardancy and compressive performance. The cell size of the foams with PGO was reduced to 196 µm and the thermal conductivity of BIO2/EG/PGO was decreased up to an 8 % compared to BIO2/EG and 11 % compared to a commercial foam. The covalent bonds between PGO and PU matrix increased the density of the foams and the barrier effect of GO improved the insulation capacity of the foam. BIO2/EG/PGO obtained a LOI of 27.6 % along with a V-0 rating in the vertical burning test, compared to 24.0 % and no rating obtained by BIO2 foam. Cone calorimeter test showed that BIO2/EG/PGO reduced the PHRR and the THR by a 50 % and 7 % with respect to BIO2 foam. A FR mechanism was proposed consisting of the combination of a condensed phase barrier insulation effect against heat and mass transfer from EG and PGO towards a gas-phase radical-scavenging effect produced by the FR polyol (CPPA) and FP1 grafted under the GO surface. Furthermore, the compressive strength of BIO2/EG/PGO dramatically increased a 25 % compared to BIO2 and an impressive 63 % compared to BIO2/EG/GO. The good interfacial

adhesion of GO structures and the PU matrix together with the covalent interactions of FP1 grafted GO and -NCO from the PU end chains, increase the stiffness of the structure and the foam density, allowing an effective load stress transfer from PU to PGO which increased the mechanical strength of the foam.

CHAPTER 8

8. Conclusions

"There is no talent, neither genius without hard work"

- Dmitri Mendeléyev

The main conclusions of this investigation can be summarized as follows:

- RPUF has extraordinary properties as insulator and mechanical reinforcement in many different industries, used mainly in the construction and automotive industrial sectors. However, their cellular and porous structure along with the petroleum nature of its components, make RPUFs very favorable to initiate a fire accident.
- EG as an additive FR has a strong an effective condensed-phase flame inhibition effect by forming an intumescent char barrier under the surface of the polymer. Three EGs were tested. Among them, EG3; with big particle size and high rate of expansion (500 μm, 350 m^3/g), obtained the maximum standards on the FR tests at only 8 wt. % loading in a RPUF of about 100 Kg/m^3 as density. However, the thermal conductivity of the foam increased; although the cell size was reduced, due to the intrinsic thermal conductivity of EG, being the EG-filled foam worse than the neat RPUF. Moreover, due to an incompatibility between EG and the PU matrix, slippage between components occur and the big size of EG3 influences negatively on the mechanical performance of the RPUF. For that reason, we encouraged to find new synergistic agents that can improve the gas-phase FR effect and improve the compatibility and compressive performance with the RPUF.
- P-N FRs work very well as synergistic agents with EG. We synthetized a new FR (FR1) based on the P-N Chemistry and with a rigid phenyl structure. The combination of EG and FR1 at 8 wt. % was performed to obtain an optimal ratio (12/1) between those additives and find a balance between flame retardancy and compressive strength. A synergistic effect in terms of flame retardancy was confirmed due to the combination of a condensed-phase effect from EG3 and a gas-phase effect from FR1. Besides, the compressive strength

increased up to a 5 % with respect to neat PU. However, the thermal insulation was indeed worse than neat RPUF and the presence of materials from petroleum nature is still high.

- Castor oil can be used to substitute petroleum-based polyols. However, it is necessary to modify it to obtain a suitable polyol for a RPUF. Following this, castor oil was firstly modified via transamidization (CODEOA). CODEOA as polyol will end on a RPUF with enormous porous structure, which increased the thermal conductivity and flammability of the RPUF. For that reason, CODEOA was epoxidized to ECODEOA and then PPA was introduced through the epoxy ring to create CPPA and impart high flame retardancy and thermal insulation. Compared to a commercial RPUF, the thermal conductivity of BIO2 decreased to an impressive 14 % and the LOI increased to 24.0 %.
- GO, a derivative novel material from EG, was obtained through a modification of a reported method on the literature. BIO2 foams with a loading of 5.5 wt. % of EG and 0.5 wt. % of GO (BIO2/EG/GO) was confirmed GO as a good insulation material to RPUFs. The cell size of the foam was reduced by GO, opposite to the effect of EG. Going forward, BIO2/EG/GO obtained 27.2 % in the LOI test and a V-0 rating in the UL94 test. Then, in the CCT, GO obtained remarkable results compared to BIO2. Despite that, BIO2/EG/GO decreased the compressive performance by a 23 % compared to BIO2. So, both additives affected negatively to the cellular structure of the foam and the interaction with -NCO was weak. New methods should be studied to improve both flame retardancy, thermal insulation and compressive strength at the same time.
- PGO was obtained through the reaction of an amine bond from FP1; a synthetized P-N FR, and the oxygen functionalities on GO surface, mostly the epoxy ring and carboxylic acid. Also, hydrogen bonds can be formed between PGO and the PU matrix. PGO maintained the thermal conductivity value obtained by GO with only a small rise due to the increase of the density. The LOI test increased to 27.6 % and obtained a very clear V-0 rating in the UL94 test, being even only 1.6 s the average after-flame time. The CCT showed impressive results, decreasing the PHRR, THR, and TSP compared to GO as additive. The most incredible result was that the compressive strength increased by a remarkable 25 % compared to BIO2. These fantastic results were obtained principally by the good interaction between PGO and PU matrix, where PGO can make bonds between -NH and -NCO at the end of the PU chains as well as H-bonding between the linkages formed. These interactions increased the density; thus improving the compressive strength, and imparted an additional gas-phase FR effect combined with a condensed phase FR effect from EG and GO.

9. Recommendations for future work

On basis of the results obtained in this thesis, some important areas for future research were found:

1) Improvements in the synthesis and characterization of CPPA and similar bio-based polyols.

   a. Increase the -OH number at the initial step by other methods, such as transesterification (with other alcohols like glycerol or pentaerythritol). Also, the epoxidation can be performed in a first stage. Multiple options available.
   b. Control the oxirane number; it is the number of epoxide groups in the polyol, to perfectly address the introduction of a FR into the epoxy ring from the epoxidation (ECODEOA) product.
   c. New structures can be introduced, such as blend with other polyols, H-reactive compounds (i.e. amines) or other P-FRs (DOPO, DMMP and etc.).
   d. Use of other oils as green source for the polyol synthesis i.e. Soybean oil, Linseed oil, olive oil …etc, which could potentially open the scenario to a new chemistry based on natural raw materials of high abundance without petroleum dependency.

2) Explore different loadings of GO and PGO to improve the FR, insulation and gas barrier properties or the compressive strength.

   a. The use of higher loadings of GO or PGO could impart higher density, rise the compressive strength and improve the flame retardancy, which could address even higher standards for the RPUF system.
   b. Functionalization of GO with other reactive compounds to create novel nanostructures with addressed properties as desired by the researcher.

3) Due to the current knowledge about PU, the method proposed in **Chapter 6** and **Chapter 7** can be addressed to other PU-based materials, such as coatings, elastomers,

adhesives, and sealants (CASE). It opens the possibility to use biobased insulating FR adhesives, thermoplastics, FPUF and so on.

References

[1] L. Qian, F. Feng, and S. Tang, "Bi-phase flame-retardant effect of hexa-phenoxy-cyclotriphosphazene on rigid polyurethane foams containing expandable graphite," *Polym. (United Kingdom)*, vol. 55, no. 1, pp. 95–101, 2014.

[2] S. Wang, L. Qian, and F. Xin, "The synergistic flame-retardant behaviors of pentaerythritol phosphate and expandable graphite in rigid polyurethane foams," *Polym. Compos.*, vol. 39, no. 2, pp. 329–336, Feb. 2016.

[3] B. C. Levin, M. Paabo, and C. S. Bailey, "Generation of Hydrogen Cyanide from Flexible Polyurethane Foam Decomposed under Different Combustion Conditions," *Fire Mater.*, vol. 9, no. 3, pp. 125–134, 1985.

[4] The Editors of Encyclopaedia Britannica, "hydrogen cyanide chemical compound," *October 12,* 2018. [Online]. Available: https://www.britannica.com/science/hydrogen-cyanide. [Accessed: 01-Apr-2019].

[5] NHS (UK), "Carbon monoxide poisoning - NHS," *23/05/2016*, 2016. [Online]. Available: https://www.nhs.uk/conditions/carbon-monoxide-poisoning/. [Accessed: 01-Apr-2019].

[6] F. Fang, S. Ran, Z. Fang, P. Song, and H. Wang, "Improved flame resistance and thermo-mechanical properties of epoxy resin nanocomposites from functionalized graphene oxide via self-assembly in water," *Compos. Part B Eng.*, vol. 165, pp. 406–416, May 2019.

[7] Leopoldo Rojo Serrano (Ministerio de Medio Ambiente y Medio Rural y Marino), Araceli Martínez Ruiz (Tecnologías y Servicios Agrarios S.A.), and Beatriz Vila Molina (Tecnologías y Servicios Agrarios S.A.), "Mapa de Riesgo de Desertificación en España. Programa de Acción Nacional contra la Desertificación (PAND) Ministerio de Medio Ambiente, Medio Rural y Marino. Madrid (2008)," 2020. [Online]. Available: https://www.mapa.gob.es/es/desarrollo-rural/temas/politica-forestal/desertificacion-restauracion-forestal/lucha-contra-la-desertificacion/lch_espana.aspx. [Accessed: 08-Mar-2020].

[8] M. Rey and J. V. Lado, "La nave de Cepsa de Cerceda sufre su segundo incendio en dos años," *La voz de Galicia*, 21-Sep-2015. [Online]. Available:

https://www.lavozdegalicia.es/noticia/carballo/cerceda/2015/09/21/nave-cespa-cerceda-sufre-segundo-incendio-dos-anos/0003_201509C21C3992.htm. [Accessed: 08-Mar-2020].

[9] F. G. Sas and U. Foces, "Un gran incendio destruye 3 frigoríficos y una planta de congelados de Fandicosta," *Faro de Vigo*, 2016. [Online]. Available: https://www.farodevigo.es/portada-o-morrazo/2016/05/10/gran-incendio-destruye-tres-frigorificos/1458028.html. [Accessed: 08-Mar-2020].

[10] M. Fontán, "Dos heridos leves en el incendio de una nave frigorífica en Bouzas," *Faro de Vigo*, 2018. [Online]. Available: https://www.farodevigo.es/gran-vigo/2018/09/27/alarma-bouzas-incendio-nave-frigorifica/1969229.html. [Accessed: 01-Apr-2019].

[11] J. M. Sanchis Bernat, I. Cabanes, M. Vázquez, and M. Domínguez, "Un incendio obliga a desalojar el Oceanogràfic de Valencia," *La opinión de Murcia*, 2019. [Online]. Available: https://www.laopiniondemurcia.es/sucesos/2019/07/09/incendio-oceanografic-valencia/1036730.html. [Accessed: 08-Mar-2020].

[12] ACN, "Diez intoxicados en el incendio de unos palets con espuma de poliuretano en una empresa de Sant Cugat del Vallès," *Diari Més Digital*, 2020. [Online]. Available: https://www.diarimes.com/es/noticias/actualidad/2020/09/05/diez_intoxicados_incendio_unos_palets_con_espuma_poliuretano_una_empresa_sant_cugat_del_valles_88580_1095.html? [Accessed: 13-Oct-2020].

[13] Redacción Interempresas, "75 años de poliuretano - Plástico," 2012. [Online]. Available: http://www.interempresas.net/Plastico/Articulos/98006-75-anos-de-poliuretano.html. [Accessed: 01-Apr-2019].

[14] Alison A. Nieder, "Invista Launching Bio-Based Lycra | California Apparel News," 2014. [Online]. Available: https://www.apparelnews.net/news/2014/may/15/invista-launching-bio-based-lycra/. [Accessed: 19-Oct-2020].

[15] E. Sharmin and F. Zafar, *Polyurethane : An Introduction*. 2012.

[16] M. M. Ionescu, *Chemistry and technology of polyols for polyurethanes*, vol. 56. Shawbury, Shrewsbury, Shropshire, SY4 4NR, United Kingdom: Rapra Technology, 2005.

[17] I. Grand View Research, "Global Polyurethane (PU) Market Size & Share, 2025 | Industry Report," 2017. [Online]. Available: https://www.grandviewresearch.com/industry-analysis/polyurethane-pu-market.

[Accessed: 01-Apr-2019].

[18] W. Xi, L. Qian, Y. Chen, J. Wang, and X. Liu, "Addition flame-retardant behaviors of expandable graphite and [bis(2-hydroxyethyl)amino]-methyl-phosphonic acid dimethyl ester in rigid polyurethane foams," *Polym. Degrad. Stab.*, vol. 122, pp. 36–43, 2015.

[19] I. Grand View Research, "Europe Polyurethane (PU) Market Size | Industry Report, 2024," 2016. [Online]. Available: https://www.grandviewresearch.com/industry-analysis/europe-polyurethane-pu-market. [Accessed: 01-Apr-2019].

[20] J. O. Akindoyo, M. D. H. Beg, S. Ghazali, M. R. Islam, N. Jeyaratnam, and A. R. Yuvaraj, "Polyurethane types, synthesis and applications – a review," *RSC Adv.*, vol. 6, no. 115, pp. 114453–114482, 2016.

[21] J. Datta and P. Kasprzyk, "Thermoplastic polyurethanes derived from petrochemical or renewable resources: A comprehensive review," *Polym. Eng. Sci.*, vol. 58, pp. E14–E35, 2018.

[22] Z. S. Petrovic, "Polyurethanes from vegetable oils," *Polym. Rev.*, vol. 48, no. 1, pp. 109–155, 2008.

[23] A. S. Dutta, "Polyurethane Foam Chemistry," in *Recycling of Polyurethane Foams*, 2018.

[24] M. Fuensanta and J. M. Martin-Martínez, "Thermoplastic polyurethane pressure sensitive adhesives made with mixtures of polypropylene glycols of different molecular weights," *Int. J. Adhes. Adhes.*, vol. 88, pp. 81–90, 2019.

[25] K. Hyung Choe, D. Soo Lee, W. Jin Seo, and W. Nyon Kim, "Properties of Rigid Polyurethane Foams with Blowing Agents and Catalysts," *Polym. J.*, vol. 36, no. 5, pp. 368–373, 2004.

[26] A. Fangareggi and L. Bertucelli, "Thermoset insulation materials in appliances, buildings and other applications," in *Thermosets*, Elsevier, 2012, pp. 254–288.

[27] K. Hill, "A special topic issue on green chemistry. Fats and oils as oleochemical raw materials," 2000.

[28] The Dow Chemical Company, "Describe the role of surfactants in a flexible polyurethane foam formulation," *Dow Answer center*, 2018. [Online]. Available: https://dowservice.custhelp.com/app/answers/detail/a_id/17054/kw/surfactant. [Accessed: 01-Apr-2019].

[29] H. Lim, S. H. Kim, and B. K. Kim, "Effects of silicon surfactant in rigid polyurethane foams," *Express Polym. Lett.*, vol. 2, no. 3, pp. 194–200, 2008.

[30] M. F. Sonnenschein, *Polyurethanes: Science, Technology, Markets, and Trends*. John Wiley & Sons, Inc., 2014.

[31] A. Lapprand, F. Boisson, F. Delolme, F. Méchin, and J. Pascault, "Reactivity of isocyanates with urethanes : Conditions for allophanate formation," *Polym. Degrad. Stab.*, vol. 90, pp. 363–373, 2005.

[32] S. Dworakowska, D. Bogdał, F. Zaccheria, and N. Ravasio, "The role of catalysis in the synthesis of polyurethane foams based on renewable raw materials," *Catal. Today*, vol. 223, pp. 148–156, 2014.

[33] M. Santiago-Calvo, V. Blasco, C. Ruiz, R. París, F. Villafañe, and M. Á. Rodríguez-Pérez, "Improvement of thermal and mechanical properties by control of formulations in rigid polyurethane foams from polyols functionalized with graphene oxide," *J. Appl. Polym. Sci.*, vol. 136, no. 19, p. 47474, 2019.

[34] R. Van Maris, Y. Tamano, H. Yoshimura, and K. M. Gay, "Polyurethane Catalysis by Tertiary Amines," *J. Cell. Plast.*, vol. 41, no. 4, pp. 305–322, 2005.

[35] Anton Demharter, "Polyurethane rigid foam, a proven thermalinsulating material for applicationsbetween+130°C and−196°C," *Cryogenics (Guildf).*, vol. 38, pp. 113–117, 1998.

[36] D. Randall and S. Lee, *The polyurethanes book*. [Huntsman Polyurethanes], 2002.

[37] G. Woods, *Flexible Polyurethane Foams: Chemistry and Technology*. London: Applied Science Publishers, 1982.

[38] K. Schwetlick and R. Noack, "Kinetics and catalysis of consecutive isocyanate reactions. Formation of carbamates, allophanates and isocyanurates," *J. Chem. Soc. Perkin Trans. 2*, no. 2, p. 395, 1995.

[39] K. Tokumoto, Y. Tamano, and S. Okuzono, "Amine catalyst for producing polyurethane and polyisocyanurate," US6307102B1, 23-Oct-2001.

[40] J. Grimminger, "Trimerization catalysts for making polyisocyanurate foams," US005958990, 23-Nov-1999.

[41] A. L. Silva and J. C. Bordado, "Recent Developments in Polyurethane Catalysis: Catalytic Mechanisms Review," *Catal. Rev.*, vol. 46, no. 1, pp. 31–51, Dec. 2004.

[42] F. Laoutid, L. Bonnaud, M. Alexandre, J.-M. Lopez-Cuesta, and P. Dubois, "New prospects in flame retardant polymer materials: From fundamentals to nanocomposites," *Mater. Sci. Eng. R Reports*, vol. 63, no. 3, pp. 100–125, Jan. 2009.

[43] N. P. Cheremisinoff, *Handbook of Polymer Science and Technology: Vol 2:*

Performance Properties of Plastics and Elastomers. New York-Basel: Marcel Dekker Inc., 1989.

[44] M. Lewin and E. D. Weil, "Mechanisms and modes of action in flame retardancy of polymers," in *Fire Retardant Materials*, Elsevier, 2001, p. 32.

[45] A. Dasari, Z. Yu, G. Cai, and Y. Mai, "Progress in Polymer Science Recent developments in the fire retardancy of polymeric materials," *Prog. Polym. Sci.*, vol. 38, no. 9, pp. 1357–1387, 2013.

[46] L. Jiao, H. Xiao, Q. Wang, and J. Sun, "Thermal degradation characteristics of rigid polyurethane foam and the volatile products analysis with TG-FTIR-MS," *Polym. Degrad. Stab.*, vol. 98, no. 12, pp. 2687–2696, 2013.

[47] Y. Li *et al.*, "Effect of expandable graphite particle size on the flame retardant, mechanical, and thermal properties of water-blown semi-rigid polyurethane foam," *J. Appl. Polym. Sci.*, vol. 131, no. 3, pp. 1–9, 2014.

[48] D. K. Chattopadhyay and D. C. Webster, "Thermal stability and flame retardancy of polyurethanes," *Prog. Polym. Sci.*, vol. 34, no. 10, pp. 1068–1133, 2009.

[49] EFRA-The European Flame Retardants Association, "Flame Retardants Frequently Asked Questions," Brussels, Belgium, 2007.

[50] https://www.flameretardants-online.com/, "Flame Retardants-Mode of action." [Online]. Available: https://www.flameretardants-online.com/flame-retardants/mode-of-action. [Accessed: 02-Apr-2019].

[51] C. X. Zhao, Y. Liu, D. Y. Wang, D. L. Wang, and Y. Z. Wang, "Synergistic effect of ammonium polyphosphate and layered double hydroxide on flame retardant properties of poly(vinyl alcohol)," *Polym. Degrad. Stab.*, vol. 93, no. 7, pp. 1323–1331, 2008.

[52] D. M. Stavert, D. C. Archuleta, M. J. Behr, and B. E. Lehnert, "Relative acute toxicities of hydrogen fluoride, hydrogen chloride, and hydrogen bromide in nose- and pseudo-mouth-breathing rats," *Fundam. Appl. Toxicol.*, vol. 16, no. 4, pp. 636–655, May 1991.

[53] S. Burreau, Y. Zebühr, D. Broman, and R. Ishaq, "Biomagnification of PBDEs and PCBs in food webs from the Baltic Sea and the northern Atlantic Ocean," *Sci. Total Environ.*, vol. 366, no. 2–3, pp. 659–672, Aug. 2006.

[54] L. G. Costa and G. Giordano, "Developmental neurotoxicity of polybrominated diphenyl ether (PBDE) flame retardants," *Neurotoxicology*, vol. 28, no. 6, pp. 1047–1067, Nov. 2007.

[55] M. Roggeman, "Call for evidence on flame retardants TCEP, TCPP and TDCP in

polyurethane foams," Helsinki, Finland, 2018.

[56] SCHER, "SCHER Opinion on the risk assessment report on 2,2-bis(chloromethyl)trimethylene bis[bis(2-chloroethyl)phosphate], (V6), environmental part, CAS 38051-10-4, 29 November 2007," 2007.

[57] SCHER, "SCHER Opinion on the risk assessment report on tris(2-chloro-1-methylethyl) phosphate (TCPP), CAS no. 13674-84-5, environmental part, 20 September 2007," Brussels, Belgium, 2007.

[58] F. Meng, X. Ding, L. Yang, and Y. Wang, "Research Progress of Flame Retardant Modified Flexible Polyurethane Foam," vol. 1, no. 4, pp. 155–160, 2015.

[59] IHS Consulting (2017), "The flame retardants market | FLAMERETARDANTS-ONLINE." [Online]. Available: https://www.flameretardants-online.com/flame-retardants/market. [Accessed: 02-Apr-2019].

[60] "Flame Retardant Additives | Smoke Suppressant | Huber Engineered Materials." [Online]. Available: https://www.hubermaterials.com/products/flame-retardants-smoke-suppressants.aspx. [Accessed: 02-Apr-2019].

[61] J. Jin, Q. X. Dong, Z. J. Shu, W. J. Wang, and K. He, "Flame retardant Properties of Polyurethane/expandable Praphite Composites," *Procedia Eng.*, vol. 71, pp. 304–309, 2014.

[62] W. J. Wang *et al.*, "Influence of Aluminum Hydroxide and Expandable Graphite on the Flammability of Polyisocyanurate-Polyurethane Foams," *Appl. Mech. Mater.*, vol. 368–370, pp. 741–746, 2013.

[63] C. Xiling, S. Kemin, L. Jihui, and L. Jinpeng, "Preparation of lower-sulfur content and expandable graphite," *Carbon N. Y.*, vol. 34, no. 12, pp. 1599–1600, Jan. 1996.

[64] G. Camino, S. Duquesne, R. Delobel, B. Eling, C. Lindsay, and T. Roels, "Mechanism of Expandable Graphite Fire Retardant Action in Polyurethanes," *ACS Symp. Ser.*, vol. 797, 2001.

[65] L. Shi *et al.*, "Expandable Graphite For Halogen-Free Flame-Retardant of High-Density Rigid Polyurethane Foams," *Polym. Plast. Technol. Eng.*, vol. 44, no. 7, pp. 1323–1337, 2005.

[66] X. Chen, J. Zhuo, W. Song, C. Jiao, Y. Qian, and S. Li, "Flame retardant effects of organic inorganic hybrid intumescent flame retardant based on expandable graphite in silicone rubber composites," *Polym. Adv. Technol.*, vol. 25, no. 12, pp. 1530–1537, 2014.

[67] M. Kirpluks, U. Cabulis, V. Zeltins, L. Stiebra, and A. Avots, "Rigid polyurethane foam

thermal insulation protected with mineral intumescent mat," *Autex Res. J.*, vol. 14, no. 4, pp. 259–269, 2014.

[68] William Reusch, "Properties of Phosphorus Compounds - Chemistry LibreTexts," *Oxidation States of Phosphorus Compounds*, 2014. [Online]. Available: https://chem.libretexts.org/Bookshelves/Organic_Chemistry/Supplemental_Modules_(Organic_Chemistry)/Organo-phosphorus_Compounds/Properties_of_Phosphorus_Compounds. [Accessed: 02-Apr-2019].

[69] S. Yang, J. Wang, S. Huo, M. Wang, J. Wang, and B. Zhang, "Synergistic flame-retardant effect of expandable graphite and phosphorus-containing compounds for epoxy resin: Strong bonding of different carbon residues," *Polym. Degrad. Stab.*, vol. 128, pp. 89–98, 2016.

[70] S. Wang *et al.*, "Synergetic enhancement of mechanical and fire-resistance performance of waterborne polyurethane by introducing two kinds of phosphorus–nitrogen flame retardant," *J. Colloid Interface Sci.*, vol. 537, pp. 197–205, Mar. 2019.

[71] U. Braun *et al.*, "Influence of the oxidation state of phosphorus on the decomposition and fire behaviour of flame-retarded epoxy resin composites," *Polymer (Guildf).*, vol. 47, no. 26, pp. 8495–8508, Dec. 2006.

[72] B. Schartel, "Phosphorus-based flame retardancy mechanisms-old hat or a starting point for future development?," *Materials (Basel).*, vol. 3, no. 10, pp. 4710–4745, 2010.

[73] F. Feng and L. Qian, "The flame retardant behaviors and synergistic effect of expandable graphite and dimethyl methylphosphonate in rigid polyurethane foams," *Polym. Compos.*, vol. 35, no. 2, pp. 301–309, Feb. 2014.

[74] W. Xi, L. Qian, Z. Huang, Y. Cao, and L. Li, "Continuous flame-retardant actions of two phosphate esters with expandable graphite in rigid polyurethane foams," *Polym. Degrad. Stab.*, vol. 130, pp. 97–102, 2016.

[75] Matthew D. Phillips, R. S. Rose, and S. B. Falloon, "Blends of (alkyl substituted) triaryl phosphate esters with phosphorus-containing flame retardants for polyurethane foams," 20-May-2003.

[76] S. Liang, M. Neisius, H. Mispreuve, R. Naescher, and S. Gaan, "Flame retardancy and thermal decomposition of flexible polyurethane foams: Structural influence of organophosphorus compounds," *Polym. Degrad. Stab.*, vol. 97, no. 11, pp. 2428–2440, 2012.

[77] Z.-J. J. Cao, X. Dong, T. Fu, S.-B. B. Deng, W. Liao, and Y.-Z. Z. Wang, "Coated vs. naked red phosphorus: A comparative study on their fire retardancy and smoke suppression for rigid polyurethane foams," *Polym. Degrad. Stab.*, vol. 136, pp. 103–111, Feb. 2017.

[78] R. Yang, B. Wang, X. Han, B. Ma, and J. Li, "Synthesis and characterization of flame retardant rigid polyurethane foam based on a reactive flame retardant containing phosphazene and cyclophosphonate," *Polym. Degrad. Stab.*, vol. 144, pp. 62–69, 2017.

[79] R. Yang, W. Hu, L. Xu, Y. Song, and J. Li, "Synthesis, mechanical properties and fire behaviors of rigid polyurethane foam with a reactive flame retardant containing phosphazene and phosphate," *Polym. Degrad. Stab.*, vol. 122, pp. 102–109, 2015.

[80] Y. Yuan, C. Ma, Y. Shi, L. Song, Y. Hu, and W. Hu, "Highly-efficient reinforcement and flame retardancy of rigid polyurethane foam with phosphorus-containing additive and nitrogen-containing compound," *Mater. Chem. Phys.*, vol. 211, pp. 42–53, Jun. 2018.

[81] X. Liu, K. A. Salmeia, D. Rentsch, J. Hao, and S. Gaan, "Thermal decomposition and flammability of rigid PU foams containing some DOPO derivatives and other phosphorus compounds," *J. Anal. Appl. Pyrolysis*, vol. 124, pp. 219–229, 2017.

[82] M. Zhang, Z. Luo, J. Zhang, S. Chen, and Y. Zhou, "Effects of a novel phosphorus-nitrogen flame retardant on rosin-based rigid polyurethane foams," *Polym. Degrad. Stab.*, vol. 120, pp. 427–434, 2015.

[83] Q. Zhao, C. Chen, R. Fan, Y. Yuan, Y. Xing, and X. Ma, "Halogen-free flame-retardant rigid polyurethane foam with a nitrogen-phosphorus flame retardant," *J. Fire Sci.*, vol. 35, no. 2, pp. 99–117, 2017.

[84] H. Ding, J. Wang, C. Wang, and F. Chu, "Synthesis of a novel phosphorus and nitrogen-containing bio-based polyols and its application in flame retardant polyurethane sealant," *Polym. Degrad. Stab.*, vol. 124, pp. 43–50, 2016.

[85] P. Jia, L. Hu, M. Zhang, G. Feng, and Y. Zhou, "Phosphorus containing castor oil based derivatives: Potential non-migratory flame retardant plasticizer," *Eur. Polym. J.*, vol. 87, pp. 209–220, 2017.

[86] D. H. Wu, P. H. Zhao, Y. Q. Liu, X. Y. Liu, and X. F. Wang, "Halogen Free flame retardant rigid polyurethane foam with a novel phosphorus-nitrogen intumescent flame retardant," *J. Appl. Polym. Sci.*, vol. 131, no. 11, 2014.

[87] M. Thirumal, D. Khastgir, G. B. Nando, Y. P. Naik, and N. K. Singha, "Halogen-free

flame retardant PUF: Effect of melamine compounds on mechanical, thermal and flame retardant properties," *Polym. Degrad. Stab.*, vol. 95, no. 6, pp. 1138–1145, 2010.

[88] L. Liu, Z. Wang, and X. Xu, "Melamine amino trimethylene phosphate as a novel flame retardant for rigid polyurethane foams with improved flame retardant, mechanical and thermal properties," *J. Appl. Polym. Sci.*, vol. 134, no. 39, p. 45234, Oct. 2017.

[89] F. Luo, K. Wu, Y. Li, J. Zheng, H. Guo, and M. Lu, "Reactive flame retardant with core-shell structure and its flame retardancy in rigid polyurethane foam," *J. Appl. Polym. Sci.*, vol. 132, no. 46, p. n/a-n/a, Dec. 2015.

[90] S. Bourbigot, M. Le Bras, L. Gengembre, and R. Delobel, "XPS study of an intumescent coating application to the ammonium polyphosphate/pentaerythritol fire-retardant system," *Appl. Surf. Sci.*, vol. 81, no. 3, pp. 299–307, Nov. 1994.

[91] H. Zhu and S. Xu, "Synthesis and properties of rigid polyurethane foams synthesized from modified urea-formaldehyde resin," *Constr. Build. Mater.*, vol. 202, pp. 718–726, Mar. 2019.

[92] A. Satdive, S. Mestry, D. Patil, and S. T. Mhaske, "Synthesis of melamine formaldehyde cured castor oil based hydroxyl functional alkyd for coating application," *Prog. Org. Coatings*, vol. 131, pp. 165–175, Jun. 2019.

[93] S.-H. Liu, C.-F. Kuan, H.-C. Kuan, M.-Y. Shen, J.-M. Yang, and C.-L. Chiang, "Preparation and Flame Retardance of Polyurethane Composites Containing Microencapsulated Melamine Polyphosphate," *Polymers (Basel).*, vol. 9, no. 12, p. 407, Aug. 2017.

[94] A. Sut, E. Metzsch-Zilligen, M. Großhauser, R. Pfaendner, and B. Schartel, "Synergy between melamine cyanurate, melamine polyphosphate and aluminum diethylphosphinate in flame retarded thermoplastic polyurethane," *Polym. Test.*, vol. 74, pp. 196–204, Apr. 2019.

[95] W.-H. Rao *et al.*, "Flame-Retardant Flexible Polyurethane Foams with Highly Efficient Melamine Salt," *Ind. Eng. Chem. Res.*, vol. 56, no. 25, pp. 7112–7119, Jun. 2017.

[96] M.-J. Chen, Z.-B. Shao, X.-L. Wang, L. Chen, and Y.-Z. Wang, "Halogen-Free Flame-Retardant Flexible Polyurethane Foam with a Novel Nitrogen–Phosphorus Flame Retardant," *Ind. Eng. Chem. Res.*, vol. 51, no. 29, pp. 9769–9776, Jul. 2012.

[97] M. Zhang, J. Zhang, S. Chen, and Y. Zhou, "Synthesis and fire properties of rigid polyurethane foams made from a polyol derived from melamine and cardanol," *Polym. Degrad. Stab.*, vol. 110, pp. 27–34, 2014.

[98] C. Wang *et al.*, "Flame-retardant rigid polyurethane foam with a phosphorus-nitrogen single intumescent flame retardant," *Polym. Adv. Technol.*, vol. 29, no. 1, pp. 668–676, 2018.

[99] Y. Feng *et al.*, "Improving thermal and flame retardant properties of epoxy resin by functionalized graphene containing phosphorous, nitrogen and silicon elements," *Compos. Part A Appl. Sci. Manuf.*, vol. 103, pp. 74–83, 2017.

[100] H.-B. Zhao *et al.*, "Inherently flame-retardant rigid polyurethane foams with excellent thermal insulation and mechanical properties," *Polymer (Guildf).*, vol. 153, no. July, pp. 616–625, 2018.

[101] Y. Liu, J. He, and R. Yang, "The effects of aluminum hydroxide and ammonium polyphosphate on the flame retardancy and mechanical property of polyisocyanurate-polyurethane foams," *J. Fire Sci.*, vol. 33, no. 6, pp. 459–472, 2015.

[102] Y. Liu, J. He, and R. Yang, "Effects of Dimethyl Methylphosphonate, Aluminum Hydroxide, Ammonium Polyphosphate, and Expandable Graphite on the Flame Retardancy and Thermal Properties of Polyisocyanurate–Polyurethane Foams," *Ind. Eng. Chem. Res.*, vol. 54, no. 22, pp. 5876–5884, 2015.

[103] S. Duquesne *et al.*, "Mechanism of fire retardancy of polyurethanes using ammonium polyphosphate," *J. Appl. Polym. Sci.*, vol. 82, no. 13, pp. 3262–3274, 2001.

[104] X. Wang *et al.*, "Flame Retardancy and Thermal Degradation of Intumescent Flame Retardant Poly(lactic acid)/Starch Biocomposites," *Ind. Eng. Chem. Res.*, vol. 50, no. 2, pp. 713–720, Jan. 2011.

[105] "Intumescent flame retardant systems | FLAMERETARDANTS-ONLINE." [Online]. Available: https://www.flameretardants-online.com/flame-retardants/intumescence. [Accessed: 03-Apr-2019].

[106] X. Chen, Y. Liu, S. Bai, and Q. Wang, "Macromolecular Nitrogen-Phosphorous Compound/Expandable Graphite Synchronous Expansion Flame Retardant Polystyrene Foam," *Polym. Plast. Technol. Eng.*, vol. 53, no. 13, pp. 1402–1407, 2014.

[107] F. Saint-Michel, L. Chazeau, and J. Y. Cavaillé, "Mechanical properties of high density polyurethane foams: II Effect of the filler size," *Compos. Sci. Technol.*, vol. 66, no. 15, pp. 2709–2718, 2006.

[108] A. Yaghoubi and M. M. Alavi Nikje, "Silanization of multi-walled carbon nanotubes and the study of its effects on the properties of polyurethane rigid foam nanocomposites," *Compos. Part A Appl. Sci. Manuf.*, vol. 109, no. March, pp. 338–344, 2018.

[109] U. Khan, A. O'Neill, H. Porwal, P. May, K. Nawaz, and J. N. Coleman, "Size selection of dispersed, exfoliated graphene flakes by controlled centrifugation," *Carbon N. Y.*, vol. 50, no. 2, pp. 470–475, 2012.

[110] H.-K. Peng *et al.*, "Effects of hydrotalcite on rigid polyurethane foam composites containing a fire retarding agent: compressive stress, combustion resistance, sound absorption, and electromagnetic shielding effectiveness," *RSC Adv.*, vol. 8, no. 58, pp. 33542–33550, Sep. 2018.

[111] S. Gómez-Fernández, L. Ugarte, C. Peña-Rodriguez, M. Á. Corcuera, and A. Eceiza, "The effect of phosphorus containing polyol and layered double hydroxides on the properties of a castor oil based flexible polyurethane foam," *Polym. Degrad. Stab.*, vol. 132, pp. 41–51, 2016.

[112] L. Gao, G. Zheng, Y. Zhou, L. Hu, G. Feng, and Y. Xie, "Synergistic effect of expandable graphite, melamine polyphosphate and layered double hydroxide on improving the fire behavior of rosin-based rigid polyurethane foam," *Ind. Crops Prod.*, vol. 50, pp. 638–647, 2013.

[113] G. Huang, J. Gao, Y. Li, L. Han, and X. Wang, "Functionalizing nano-montmorillonites by modified with intumescent flame retardant: Preparation and application in polyurethane," *Polym. Degrad. Stab.*, vol. 95, no. 2, pp. 245–253, 2010.

[114] L. Gao, G. Zheng, Y. Zhou, L. Hu, G. Feng, and M. Zhang, "Synergistic effect of expandable graphite, diethyl ethylphosphonate and organically-modified layered double hydroxide on flame retardancy and fire behavior of polyisocyanurate-polyurethane foam nanocomposite," *Polym. Degrad. Stab.*, vol. 101, no. 1, pp. 92–101, 2014.

[115] M. Antunes, Á. Cano, V. Realinho, D. Arencón, and J. I. Velasco, "Compression Properties and Cellular Structure of Polyurethane Composite Foams Combining Nanoclay and Different Reinforcements," *Int. J. Compos. Mater.*, vol. 4, no. 5A, pp. 27–34, 2014.

[116] N. N. P. Nik Pauzi, R. A. Majid, M. H. Dzulkifli, and M. Y. Yahya, "Development of rigid bio-based polyurethane foam reinforced with nanoclay," *Compos. Part B Eng.*, vol. 67, pp. 521–526, 2014.

[117] F. Wang, J. S. Liang, and Q. G. Tang, "Preparation and Properties of Rigid Polyurethane Foams Reinforced by Sepiolite Minerals Nanofibers," *Key Eng. Mater.*, vol. 512–515, pp. 280–283, 2012.

[118] M. Kotal and A. K. Bhowmick, "Polymer nanocomposites from modified clays: Recent

advances and challenges," *Prog. Polym. Sci.*, vol. 51, pp. 127–187, 2015.

[119] X. Li, Z. Wang, L. Wu, and T. Tsai, "One-step: In situ synthesis of a novel α-zirconium phosphate/graphene oxide hybrid and its application in phenolic foam with enhanced mechanical strength, flame retardancy and thermal stability," *RSC Adv.*, vol. 6, no. 78, pp. 74903–74912, 2016.

[120] S. Gaan and G. Sun, "Effect of phosphorus and nitrogen on flame retardant cellulose: A study of phosphorus compounds," *J. Anal. Appl. Pyrolysis*, vol. 78, no. 2, pp. 371–377, 2007.

[121] A. Hadjadj *et al.*, "Effects of cellulose fiber content on physical properties of polyurethane based composites," *Compos. Struct.*, vol. 135, pp. 217–223, 2015.

[122] E. R. P. Pinto, H. S. Barud, W. L. Polito, S. J. L. Ribeiro, and Y. Messaddeq, "Preparation and characterization of the bacterial cellulose/polyurethane nanocomposites," *J. Therm. Anal. Calorim.*, vol. 114, no. 2, pp. 549–555, 2013.

[123] F. Luo, K. Wu, H. Guo, Q. Zhao, L. Liang, and M. Lu, "Effect of cellulose whisker and ammonium polyphosphate on thermal properties and flammability performance of rigid polyurethane foam," *J. Therm. Anal. Calorim.*, vol. 122, no. 2, pp. 717–723, 2015.

[124] X. Wang, E. N. Kalali, J.-T. Wan, and D.-Y. Wang, "Carbon-family materials for flame retardant polymeric materials," *Prog. Polym. Sci.*, vol. 69, pp. 22–46, Jun. 2017.

[125] Y. Zhu *et al.*, "Graphene and Graphene Oxide: Synthesis, Properties, and Applications," *Adv. Mater.*, vol. 22, no. 35, pp. 3906–3924, Sep. 2010.

[126] M. Bera and P. K. Maji, "Effect of structural disparity of graphene-based materials on thermo-mechanical and surface properties of thermoplastic polyurethane nanocomposites," *Polymer (Guildf).*, vol. 119, pp. 118–133, Jun. 2017.

[127] A. T. Smith, A. M. LaChance, S. Zeng, B. Liu, and L. Sun, "Synthesis, properties, and applications of graphene oxide/reduced graphene oxide and their nanocomposites," *Nano Mater. Sci.*, vol. 1, no. 1, pp. 31–47, Mar. 2019.

[128] P. Pokharel, S. H. Lee, and D. S. Lee, "Thermal, Mechanical, and Electrical Properties of Graphene Nanoplatelet/Graphene Oxide/ Polyurethane Hybrid Nanocomposite.," *J. Nanosci. Nanotechnol.*, vol. 15, no. 1, pp. 211–4, Jan. 2015.

[129] M. Strankowski, D. Włodarczyk, Ł. Piszczyk, and J. Strankowska, "Polyurethane Nanocomposites Containing Reduced Graphene Oxide, FTIR, Raman, and XRD Studies," *J. Spectrosc.*, vol. 2016, pp. 1–6, Aug. 2016.

[130] S. Thakur and N. Karak, "Ultratough, Ductile, Castor Oil-Based, Hyperbranched,

Polyurethane Nanocomposite Using Functionalized Reduced Graphene Oxide," *ACS Sustain. Chem. Eng.*, vol. 2, no. 5, pp. 1195–1202, May 2014.

[131] P. Pokharel and D. S. Lee, "Thermal and Mechanical Properties of Reduced Graphene Oxide/Polyurethane Nanocomposite," *J. Nanosci. Nanotechnol.*, vol. 14, no. 8, pp. 5718–5721, Aug. 2014.

[132] C. Lee, X. Wei, J. W. Kysar, and J. Hone, "Measurement of the elastic properties and intrinsic strength of monolayer graphene.," *Science*, vol. 321, no. 5887, pp. 385–8, Jul. 2008.

[133] R. Yan *et al.*, "Synthesis and in-situ functionalization of graphene films through graphite charging in aqueous Fe2(SO4)3," *Carbon N. Y.*, vol. 107, pp. 379–387, 2016.

[134] M. Bera, P. Chandravati, P. Gupta, and P. K. Maji, "Facile One-Pot Synthesis of Graphene Oxide by Sonication Assisted Mechanochemical Approach and Its Surface Chemistry," *J. Nanosci. Nanotechnol.*, vol. 18, no. 2, pp. 902–912, Feb. 2018.

[135] T. Kavinkumar, D. Sastikumar, and S. Manivannan, "Effect of functional groups on dielectric, optical gas sensing properties of graphene oxide and reduced graphene oxide at room temperature," *RSC Adv.*, vol. 5, no. 14, pp. 10816–10825, Jan. 2015.

[136] A. L. Higginbotham, J. R. Lomeda, A. B. Morgan, and J. M. Tour, "Graphite oxide flame-retardant polymer nanocomposites," *ACS Appl. Mater. Interfaces*, vol. 1, no. 10, pp. 2256–2261, Oct. 2009.

[137] D. R. Dreyer, S. Park, C. W. Bielawski, and R. S. Ruoff, "The chemistry of graphene oxide," *Chem. Soc. Rev.*, vol. 39, no. 1, pp. 228–240, Dec. 2010.

[138] A. Lorenzetti, M. Roso, A. Bruschetta, C. Boaretti, and M. Modesti, "Polyurethane-graphene nanocomposite foams with enhanced thermal insulating properties," *Polym. Adv. Technol.*, vol. 27, no. 3, pp. 303–307, Mar. 2016.

[139] J. H. Warner *et al.*, "Graphene, Fundamentals and emergent applications," in *Graphene*, vol. 17, Elsevier, 2013, p. Chapter 6-pp. 333–437.

[140] J. D. Renteria *et al.*, "Strongly Anisotropic Thermal Conductivity of Free-Standing Reduced Graphene Oxide Films Annealed at High Temperature," *Adv. Funct. Mater.*, vol. 25, no. 29, pp. 4664–4672, Aug. 2015.

[141] X. Xinzhao, L. Guoming, L. Dongyan, S. Guoxin, and Y. Rui, "Electrically conductive graphene-coated polyurethane foam and its epoxy composites," *Compos. Commun.*, vol. 7, pp. 1–6, Mar. 2018.

[142] L. Ugarte, S. Gómez-Fernández, A. Tercjak, A. Martínez-Amesti, M. A. Corcuera, and

A. Eceiza, “Strain sensitive conductive polyurethane foam/graphene nanocomposites prepared by impregnation method,” *Eur. Polym. J.*, vol. 90, no. March, pp. 323–333, 2017.

[143] R. M. M. Hodlur and M. K. K. Rabinal, “Self assembled graphene layers on polyurethane foam as a highly pressure sensitive conducting composite,” *Compos. Sci. Technol.*, vol. 90, pp. 160–165, Jan. 2014.

[144] X. Wang, Y. Hu, L. Song, H. Yang, W. Xing, and H. Lu, “In situ polymerization of graphene nanosheets and polyurethane with enhanced mechanical and thermal properties,” *J. Mater. Chem.*, vol. 21, no. 12, p. 4222, Mar. 2011.

[145] J. N. Gavgani, H. Adelnia, and M. M. Gudarzi, “Intumescent flame retardant polyurethane/reduced graphene oxide composites with improved mechanical, thermal, and barrier properties,” *J. Mater. Sci.*, vol. 49, no. 1, pp. 243–254, Jan. 2014.

[146] P. Pokharel and D. S. Lee, “High performance polyurethane nanocomposite films prepared from a masterbatch of graphene oxide in polyether polyol,” *Chem. Eng. J.*, vol. 253, pp. 356–365, Oct. 2014.

[147] P. Pokharel, S. Choi, and D. S. Lee, “The effect of hard segment length on the thermal and mechanical properties of polyurethane/graphene oxide nanocomposites,” *Compos. Part A Appl. Sci. Manuf.*, vol. 69, pp. 168–177, Feb. 2015.

[148] M. Santiago-Calvo, V. Blasco, C. Ruiz, R. París, F. Villafañe, and M. Á. Rodríguez-Pérez, “Synthesis, characterization and physical properties of rigid polyurethane foams prepared with poly(propylene oxide) polyols containing graphene oxide,” *Eur. Polym. J.*, vol. 97, no. July, pp. 230–240, Dec. 2017.

[149] J.-M. J.-D. J.-H. J.-M. J.-D. J.-H. Kim *et al.*, “Synthesis of nanoparticle-enhanced polyurethane foams and evaluation of mechanical characteristics,” *Compos. Part B Eng.*, vol. 136, pp. 28–38, Mar. 2018.

[150] X. Shi *et al.*, “Bi-phase fire-resistant polyethylenimine/graphene oxide/melanin coatings using layer by layer assembly technique: Smoke suppression and thermal stability of flexible polyurethane foams,” *Polymer (Guildf).*, vol. 170, pp. 65–75, Apr. 2019.

[151] B. Wicklein *et al.*, “Thermally insulating and fire-retardant lightweight anisotropic foams based on nanocellulose and graphene oxide,” *Nat. Nanotechnol.*, vol. 10, no. 3, pp. 277–283, Mar. 2015.

[152] X. Shi, X. Peng, J. Zhu, G. Lin, and T. Kuang, “Synthesis of DOPO-HQ-functionalized graphene oxide as a novel and efficient flame retardant and its application on polylactic

acid: Thermal property, flame retardancy, and mechanical performance," *J. Colloid Interface Sci.*, vol. 524, pp. 267–278, Aug. 2018.

[153] B. Yu *et al.*, "Functionalized graphene oxide/phosphoramide oligomer hybrids flame retardant prepared via in situ polymerization for improving the fire safety of polypropylene," *RSC Adv.*, vol. 4, no. 60, p. 31782, Jun. 2014.

[154] G. Huang, S. Chen, S. Tang, and J. Gao, "A novel intumescent flame retardant-functionalized graphene: Nanocomposite synthesis, characterization, and flammability properties," *Mater. Chem. Phys.*, vol. 135, no. 2–3, pp. 938–947, Aug. 2012.

[155] Z.-J. J. Cao, W. Liao, S.-X. X. Wang, H.-B. B. Zhao, and Y.-Z. Z. Wang, "Polyurethane foams with functionalized graphene towards high fire-resistance, low smoke release, superior thermal insulation," *Chem. Eng. J.*, vol. 361, no. September 2018, pp. 1245–1254, Apr. 2019.

[156] C. Zhang and M. R. Kessler, "Bio-based Polyurethane Foam Made from Compatible Blends of Vegetable-Oil-based Polyol and Petroleum-based Polyol," *ACS Sustain. Chem. Eng.*, vol. 3, no. 4, pp. 743–749, Apr. 2015.

[157] G. Gaidukova, A. Ivdre, A. Fridrihsone, A. Verovkins, U. Cabulis, and S. Gaidukovs, "Polyurethane rigid foams obtained from polyols containing bio-based and recycled components and functional additives," *Ind. Crops Prod.*, vol. 102, pp. 133–143, Aug. 2017.

[158] M. Kurańska and A. Prociak, "The influence of rapeseed oil-based polyols on the foaming process of rigid polyurethane foams," *Ind. Crops Prod.*, vol. 89, pp. 182–187, Oct. 2016.

[159] M. Kurańska, A. Prociak, U. Cabulis, M. Kirpluks, J. Ryszkowska, and M. Auguścik, "Innovative porous polyurethane-polyisocyanurate foams based on rapeseed oil and modified with expandable graphite," *Ind. Crops Prod.*, vol. 95, pp. 316–323, Jan. 2017.

[160] X. Zhou, M. M. Sain, and K. Oksman, "Semi-rigid biopolyurethane foams based on palm-oil polyol and reinforced with cellulose nanocrystals," *Compos. Part A Appl. Sci. Manuf.*, vol. 83, no. April 2016, pp. 56–62, 2016.

[161] C. S. Lee, T. L. Ooi, C. H. Chuah, and S. Ahmad, "Synthesis of Palm Oil-Based Diethanolamides," *J. Am. Oil Chem. Soc.*, vol. 84, no. 10, pp. 945–952, Sep. 2007.

[162] R. Tanaka, S. Hirose, and H. Hatakeyama, "Preparation and characterization of polyurethane foams using a palm oil-based polyol," *Bioresour. Technol.*, vol. 99, no. 9, pp. 3810–3816, Jun. 2008.

[163] S. Tan, T. Abraham, D. Ference, and C. W. Macosko, "Rigid polyurethane foams from a soybean oil-based Polyol," *Polymer (Guildf).*, vol. 52, no. 13, pp. 2840–2846, Jun. 2011.

[164] G. S. Dhaliwal, S. Anandan, K. Chandrashekhara, J. Lees, and P. Nam, "Development and characterization of polyurethane foams with substitution of polyether polyol with soy-based polyol," *Eur. Polym. J.*, vol. 107, pp. 105–117, Oct. 2018.

[165] D. Ji *et al.*, "Polyurethane rigid foams formed from different soy-based polyols by the ring opening of epoxidised soybean oil with methanol, phenol, and cyclohexanol," *Ind. Crops Prod.*, vol. 74, pp. 76–82, 2015.

[166] L. Zhang, M. Zhang, L. Hu, and Y. Zhou, "Synthesis of rigid polyurethane foams with castor oil-based flame retardant polyols," *Ind. Crops Prod.*, vol. 52, pp. 380–388, 2014.

[167] M. A. Mosiewicki, G. A. Dell'arciprete, M. I. Aranguren, and N. E. Marcovich, "Polyurethane foams obtained from castor oil-based polyol and filled with wood flour," *J. Compos. Mater.*, vol. 43, no. 25, pp. 3057–3072, 2009.

[168] T. Kattiyaboot and C. Thongpin, "Effect of Natural Oil Based Polyols on the Properties of Flexible Polyurethane Foams Blown by Distilled Water," *Energy Procedia*, vol. 89, pp. 177–185, Jun. 2016.

[169] A. Prociak, "Properties of Polyurethane Foams Modified with Natural Oil-Based Polyols," *Cell. Polym.*, vol. 26, no. 6, pp. 381–392, Nov. 2007.

[170] H. Mutlu and M. A. R. Meier, "Castor oil as a renewable resource for the chemical industry," *Eur. J. Lipid Sci. Technol.*, vol. 112, no. 1, pp. 10–30, Jan. 2010.

[171] S. S. Narine, X. Kong, L. Bouzidi, and P. Sporns, "Physical Properties of Polyurethanes Produced from Polyols from Seed Oils: II. Foams," *J. Am. Oil Chem. Soc.*, vol. 84, no. 1, pp. 65–72, Jan. 2007.

[172] P. Furtwengler, R. Perrin, A. Redl, and L. Avérous, "Synthesis and characterization of polyurethane foams derived of fully renewable polyester polyols from sorbitol," *Eur. Polym. J.*, vol. 97, no. September, pp. 319–327, 2017.

[173] M. Ionescu, Z. S. Petrović, and X. Wan, "Primary Hydroxyl Content of Soybean Polyols," *J. Am. Oil Chem. Soc.*, vol. 85, no. 5, pp. 465–473, May 2008.

[174] A. Palanisamy, B. S. Rao, and S. Mehazabeen, "Diethanolamides of Castor Oil as Polyols for the Development of Water-Blown Polyurethane Foam," *J. Polym. Environ.*, vol. 19, no. 3, pp. 698–705, Sep. 2011.

[175] U. Stirna *et al.*, "Structure and properties of the polyurethane and polyurethane foam

synthesized from castor oil polyols," *J. Cell. Plast.*, vol. 48, no. 6, pp. 476–488, Nov. 2012.

[176] L. Zhang, M. Zhang, Y. Zhou, and L. Hu, "The study of mechanical behavior and flame retardancy of castor oil phosphate-based rigid polyurethane foam composites containing expanded graphite and triethyl phosphate," *Polym. Degrad. Stab.*, vol. 98, no. 12, pp. 2784–2794, 2013.

[177] S. T. Keera, S. M. El Sabagh, and A. R. Taman, "Castor oil biodiesel production and optimization," *Egypt. J. Pet.*, vol. 27, no. 4, pp. 979–984, 2018.

[178] M. F. Valero and A. Gonzalez, "Polyurethane adhesive system from castor oil modified by a transesterification reaction," *J. Elastomers Plast.*, vol. 44, no. 5, pp. 433–442, 2012.

[179] M. Zhang, H. Pan, L. Zhang, L. Hu, and Y. Zhou, "Study of the mechanical, thermal properties and flame retardancy of rigid polyurethane foams prepared from modified castor-oil-based polyols," *Ind. Crops Prod.*, vol. 59, pp. 135–143, 2014.

[180] M. Kirpluks, D. Kalnbunde, Z. Walterova, and U. Cabulis, "Rapeseed Oil as feedstock for high functionality polyol synthesis," *J. Renew. Mater.*, vol. 5, no. 3–4, pp. 258–270, 2017.

[181] S. Bhoyate, M. Ionescu, P. K. Kahol, J. Chen, S. R. Mishra, and R. K. Gupta, "Highly flame-retardant polyurethane foam based on reactive phosphorus polyol and limonene-based polyol," *J. Appl. Polym. Sci.*, vol. 135, no. 21, pp. 16–19, 2018.

[182] K. Gosz, J. Haponiuk, and Ł. Piszczyk, "The Influence of Substitution of a Phosphorus-Containing Polyol with the Bio-polyol on the Properties of Bio-based PUR/PIR Foams," *J. Polym. Environ.*, vol. 26, no. 9, pp. 3877–3888, Sep. 2018.

[183] W.-H. H. Rao *et al.*, "A reactive phosphorus-containing polyol incorporated into flexible polyurethane foam: Self-extinguishing behavior and mechanism," *Polym. Degrad. Stab.*, vol. 153, pp. 192–200, Jul. 2018.

[184] H.-B. Zhao and Y.-Z. Wang, "Design and Synthesis of PET-Based Copolyesters with Flame-Retardant and Antidripping Performance," *Macromol. Rapid Commun.*, vol. 38, no. 23, p. 1700451, Dec. 2017.

[185] M. C. Saha, M. E. Kabir, and S. Jeelani, "Enhancement in thermal and mechanical properties of polyurethane foam infused with nanoparticles," *Mater. Sci. Eng. A*, vol. 479, no. 1–2, pp. 213–222, 2008.

[186] ASTM international, "ASTM E1899 - 16 Standard Test Method for Hydroxyl Groups Using Reaction with -Toluenesulfonyl Isocyanate (TSI) and Potentiometric Titration

with Tetrabutylammonium Hydroxide." 2016.

[187] ISO, "ISO - ISO 22007-2:2008 - Plastics — Determination of thermal conductivity and thermal diffusivity — Part 2: Transient plane heat source (hot disc) method." .

[188] ASTM, "ASTM D2863 - 19-Standard Test Method for Measuring the Minimum Oxygen Concentration to Support Candle-Like Combustion of Plastics (Oxygen Index)." 2019.

[189] M. E. Mngomezulu, M. J. John, V. Jacobs, and A. S. Luyt, "Review on flammability of biofibres and biocomposites," *Carbohydr. Polym.*, vol. 111, pp. 149–182, 2014.

[190] X. Chen, J. Li, and M. Gao, "Thermal degradation and flame retardant mechanism of the rigid polyurethane foam including functionalized graphene oxide," *Polymers (Basel).*, vol. 11, no. 1, Jan. 2019.

[191] ASTM International, "ASTM D3801-10. Standard Test Method for Measuring the Comparative Burning Characteristics of Solid Plastics in a Vertical Position," *Annual Book of ASTM Standards*, no. October. pp. 1–5, 2000.

[192] B. Schartel and T. R. Hull, "Development of fire-retarded materials—Interpretation of cone calorimeter data," *Fire Mater.*, vol. 31, no. 5, pp. 327–354, Aug. 2007.

[193] J. Lindholm, A. Brink, and M. Hupa, "Cone calorimeter – a tool for measuring heat release rate," *Finnish-Swedish Flame Days 2009*, p. 4B, 2009.

[194] J. Lefebvre *et al.*, "Flame spread of flexible polyurethane foam: comprehensive study," *Polym. Test.*, vol. 23, no. 3, pp. 281–290, May 2004.

[195] V. Babrauskas, "The Cone Calorimeter," in *SFPE Handbook of Fire Protection Engineering*, 5th ed., New York: Springer, 2016, pp. 952–980.

[196] ISO, "ISO 5660-1:2015 Reaction-to-fire tests — Heat release, smoke production and mass loss rate — Part 1: Heat release rate (cone calorimeter method) and smoke production rate (dynamic measurement)." 2015.

[197] ASTM International, "ASTM D1621 - 00-Standard Test Method for Compressive Properties Of Rigid Cellular Plastics." 2000.

[198] M. Heinen, A. E. Gerbase, and C. L. Petzhold, "Vegetable oil-based rigid polyurethanes and phosphorylated flame-retardants derived from epoxydized soybean oil," *Polym. Degrad. Stab.*, vol. 108, pp. 76–86, 2014.

[199] H. M. Stapleton *et al.*, "Detection of organophosphate flame retardants in furniture foam and U.S. house dust.," *Environ. Sci. Technol.*, vol. 43, no. 19, pp. 7490–5, Oct. 2009.

[200] Y. Wang *et al.*, "Core-shell expandable graphite @ aluminum hydroxide as a flame-retardant for rigid polyurethane foams," *Polym. Degrad. Stab.*, vol. 146, no. November,

pp. 267–276, 2017.

[201] M. Modesti, A. Lorenzetti, F. Simioni, and G. Camino, “Expandable graphite as an intumescent flame retardant in polyisocyanurate-polyurethane foams,” *Polym. Degrad. Stab.*, vol. 77, no. 2, pp. 195–202, 2002.

[202] T. Guler, U. Tayfun, E. Bayramli, and M. Dogan, “Effect of expandable graphite on flame retardant, thermal and mechanical properties of thermoplastic polyurethane composites filled with huntite&hydromagnesite mineral,” *Thermochim. Acta*, vol. 647, pp. 70–80, 2017.

[203] M. Thirumal, D. Khastgir, N. K. Singha, B. S. Manjunath, and Y. P. Naik, “Effect of foam density on the properties of water blown rigid polyurethane foam,” *J. Appl. Polym. Sci.*, vol. 108, no. 3, pp. 1810–1817, May 2008.

[204] A. Lorenzetti, B. Dittrich, B. Schartel, M. Roso, and M. Modesti, “Expandable graphite in polyurethane foams: The effect of expansion volume and intercalants on flame retardancy,” *J. Appl. Polym. Sci.*, vol. 134, no. 31, pp. 1–8, 2017.

[205] X. L. Zhang *et al.*, “A facile strategy to fabricate microencapsulated expandable graphite as a flame-retardant for rigid polyurethane foams,” *J. Appl. Polym. Sci.*, vol. 132, no. 31, pp. 1–9, 2015.

[206] Jihui-Li, Huifang-Da, Qian-Liu, and Shufen-Liu, “Preparation of sulfur-free expanded graphite with 320 μm mesh of flake graphite,” *Mater. Lett.*, vol. 60, no. 29–30, pp. 3927–3930, 2006.

[207] W. Luo, Y. Li, H. Zou, and M. Liang, “Study of different-sized sulfur-free expandable graphite on morphology and properties of water-blown semi-rigid polyurethane foams,” *RSC Adv.*, vol. 4, no. 70, pp. 37302–37310, Aug. 2014.

[208] L. Ye, X. Y. Meng, X. Ji, Z. M. Li, and J. H. Tang, “Synthesis and characterization of expandable graphite-poly(methyl methacrylate) composite particles and their application to flame retardation of rigid polyurethane foams,” *Polym. Degrad. Stab.*, vol. 94, no. 6, pp. 971–979, 2009.

[209] X.-C. Bian, J.-H. Tang, Z.-M. Li, Z.-Y. Lu, and A. Lu, “Dependence of flame-retardant properties on density of expandable graphite filled rigid polyurethane foam,” *J. Appl. Polym. Sci.*, vol. 104, no. 5, pp. 3347–3355, Jun. 2007.

[210] M. Thirumal, D. Khastgir, N. K. Singha, B. S. Manjunath, and Y. P. Naik, “Effect of expandable graphite on the properties of intumescent flame-retardant polyurethane foam,” *J. Appl. Polym. Sci.*, vol. 110, no. 5, pp. 2586–2594, Dec. 2008.

[211] P. Acuña, Z. Li, M. Santiago-Calvo, F. Villafañe, M. ángel Rodríguez-Perez, and D.-Y. D. Y. D.-Y. Wang, "Influence of the characteristics of expandable graphite on the morphology, thermal properties, fire behaviour and compression performance of a rigid polyurethane foam," *Polymers (Basel).*, vol. 11, no. 1, p. 168, 2019.

[212] P. Acuña, M. Santiago-Calvo, F. Villafañe, M. A. M. A. Rodríguez-Perez, J. Rosas, and D. Y. D.-Y. Wang, "Impact of expandable graphite on flame retardancy and mechanical properties of rigid polyurethane foam," *Polym. Compos.*, vol. 40, no. S2, pp. E1705–E1715, 2018.

[213] S. Estravís, J. Tirado-Mediavilla, M. Santiago-Calvo, J. Luis Ruiz-Herrero, F. Villafañe, and M. Ángel Rodríguez-Pérez, "Rigid polyurethane foams with infused nanoclays: Relationship between cellular structure and thermal conductivity," *Eur. Polym. J.*, vol. 80, pp. 1–15, 2016.

[214] S. W. Choi, J. M. Jung, H. M. Yoo, S. H. Kim, and W. Il Lee, "Analysis of thermal properties and heat transfer mechanisms for polyurethane foams blown with water," *J. Therm. Anal. Calorim.*, vol. 132, no. 2, pp. 1253–1262, 2018.

[215] D. Yan, L. Xu, C. Chen, J. Tang, X. Ji, and Z. Li, "Enhanced mechanical and thermal properties of rigid polyurethane foam composites containing graphene nanosheets and carbon nanotubes," *Polym. Int.*, vol. 61, no. 7, pp. 1107–1114, Jul. 2012.

[216] H. J. Duan, H. Q. Kang, W. Q. Zhang, X. Ji, Z. M. Li, and J. H. Tang, "Core-shell structure design of pulverized expandable graphite particles and their application in flame-retardant rigid polyurethane foams," *Polym. Int.*, vol. 63, no. 1, pp. 72–83, 2014.

[217] F. S. Chuang, "Analysis of thermal degradation of diacetylene-containing polyurethane copolymers," *Polym. Degrad. Stab.*, vol. 92, no. 7, pp. 1393–1407, Jul. 2007.

[218] S. Duquesne *et al.*, "Thermal degradation of polyurethane and polyurethane/expandable graphite coatings," *Polym. Degrad. Stab.*, vol. 74, no. 3, pp. 493–499, 2001.

[219] M. Kurańska, U. Cabulis, M. Auguścik, A. Prociak, J. Ryszkowska, and M. Kirpluks, "Bio-based polyurethane-polyisocyanurate composites with an intumescent flame retardant," *Polym. Degrad. Stab.*, vol. 127, pp. 11–19, 2016.

[220] Y. Leng, J. Gu, W. Cao, and T.-Y. Zhang, "Influences of density and flake size on the mechanical properties of flexible graphite," *Carbon N. Y.*, vol. 36, no. 7–8, pp. 875–881, Jan. 1998.

[221] X. Chen, J. Yu, S. Guo, Z. Luo, and M. He, "Flammability and Thermal Oxidative Degradation Kinetics of Magnesium Hydroxide and Expandable Graphite Flame

Retarded Polypropylene Composites," *J. Macromol. Sci. Part A*, vol. 45, no. 9, pp. 712–720, Jul. 2008.

[222] X. Chen, J. Yu, S. Lu, H. Wu, S. Guo, and Z. Luo, "Combustion Characteristics of Polypropylene/Magnesium Hydroxide/Expandable Graphite Composites," *J. Macromol. Sci. Part B*, vol. 48, no. 6, pp. 1081–1092, Oct. 2009.

[223] X. Chen, H. Wu, Z. Luo, B. Yang, S. Guo, and J. Yu, "Synergistic effects of expandable graphite with magnesium hydroxide on the flame retardancy and thermal properties of polypropylene," *Polym. Eng. Sci.*, vol. 47, no. 11, pp. 1756–1760, Nov. 2007.

[224] L. Du, Y. Zhang, X. Yuan, and J. Chen, "Combustion Characteristics and Synergistic Effect of Halogen-Free Flame-Retarded EVA/Hydrotalcite Blends with Expandable Graphite and Fumed Silica," *Polym. Plast. Technol. Eng.*, vol. 48, no. 10, pp. 1002–1007, Sep. 2009.

[225] B. Debelak and K. Lafdi, "Use of exfoliated graphite filler to enhance polymer physical properties," *Carbon N. Y.*, vol. 45, no. 9, pp. 1727–1734, Aug. 2007.

[226] M. Modesti and A. Lorenzetti, "Flame retardancy of polyisocyanurate-polyurethane foams: Use of different charring agents," *Polym. Degrad. Stab.*, vol. 78, no. 2, pp. 341–347, 2002.

[227] X.-C. Bian, J.-H. Tang, and Z.-M. Li, "Flame retardancy of hollow glass microsphere/rigid polyurethane foams in the presence of expandable graphite," *J. Appl. Polym. Sci.*, vol. 109, no. 3, pp. 1935–1943, Aug. 2008.

[228] P. Acuña *et al.*, "Synergistic effect of expandable graphite and phenylphosphonic-aniline salt on flame retardancy of rigid polyurethane foam," *Polym. Degrad. Stab.*, vol. 179, 2020.

[229] S. Wang, F. Xin, Y. Chen, L. Qian, and Y. Chen, "Phosphorus-nitrogen containing polymer wrapped carbon nanotubes and their flame-retardant effect on epoxy resin," *Polym. Degrad. Stab.*, vol. 129, pp. 133–141, Jul. 2016.

[230] M.-J. Chen *et al.*, "Full substitution of petroleum-based polyols by phosphorus-containing soy-based polyols for fabricating highly flame-retardant polyisocyanurate foams," *Polym. Degrad. Stab.*, vol. 154, pp. 312–322, Aug. 2018.

[231] B. Zhao, D. Y. Liu, W. J. Liang, F. Li, J. S. Wang, and Y. Q. Liu, "Bi-phase flame-retardant actions of water-blown rigid polyurethane foam containing diethyl-N,N-bis(2-hydroxyethyl) phosphoramide and expandable graphite," *J. Anal. Appl. Pyrolysis*, vol. 124, pp. 247–255, 2017.

[232] M. J. Xu, G. R. Xu, Y. Leng, and B. Li, "Synthesis of a novel flame retardant based on cyclotriphosphazene and DOPO groups and its application in epoxy resins," *Polym. Degrad. Stab.*, vol. 123, pp. 105–114, 2016.

[233] S. Bhoyate, M. Ionescu, P. K. Kahol, and R. K. Gupta, "Sustainable flame-retardant polyurethanes using renewable resources," *Ind. Crops Prod.*, vol. 123, pp. 480–488, Nov. 2018.

[234] T. T. Li *et al.*, "Nitrogen/phosphorus synergistic flame retardant-filled flexible polyurethane foams: Microstructure, compressive stress, sound absorption, and combustion resistance," *RSC Adv.*, vol. 9, no. 37, pp. 21192–21201, Jul. 2019.

[235] J. Shen, X. Han, and L. J. Lee, "Nanoscaled Reinforcement of Polystyrene Foams using Carbon Nanofibers," *J. Cell. Plast.*, vol. 42, no. 2, pp. 105–126, Mar. 2006.

[236] M. M. Velencoso, M. J. Ramos, R. Klein, A. De Lucas, and J. F. Rodriguez, "Thermal degradation and fire behaviour of novel polyurethanes based on phosphate polyols," *Polym. Degrad. Stab.*, vol. 101, no. 1, pp. 40–51, 2014.

[237] B. Zhao, L. Chen, J.-W. Long, H.-B. Chen, and Y.-Z. Wang, "Aluminum Hypophosphite versus Alkyl-Substituted Phosphinate in Polyamide 6: Flame Retardance, Thermal Degradation, and Pyrolysis Behavior," *Ind. Eng. Chem. Res.*, vol. 52, no. 8, pp. 2875–2886, Feb. 2013.

[238] X. Wang, W. Xing, X. Feng, B. Yu, L. Song, and Y. Hu, "Functionalization of graphene with grafted polyphosphamide for flame retardant epoxy composites: synthesis, flammability and mechanism," *Polym. Chem.*, vol. 5, no. 4, pp. 1145–1154, 2014.

[239] N. Wu, G. Fu, Y. Yang, M. Xia, H. Yun, and Q. Wang, "Fire safety enhancement of a highly efficient flame retardant poly(phenylphosphoryl phenylenediamine) in biodegradable poly(lactic acid)," *J. Hazard. Mater.*, vol. 363, no. September 2018, pp. 1–9, 2019.

[240] Y. Chen, W. Wang, Y. Qiu, L. Li, L. Qian, and F. Xin, "Terminal group effects of phosphazene-triazine bi-group flame retardant additives in flame retardant polylactic acid composites," *Polym. Degrad. Stab.*, vol. 140, pp. 166–175, 2017.

[241] S. Ramanujam, C. Zequine, S. Bhoyate, B. Neria, P. Kahol, and R. Gupta, "Novel Biobased Polyol Using Corn Oil for Highly Flame-Retardant Polyurethane Foams," *C*, vol. 5, no. 1, p. 13, 2019.

[242] C. K. Ranaweera, M. Ionescu, N. Bilic, X. Wan, P. K. Kahol, and R. K. Gupta, "Biobased Polyols Using Thiol-Ene Chemistry for Rigid Polyurethane Foams with Enhanced

Flame-Retardant Properties," *J. Renew. Mater.*, vol. 5, no. 1, pp. 1–12, 2017.

[243] W. Yao, D. Zhang, Y. Zhang, T. Fu, D. Guan, and Y. Dou, "Synergistic Flame Retardant Effects of Expandable Graphite and Ammonium Polyphosphate in Water-Blow Polyurethane Foam," *Adv. Mater. Sci. Eng.*, vol. 2019, pp. 1–8, Jan. 2019.

[244] X. Hu, D. Wang, and S. Wang, "Synergistic effects of expandable graphite and dimethyl methyl phosphonate on the mechanical properties, fire behavior, and thermal stability of a polyisocyanurate–polyurethane foam," *Int. J. Min. Sci. Technol.*, vol. 23, no. 1, pp. 13–20, Jan. 2013.

[245] S. Gómez-Fernández, M. Günther, B. Schartel, M. A. Corcuera, and A. Eceiza, "Impact of the combined use of layered double hydroxides, lignin and phosphorous polyol on the fire behavior of flexible polyurethane foams," *Ind. Crops Prod.*, vol. 125, pp. 346–359, Dec. 2018.

[246] W. Luo, J. Qin, M. Xiao, D. Han, S. Wang, and Y. Meng, "Synthesis of Aliphatic Carbonate Macrodiols and Their Application as Sustainable Feedstock for Polyurethane," *ACS Omega*, vol. 2, no. 7, pp. 3205–3213, Jul. 2017.

[247] C. Wang, Y. Zheng, Y. Xie, K. Qiao, Y. Sun, and L. Yue, "Synthesis of bio-castor oil polyurethane flexible foams and the influence of biotic component on their performance," *J. Polym. Res.*, vol. 22, no. 8, 2015.

[248] H. Ding, K. Huang, S. Li, L. Xu, J. Xia, and M. Li, "Synthesis of a novel phosphorus and nitrogen-containing bio-based polyol and its application in flame retardant polyurethane foam," *J. Anal. Appl. Pyrolysis*, vol. 128, no. November, pp. 102–113, Feb. 2017.

[249] S. Rabe, Y. Chuenban, and B. Schartel, "Exploring the Modes of Action of Phosphorus-Based Flame Retardants in Polymeric Systems," *Materials (Basel).*, vol. 10, no. 5, p. 455, Apr. 2017.

[250] M. Strankowski, P. Korzeniewski, J. Strankowska, A. S. Anu, and S. Thomas, "Morphology, mechanical and thermal properties of thermoplastic polyurethane containing reduced graphene oxide and graphene nanoplatelets," *Materials (Basel).*, vol. 11, no. 1, p. 82, Jan. 2018.

[251] N. Wu, X. She, D. Yang, X. Wu, F. Su, and Y. Chen, "Synthesis of network reduced graphene oxide in polystyrene matrix by a two-step reduction method for superior conductivity of the composite," *J. Mater. Chem.*, vol. 22, no. 33, p. 17254, Jul. 2012.

[252] D. C. Marcano *et al.*, "Improved Synthesis of Graphene Oxide," *ACS Nano*, vol. 12, no.

2, pp. 2078–2078, Aug. 2018.

[253] M. Rafiee, F. Nitzsche, J. Laliberte, S. Hind, F. Robitaille, and M. R. Labrosse, "Thermal properties of doubly reinforced fiberglass/epoxy composites with graphene nanoplatelets, graphene oxide and reduced-graphene oxide," *Compos. Part B Eng.*, vol. 164, pp. 1–9, May 2019.

[254] H. Liu *et al.*, "Lightweight conductive graphene/thermoplastic polyurethane foams with ultrahigh compressibility for piezoresistive sensing," *J. Mater. Chem. C*, vol. 5, no. 1, pp. 73–83, Dec. 2017.

[255] S. Jiang *et al.*, "Effect of carbon fiber-graphene oxide multiscale reinforcements on the thermo-mechanical properties of polyurethane elastomer," *Polym. Compos.*, vol. 40, no. S2, pp. E953–E961, Mar. 2019.

[256] P. Acuña, J. Zhang, G.-Z. Yin, X.-Q. Liu, and D.-Y. Wang, "Bio-based rigid polyurethane foam from castor oil with excellent flame retardancy and high insulation capacity via cooperation with carbon-based materials," *J. Mater. Sci.*, vol. 56, pp. 2684–2701, 2020.

[257] V. Yakushin, U. Stirna, O. Bikovens, M. Misane, I. Sevastyanova, and D. Vilsone, "Synthesis and Characterization of Novel Polyurethanes Based on Vegetable Oils Amide and Ester Polyols," *Mater. Sci.*, vol. 20, no. 3, 2014.

[258] L. J. Bellamy, *Introduction. In: The Infra-red Spectra of Complex Molecules*, 1st ed. Dordrecht: Springer, Dordrecht, 1975.

[259] P. Y. Jia, C. Y. Bo, L. Q. Zhang, L. H. Hu, M. Zhang, and Y. H. Zhou, "Synthesis of castor oil based plasticizers containing flame retarded group and their application in poly (vinyl chloride) as secondary plasticizer," *J. Ind. Eng. Chem.*, vol. 28, pp. 217–224, 2015.

[260] S. Sinadinović-Fišer, M. Janković, and O. Borota, "Epoxidation of castor oil with peracetic acid formed in situ in the presence of an ion exchange resin," *Chem. Eng. Process. Process Intensif.*, vol. 62, pp. 106–113, 2012.

[261] F. Sun, T. Yu, C. Hu, and Y. Li, "Influence of functionalized graphene by grafted phosphorus containing flame retardant on the flammability of carbon fiber/epoxy resin (CF/ER) composite," *Compos. Sci. Technol.*, vol. 136, pp. 76–84, Nov. 2016.

[262] R. Yuan, J. Yuan, Y. Wu, L. Chen, H. Zhou, and J. Chen, "Efficient synthesis of graphene oxide and the mechanisms of oxidation and exfoliation," *Appl. Surf. Sci.*, vol. 416, pp. 868–877, Sep. 2017.

[263] Y. Guo, C. Bao, L. Song, B. Yuan, and Y. Hu, "In situ polymerization of graphene, graphite oxide, and functionalized graphite oxide into epoxy resin and comparison study of on-the-flame behavior," *Ind. Eng. Chem. Res.*, vol. 50, no. 13, pp. 7772–7783, 2011.

[264] Z. Ying, X. Lin, Y. Qi, and J. Luo, "Preparation and characterization of low-temperature expandable graphite," *Mater. Res. Bull.*, vol. 43, no. 10, pp. 2677–2686, 2008.

[265] X. Jing, H.-Y. Mi, M. R. Salick, X.-F. Peng, and L.-S. Turng, "Preparation of thermoplastic polyurethane/graphene oxide composite scaffolds by thermally induced phase separation," *Polym. Compos.*, vol. 35, no. 7, pp. 1408–1417, Jul. 2014.

[266] D. Cai, J. Jin, K. Yusoh, R. Rafiq, and M. Song, "High performance polyurethane/functionalized graphene nanocomposites with improved mechanical and thermal properties," *Compos. Sci. Technol.*, vol. 72, no. 6, pp. 702–707, 2012.

[267] X. M. Hu and D. M. Wang, "Enhanced fire behavior of rigid polyurethane foam by intumescent flame retardants," *J. Appl. Polym. Sci.*, vol. 129, no. 1, pp. 238–246, 2013.

[268] A. Hejna, M. Kirpluks, P. Kosmela, U. Cabulis, J. Haponiuk, and Ł. Piszczyk, "The influence of crude glycerol and castor oil-based polyol on the structure and performance of rigid polyurethane-polyisocyanurate foams," *Ind. Crops Prod.*, vol. 95, pp. 113–125, 2017.

[269] N. Gama, L. C. Costa, V. Amaral, A. Ferreira, and A. Barros-Timmons, "Insights into the physical properties of biobased polyurethane/expanded graphite composite foams," *Compos. Sci. Technol.*, vol. 138, pp. 24–31, Jan. 2017.

[270] C. Bernard *et al.*, "Graphene oxide/waterborne polyurethane nanocoatings: effects of graphene oxide content on performance properties," *J. Coatings Technol. Res.*, vol. 17, no. 1, pp. 255–269, 2020.

[271] H. Kim, Y. Miura, and C. W. Macosko, "Graphene/Polyurethane Nanocomposites for Improved Gas Barrier and Electrical Conductivity," *Chem. Mater.*, vol. 22, no. 11, pp. 3441–3450, Jun. 2010.

[272] J. Bian, H. L. Lin, F. X. He, X. W. Wei, I.-T. Chang, and E. Sancaktar, "Fabrication of microwave exfoliated graphite oxide reinforced thermoplastic polyurethane nanocomposites: Effects of filler on morphology, mechanical, thermal and conductive properties," *Compos. Part A Appl. Sci. Manuf.*, vol. 47, pp. 72–82, Apr. 2013.

[273] M. Modesti *et al.*, "Synergism between flame retardant and modified layered silicate on thermal stability and fire behaviour of polyurethane nanocomposite foams," *Polym. Degrad. Stab.*, vol. 93, no. 12, pp. 2166–2171, 2008.

[274] W. Xu, G. Wang, and X. Zheng, "Research on highly flame-retardant rigid PU foams by combination of nanostructured additives and phosphorus flame retardants," *Polym. Degrad. Stab.*, vol. 111, pp. 142–150, 2015.

[275] J. Alongi, Z. Han, and S. Bourbigot, "Intumescence: Tradition versus novelty. A comprehensive review," *Prog. Polym. Sci.*, vol. 51, pp. 28–73, 2015.

[276] S. Bourbigot and S. Duquesne, "Fire retardant polymers: Recent developments and opportunities," *J. Mater. Chem.*, vol. 17, no. 22, pp. 2283–2300, 2007.

[277] M. Shams *et al.*, "Influence of functional groups on the degradation of graphene oxide nanomaterials," *Environ. Sci. Nano*, vol. 6, no. 7, pp. 2203–2214, 2019.

[278] V. D. Punetha *et al.*, "Functionalization of carbon nanomaterials for advanced polymer nanocomposites: A comparison study between CNT and graphene," *Prog. Polym. Sci.*, vol. 67, pp. 1–47, 2017.

[279] Y. Yang *et al.*, "Thermal conductivity of defective graphene oxide: A molecular dynamic study," *Molecules*, vol. 24, no. 6, 2019.

[280] W. Yu, L. Sisi, Y. Haiyan, and L. Jie, "Progress in the functional modification of graphene/graphene oxide: a review," *RSC Adv.*, vol. 10, p. 15328, 2020.

[281] S. Zhou *et al.*, "One-pot synthesis of robust superhydrophobic, functionalized graphene/polyurethane sponge for effective continuous oil–water separation," *Chem. Eng. J.*, vol. 302, pp. 155–162, Oct. 2016.

[282] Y. J. Ning *et al.*, "Anti-corrosion reinforcement of waterborne polyurethane coating with polymerized graphene oxide by the one-pot method," *J. Mater. Sci.*, no. ii, 2020.

[283] X. Zhao, H. V. Babu, J. Llorca, and D. Y. Wang, "Impact of halogen-free flame retardant with varied phosphorus chemical surrounding on the properties of diglycidyl ether of bisphenol-A type epoxy resin: Synthesis, fire behaviour, flame-retardant mechanism and mechanical properties," *RSC Adv.*, vol. 6, no. 64, pp. 59226–59236, 2016.

[284] Y. Bykov *et al.*, "Synthesis of new dibenzo[c.e][1,2]oxaphosphorine 2-oxide containing diols based on diethanolamine," *Heteroat. Chem.*, vol. 23, no. 2, pp. 146–153, 2012.

[285] M. Acik *et al.*, "The role of intercalated water in multilayered graphene oxide," *ACS Nano*, vol. 4, no. 10, pp. 5861–5868, Oct. 2010.

[286] J. He and L. Fang, "Controllable synthesis of reduced graphene oxide," *Curr. Appl. Phys.*, vol. 16, no. 9, pp. 1152–1158, 2016.

[287] W.-H. Liao *et al.*, "Effect of Molecular Chain Length on the Mechanical and Thermal Properties of Amine-Functionalized Graphene Oxide/Polyimide Composite Films

Prepared by In Situ Polymerization," *Appl. Mater. Interfaces*, vol. 5, pp. 869–877, May 2013.

[288] Q. Jing, W. Liu, Y. Pan, V. V. Silberschmidt, L. Li, and Z. L. Dong, "Chemical functionalization of graphene oxide for improving mechanical and thermal properties of polyurethane composites," *Mater. Des.*, vol. 85, pp. 808–814, 2015.

[289] Y. Shi, B. Yu, Y. Zheng, J. Yang, Z. Duan, and Y. Hu, "Design of reduced graphene oxide decorated with DOPO-phosphanomidate for enhanced fire safety of epoxy resin," *J. Colloid Interface Sci.*, vol. 521, pp. 160–171, Jul. 2018.

[290] F. Fang, P. Song, S. Ran, Z. Guo, H. Wang, and Z. Fang, "A facile way to prepare phosphorus-nitrogen-functionalized graphene oxide for enhancing the flame retardancy of epoxy resin," *Compos. Commun.*, vol. 10, pp. 97–102, Dec. 2018.

[291] O. C. Compton, D. A. Dikin, K. W. Putz, L. C. Brinson, and S. T. Nguyen, "Electrically conductive 'alkylated' graphene paper via chemical reduction of amine-functionalized graphene oxide paper," *Adv. Mater.*, vol. 22, no. 8, pp. 892–896, 2010.

[292] T. T. Nguyen, P. Bandyopadhyay, X. Li, N. H. Kim, and J. H. Lee, "Effects of grafting methods for functionalization of graphene oxide by dodecylamine on the physical properties of its polyurethane nanocomposites," *J. Memb. Sci.*, vol. 540, no. May, pp. 108–119, 2017.

[293] B. C. Smith, "Chapter 5: Organic Nitrogen Compounds," in *Infrared Spectral Interpretation: A Systematic Approach*, 1st ed., vol. 2, B. C. Smith, Ed. Boca Raton, London, New York, Washington, D.C.: CRC Press, 1998, pp. 128–132.

[294] M. Bera, P. Gupta, and P. K. Maji, "Efficacy of ultra-low loading of amine functionalized graphene oxide into glycidol-terminated polyurethane for high-performance composite material," *React. Funct. Polym.*, vol. 139, no. February, pp. 60–74, 2019.

[295] Z. Wang, P. Wei, Y. Qian, and J. Liu, "The synthesis of a novel graphene-based inorganic-organic hybrid flame retardant and its application in epoxy resin," *Compos. Part B Eng.*, vol. 60, pp. 341–349, 2014.

[296] W. Guo, B. Yu, Y. Yuan, L. Song, and Y. Hu, "In situ preparation of reduced graphene oxide/DOPO-based phosphonamidate hybrids towards high-performance epoxy nanocomposites," *Compos. Part B Eng.*, vol. 123, pp. 154–164, Aug. 2017.

[297] J. J. Shea, *Polymeric foams: mechanisms and materials [Book review]*, vol. 21, no. 2. 2005.

[298] M. Bera, A. Prabhakar, and P. K. Maji, "Nanotailoring of thermoplastic polyurethane by

amine functionalized graphene oxide: Effect of different amine modifier on final properties," *Compos. Part B Eng.*, vol. 195, no. March, p. 108075, 2020.

[299] A. Tounici and J. M. Martín-Martínez, "Addition of small amounts of graphene oxide in the polyol during the synthesis of waterborne polyurethane urea adhesives for improving their adhesion properties," *Int. J. Adhes. Adhes.*, vol. 104, no. September 2020, 2021.

[300] Q. Zhang, M. Hao, X. Xu, G. Xiong, H. Li, and T. S. Fisher, "Flyweight 3D Graphene Scaffolds with Microinterface Barrier-Derived Tunable Thermal Insulation and Flame Retardancy," *ACS Appl. Mater. Interfaces*, vol. 9, no. 16, pp. 14232–14241, 2017.

[301] F. Liu, L. Wu, Y. Song, W. Xia, and K. Guo, "Effect of molecular chain length on the properties of amine-functionalized graphene oxide nanosheets/epoxy resins nanocomposites," *RSC Adv.*, vol. 5, no. 57, pp. 45987–45995, 2015.

[302] Y. Feng *et al.*, "Superior flame retardancy and smoke suppression of epoxy-based composites with phosphorus/nitrogen co-doped graphene," *J. Hazard. Mater.*, vol. 346, pp. 140–151, 2018.

[303] X. Wu *et al.*, "Influence of char residues on flammability of EVA/EG, EVA/NG and EVA/GO composites," *Polym. Degrad. Stab.*, vol. 97, no. 1, pp. 54–63, Jan. 2012.

[304] G. Wu, X. Xu, X. He, and Y. Yan, "Preparation and Characterization of Graphene Oxide-Modified Sapium sebiferum Oil-Based Polyurethane Composites with Improved Thermal and Mechanical Properties," *Polymers (Basel).*, vol. 10, no. 133, 2018.

[305] M. Kumar, J. S. Chung, B.-S. Kong, E. J. Kim, and H. Hur, "Synthesis of graphene-polyurethane nanocomposite using highly functionalized graphene oxide as pseudo-crosslinker," *Mater. Lett.*, vol. 106, pp. 319–321, 2013.

[306] J. Jing *et al.*, "Layer by layer deposition of polyethylenimine and bio-based polyphosphate on ammonium polyphosphate: A novel hybrid for simultaneously improving the flame retardancy and toughness of polylactic acid," *Polymer (Guildf).*, vol. 108, pp. 361–371, Jan. 2017.

[307] X. Hu, D. Wang, and W. Cheng, "Effect of dosage of expandable graphite, dimethyl methylphosphonate, triethanolamine, and isocyanate on fluidity, mechanical, and flame retardant properties of polyurethane materials in coal reinforcement," *Int. J. Min. Sci. Technol.*, vol. 26, no. 2, pp. 345–352, 2016.

[308] Y. Wang, Y. Yu, X. Hu, A. Feng, F. Jiang, and L. Song, "p-Phenylenediamine strengthened graphene oxide for the fabrication of superhydrophobic surface," *Mater. Des.*, vol. 127, no. January, pp. 22–29, 2017.

[309] M. Szycher, P. D, and M. Szycher, “Structure–Property Relations in Polyurethanes,” in *Szycher’s Handbook of Polyurethanes, Second Edition*, 2012, pp. 37–86.